

Eye controlled semi-Robotic Wheelchair for quadriplegic users embedding Mixed Reality tools



Luca Maule

Supervisors: Prof. M. De Cecco

Dr. M. Tavernini

Department of Industrial Engineering
University of Trento

This dissertation is submitted for the degree of
Doctor of Materials, Mechatronics and Systems Engineering
XXXI cycle

June 2019

I would like to dedicate this thesis to my loving parents.

Declaration

I hereby declare that except where specific reference, the contents of this dissertation are original and have not been submitted in whole or in part for consideration for any other degree or qualification in this, or any other University. This dissertation includes organically the work published or submitted on scientific journals and international conference proceedings. This dissertation contains less than 65,000 words including appendices, bibliography, footnotes, tables and equations and has fewer than 150 figures.

Luca Maule
June 2019

Acknowledgements

First and foremost I want to thank my advisor Prof. Mariolino De Cecco for the continuous support of my Ph.D. study and related research, for his patience, motivation, and immense knowledge. It has been an honour to be his Ph.D. student. The enthusiasm he has for the research was contagious and motivational for me, even during tough times during the Ph.D. pursuit. My sincere thank also goes to all the team of the Measurement Instrumentation and Robotic (MiRo) laboratory. They have all contributed immensely to my personal and professional time being a source of friendships as well as good advice and collaboration. I am especially grateful to two of the original group members Mattia Tavernini and Alberto Fornaser for the constant help they gave me during the last five years. Their support on the development, data analysis, and scientific production was fundamental for the overall outcome of my Ph.D. work. Furthermore, I thank Paolo Tomasin, another important member of the team who helped me a lot as a graduating student at the beginning and then, as a research fellow. His contribution to the development of the prototype was very important during the last four years. Last but not least, I want to address big thanks to Matteo Zanetti for the support during almost all my university career. Since the beginning of our friendship, he has been a good fellow traveller friend.

Recently, the MiRo team has expanded with the entrance of Alessandro Luchetti and Nicola Covre. A thank goes also to them for the good time spent during this time inside the laboratory.

Other past and present group members that I have had the pleasure to work with or alongside are the graduated students Malvina Leuci, Gabriele Minotto, Aibike Yessimbekova, and Matteo Dallapiccola. I would like to acknowledge them for working on the various part of the research related to my Ph.D. study. Also their contribution was fundamental for the overall outcome of the project.

This research was supported by the company Nuova Blandino Srl, Alberto Tassone, and Andrea Gravina, who provided the necessary devices and technology.

I would also like to thank the Abilita service of APSS, with the head Dr. Giovanni Guandalini, and the people involved in the project who provided insight and expertise that greatly assisted the research. I thanks all the volunteers that participated in the test campaign.

Their availability to help us was fundamental for the realization of the device and this work. A special thank goes to Mr. Moreno Corsi, for his inestimable help and strong will. His inexhaustible desire to live pushed me, as well as all the MiRo team, to work harder.

I would like to express my thank to all my big family composed by aunts, uncles, and cousins. Sara, Carlo, Massimiliano, Stefano as well as all my other relatives demonstrated a constant availability, first of all, to support me with advice or suggestions, but also to participate to "funny" evening. All these contributions were very important during my academic career.

To my friends, thank you for listening, offering me advice, and supporting me at any time I need. A special thanks go also to Filippo, Fabio, Desireè, Federica, Alessandra, Francesca, Nadia, Romina, Claudia, Andrea, Barbara and Sara for their moral support and motivation, which drives me to give my best at any time. They remember me every day the importance of friendship.

In conclusion, I want to dedicate the bigger thanks to my parents Giuseppe e Carmen and to my sisters Daniela and Laura for all of the sacrifices that they've made on my behalf. Thank you for teaching me that my job in life was to learn, to be happy, and to know and understand myself. A final thought is dedicated to my grandparents to be on my side every day.

Abstract

Mobile assistive robotics can play a key role to improve the autonomy and lifestyle of patients. In this context, RoboEye project aims to support people affected by mobility problems that range from very impairing pathologies (like ALS, amyotrophic lateral sclerosis) to old age.

Any severe motor disability is a condition that limits the capability of interacting with the environment, even the domestic one, caused by the loss of the control on our own mobility. Although these pathologies are relatively rare, the number of people affected by this disease are increasing during the years.

The focus of this project is the restore of persons' mobility using novel technologies based on the gaze on a power wheelchair designed to enable the user to move easily and autonomously inside his home. A novel and intuitive control system was designed to achieve such a goal, in which a non-invasive eye tracker, a monitor, and a 3D camera represent some of the core elements. The developed prototype integrates, on a standard power wheelchair, functionalities from the mobile robotics field, with the main benefit of providing to the user two driving options and comfortable navigation.

The most intuitive, and direct, modality foresees the continuous control of the frontal and angular velocities of the wheelchair by gazing at different areas of the monitor. The second, semi-autonomous, enables the navigation toward a selected point in the environment by just pointing and activating the wished destination while the system autonomously plans and follows the trajectory that brings the wheelchair there. The main goal is the development of shared control, combining direct control by the user with the comfort of autonomous navigation based on augmented reality markers.

A first evaluation has been performed on a real test bed where specific motion metrics are evaluated. The designs of the control structure and driving interfaces were tuned thanks to the testing of some volunteers, habitual users of standard power wheelchairs. The driving modalities, especially the semi-autonomous one, were modelled and qualified to verify their efficiency, reliability, and safety for domestic usage.

Table of contents

List of figures	xv
List of tables	xxi
Nomenclature	xxiii
1 Introduction	1
1.1 Motivation	1
1.2 Related efforts	3
1.3 Thesis summary	4
2 Requirements	7
2.1 Amyotrophic Lateral Sclerosis (ALS)	7
2.1.1 Who gets ALS?	8
2.1.2 Symptoms	10
3 State of art	13
3.1 Eye driven wheelchairs	15
4 Eye Tracking Technology and uncertainty analysis	17
4.1 Uncertainty analysis	25
4.1.1 Eye tracker repeatability and accuracy characterization	26
5 Wheelchair	31
5.1 Mechanical structure	32
5.1.1 AGV	36
5.2 Differential drive kinematic model	38
5.3 Prototype: hardware	40
5.3.1 Devices	45

5.4	Calibration of the wheelchair kinematic parameters	50
5.5	Prototype: software	56
5.5.1	Human Machine Interface	57
5.5.2	Camera acquisition	58
5.5.3	Path planning	59
5.5.4	Path following	59
5.5.5	Serial communication	62
5.5.6	Management of the wheelchair layout	62
5.5.7	Status management of the system	62
6	Wheelchair Direct Eye Control	65
6.1	Direct Drive Modality	65
6.1.1	Interaction design in VR simulated environment	66
6.1.2	Interaction design on the eye controlled wheelchair	69
6.1.3	Test plan	72
6.2	HMI performance evaluation in VR environment	77
6.2.1	Results analysis of the circuit metric	77
6.2.2	Results analysis of comfort metric	81
6.2.3	Results analysis of manoeuvring metric	81
6.2.4	Results analysis of depth perception metric	85
6.2.5	Discussion of the results	89
6.3	HMI performance evaluation in real environment	90
6.3.1	Test environment design	90
6.3.2	Testing protocol	99
6.3.3	Metrics evaluation features	100
6.3.4	Subjective evaluation features	106
6.3.5	Experimental results	108
6.3.6	Influence factors in the usage of ocular HMI	160
6.3.7	Human metrics	166
6.3.8	Workload	166
6.3.9	Discussion of the results	173
7	Robotic feature modality using mixed reality	175
7.1	Semi-autonomous driving technique	178
7.1.1	Navigation	180
7.2	Experimental verification	184
7.2.1	Manoeuvre modelling	186

Table of contents	xiii
7.2.2 Experimental testing	192
7.3 Discussion of the results	196
8 Conclusions	197
References	199

List of figures

1.1	Conceptual model of the project	3
2.1	ALS Projection	9
4.1	Eye Tracker Technology	18
4.2	Raw data collected for accuracy and repeatability characterization of the eye tracker uncertainty	27
4.3	Mean and covariance of accuracy and repeatability characterization of the eye tracker uncertainty	28
4.4	Eye tracker repeatability analysis including different calibrations	29
4.5	Values of the covariance ellipse's angle	30
4.6	Covariance <i>circle</i> with radius $R=114$ pixels	30
5.1	Synchro-drive mobile robot	33
5.2	Differential-drive mobile robot	34
5.3	Tricycle mobile robot	34
5.4	Car-like mobile robot	35
5.5	Differential drive kinematic model schema	38
5.6	Prototype of semi-robotic eye controlled wheelchair	41
5.7	Tobii 4C eye tracker	45
5.8	RoboteQ devices	46
5.9	Bearingless magnetic encoder	47
5.10	3D cameras: Kinect v2 vs Intel RealSense D435	49
5.11	Point cloud frames collected with Kinect v2 and Intel RealSense D435	51
5.12	Testbed for the calibration of the wheelchair kinematic parameters	52
5.13	Velocity profiles resultng from the aylisis on the commercial wheelchair	53
5.14	Theoretical open loop system step response	55
5.15	Measured open loop system step response	56
5.16	The Human Machine Interface shown on the frontal monitor	58

5.17	Path planning process	60
5.18	Path following graphical representation	61
6.1	HMI with 3X3 grid buttons	67
6.2	HMI with control functions for translation and rotation	68
6.3	VR environment	68
6.4	Control laws of the velocity profiles	71
6.5	UNITY virtual test environment	75
6.6	Rendering of the real test environment	76
6.7	Paths of circuit test in VR	78
6.8	HMIs penalties comparison for the circuit test in VR	80
6.9	Paths of manoeuvring test in VR	82
6.10	HMIs penalties comparison for the manoeuvring test in VR	85
6.11	Speed of the virtual wheelchair during the depth perception test in VR	86
6.12	HMIs penalties comparison for the depth perception test in VR	88
6.13	"OptiTrack" simulated environment	91
6.14	Drone arena	92
6.15	Optitrack uncertainty analysis	94
6.16	"OptiTrack" tracking object	95
6.17	Drone arena with the drawn paths	98
6.18	Schematic representation of the sections considered in the analysis.	101
6.19	Example of acceleration data from a specific subject	102
6.20	Wheelchair reference system	102
6.21	Path segmentation for the path following test.	103
6.22	Questionnaire on personal interests	107
6.23	Workload questionnaire	110
6.24	Interface questionnaire	111
6.25	Interface questionnaire (page 2).	112
6.26	Interface questionnaire (page 3).	113
6.27	Interface questionnaire (page 4).	114
6.28	Full set of paths recorded during the tests.	115
6.29	Comparison of the deviation from the reference path related to the full population along the straight part of the path following test (section 1)	116
6.30	Comparison of the deviation from the reference path between interfaces along the straight part of the path following test (section 1)	117
6.31	Comparison of the deviation from the reference path between subjects along the straight part of the path following test (section 1)	118

6.32 ANOVA analysis for the mean deviation (e_m) for the path following test, along the section 1	119
6.33 ANOVA analysis for the efficiency in speed control ($v_{\hat{eff}}$) for the path following test, along the section 1	120
6.34 ANOVA analysis for the frontal weighted average acceleration (a_{wf}) for the path following test, along the section 1	121
6.35 ANOVA analysis for the lateral weighted average acceleration (a_{wl}) for the path following test, along the section 1	122
6.36 Comparison of the deviation from the reference path related to the full population along the bumpy part of the path following test (section 2) . . .	124
6.37 Comparison of the deviation from the reference path between interfaces along the bumpy part of the path following test (section 2)	125
6.38 Comparison of the deviation from the reference path between subjects along the bumpy part of the path following test (section 2)	126
6.39 ANOVA analysis for the mean deviation (e_m) for the path following test, along the section 2	127
6.40 ANOVA analysis for the efficiency in speed control ($v_{\hat{eff}}$) for the path following test, along the section 2	128
6.41 ANOVA analysis for the frontal weighted average acceleration (a_{wf}) for the path following test, along the section 2	129
6.42 ANOVA analysis for the lateral weighted average acceleration (a_{wl}) for the path following test, along the section 2	130
6.43 Comparison of the deviation from the reference path related to the full population along the curved part of the path following test (section 3) . . .	133
6.44 Comparison of the deviation from the reference path between interfaces along the curved part of the path following test (section 3)	134
6.45 Comparison of the deviation from the reference path between subjects along the curved part of the path following test (section 3)	135
6.46 Full set of paths related to the path following test	136
6.47 ANOVA analysis for the mean deviation (e_m) for the path following test, along the section 3	137
6.48 ANOVA analysis for the efficiency in speed control ($v_{\hat{eff}}$) for the path following test, along the section 3	138
6.49 ANOVA analysis for the frontal weighted average acceleration (a_{wf}) for the path following test, along the section 3	139

6.50	ANOVA analysis for the lateral weighted average acceleration (a_{wl}) for the path following test, along the section 3	140
6.51	Comparison of the deviation from the reference path related to the full population along the parking test (section 4)	142
6.52	Comparison of the deviation from the reference path between interfaces along the parking test (section 4)	143
6.53	Comparison of the deviation from the reference path between subjects along the parking test (section 4)	144
6.54	Full set of paths related to the parking test	146
6.55	ANOVA analysis for the mean deviation (e_m) for the parking test	147
6.56	ANOVA analysis for the efficiency in speed control (v_{eff}) for the parking test	148
6.57	ANOVA analysis for the entrance angle (θ_s) for the parking test	149
6.58	ANOVA analysis for the exit angle (θ_e) for the parking test	150
6.59	Comparison of the deviation from the reference path related to the full population along the braking test (section 5)	153
6.60	Comparison of the deviation from the reference path between interfaces along the braking test (section 5)	154
6.61	Comparison of the deviation from the reference path between subjects along the braking test (section 5)	155
6.62	ANOVA analysis for the braking distance (e_b) for the braking test	157
6.63	ANOVA analysis for the efficiency in speed control (v_{eff}) for the braking test	158
6.64	Influence factors evaluation on the mean deviation (e_m) of the wheelchair along the straight part of the path following test	161
6.65	Influence factors evaluation on the mean deviation (e_m) of the wheelchair along the bumpy part of the path following test	162
6.66	Influence factors evaluation on the mean deviation (e_m) of the wheelchair along the curved part of the path following test	163
6.67	Influence factors evaluation on the mean deviation (e_m) of the wheelchair along parking test	164
6.68	Influence factors evaluation on the mean deviation (e_m) of the wheelchair along braking test	165
6.69	Interaction plot of the module of the mean deviation (e_m) of the wheelchair along the straight part of the path following test	167
6.70	Interaction plot of the module of the mean deviation (e_m) of the wheelchair along the bumpy part of the path following test	168

6.71	Interaction plot of the module of the mean deviation (e_m) of the wheelchair along the curved part of the path following test	169
6.72	Interaction plot of the module of the mean deviation (e_m) of the wheelchair along the parking test	170
6.73	Interaction plot of the module of the mean deviation (e_m) of the wheelchair along braking test	171
7.1	Robotics: a collaboration concept	176
7.2	Reality-Virtuality (RV) Continuum	178
7.3	The Human Machine Interface shown on the frontal monitor	179
7.4	Relation between the standard deviation in the marker localization versus the number of points associated to a marker	185
7.5	The scheme of the tests used in the Monte Carlo simulation	186
7.7	Scheme for the assessment of the minimum door clearance	189
7.8	Distributions of door clearance	190
7.9	Success rate in door passage, clearance versus σ_s	191
7.10	Test scenario related to the semi-autonomous navigation	193
7.11	Semi-autonomous navigation action sequence adopted for the repeatability analysis	194
7.12	Repeatability analysis results on semi-autonomous navigation	195

List of tables

5.1	Tobii Eye Tracker 4C technical specifications.	45
5.2	Comparison between Microsoft Kinect v2 and Intel RealSense D435.	50
5.3	Pros and cons of depth Kinect v2 and Intel RealSense D435.	52
5.4	Ziegler-Nichols Tuning Formula for Step Response Method.	54
6.1	Results of circuit metric	80
6.2	Results of comfort metric	83
6.3	Results of manoeuvring metric	84
6.4	Results of depth perception metric	88
6.5	Wheelchair Skills Test skills, in bold the points considered for the design of the experiment.	96
6.6	Evaluated features for each considered section of path.	105
6.7	Subjective features evaluated.	109
6.8	P-values from ANOVA analysis among the considered feature for the vehicle metrics. The considered factors are: subject, non-disabled vs. disables, and interface, joystick vs. ocular. S-H represents the interaction between subject and interface.	159
6.9	Classification of the influence factor	160
6.10	Subjective features results.	172
6.11	Workload results.	173
7.1	Initial conditions of the repeatability analysis.	194
7.2	Results of repeatability analysis.	194

Nomenclature

Acronyms / Abbreviations

ALS Amyotrophic Lateral Sclerosis

APF Arc Path Following

AR Augmented Reality

DC Direct Current

FoV Field of View

HCI Human Computer Interaction

HMI Human Machine Interaction

ICR Instantaneous Centre of Rotation

IR Infra-Red

MNDs MotorNeuron Diseases

MR Mixed Reality

NAZ Normalized At Zero

PBP Progressive Bulbar Palsy

PDF Probability Density Function

PLC Programmable Logic Controller

PLS Primary Lateral Sclerosis

PMA Progressive Muscular Atrophy

POI Point Of Interest

PoR Point of Regard

RMS Root Mean Square

RV Reality-Virtuality

SMA Spinal Muscular Atrophy

VOG Video OculoGraphy

VR Virtual Reality

WSP Wheelchair Skills Program

WSTP Wheelchair Skills Training Program

WST Wheelchair Skills Test

Chapter 1

Introduction

1.1 Motivation

Disability is an impairment that affects people at different levels and timing. It may be present from the birth or occur during life and it may involve different human function such as cognitive, intellectual, physical, sensory or a combination of these.

The work presented in this thesis aims to support people affected by some severe mobility problems like spinal cord injuries or degenerative diseases such as Amyotrophic Lateral Sclerosis (ALS) or muscular dystrophy that foresee a progressive loss of mobility starting from the peripheral arts. Of course, any severe motor disability is a condition that limits the capability of interacting with the environment, even the domestic one, caused by the loss of the control on our own mobility.

Due to the delicate health condition of the patients, it would be highly desirable to have interfaces that are the least tiring and invasive possible. The usage of common aids, like a power wheelchair, becomes very difficult and often even impossible. In this context, eye tracker technologies have become a promising tool as the control input for any kind of user. The eye is one of the muscles less affected by the above-mentioned pathologies or it is involved only in the last part of the diseases (ALS). Due to this reason, the eye can have a fundamental role in the daily life of the patients if it were able to interface with the outside world.

This work presents RoboEYE, a power wheelchair designed to enable the user to move easily and autonomously inside his home. The research work here presented aims to develop a prototype of the eye-controlled wheelchair including innovative control strategies through mixed reality tool. A novel and intuitive control system was designed to achieve such goal, in which a non-invasive eye tracker, a monitor, and a 3D camera represent some of the core elements. RoboEYE integrates, on a standard power wheelchair, functionalities from

mobile robotics field, with the main benefit of providing to the user two driving options and comfortable navigation.

The first part of the work involves the development of an intuitive, and direct driving modality foreseeing the continuous control of the frontal and angular velocities of the wheelchair by gazing at different areas of the monitor. The design of this novel paradigm of Human-Computer Interaction (HCI) includes a Virtual Reality (VR) environment as well as the information gathered by an eye tracker. A virtual reality platform based on a game engine has been chosen for the HMI evaluation, and optimization of a so-called “natural gaze-based wheelchair driving”. The designs of the control structure and driving interfaces were tuned thanks to the testing of some volunteers, habitual users of standard power wheelchairs.

The second, semi-autonomous, enables the navigation toward a selected point in the environment by just pointing and activating the wished destination while the system autonomously plans and follows the trajectory that brings the wheelchair there. The driving modalities, especially the semi-autonomous one, were modelled and qualified to verify their efficiency, reliability, and safety for domestic usage. Regarding the direct drive interaction modalities, the interface requires a continuous control by the user resulting very tiring for the patients because the user has to keep all the time the attention on the monitor.

Moreover, houses are usually characterized by small spaces and narrow passages. Unfortunately, not all disabled people have the possibility to adapt their house to the required particular necessities. For these reasons, the exploitation of a robotic path planning control of power wheelchair would be of great benefit to relief the patient. Indeed, in this manner, he/she does not have to keep attention on the HMI. An assisted guide could be very useful and comfortable especially for the movement in narrow spaces. The solution presented in this thesis aims to create a novel technology to support the control of a power wheelchair during difficult manoeuvres. Furthermore, using an autonomous wheelchair, the patient does not need to keep the attention on the monitor, resulting in less tiring. This part of the work is an integration of the previous gaze-based HMI, used for the direct drive technique, with a robotic framework able to plan and control a part of the route according to a normal HMI based on AR. This novel technology aims to guarantee the freedom of movement and at the same time the comfort of the assisted guide.

Fig. 1.1 presents a schematic representation of the system. In the left part a commercial device (power wheelchair) where the proposed technology is integrated. In the central part, the module developed, and added on the wheelchair, represented by a Windows PC that reads the navigation camera, acquires the information about the gaze position and shows the HMI on the monitor. The surrounding environment is shown in the right part, where some markers are used to define all the point of interest for the user.

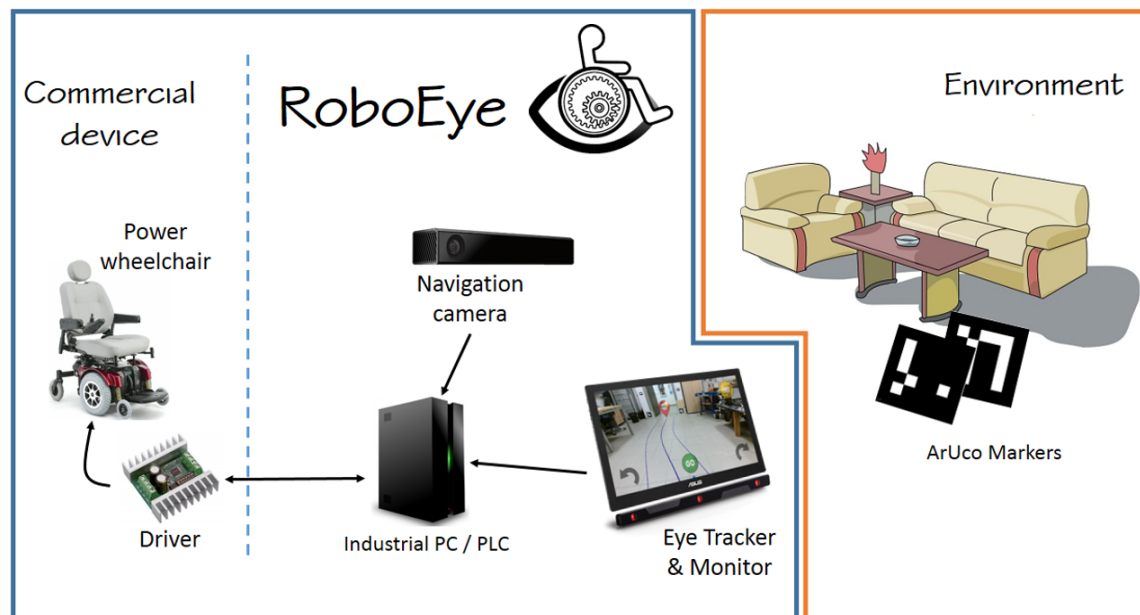


Fig. 1.1 Conceptual model of the project

1.2 Related efforts

The research activity related to this thesis involves the development of an eye gaze controlled wheelchair including the design of an innovative human-machine interface (HMI). The system was designed in order to enhance the mobility of the user giving him/her the possibility to control the wheelchair through both manual and autonomous navigation via gaze-based technique. As a fundamental concept, the development of the wheelchair prototype, as well as some HMIs and VR environment for the test, were carried out together with some test phases involving some volunteers. In this way, the HMI was optimized on a real patient by considering the feedback from the users.

The work started with the study of some commercial eye tracker, accuracy and precision were characterized to determine the best device. In this sense, two innovative HMI strategies for eye-controlled wheelchairs in Virtual Reality was designed and evaluated inside a VR simulation engine. Both the HMIs and the VR-based simulation engine was developed using one of the current states of the art game engine, UNITY. The performance evaluation of the two HMIs was carried considering different metrics, related to the vehicle management and comfort of the passengers, but also to the cognitive and emotive response of the subject to different stimuli. A pool of subjects tested the two HMIs.

The activities continued with the realization of the first wheelchair prototype from a mechanical and electrical point of view. An old wheelchair was modified adding devices such

as PLC, Pc and some other devices. After that, the developer focuses on the development of the software able to interact with the user and drive the wheelchair in the proper way. With regard to the navigation of the wheelchair, during this phase was integrated on the vehicle the best HMI previously evaluated, realizing the direct driving mode. This is the first driving modality, with which the user acts directly on the wheels by selecting the forward and the rotational speed through gaze position on the screen. Moreover, on this prototype was developed and tested the "so-called" semi-autonomous driving strategy. With semi-autonomous navigation, the wheelchair is able to reach a selected target without any other input from the user. All this technology was moved on a new prototype of a wheelchair. This part of the project involved the integration of a hardware and software module on a commercial wheelchair.

The last phases of the work involved a test campaign in order to obtain an evaluation of the prototype from an objective and a subjective point of view.

1.3 Thesis summary

The structure of the thesis is the following:

Chapter 2: The second chapter is focused on the requirements that the technology here presented aims to solve. It provides an overview of the neuro-degenerative diseases focusing, in particular, on the Amyotrophic Lateral Sclerosis (ALS). It describes the diffusion of ALS, current and predicted, of the disease as well as its causes and symptoms.

Chapter 3: The third chapter is focused on the state of the art related to the technology involved in the project: eye tracking, robotic power wheelchair, and mixed reality. Different works are presented based on eye-tracking technology that involves the usage of several devices in order to create applications as effective human-machine interfaces. Furthermore, the chapter gives an overview of the eye driven wheelchair for real application but also for simulated environments to achieve a safe training tool.

Chapter 4: The fourth chapter describes the eye-tracking technology focusing, among other things, on its field of application and performances. In addition, are reported the details about the main parameters that influence the performances of the technology. Furthermore, the chapter describes the experimental campaign, carried out on a commercial eye tracker, to perform an uncertainty analysis as well as the repeatability and accuracy obtained.

Chapter 5: The fifth chapter starts reporting an overview of the commercial wheelchairs, some mean feature related to typical mechanical structure characterizing a mobile robot. Then, it includes a brief description of the AGV, a particular mobile robot devoted to performing transfers of materials inside industrial environments. The chapter continues with the kinematic model of a differential drive vehicle that is the one characterizing the wheelchair used in the project. The developed prototype is then described from a mechanical point of view focusing on the devices used, on the commercial wheelchair used and on the integrations performed on it. Furthermore, it is reported the procedure adopted for the calibration of the wheelchair kinematic parameters as well as the gains of the feedback control system. The last part of the chapter described the software developed on the eye-controlled wheelchair focusing on the micro-services architecture adopted.

Chapter 6: With the sixth chapter starts the description of the two driving modalities designed for the gaze control of the wheelchair. This chapter reports the first one, the direct drive modality, also called "manual navigation", with which the user can manoeuvre directly the wheelchair by selecting the desired velocities that are proportional to the gaze position on the screen. This part reports the details of the interaction design inside a virtual reality simulated environment as well as on the real prototype of eye-controlled wheelchair. This chapter reports, therefore, the test plan planned for the assessment of the driving performance through a test campaign during which was evaluated the gaze-based interface. This test plan includes the metrics considered but also the testing protocol and the feature evaluated. The final part of the chapter reports the results of the tests on both the simulated and the real environment as well as a brief final discussion.

Chapter 7: The seventh chapter is devoted to the description of the second driving modality, the semi-autonomous navigation. This part starts with a brief description of assistive robotics followed by the concept of mixed reality. After that, the semi-autonomous driving technique is reported focusing on the localization process of the vehicle. Also in this chapter are reported the test procedure based on a Monte Carlo simulation but also on a real test bed. As in the previous case, the chapter is concluded with a brief discussion of the results obtained.

Chapter 8: The eighth chapter is devoted to the final conclusion of the project and to hypnotize possible future development.

Chapter 2

Requirements

Nowadays, a large number of people is affected by mobility problems on different levels. Rheumatic, muscular and joint pains are probably the most common health problems affecting especially elderly people that reduce mobility. However, specific medicines allow persons affected by these diseases to have a regular life. Others most serious pathologies have a stronger impact on the human body. Neuro-degenerative diseases such as Alzheimer, Amyotrophic Lateral Sclerosis (ALS), Parkinson's or spinal muscular atrophy are probably the worst. They involve many of the body's activities like balance, movement, talking, breathing and hearth functions. The causes for these could be different: genetic attitude, medical condition (like alcoholism, tumor, or stroke), toxins, chemicals or also viruses. Sometimes the causes are not known.

2.1 Amyotrophic Lateral Sclerosis (ALS)

Amyotrophic lateral sclerosis (ALS) is a rare neurological disease involving motoneurons that are responsible for the control of voluntary muscle movement such as chewing, walking, and talking. It causes a gradual degradation and then the death of the motoneurons.

Motoneurons are nerve cells used to connect the brain with the voluntary muscles, the glands, a part of the heart and the smooth muscles. They extend from the brain to the spinal cord and to the muscles. The messages start from the brain, where are located the upper motoneurons, and arrive to the motoneurons of the spinal cord and to the motor nuclei of the brain, that are called lower motoneurons. Subsequently, the information goes from the spinal cord and from the motor nuclei to a specific muscle or to a group of muscles. If the motoneurons are damaged the execution of a certain activity is compromised; the movement becomes increasingly difficult and the muscle mass decreases.

ALS is the most famous and serious motoneuron disease but it is not the only ones. Pathologies like the primary lateral sclerosis (PLS), the progressive muscular atrophy (PMA), the progressive bulbar palsy (PBP), the pseudobulbar palsy or the spinal muscular atrophy (SMA) are included in the group of the motoneuron diseases (MNDs). Motoneuron diseases affect specifically the good health and the good functioning of the motoneurons, causing neurodegenerative conditions. Actually, the causes of the motoneurons diseases are unknown as well as a cure to halt or reverse the progression of the pathologies. In this sense, the research has a fundamental role in order to improve scientific knowledge and identify new therapeutic approaches, Clinic [19].

ALS affects both the upper and the lower motoneurons, preventing the sending of messages from the brain that is unable to control the muscles. Without any type of input, the muscles weaken, start to degrade and then waste away. This last process is also called atrophy. ALS, as all the motoneuron diseases have a progressive deterioration of the health condition. It means that the symptoms get worse over time

Usually, the first symptoms of ALS include weakness or stiffness. Progressively, ALS involves all the muscles under voluntary control. Therefore, the patients lose both their strength and the ability to speak, eat, move and at the end even breathe.

Most of the patient affected by SLA die due to respiratory failure, usually within a time ranging from 3 to 5 years from when the first symptoms appear. However, about 10 percent of patients with ALS survive for 10 or more years.

2.1.1 Who gets ALS?

Although ALS is relatively rare, the number of people affected by this disease are increasing during the years. As mentioned previously, ALS is a common neuromuscular disease worldwide affecting people of all races and ethnic backgrounds. Arthur et al. [5] focus on the estimation of the individuals suffering from ALS. During the period between 2015 and 2040, the total number of people affected by ALS is expected to grow from 80,162 to 105,693 with an increase of 31.85%. Fig. 2.1 shows the geographical distribution of this increase in case numbers. However, it is necessary to consider also the worldwide population increase that is estimated from 1.89 to 2.04 billion. Under this hypothesis, the projected number of individuals with ALS will grow of 22.15%.

Considering other sources, in 2016 the Centers for Disease Control and Prevention estimated the number of the patients affected by ALS between 14,000 - 15,000 in America.

The most potential risk factors related to the ALS include:

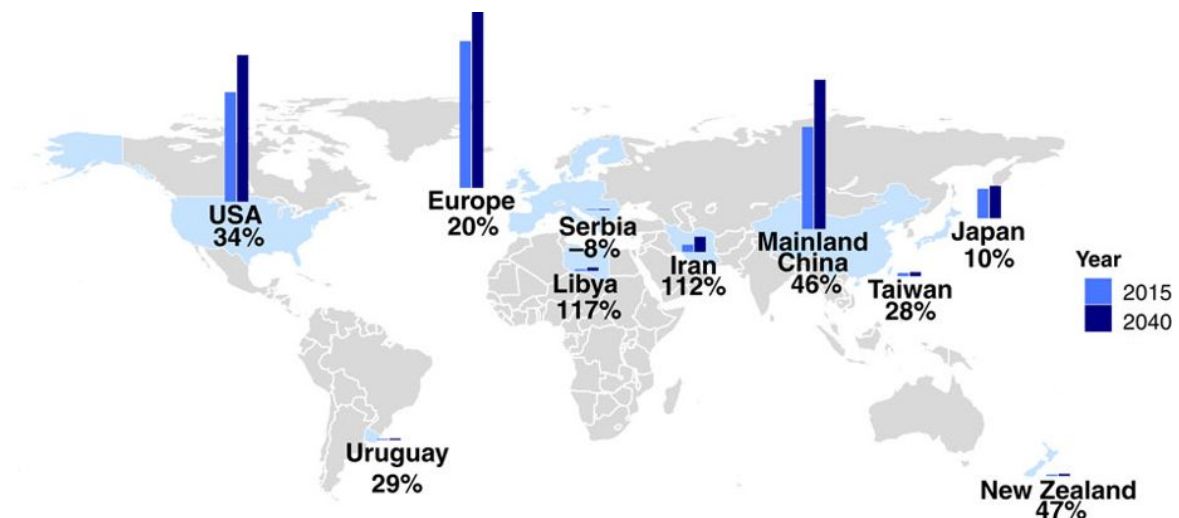


Fig. 2.1 Worldwide ALS projection from 2015 to 2040, Arthur et al. [5]

Age: the symptoms most occurs peoples with age that range from 55 to 75 years although the disease can strike at any age;

Gender: Currently, men develop ALS slightly more likely than women. Nevertheless, as we age the difference between men and women disappears;

Race and ethnicity: Caucasians and non-Hispanics people are most likely to develop the disease.

Some studies suggest that military veterans develop ALS more likely, of about 1.5 to 2 times, with respect to civil people. The reasons for this fact are still unclear. However possible risk factors for veterans include exposure to lead, pesticides, and other environmental toxins. In particular, the U.S. Department of Veterans Affairs recognizes the ALS as a service-connected disease.

The majority of ALS cases (90 percent or more) are considered sporadic. This means the disease seems to occur randomly without clear association with both risk factors and family history of the disease. Even though relatives of patients affected by sporadic ALS present increased risk for the disease, the overall risk is very low and most of them will not develop ALS.

On the other hand, a percentage of people ranging from 5 and 10 percent of all the people affected by ALS are familiar. This means that the patient inherits the disease from members of the family. Usually, this particular form of ALS requires only one parent to carry the gene responsible for the disease. One of the causes of familial ALS is the mutation in more than a dozen genes. A defect in a gene known as “chromosome 9 open reading frame

72” or C9ORF72 causes about 25 and 40 percent of all familial cases of ALS as well as a small percentage of sporadic cases. Interestingly, the same mutation can be associated with atrophy of frontal-temporal lobes of the brain that cause frontal-temporal lobe dementia. Moreover, some patients carrying this mutation may highlight signs of both motor neuron and dementia symptoms (ALS-FTD). Finally, another 12 to 20 percent of familial cases result from mutations in the gene that provides instructions for the production of the enzyme copper-zinc superoxide dismutase 1 (SOD1).

2.1.2 Symptoms

At the beginning of the disease, the onset can be very subtle. Indeed, the symptoms are ignored until these symptoms develop into more obvious weakness or atrophy that may cause a physician to suspect ALS.

Some early symptoms of ALS include:

- Fasciculations or muscle twitches which are small, local, involuntary muscle contractions and relaxations of arms, legs, shoulders or tongue;
- Muscle cramps;
- Tight and stiff muscles (spasticity);
- Muscle weakness affecting arms, legs, neck or diaphragm;
- Slurred and nasal speech;
- Difficulty in chewing or swallowing;

For many individuals, the first sign of ALS appears in the hand or arm. They have difficulty with simple tasks such as buttoning a shirt, writing or turning a key in a lock. In other cases, the symptoms start affecting one of the legs. The patients experience awkwardness when walking or running or they notice that they trip or stumble more often.

If the symptoms begin in the arms or legs, it is referred to as “limb onset” ALS. In other cases, individuals first notice speech or swallowing problems, termed “bulbar onset” ALS.

The muscle weakness and atrophy spread to other parts of the body during the disease progression independently of where the symptoms appear first. The subjects may develop problems with moving, swallowing (dysphagia), speaking or forming words (dysarthria) as well as breathing (dyspnea).

Generally, the sequence of emerging symptoms, as well as the progression rate of the disease, changes from subject to subject. However, eventually, the patients will not be able to stand or walk, get in or out of bed on their own as well as use their hands and arms.

Individuals affected by ALS experience also difficulty swallowing and chewing food. This fact makes it hard to eat normally and increases the risk of choking. Moreover, they also burn calories at a faster rate than most healthy people, losing in this way their weight rapidly becoming malnourished.

However, the people with ALS usually maintain the ability to perform higher mental process like reasoning, remembering, understanding and problem-solving. In other words, they are aware of their progressive loss of function and may suffer from anxiety and depression.

A small percentage of individuals may have problems with language and decision making. There is growing evidence that some of them may develop a form of dementia over time.

Subject affected by ALS present difficulties breathing while the muscle weakness of the respiratory system increases. At the end, they lose also the capability to breathe on their own. They must depend on a mechanical ventilator. Moreover, affected individuals face also an increasing risk of pneumonia during the final part of the disease. Finally, besides muscle cramps causing discomfort, some ALS patients may develop painful neuropathy, nerve disease or damage.

Chapter 3

State of art

Collaborative Assistive Robotics is the discipline that studies the support of automatic machines to people in the execution of many different tasks involving the specific design of human-machine interaction HMI. Applications of this kind range from industrial application to medicine. Power wheelchairs represent a good example of an assistive tool that could benefit from the technological transfer from the industrial mobile robotic field. Indeed, the wheelchair has a strong impact on the quality of life of patients affected by mobility limitations.

The support and the assistance of patients suffering from mobility problems such as spinal cord injuries or degenerative diseases as ALS (Amyotrophic Lateral Sclerosis), is a very relevant research branch in the field of Assistive Robotics. In addition to the physical deficit, these kinds of pathologies are often cause of psychological distress. Of course, the capability of moving autonomously plays, therefore, an important role for their quality of daily life. In order to alleviate the loss of mobility and the capability of interacting with the surrounding world, the market offers solutions based on motorized wheelchairs and combined with a suitable HMI. In this context, an assistive technology should be designed to be as much comfortable as possible and not invasive in order to improve the autonomy of the patients. For this reason, a robotic wheelchair can be of great benefits restoring human mobility. Common techniques to control a wheelchair are based on physical interaction between the user and a device such as joysticks, keyboards, breath or voice [3]. Others innovative approaches involve the usage Brain Computer Interface (BCI), with the help of Electroencephalogram (EEG) signal, to control a power wheelchair, [49, 28].

Recently, a very promising yet challenging interface is the adoption of eye tracking technologies. This technique provides a measurement of the gazed point, or area, on a monitor. More than the medical and commercial application [8, 30], this technology has improved to a maturity suitable for its application as an effective human-machine interface

(HMI). Effectively, eye movement is one of the fastest human movement, although are mainly conceived for exploration, less for control [35]. This kind of interaction paradigm is indeed very useful since it can help to enhance user mobility, consisting of valuable support also until the last and most critical phases of the disease. Therefore, as explained in the following chapters, pathologies like ALS affect people starting from the peripheral organs, moving progressively to the rest of the body. The last part involved are the eye muscles. On top of this, the Human Machine Interface (HMI) based on eye tracking can play a fundamental role in actual usability and manoeuvrability of a wheelchair. As the main advantage, the usage of eyes as input [75] enables those users that, because of disease or physiological state, cannot use standard interfaces such as a joystick or a keyboard, to interact with other people or the environment in a quite efficient way. The main drawback that affects such technology is represented by the sensibility to various factors like the light condition, the colour of the iris, motion of the head [40, 12]. Holmqvist et al. [43], Cerrolaza et al. [15], Fornaser et al. [34] analysed those elements and provided a more detailed characterization of the measurement process together with a method for the assessment and compensation [27, 80] of the uncertainty in eye tracking. This last element was considered in the proposed solution, and it resulted in a key element for the smooth control of the wheelchair by means of a non-invasive, commercial, eye tracker.

Existing solutions for gaze-based interaction are quite invasive due to the necessity to often wear external devices such as glasses [44] or electrodes for Electrooculography [16]. Others are based on less invasive solutions as for example Video Oculography (VOG). However, due to patient health conditions, it would be highly desirable to develop HMIs that are least tiring and invasive as possible. Moreover, the user needs a certain amount of time to become familiar with it [20], the designer is often required to develop customized HMIs [48] and clinicians need assistance in performing standardized wheelchair driving assessments [54].

Unfortunately, VOG, although being minimally invasive, achieves lower performances in terms of eye gaze estimation accuracy compared to more traditional interaction paradigms. This is due to the different elements and environmental conditions that influence the system performances and cannot be fully kept under control. Among them, illumination, relative motion between the user and the instrument (rotation and translation), objects in front of the eyes, physiology of the different users [35]. Another problem underlined from many authors is that the performances provided by the manufacturers seem to be neither repeatable nor representative as they are obtained in ideal conditions [18].

From the considerations above it is evident the need to have an instrument able to train the user, let the designer develop optimized HMIs taking into account also the instrument

accuracy, and eventually assist clinicians in performing standardized wheelchair driving assessments. Buxbaum et al. [13] used VR to assess lateralized spatial attention and neglect for users hit by right hemisphere strokes, adopting a complex hardware simulator based on a treadmill. In [48] a virtual reality platform based on a game engine (Unreal Engine™) has been chosen for training, HMI evaluation, and optimization of a so-called “natural gaze-based wheelchair driving”. The first part of the work here presented proposes a VR-based simulation engine to develop an innovative HMI for VOG that uses, for the first time, the information on the eye tracker accuracy to achieve better performances in usability, comfort during navigation and fault tolerance to noise induced by the intrinsically low accuracy of the interface, as previously described. With respect to [13] this research using one of the current states of the art game engine, Unity 3D, to develop a VR tool, as it is able to provide immersive and high-quality 3D graphics in a much simpler and reconfigurable platform. The work of [48] is quite interesting and very close to the goals and the general approach of this thesis.

Compared to them one of the contributions of this research consists of the inclusion in the model of the eye tracker accuracy. Different more “natural” HMI interfaces were developed by using used a more complete set of metrics to assess the user performances.

3.1 Eye driven wheelchairs

With reference to the availability of systems that exploit the gaze information to control and drive a wheelchair or more in general for mobility enhancement in patients affected by severe motor disabilities, the literature presents some works carried out in the past years that have been considered as a reference and starting point for our application. The first attempts in this area can be found in [52], where the authors propose a model to drive the wheelchair using, as a driver, the information gathered by a glass-mounted camera that takes a close look on the users’ eye. A rather simple yet effective method to control the wheelchair by interpreting the position of the eye was proposed more recently by Gajwani and Chhabria [37]. The method exploits the positioning of the eye and the blinking information to extract basic commands, as moving ahead, left and right. Such approach, like many others based on different technologies [63, 57], foresaw the usage of wearable technology, the only available in the past due to the incapability of dealing with head motion, both systems require a head-mounted device for tracking. However, these can provide only a limited number of commands, may turn out to be fatiguing [11], and therefore not suitable in the case of long usage.

Electrooculography [63] has also been recently used as a tool to understand the users' intentions and control the wheelchair accordingly. Besides requiring the use of a wearable device, electrooculography is an efficient diagnosis tool, but also, in this case, it may turn out to be fatiguing, and the number of commands that can be configured is somehow limited.

It is worth noting that wearing additional equipment may result uncomfortable for the user and therefore it would be highly desirable to reduce the invasiveness of the technology. To this aim, other researches in this area have proven that the task can also be solved adopting external devices.

As for non-wearable (and less invasive) technology, [65] proposed a solution based on a webcam and the analysis of the gaze direction. The solution is interesting but both the camera position (almost in front of the face of the user) and the lack of a video interface could lead to poor management of the system and complex driving practice. Wastlund et al. [76] used a rather expensive eye-tracking system, definitely more promising and probably efficient than the previous. However, an eye-tracking system as the one used for their experiments is rather expensive, considerably reducing the affordability of a complete system especially by a private user.

As for the usage of these systems, [73] proved as a matter of fact that drive-by mean of eyes achieves better performances than more standard control techniques and interfaces. So as [55], in which the interaction with the eye tracker was included in a simulated environment, achieving a safer training environment than a real space, but also useful for the optimization of the design of HMIs and navigation modalities.

The main contribution of the here presented work to this area comes from the inclusion of the uncertainty information on the gazed position in the human-machine interaction and thus the creation of a smart HMI that is capable of adapting with respect to such parameter. Moreover, the problems of fatigue and safety during the drive were considered, proposing as a solution a semi-autonomous navigation modality that enables the system to navigate safely through narrow passages. The development of the eye-controlled wheelchair prototype involved the usage of an external device, similarly to previous studies [76], but adopting an affordable system that can be easily configured and customized to fit the requirements of the specific application context. Last but not least, the design of the system considered the affordability of the technology, its capability in being configured, customized, and then transferred to the end user.

Chapter 4

Eye Tracking Technology and uncertainty analysis

Techniques for tracking the eyes took place for several decades for different applications that range from military to education, entertainment, and clinics, [29]. The existing systems are in general of two categories: precise but intrusive or comfortable but less accurate.

The eye tracker is an instrument that allows determining the point where the user is looking at. This kind of technology has two principal fields of application:

1. Analysis of visual scanning patterns;
2. Human Machine Interaction (HMI).

Since it is commonly agreed that the point or region a person is looking at is the point where that person is focusing his attention, except in some cases with very simple tasks as stated by Rayner [66], knowing the visual scanning pattern it's a great way to study human cognitive processes. The application may be multiple starting from market to web searches. Moreover, the study of visual scanning path may be used in medicine to diagnose mood, perception, learning and attention disorders. In the field of human-machine interface, the use of the eye as input may have multiple advantages. The first and more evident reason to use the eye as input is to allow users that are not able to use other input, such as joystick and keyboard, due to some diseases that partially or completely limit their movement. Anyway, the eye tracker may be useful to any kind of user. Let's think of a person that want to select an icon or a link, he will first look at that point and then move the mouse in that position. That makes the eye a faster way to communicate, a better explanation can be found in [39]. Of course, this kind of technology needs to be improved before. Indeed, all the systems available nowadays has some drawbacks. We target the use of eye trackers for assistive



Fig. 4.1 Eye Tracker Technology

robotics in order to allow severely impaired users moving autonomously. So, our interest is focused more on the field of HMI.

There are lots of different technology implemented in order to track the eye. Through all this technology it is possible at first to distinguish between intrusive and non-intrusive one. In the first category falls all that kind of devices that are in some way fixed with the user's head. Some examples are contact lenses, electrodes, and head-mounted devices. This kind of technology has two main advantages: accuracy and robustness with respect to head movement. The main drawback of intrusive devices is that may be tedious for the user. The alternative is the non-intrusive, or remote, eye tracker. This kind of devices is mostly based on computer vision techniques. They consist of one or more cameras to capture the eye's image, [4, 74]. Those kinds of system are more comfortable and can be used for long periods. This makes them suitable to be used as HMI. A better description and list of some of these techniques can be found in [2]. Due to the scope of this work we are more interested in remote eye trackers. A state of the art that focuses on REGT(remote eye gaze trackers) techniques is presented in [60].

The most popular kind of remote eye trackers uses features detection to track the eye. Eye's characteristic that can be tracked is, e.g., the limbus and the pupil. The problem of the limbus is that it's covered by the eyelids. On the other hand, the problem of the pupil is the weaker contrast with the iris, that makes it harder to detect it in the image. This will obviously depend also on the specific user characteristics, such as shape and size of the eye and also the color, [41]. Anyway, a solution commonly adopted is the usage of infrared light. Indeed, IR light enhances the above-mentioned contrast. Since IR is not visible it won't

distract the user. Due to this property, this is one of the most used solutions, and in particular, is the one used from the system considered in this work.

The presence of a lot of different techniques and implementation is due to the fact that none of them has been claimed to be the best with respect to all the others. Moreover, not a lot of work has been done in finding a common way to estimate the performances so that the various eye tracker system and techniques can be easily compared. This issue has been discussed by Holmqvist et al. [43]. In particular, they determine three principle characteristics in order to determine the performances of eye tracking devices:

- Accuracy: is the bias (systematic effect), i.e. the difference between the estimated PoR (mean of the collected data) and the point the user is actually looking at;
- Precision: that is the repeatability of the estimate. It is usually estimated as the RMS or as the standard deviation of the available data;
- Robustness: capability to work with different users. Usually, eye trackers do not work with everybody or anyway do not have the same performances changing users. This may be due to different characteristics of the user, both cognitive (e.g. the ability to follow a task) and physics (e.g. the physiology of the eye);

Another problem underlined from many authors is that the values provided by the manufacturers seem not to be repeatable. This is mainly due to the fact that the values obtained by the manufacturers are obtained in an ideal situation. As demonstrated by Clemotte et al. [18] the use in normal condition bring to values of accuracy and precision quite different from the ones given by the manufacturers. Knowing the real accuracy and precision allow better design of software or programs that use eyes as input. For example, it is possible to determine the optimized size of buttons. Clemotte et al. [18] claimed to use precision as the minimum size of the target.

In addition, to overcome the problem of the difference between real and ideal condition it was estimated the influence on the performance of some parameters. In particular, it was founded a relationship between those parameters and the covariance so that the information given by the eye tracker will be a function of the operating conditions. The parameter of influence we have considered are the following:

- Illumination;
- Relative motion between the user and the instrument (rotation and translation);
- Objects in front of the eyes;

- Different user;

Regarding this problem in the literature, many papers have tried to identify the influencing parameters and to find a way to decrease their effect on the results. It is commonly considered that two of the main problem of the remote eye tracking systems, as we have hypnotized, are illumination change and head movement.

Illumination: The influence of light largely depends on the usage of the eye tracker. For example, if it is used as HMI on a computer it is possible to place that computer in a spot with optimal illumination. For example, far from windows (illumination change during the day). Hansen and Pece [42] propose a system that uses image statistic instead of features detection. As described by the authors “the underlying idea is that a large image gradient is likely to arise from a boundary between object and background”. Indeed, they obtain a system that is robust with respect to light changes. They use an algorithm based on particle filters and EM Contour, the main drawback is that head movement must be very limited.

Relative motion between the user and the instrument: The problem of head movements will largely depend on the user characteristics: several disabled users may not be able to move the head or may not be able to keep it fixed depending on the diseases. Also, a healthy user will slightly move the head in most activities. Usually, to test the eye tracker it is used a chin rest or a bite bar that eliminate that kind of movements. The results obtained will be largely different from the ones achievable in real operating conditions. In literature multiple solutions to the head movement problem can be found: White et al. [77] propose to include a second reference light source to distinguish between head and eye rotation. They proved the validity of the solution for large lateral displacement, but only with simulated data. Cerrolaza et al. [15] instead consider the problem of head displacements in the direction perpendicular to the screen. In particular, they proposed two methods. The first one is to include information about the different positions in the calibration procedure in order to improve the tolerance to this kind of displacement. A noticeable drawback for this method is the increase of the calibration time. For this kind of system, a too long calibration time may increase the stress of the user and the distraction. The second method is based on the hypothesis that the PoR estimation error mainly depends on the system and not on the different user. Hence the error can be modelled for a particular configuration and used to compensate the estimation. Both methods seem to improve the robustness to head movement. Guestrin and Eizenman [40] stated that with more than one light source, as in the case of the system used in this research, it is possible to tolerate certain movement of the head. That is from 2 to 4 cm depending on the direction of the displacement. That requires a multiple point calibration. In addition,

they show that the same results can be obtained with a single point calibration using both multiple light sources and multiple cameras. The idea of using more than one camera to change the behaviour of the eye tracking system is exploited in more than one paper. For example, in [68] multiple cameras and multiple lights are used to eliminate the usage of the user dependent parameters. The estimate is done using 3D computer vision technique and allows to completely eliminate the calibration phase. On the other hand, in [12] the new camera is used in order to allow free head movement in a volume with 40 cm of diameter. This may result very interesting in the case of a user in front of a computer screen since the natural movement won't be much bigger than that.

Anyway, what this research is actually interested in is not to change how the eye tracker works but to determine:

1. the accuracy estimated in 2D LCD plane in relation to the influencing factors;
2. to map the influencing factor on eye tracker accuracy in real time.

The first goal is something similar to what Nyström et al. [61] reported. Here the authors consider calibration method and eye physiology as influencing parameters and study their effect on data quality. The tests are done with a tower mounted video-based eye tracker. In particular, they study three different calibration procedures to verify which one works better. The difference through the three is the way to determine if the calibration has to be considered good or discard. The three kinds are operator controlled, participant controlled and automatic calibration. From the experimental data, it seems that participant controlled calibration is the one that gives better results, followed by an operator controlled one. Actually, this work is not interested in changing the calibration procedure, anyway in the system used to decide whether the calibration is good enough there is a testing phase. During the test, both the user and the operator can see if the system is capturing the eye position in the right way. In addition, they develop a series of test to verify how accuracy, precision, and the number of valid fixation samples vary changing some influences parameters that are the position on the screen, time, eye physiology and visual aids. In the following the results they obtain:

Position on the screen:

- Accuracy (systematic effect): better in the top left part of the screen;
- Precision (repeatability): worst for targets located off-centre or father down on the screen;
- Valid fixation samples: again worst for targets located off-centre or father down on the screen;

This can be explained considering that off centre positions mean a higher visual angle that makes it harder to distinguish the eye, e.g. the pupil may be covered by eyelashes.

Time: For all the participant were taken to set of data one soon after the calibration, the other after a certain time making the user move from the calibration position. Data quality get worst with time, all the second sets have worst accuracy (systematic effect), precision (repeatability) and less valid samples. This may be due to the fact that the person has moved, even if with the chin rest this should not be a problem. The problem of moving from the calibration position will be discussed later also in this work.

Eye physiology:

- Accuracy (systematic effect): Eyelashes pointing downwards, and smaller pupil has a negative effect on accuracy. There is no significative difference between right and left eye, while the dominant eye gives better accuracy. Also, the color of the eye has no effect;
- Precision (repeatability): worst for blue eyes. This is mainly due to the fact that blue eyes have a lower contrast between iris and pupil. The right eye, no matter which eye is the dominant one, seems to be less precise. Eyelashes have no influence;
- Valid fixation samples: Nor eye color nor eyelashes direction change the ability to acquire valid data. The right eye, no matter which eye is the dominant one, produce slightly more valid samples;

Visual aids:

- Accuracy (systematic effect): worst using contact lenses, while glasses have not such a great effect;
- Precision (repeatability): worst using glasses, while contact lenses improve precision also with respect to no usage of visual aids;
- Valid fixation samples: worst using contact lenses, while glasses have not such a great effect;

In this article, the authors provide “the first comprehensive set of data showing how the calibration method, the operator, participants’ eye physiology, and visual aids affect the quality of data”. Anyway, they do not exclude that different eye trackers may provide different results. A step forward can be done applying this kind of test to a wider set of eye

trackers. Note that here the authors determine the scalar uncertainty, while in this work is calculated the 2D covariance ellipse.

Based on the work of Holmqvist et al. [43], it has been developed a software 'Accuracy Test Tool', for precision and accuracy measure by Tobii Technology. In particular, a description of the software and test specification can be found in [46]. As said by the authors themselves: "This document presents a suitable methodology to test and compare the performance of different remote eye tracking systems. It outlines a series of extensive tests that identify and control for external parameters that illustrate the accuracy and the precision of the system under usage scenarios (e.g. subjects' position in the track box, environmental light levels, and large gaze angles)". In this paper, they do not take into account the influence parameters that depend on user characteristics (eye physiology, glasses...). Indeed, they consider only data acquired by "suitable eye tracking individuals". This means that people with glasses, lenses or anyhow poor performances are excluded. The different scenarios they consider are:

- Ideal conditions: best scenario, unattainable in real working conditions;
- Large gaze angles: stimuli placed far from the center;
- Varying illumination: variation of illumination level. In particular, they reproduce four conditions: dark, normal illumination, one target light over the work area, multiple target light. They conduct also a test varying the background illumination;
- Head positions: the eye tracker is moved of 5 cm in one direction (X, Y or Z) for the test. The head always remain on the chin rest;

It has to be noticed that in all this test the user's head lay on a chin rest. This is not what happened in a real situation where the user may move the head. Another experiment based on this idea was carried out by Clemotte et al. [18]. The purpose of the work is to "identify the precision and accuracy of the Tobii x2-30 with non-disabled people under non-ideal conditions (without any chin rest)". They found out that accuracy (systematic effect) and precision (repeatability) values obtained in these conditions highly differ from the ones reported on the data sheets. The accuracy (systematic effect) change from 0.4 to 2.46 degrees, while the precision (repeatability) grows from 0.2 to 1.91 degrees.

The authors stated that the values they found are "better descriptor of the device's performance since were calculated in real conditions". Those values are more as an input to command a wheelchair. This will let the disabled user move freely in the environment. Some prototype similar to what this work points to obtain has already been developed.

An example is the prototype presented in [62]. Here an eye tracker system connected with Arduino is used to command an electronic hand unit. The electronic hand, essentially made of servomotors, is the one that controls the wheelchair's joystick. This solution is obtained utilizing "the existing hardware that the UK government provides for those with MND: a motorized wheelchair and an eye gaze computer". The main advantage of this solution is that it has been developed by final users, Patrick Joyce and Steve Evans. According to the developers eyedrivomatic now works well and is:

- Easy to use;
- Safe;
- Expandable - the system is able to control other external devices according to the needs of the user;
- Totally open, both open hardware and open source software;
- Capable of being built at home - by an unskilled person;
- Soon to be a manufactured product as well;

The main drawback is the interface that does not allow to see the environment, hence it may become difficult to see obstacles, and use a command such as forward, backward, turn left and right. Even though the use of this kind of command has been exploited in a lot of work, see also [18], we would like to let the user decide where he wants to go by only looking at that specific point.

Another interesting solution can be seen in [53]. Here "the wheelchair user's eye movements are monitored by a £20 eye-tracking device and translated into instructions that are fed through to the wheelchair's joystick control pad. The user "drives" the wheelchair by blinking". This prototype, developed at the London Imperial College, has the main advantage to go where the user is looking in the environment. This will let more freedom to the user and the chance to move in whatever environment. The main drawback is that nowadays it still remains a clunky prototype.

Another possible solution to the issue of how to control the wheelchair may be to specify the final point where the user wants to arrive. Puanhvuan et al. [64] present a system that is able to do that. Their system works both with autonomous and direct control. For the direct control, they allow the user to control the wheelchair forward, backward, turn left and right. This causes fatigue as the authors declare. For this reason, they develop the autonomous functionality that allows defining only the final destination. It has to be noticed that here the

possibility to define navigation zones in a proper CAD is lacking. Moreover, this technology cannot be used in the cluttered and frequently changing home environment.

4.1 Uncertainty analysis

In the experimental campaign has been adopted the EyeAssist developed by Xtensa, a low-cost eye-tracking platform developed for clinical purposes. Using an infra-red camera, it maps the gaze of the user on the screen by detecting the location of the pupil with respect to a known pattern of light. This system requires a first phase of calibration to fit the different users. This phase consists in a point moving on the screen in a random way between 9 possible positions. In particular, we target the PoR together with its covariance that we estimate as a function of the operating conditions in real time, namely the lighting, head position and rotation, target position on the screen, number of eyes detected and user characteristics.

The eye tracker communicates data obtained on a UDP port. The software developed in Unity was able to read from this port and also to communicate messages to the eye tracker, always through the UDP. This to communicate the data needed to load the calibration. During the test, the software counts both the valid and wrong data. If the number of wrong data overcomes 130, the target is moved to the following position.

The data obtained contain:

- Timestamp;
- X and Y coordinate of the PoR obtained considering only respectively the left and the right eye;
- X and Y coordinate of the PoR obtained as a medium value;
- X and Y position of the left and the right pupil on the image;
- X and Y coordinate of the target;
- Number of wrong data.

The test procedure used to collect the data is similar to the one used for calibration. The software employed to develop the test was Unity 3D. In this case, was used Unity 3D to control a circle on the screen appearing randomly on a grid of 5x5 that covers the whole screen. The circular target remained in each location on the screen until a sufficient amount of valid data has been collected (130 samples).

A problem that was considered is the relative motion between the screen and the head. In order to minimize this effect, it was added a bar to the set up to hold the user's forehead. Moreover, it has been drawn a scheme that allows the user to verify if he lies in the centre of the camera in order to locate the head always in the same position.

Another influencing factor is light. Indeed ambient light may change during the day. This alteration is partially compensated by changing the camera exposure. Anyway, the test was conducted in as much limited time slots as possible, also verifying that the lighting condition did not change that much.

4.1.1 Eye tracker repeatability and accuracy characterization

The obtained data were elaborated to remove outliers by means of the Chauvenet's. We set the maximum allowable deviation to 2. The procedure was repeated until the difference between previous and current standard deviation was less than 10%. A higher reduction would be meaningless. In Fig. 4.2 it is evident that the noise was largely reduced.

Having the filtered data it is possible to calculate the systematic effect and repeatability for every target position. The repeatability regions were then calculated using a confidence threshold that allows to obtain a confidence level of 95%, as explained in smith1986representation [71]. Plotting the results obtained it is straightforward to see that the ellipse does not contain the true value, which is the target position.

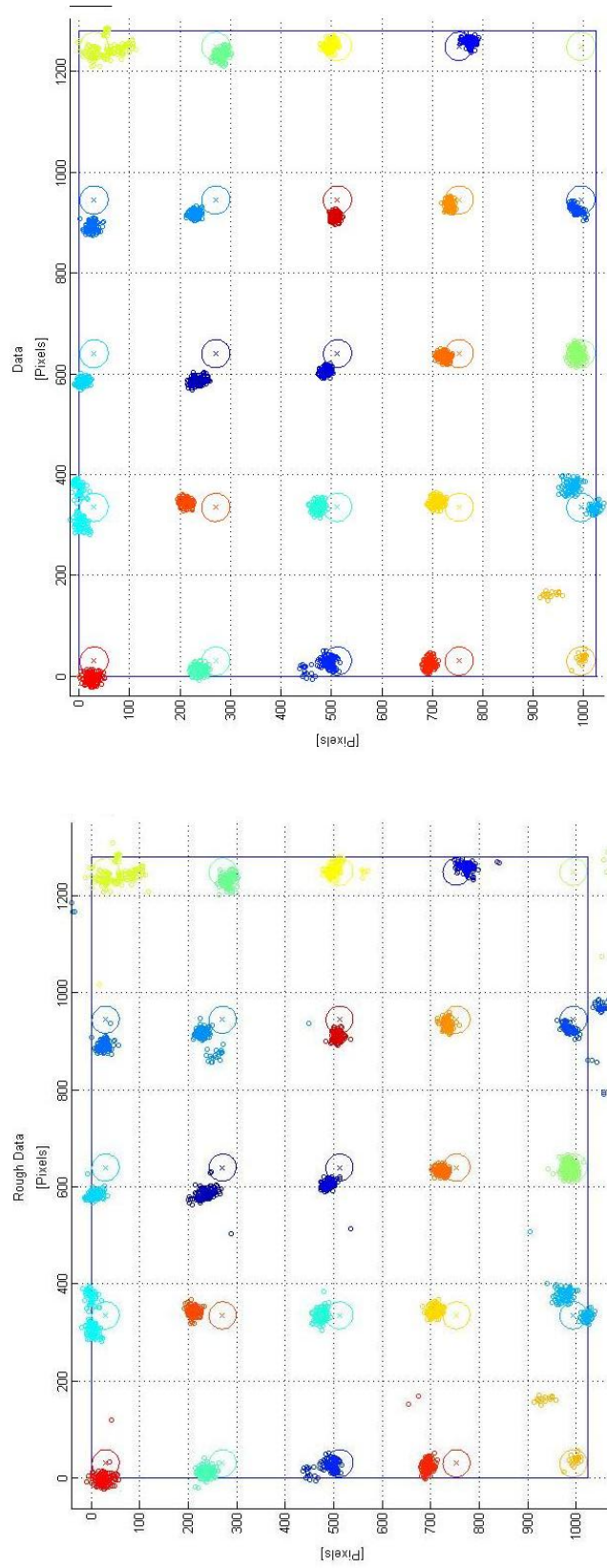


Fig. 4.2 Raw data collected for accuracy and repeatability characterization of the eye tracker uncertainty, before (left) and after (right) the application of a filter.

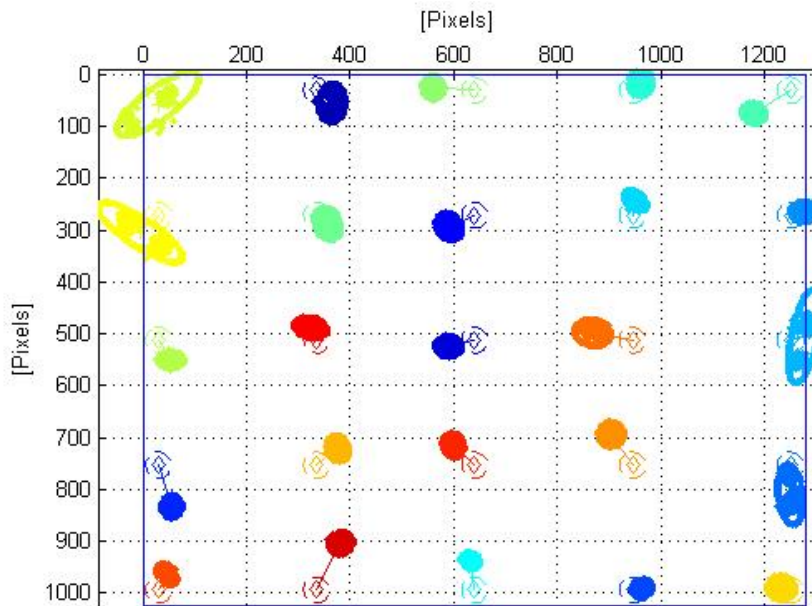


Fig. 4.3 Mean and covariance of accuracy and repeatability characterization of the eye tracker uncertainty

It is evident that this problem is mainly due to the presence of a strong systematic effect that seems to have a random nature, as evident in Fig. 4.3. In traditional measurement systems, if the results are repeatable, the systematic effect can often be determined and compensated.

In order to verify the statistic nature of the systematic effect, we tried to distinguish between repeatability for the same calibration and repeatability through different calibrations. For this aim was considered data coming from different calibrations. In Fig. 4.4 it is evident that the systematic effect is completely random.

The results presented previously underline the needed of a different method to estimate the uncertainty. It has to be noticed a good estimation of the true value, that is the target position. Even though we can not say where a person is actually looking but only where he/she thinks to look, the target position is a good approximation since the user is asked to look at the point. Hence it is possible to use this information to calculate an interval that includes the true values. With regard to this concept the residuals were calculated, as the difference between nominal value and measured values, and it was used those residuals to build the covariance matrix.

More than one test was used to collect more data as well as to have information coming from different calibrations. Indeed, data coming from different calibrations are not repeatable

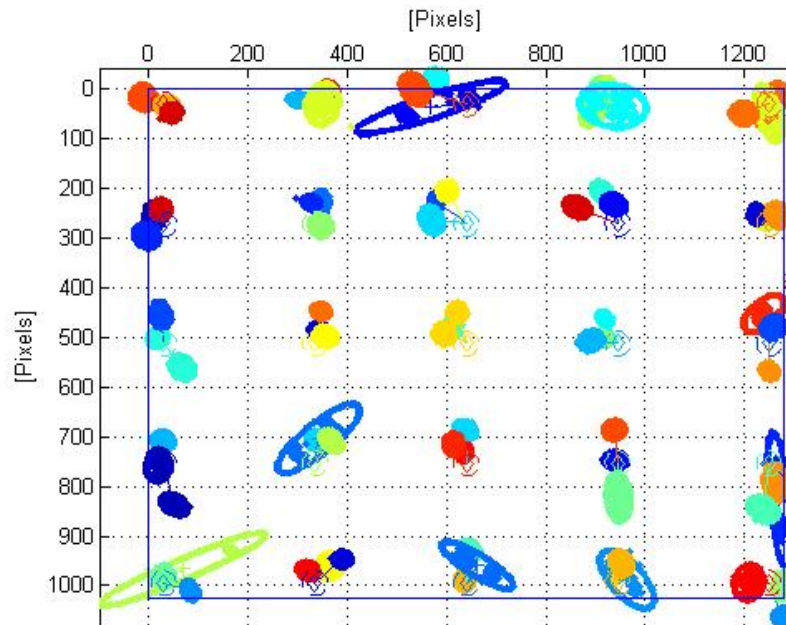


Fig. 4.4 Eye tracker repeatability analysis including different calibrations.

even if all this information are still coming from the same user. Note that the covariance calculated with the distance from the target does not need a confidence threshold of two to achieve the 95% of confidence, as in the pure repeatability case, but a confidence threshold of one is more than enough because the repetitions are always concentrated several pixels away from the reference value.

The covariance (equiprobable) ellipse can be expressed by three parameters that represent the major, the minor axis and the orientation (i.e. correlation factor). Looking at the available data, see Fig. 4.5, it is evident that the orientations are random.

Because there is not a prevalent orientation of the equiprobable ellipses it has no sense to model it as an ellipse. As a consequence, the uncertainty was modelled to be equally distributed along every direction, i.e. as a circle of radius R equal to the semi-major axis. We found the value of R that contains the 95% of the values to be $R = 114\text{pixels}$. In Fig. 4.6 can be seen this value applied to a validation set.

All the targets are now inside the covariance ellipse, that is actually a circle, except for one. A wider series of data verify that in the 95% of the cases the circle includes the true value. Since the screen used is 1280x1024, this value is more or less the 10% of the screen dimension.

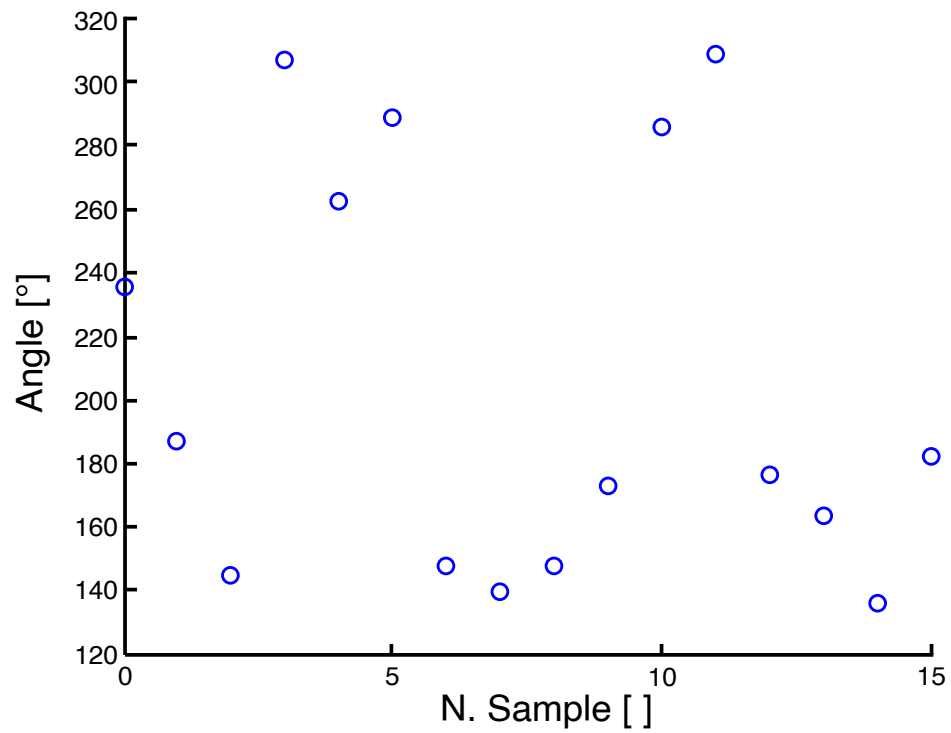


Fig. 4.5 Values of the covariance ellipse's angle.

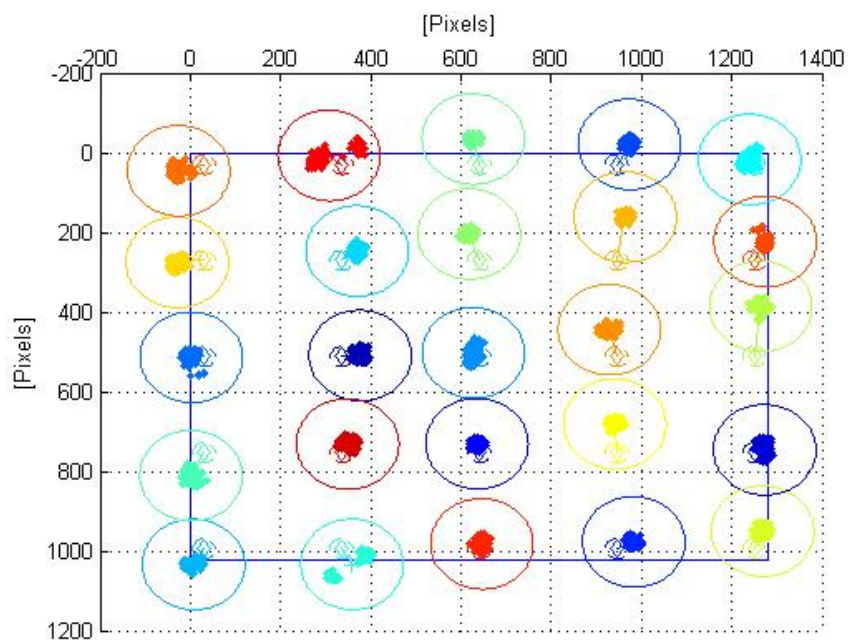


Fig. 4.6 Covariance *circle* with radius $R = 114pixels$.

Chapter 5

Wheelchair

A wheelchair is a wheeled mobile device used by people affected by some impairments due to illness, injury or disability. Wheelchairs are characterized by different format in order to satisfy the specific requirements of the users. They can include specific seating and controls or be personalized for particular activities such as sports wheelchairs. The main distinction of the wheelchairs is based on traction. In the manual wheelchair, the propulsion is provided manually by the user or by a caregiver while the powered wheelchair is equipped with batteries that power electric motors. Moreover, on the market are available different types of wheelchairs in order to perform many activities ranging from the standard manual or powered to sport or all-terrain device. Focusing on the power wheelchair, the traction can be applied on the frontal or on the rear rotation axis or integrally on all the wheels. Specific models can be equipped with tanks.

As the main advantage, using a power wheelchair, a patient is able to drive autonomously for long distances without fatiguing himself as well as without the presence of a caregiver. Typically, the commercial wheelchair is controlled with a joystick. However, it exists other kinds of input interface such as chin controller or by using voice or breath. Unfortunately, the control technique just listed are unfeasible especially for people affected by disease impairing upper limbs and respiratory organs like the ALS. In this context, the gaze control technology has a fundamental role for the mobility restore. The research work here described involved the development of an innovative strategy for an eye-controlled wheelchair including direct and semi-autonomous driving modalities. These were designed to provide to the user different experiences in driving, resulting from the focus required, the feeling resulting from the amount of control on the motion, and the level of safety provided by the system in relation to the environment. Even if the direct drive modality provides a versatile manoeuvrability, with reduced jerks, and an overall comfortable experience it resulted tiring for the patients that have to keep all the time the attention on the monitor. Indeed eye movement is one

of the fastest human movement, although are mainly conceived for exploration, less for control [35]. Using The semi-autonomous drive mode was included to solve the problem of user tiring affecting the direct mode by enabling the wheelchair to reach autonomously the selected target position. Of course, this kind of system must ensure high reliability of the control as well as a good knowledge of the work environment. One of the key feature influencing the performance of the navigation is the localization tools. The eye-controlled wheelchair prototype includes two types of localization: odometric recursion from encoders and a custom designed absolute marker based localization method.

The odometric localization uses the information about the rotation of the wheel between two steps of control. It requires the knowledge of the mechanical structure and in particular about the kinematic model of the vehicle in order to calculate the speed of the wheelchair from the velocity of the wheels.

5.1 Mechanical structure

A power wheelchair can be categorized as a mobile robot that is a device characterized by a mobile base that permits the positioning of the entire vehicle inside the work environment. One of the key topics of a robotic system is the mechanical structure that is fundamental to classify the robot. The main feature of the classification includes the base of the device. A robot with a fixed based is called robot manipulator while a mobile base characterizes the mobile robot. The following part describes the main geometrical features of a mobile robot.

Contrary to the manipulators, mobile robots need considerable motor capabilities. The mechanical structure of mobile robots is composed of one or more rigid bodies equipped with a locomotion system. In reference to the type of locomotion system, mobile robots are divided into two categories, the robot that moves by using wheels or legs.

Wheeled mobile robots are usually characterized by a rigid body (chassis) and a system of wheels that move the vehicle with respect to the ground. The wheels mounted on a mobile robot could be of different type.

Legged mobile robots are characterized by multiple rigid bodies interconnected generally by using revolute joint or sometimes with prismatic joints. The extremities, also called feet, periodically contacts the ground, realizing the displacement of the entire robot. This type of structure is generally used in biomedical field to perform research on living organisms (biomimetic robots), that range from biped humanoids to hexapod robots.

Generally, the main mechanical element characterizing the motion of a mobile robot are wheels. In particular, there are different variances:

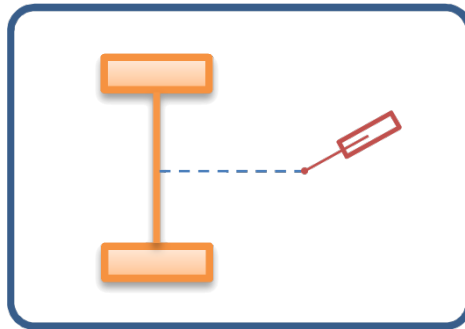


Fig. 5.1 Synchro-drive mobile robot

- The fixed wheels can rotate only around an axis placed in the center of the wheel and that is orthogonal to the wheel plane. The orientation of the wheel with respect to the base is fixed; it is rigidly attached to the chassis.
- The steerable wheels have two axes of rotation. The first is the same as the fixed wheels, while the second is vertical and it passes through the center of the wheel, allowing the orientation of the wheel with respect to the vehicle.
- The caster wheels present two axes of rotation like the steerable wheels. However, in the caster wheels, the vertical axis doesn't pass through the center of the wheel but it is displaced by a constant offset. That configuration guarantees a quick alignment of the wheel with the direction of the motion of the vehicle. This type of wheel is usually introduced to provide a static balance without affecting the mobility of the chassis.

The combination of the three conventional wheels generates the kinematic structure of the entire robot. In the following part, the most relevant kinematic structures are described.

A differential-drive vehicle is characterized by two fixed wheels that share a common rotation axis. Furthermore, one or more caster wheels guarantee the statically balance of the vehicle. Typically, the caster wheels, drawn in orange in Fig. 5.1, are smaller than the fixed wheels. The two fixed wheels are separately controlled by applying the proper value of speed to the single motor. Therefore, the vehicle can perform linear movements, as well as on spot rotations without move the midpoint between the wheels. These movements in closed environments are obtained by providing to the wheels an equal and opposite value of angular velocity.

A robot with synchro-drive kinematics presents three aligned steerable wheels, as shown in Fig. 5.2, that are driven by only two motors through a mechanical coupling, a chain or a transmission belt. The first motor provides the driving force, represented by the rotation of the wheels around the horizontal axis. The second motor controls the steering by rotating

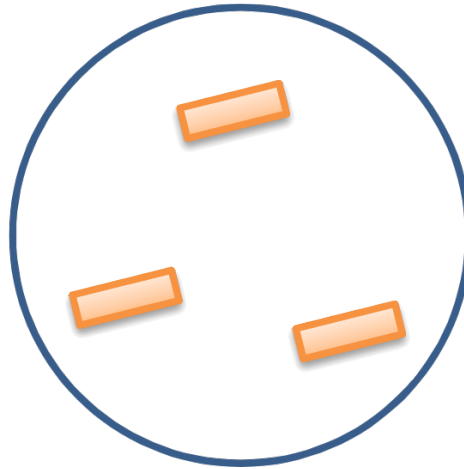


Fig. 5.2 Differential-drive mobile robot

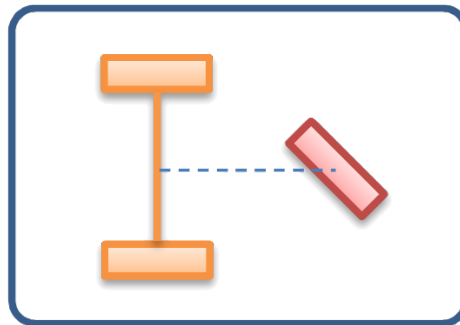


Fig. 5.3 Tricycle mobile robot

the wheels around the vertical axis. The syncro-drive kinematics have mobility like the ones obtained from the differential-drive vehicle. The only difference is in the heading of the chassis that remain fixed during the movement. However, a third motor guarantees the rotation of the upper part of the robot with respect to the lower part in order to orient for example a directional sensor.

A tricycle vehicle is equipped with two fixed wheels having common rotation axes joined to the chassis in the rear part of the robot. These wheels are acted by a single motor which controls the traction. Moreover, in the frontal part of the robot, are placed a steerable wheel driven by a single motor. The traction can be controlled by another motor that can act on both the rear wheels or, more rarely on the frontal wheel. Fig. 5.3 shows the mechanical arrangement of a tricycle mobile robot

A car-like vehicle has two steerable wheels, as shown in red in Fig. 5.4, mounted in the frontal part of the chassis and acted by a specific steering motor. The orientation of the frontal wheels during the movements along the curve must be carefully determined in order

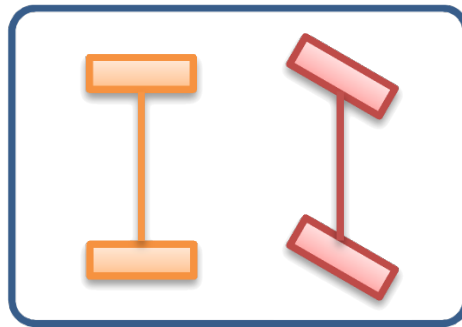


Fig. 5.4 Car-like mobile robot

to avoid slippage. In particular, the internal wheel is more steered than the external one. Devices like Ackermann steering guarantees the proper difference in the steering angle. Also in this type of vehicle are present two aligned fixed wheels mounted in the frontal part of the chassis. As in the previous case, the traction is provided by another specific motor that can act on the rear or on the frontal axis.

In addition to the conventional wheels listed above, there are other types of fixed, called Mecanum or Swedish wheels, that include passive rollers placed along the external rim. Usually, the axis of rotation of each roller has an attitude of about 45° . Using this type of fixed wheels, mounted in pairs on the two parallel axes, the robot can perform omnidirectional movements. The wheels on the same axis are mounted in such a way that the rotation axis of the rollers is incident. In this way, if the rotation speed of the two wheels has the same value and direction, the robot moves along its axis. Indeed, the lateral components of the force are compensated, while the longitudinal components have the same direction. Instead, if the rotation speeds of the two wheels have opposite directions, the sum of the longitudinal components is zero and so the robot performs a lateral movement.

The position of the wheels of a robot, and in particular the contact point between the wheels and the ground, represent the ideal vertex of a support polygon. If the center of mass of the robot falls inside the support polygon the vehicle is statically balanced. During the development of the mobile robot, an appropriate distribution of the wheels avoids problems in the mechanical balance of the structure.

In general, mobile robots present constraints in the equation of the velocity and related to the variable that describes the pose of the vehicle. This means that the system is non-holonomic and so, some of the trajectories related to the generalized variable of the system are not admitted. The equation of the velocity cited before is not integrable. The mobility of the vehicle is therefore limited due to the structure and its components. A mobile robot can reach any point of the surrounding environment, the workspace is unlimited. For example, a car is not able to move instantaneously in a direction orthogonal to the vehicle axis. The car

can however in that direction through a combination of manoeuvres allowing to reach the desired pose. In other words, the car, like other vehicles, presents limitations concerning the instantaneous direction of movement. Nevertheless, it can reach any points in the surrounding environment. In general, if the number of degree of freedom of the system is greater than the number of control variables, the equation of the velocity is non-integrable.

5.1.1 AGV

In a manufacturing process, one of the most important roles involving robots is the product transfer from a location in the factory to another in order to pass from a stage of the production to the following. The robot performs a service task without applying any physical modification to the objects.

Manipulators robots are involved in typical industrial applications such as palletizing, packaging, part sorting or warehouse loading and unloading. Moreover, another fundamental functionality is the product transfer from a location to another one at a high distance inside the factory. Mobile robots, and in particular AGV, are devoted to performing this kind of transfer. These devices are considered the evolution of the traditional transfer systems that follow a path through fixed guides (inductive, magnetic or optical). AGV can move autonomously thanks to a position sensor system (encoders, lasers, cameras) which allows it a high precision localization inside the environment. Moreover, a proper control algorithm ensures that the vehicle follows the planned path or trajectory as much precise as possible. The working environment has a strong impact on the localization systems mounted on the robot and, in particular, on the number and the type of sensor involved. The data collected from each sensor is joined by using a data fusion task that allows to combine the best feature of each localization system. The data fusion procedure aims to extract a unique value of position that is more precise and reliable than the ones coming from each single sensor with less uncertainty on the measure.

The measurements are always affected by noise factors, requiring thus a control algorithm to compare the reference with the measured values of positions, attitudes, and velocities and generate the proper correction signal. Generally, also path planning and control phases are strongly related to the working environment. It possible to define three environment categories basing on the information concerning the environment:

- **Structured environments:** the layout of the free spaces and the position of the obstacles are well known from a topological point of view. A typical example is the industrial logistic environment. The planning of paths of trajectories can be done off-line without

analysing the surrounding environment. On the other hand, the robot is not able to handle unforeseen situations like obstacles on the path.

- **Semi-structured environments:** the knowledge of the environment is not complete because there is not enough beforehand information about the target. Under these conditions, there is a planning of the spaces surrounding the robot, allowing flexible management of the path locally and in real time of the path to avoid obstacles, which are not known beforehand. The robot plans the movements off-line like the previous case, but it can change the path if an unforeseen situation happens.
- **Unstructured environment:** the plan cannot be comprehensively planned off-line in advance because the information about the environment is not enough. The only data provided is the final pose that the robot must reach. A real-time localization task is required, followed by an iterative path planning procedure. Starting from the initial and final pose of the robot, the localization and path planning algorithms generate the proper path that the vehicle shall follow in the best possible way (SLAM, Simultaneous Localization and Mapping).

A path can have different shapes basing on the profiles chosen by the designer. In particular, one of the key factors is the connection between two subsequent path sections. The trend of the path must be continuous and the derivative and the curvature of the two sections must have the same value without jerks in the connection point. Discontinuities in the curvature require instantaneous variation of the steering angle creating vibration and delay in the movement but especially stress for the motors. Due to this reason, the condition of curvature is very important. A motor has a behaviour, with regard to the frequency, similar to a low pass filter. This means that a motor cannot handle sudden variations of the input, generating a delay in the response and so a deviation from the planned path.

The curves used in the planning processes can be divided into two categories. The first is the curves with coordinate having a closed-form expression such as B-spline, fifth-degree polynomials or polar spline. The second are parametric curves in which the curvature is a function of the length of the arc (curvilinear coordinate) such as clothoids, cubic spirals or intrinsic spline.

The path planning algorithm used in this research involves the clothoids because this type of curve varies linearly with the length of the arc.

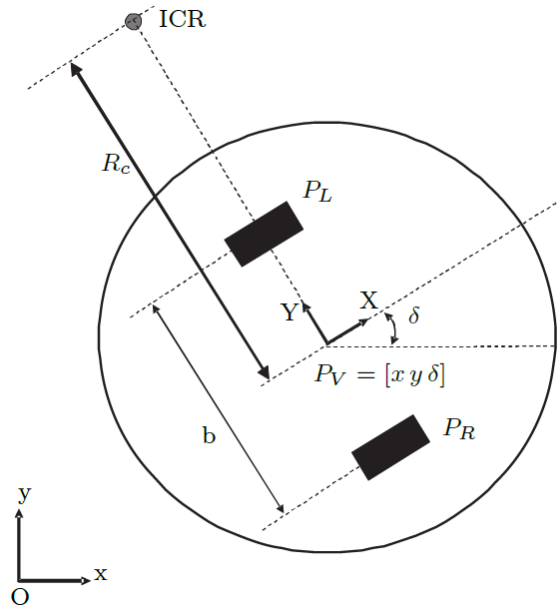


Fig. 5.5 Differential drive kinematic model schema.

5.2 Differential drive kinematic model

The kinematic model of a vehicle aims to describe the evolution over time of the variable having a significant impact on the system. These variables describe the state of the system inside the space of the possible configurations defined by the generalized coordinate vector, also called configuration variables. The number of the generalized coordinates is the same as the number of the degrees of freedom of the system and they can have, or not have physical meaning.

The definition of the kinematic model starts from one fundamental assumption: the existence of pure rolling constraint of the wheels. This constraint belongs to a non-holonomic class of vehicles having limitations in the speed of the vehicle (module and direction). As a consequence, also the feasible trajectories starting from a certain configuration are limited. However, the model of the vehicle is purely ideal. In reality, there are always some deviations from the model due to the non-ideality of the constraint.

As defined by Baglivo [7], a classic locomotion system for mobile robots is composed by two parallel driving wheels, controlled in speed or acceleration by two independent motors. Since two wheels are not enough to guarantee stable support, some caster wheels are added to maintain the vehicle with the right attitude with respect to the ground.

Taking as a reference the mean point between the two driving wheels (P_V), the system configuration is defined by three coordinates: the vector $[x, y]$ identifying the position of P_V

and the attitude angle δ that defines the instantaneous direction of the movement. This last coordinate coincides with the orientation of the driving wheels. The kinematic model is reported in Eq. 5.1.

$$\begin{bmatrix} \dot{x} \\ \dot{y} \\ \dot{\delta} \end{bmatrix} = \begin{bmatrix} v \cdot \cos(\delta) \\ v \cdot \sin(\delta) \\ \frac{v_R - v_L}{b} \end{bmatrix} = \begin{bmatrix} \frac{v_R + v_L}{2} \cdot \cos(\delta) \\ \frac{v_R + v_L}{2} \cdot \sin(\delta) \\ \frac{v_R - v_L}{b} \end{bmatrix} \quad (5.1)$$

Where:

- b is the the wheelbase (distance between the two driving wheels);
- v_R, v_L are the speed of the right and the left wheels;
- v is the speed of the reference point;

The model is obtained considering the rotation of the vehicle around its instantaneous centre of rotation (ICR) and expressing the speed v of the reference point as a function of the speed of the right and the left wheels.

The kinematic model changes depending on the generalized coordinates and on the selected controls. As for the latter, there are two examples of models related to the same system. The first one is a dynamic model controlled directly by using accelerations u_R and u_L of the wheels as reported in Eq. 5.2.

$$\begin{bmatrix} \dot{x} \\ \dot{y} \\ \dot{\delta} \\ \dot{v}_R \\ \dot{v}_L \end{bmatrix} = \begin{bmatrix} \frac{v_R + v_L}{2} \cdot \cos(\delta) \\ \frac{v_R + v_L}{2} \cdot \sin(\delta) \\ \frac{v_R - v_L}{b} \\ 0 \\ 0 \end{bmatrix} + \begin{bmatrix} 0 \\ 0 \\ 0 \\ 1 \\ 0 \end{bmatrix} u_R + \begin{bmatrix} 0 \\ 0 \\ 0 \\ 0 \\ 1 \end{bmatrix} u_L \quad (5.2)$$

The second model has as controls the speed of the middle point of the wheelbase and the angular velocity of the vehicle as reported in Eq. 5.3

$$\begin{bmatrix} \dot{x} \\ \dot{y} \\ \dot{\delta} \end{bmatrix} = \begin{bmatrix} \cos(\delta) \\ \sin(\delta) \\ 0 \end{bmatrix} v + \begin{bmatrix} 0 \\ 0 \\ 1 \end{bmatrix} w \quad (5.3)$$

5.3 Prototype: hardware

The prototype of the semi-robotic eye-controlled wheelchair, shown in Fig. 5.6, was built starting from a GR558, a commercial power wheelchair of Nuova Blandino driven through a joystick.

The base commercial wheelchair is composed by:

- **A sit** including a flatbed, a backrest, a headrest, two armrests, and two footplates;
- **A steel chassis** which represents the main load-bearing structure of the vehicle
- **Two driving wheels** having a diameter of approximately 15.6 centimeters and mounted on a gear unit with a transmission ratio of 25;
- **Two caster wheels** to guarantee the stability of the vehicle and maintain the right attitude of the wheelchair with respect to the ground;
- **Two continuous current electric motors** that is connected to the wheels through the gear units and they include mechanical braking system with electric driving;
- **A motorized extensible actuator** fused for the tilting attitude adjustment of the sit.
- **A command console** including a joystick, some other controls buttons such as the indication lamp or the speed profile selection (5 different speed levels selectable), and the status of the wheelchair like the battery life or eventually some malfunctions;
- **An driver** connected with the console, the tilt system, the two motors, the encoders, and the breaks.
- **Two DC battery** having supply voltage of 12 Volts and current of about 42 Ah;

In the commercial wheelchair, the command console is connected directly to the driver through a specific communication protocol. The driver elaborates the information and executes the required task by using advanced control algorithms. Some tests executed on the



Fig. 5.6 Prototype of semi-robotic eye controlled wheelchair.

joystick highlighted different settings that range from the acceleration ramps to the speed limit before the steering. Indeed, if during a forward movement at the maximum frontal speed, the user suddenly moves laterally the joystick, the wheelchair decelerates and then performs the steering in safe conditions.

However, there is no evidence to support all these behaviours, creating in this way possible big obstacles in the development of different control systems. Also the communication protocol between the joystick and the driver is not properly documented. The absence of information creates many limitations for the development of innovative alternative driving techniques due to the problems on the integration of new devices as well as to the possible unpredictable behaviours of the vehicle.

Therefore, the commercial wheelchair is suitable for the purpose of the research but it requires considerable modifications in order to be used for the development of the prototype of eye-controlled wheelchair.

The base commercial wheelchair was reconfigured to include some advanced robotic functionalities. The default electronics were removed and substituted with a commercial driver to power the original motors and two encoders on the wheels for the odometric localization. A Time of Flight (ToF) Microsoft Kinect V2 camera was mounted on the frontal part of the wheelchair, few centimetres above the legs of the user. A monitor was mounted in the frontal part and shows the HMI and the information coming from the TOF about the environment to the user. A Windows PC manages the logic of the system. This collects the data from the encoders, calculates the position of the wheelchair, and the control parameters required to pilot the drivers. It also manages the eye tracker (fastened below the monitor), the HMI and the ToF. Both the HMI and the hardware manager services were developed in UNITY, and the communication between the OS and the driver was structured over an RS232 serial communication.

Hereafter are reported the full list of modifications made on the base wheelchair:

Substitution of the control driver: as previously introduced the original control driver is not suitable for the development of the eye-controlled wheelchair. The very limited amount of documentation about the original driver, from both the hardware and the software point of view, makes impossible the integration of the original driver inside the new technology. Moreover, the proprietary control algorithm doesn't allow detailed and complete movement management. The speed control is not integrated on the commercial wheelchair. Due to all these reasons, the original hardware was substituted with an industrial commercial driver, the SDC2160 model of RoboteQ brushed DC motor controllers. This element is connected with a PC through serial communication.

Removal of the joystick: the controller originally installed cannot be integrated into the non-proprietary systems due to the policy of the manufacturer. Indeed there is no documentation available as the point of view of the communication protocol. This condition doesn't allow the direct use of this controller in the system. Actually, the joystick has simply been removed but, as future development, an equivalent device could be included as an alternative controller.

Integration of two encoder: the localization of the wheelchair is a fundamental task for the navigation of the vehicle. The odometric localization algorithm returns the position and the attitude of the wheelchair with respect to the initial pose of the path by using two incremental magnetic encoders. They are mounted on the hubs of the wheels, between the gear units and the wheel.

Integration of the PC: in order to perform all the functions required for the wheelchair navigation it is necessary a PC having reduced dimension as well as high computation capability and low power consumption. The integration of the peripheral devices, such as the eye tracker, is not feasible on a common driver of PLC, it requires a Windows PC. On the eye-controlled wheelchair prototype was embedded a compact PC with reduced power consumption (maximum 40 W with all the peripheral devices connected). Moreover, the integration of a PC offers the possibility to connect many other peripheral devices which would be uncontrollable with a standard drive. This fact increases the versatility of the system.

Integration of the camera: the interaction with the surrounding environment requires a specific device able to collect information about all the elements around the wheelchair. By using a ToF camera are collected information about the RGB video stream but also a depth image useful to reconstruct the three-dimensional surrounding environment. The ToF camera mainly used was a Kinect v2 of Microsoft but recently it was changed with an Intel RealSense D435 due to the withdrawal from the market of the Kinect v2. The camera position and attitude are fixed with respect to the wheelchair chassis in order to maintain the optimal view also during the tilt manoeuvres. The camera is mechanically mounted on an arm connected to the chassis through a revolute joint in order to be as much adjustable as possible in the attitude. The position was identified by considering advice from a pool of volunteer testers, habitual users of standard and special power wheelchairs: these highlighted the importance of seeing their own knees inside the driving interface, resulting in an effective strategy for a better depth perception from the video interface.

Integration of a monitor: the human-machine interaction is performed by using a portable monitor mounted on a specific support arm. The data communication is carried out through a USB cable as well as the power supply, reducing in this way the number of cables required but also avoiding the integration of specific voltage regulators. The monitor is used both to visualize the camera stream and also to show the control buttons useful for the navigation. The monitor has a fixed position with respect to the seat in order to follow the user during the tilt manoeuvres.

Integration of the eye tracker: the interaction between the user and the wheelchair prototype requires also an input device able to collect information about the desired commands. A Tobii eye tracker (model EyeC) was added to control the vehicle without the usage of the hands. As the monitor, also the eye tracker is connected to the PC through a USB cable. The eye tracker requires a quick calibration procedure whereby the geometric characteristics of a subject's eyes are estimated as the basis for a fully-customized and accurate gaze point calculation.

The first prototype of eye-controlled wheelchair was made by a power wheelchair commercialized by Invacare (model: Storm XR), integrated with some additional devices useful at including advanced robotic functionalities. Differently, from the current version, the control of the vehicle was split into two levels. The lower level used an industrial PLC running ArWin, a proprietary real-time operating system. Five X20 B&R expansion modules were connected to the industrial PLC through POWERLINK communication. Two of these modules were dedicated to reading the steps from the two encoders on the motors, two analog output was used to pilot the driver, a digital input/output was used to enable the power supply and the PLC read the data from a joystick using an analog input. The PLC calculated the control parameters (voltage related to forward and rotational speeds) and piloted the driver of the two motors. It also collects the data from the encoders.

The higher one used a Windows PC to manage the camera, the monitor and the eye tracker. It is connected to the PLC through a TCP/IP connection using PVI library from B&R.

As in the current version of the prototype, the absolute localization of the wheelchair with respect to some Points Of Interest (POI) is implemented with the Time Of Flight (TOF) camera, a Kinect V2.0, mounted on the frontal part of the wheelchair, few centimetres above the knees of the patient. The position of the sensor was the result of the advice from a pool of testers: the presence of the knees in the field of view of the camera was considered very useful in the depth perception of the surrounding environment and in particular for movements close to obstacles or narrow passages.



Fig. 5.7 Tobii 4C eye tracker

Table 5.1 Tobii Eye Tracker 4C technical specifications.

Size	17 x 15 x 335 mm
Max Screen Size	27 inches with 16:9 Aspect Ratio
Operating Distance	50 - 95 cm
CPU Load	1% (Core i7)
Power Consumption	2.0 W
Illuminators	Near Infrared (NIR 850nm)

The images coming from the camera are displayed on a monitor mounted in front of the user. On that image are overlapped the HMI and the information about the POI detected in the field of view of the camera. The patient interacts with the system using an eye tracker (TOBII EyeX5) mounted below the monitor that is similar to the one currently used.

A safety button, connected directly to the voltage supply of the motors, ensures the safety of the user during the learning and test phase. The pressure of the safety button is notified to the PLC through the input/output X2X module.

5.3.1 Devices

In this section is described the main devices used on the prototype of eye-controlled wheelchair developed during the research activities.

Eye Tracker

Eye tracking is a sensor technology that enables a device to know exactly where the user's eyes are focused. It is a device intended to determine presence, attention, focus, drowsiness, consciousness or other mental states. This information can be used to gain deep insights into consumer behaviour or to design revolutionary new user interfaces across various devices.

The eye-controlled wheelchair is equipped with a Tobii Eye Tracker 4C, one the most famous device for the eye tracking, Fig. 5.7. It is a low-cost device commonly used in PC gaming for enhanced streaming, and exports experience. Recently, eye-tracking technology is used also in different fields such as in professional application to cut the training time, improve safety and productivity. Other applications involve the eye tracker for consumer



Fig. 5.8 RoboteQ devices. SDC2160 Brushed DC Motor Controller on the left and RIOX Smart IO Expansion Card Roboteq on the right.

insight, scientific research and also in the assistive technology through augmentative and alternative communication. Table 5.1 reports the main technical specifications about Tobii Eye Tracker 4C.

Driver Roboteq

Roboteq's SDC2160 is a very compact high-performance dual-channel brushed DC motor controller, Fig. 5.8. It is designed to convert commands received from an RC radio, Analog Joystick, wireless modem, PC or microcomputer into high voltage and high current output for driving one or two DC motors. A CAN bus interface allows up to 127 controllers to communicate at up to 1 Mbit/s. The controller features a high-performance 32-bit microcomputer and quadrature encoder inputs to perform advanced motion control algorithms in open or closed loop (Speed or Position) modes. The SDC2160 features several analogs, pulse, and digital I/Os which can be remapped as command or feedback inputs, limit switches, or many other functions. For mobile robotic applications, the controller's two motor channels can either be operated independently or mixed to set the direction and rotation of a vehicle by coordinating the motion of each motor.

In addition to the SDC2160, the eye-controlled wheelchair prototype embeds also a smart input/output and communications module, the RIOX (Robot IO eXtender) of RoboteQ, Fig. 5.8. This module is an intelligent I/O expansion card, with an optional Attitude and Heading Reference System (AHRS), that seamlessly integrates with RoboteQ motor controllers. It is intended for use in robotics navigation, unmanned vehicles, machine control, industrial automation and any other applications that need interfacing to the real world. The RIOX mod-



Fig. 5.9 Bearingless magnetic encoder

ule can also be used stand-alone, or as an IO extender to PC, PLC or microcomputer-based systems. The main functions used in on the wheelchair are the configurable 12 digital/analog inputs and 16 digital outputs capable of driving loads or motors up to 1A each at 40V.

Encoder

A rotary encoder is an electro-mechanical device specifically designed to translate the motion of a rotary axis, i.e. a rotary mechanical movement such as the one of a motor or a shaft, into either analog or digital electrical signals. Alternative outputs signal can be a digital code under specific encoding. Through appropriate electronic equipment, the encoder can be used to determine information about travel, position, displacement, direction, velocity, and acceleration. An encoder can be found in the widest variety of industrial sectors, wherever a rotation has to be controlled, such as in automotive industries, robotics, packaging machinery, mechanical engineering, conveyors, among others. Each application needs a personalized solution that has to be uniquely suitable for specific aims. For example, the automotive and packaging industries need flexibility, high processing speed, and absolutely safe and reliable signal transmissions. Instead, harsh environments affected by oil, dirt, dust, moisture as well as severe temperature fluctuations require rugged and high protection rate encoders. Moreover, wood, paper, and steel industries demand robust encoders capable of withstanding both high mechanical loadings and extreme shock and vibration levels.

Rotary encoders can be divided into two main categories:

Incremental encoder: produce square waves but also sinusoidal signals. They are used to determine information about travel, position, displacement, and velocity. The estimation of the position is derived from an odometric recursion considering subsequent steps. This means that it is possible to determine if the axis is rotating and also rotating direction. However, it is not possible to get information about the absolute position of the axis. For this reason, the homing operation is always required at the beginning of the process to determine the absolute position of the system. In this way, the reference point or zero points is detected.

Absolute encoder: provide information about the absolute position of an axis. They use a unique code pattern, giving back a unique digital code for each angular position of the axis. As the main feature, using this type of encoder, it is always possible to know exactly the position of the axis also in case of temporary signal loss. Indeed, no homing operation is required to determine the absolute position. An absolute encoder provides, as output signal, a digital code that can be in pure Binary, Gray or BCD output code format through parallel or serial output circuits. Furthermore, they can afford almost all field bus interfaces available on the market. Absolute encoders can be either single-turn or multi-turn. Single-turn encoders provide the absolute position information per each revolution and the counting operation resumes again after each revolution, while multi-turn encoders use an additional internal counting process to monitor and track the number of rotations.

In general, the manufacturer divides them into categories according to the specialized application such as light-duty, industrial, feedback or heavy-duty. The eye-controlled prototype is equipped with two MRI2 series bearingless non-contact magnetic encoder having resolution of 18 000 ppr, Fig. 5.9. It was used a modular magnetic encoder for heavy-duty application due to the position of the devices on the wheelchair. They are placed on the hubs between the gear units and the wheels, in a particularly exposed position. The harshest environments affected by oil, dirt, the finest of dust particles, moisture, water jets, wash down cleaning as well as common chemical agents require rugged and high protection level encodes. Heavy-duty encoders are designed for the toughest applications. They are robust and capable of withstanding highest mechanical loadings and also extreme shock and vibration levels. Moreover, they are designed to offer outstanding reliability and absolute safety, with little maintenance.



Fig. 5.10 3D cameras: Kinect v2 on the left vs Intel RealSense D435 on the right.

3D Camera

One of the main functionalities characterizing the prototype of eye-controlled wheelchair is the semi-autonomous navigation. It requires a strong interaction with the surrounding environment in order to collect information about the element around the vehicle such as the floor, walls or obstacles. This function is performed through a 3D camera connected to the Windows PC. The first part of the development of the prototype involved the usage of the Microsoft Kinect v2, an infra-red (IR) Time of Flight (ToF) camera equipped with a 3D depth sensor (IR emitter and camera) in the central part and an RGB cameras on the left side, as shown in Fig. 5.10. From the Kinect v2, it is collected information about the RGB and depth video streams. The RGB frames are used on the HMI to show the surrounding environment and, but also in the path planning algorithm to detect the points of interest and extract the information about the target. Instead, from the depth frames are determined the point cloud of the environment. It is also used in the path planning algorithm to calculate the position of the vehicle with respect to some reference positions.

Although the Kinect v2 is a very powerful 3D camera it was substituted with the RealSense D435 of Intel because recently Microsoft withdrew its camera from the market. The RealSense is a depth camera that uses stereo vision to calculate depth. The D435 is a USB-powered depth camera and consists of a pair of depth sensors, RGB sensor, and infra-red projector. Contrary to the Kinect v2, the RealSense can work also in outdoor.

These two cameras present difference from the technological point of view. Table 5.4 reports the main features of Kinect v2 and Intel RealSense D435.

The introduction of the Intel RealSense D435 highlighted some problems during the navigation of the wheelchair and in particular in the path planning. Comparing the two cameras it is possible to notice that the RealSense provides less stability as well as higher noise of the depth image with respect to the Kinect. Fig. 5.11 shows two point cloud frames acquired respectively with the Kinect v2 and the RealSense D435. These conditions required a revision of the localization algorithm to extract the attitude of the POI from the RGB image

Table 5.2 Comparison between Microsoft Kinect v2 and Intel RealSense D435.

	Kinect v2	RealSense D435
Technology	Tof	Stereo
RGB resolution [pixel]	1920x1080	1920x1080
IR resolution [pixel]	512x424	1280x720
Depth resolution [pixel]	512x424	1280x720
Depth Field of view [degrees]	70.6x60	85.2x58
RGB Field of view [degrees]	84.1x53.8	69.4x42.5
FPS depth [FPS]	30	up to 90
Dimension (L x D x H) [mm]	90 x 25 x 25	249 x 66 x 67

instead of from the depth frame. The noise of the point cloud frame caused a high variability of the attitude values.

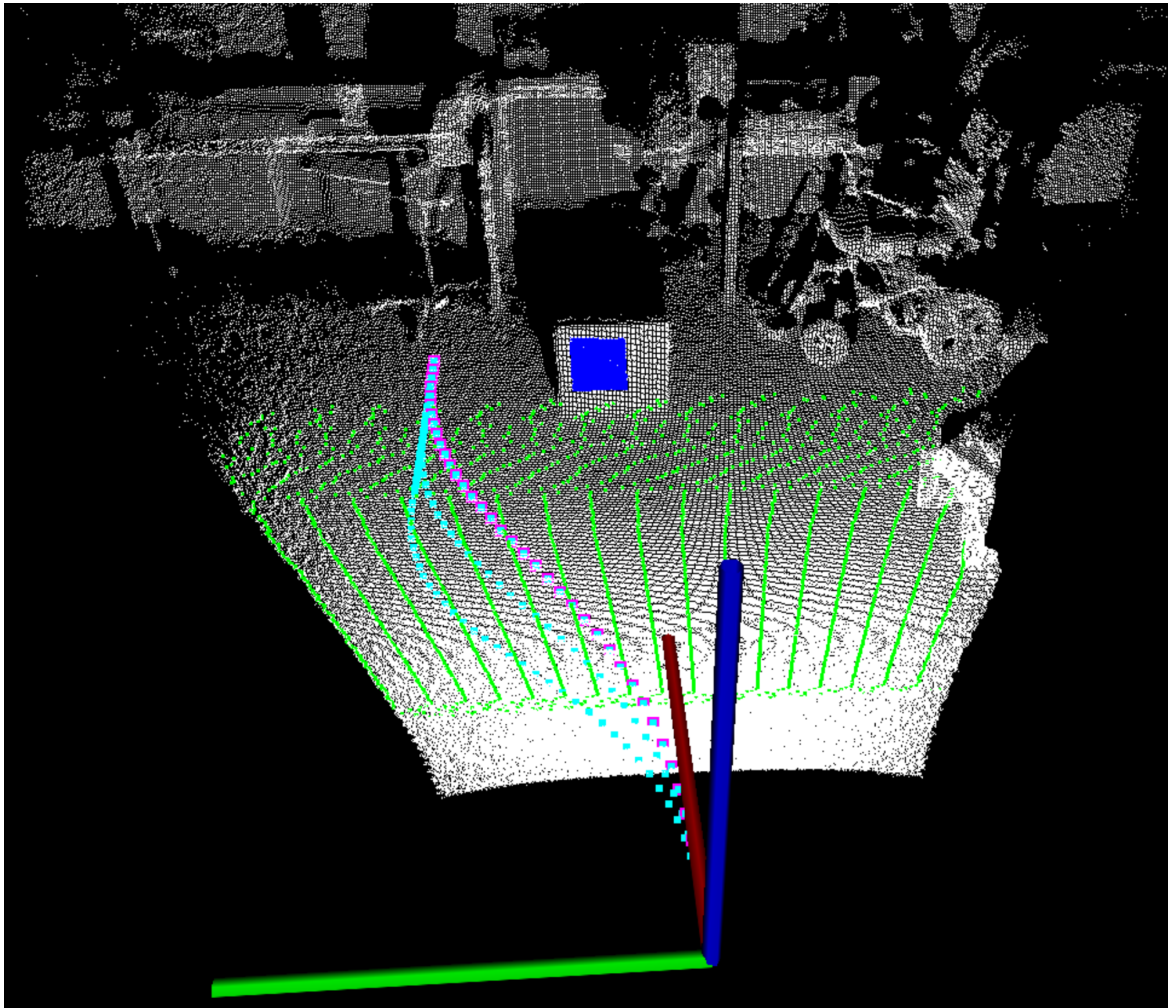
Table 5.3 summarise the major pros and cons of the two depth sensors.

5.4 Calibration of the wheelchair kinematic parameters

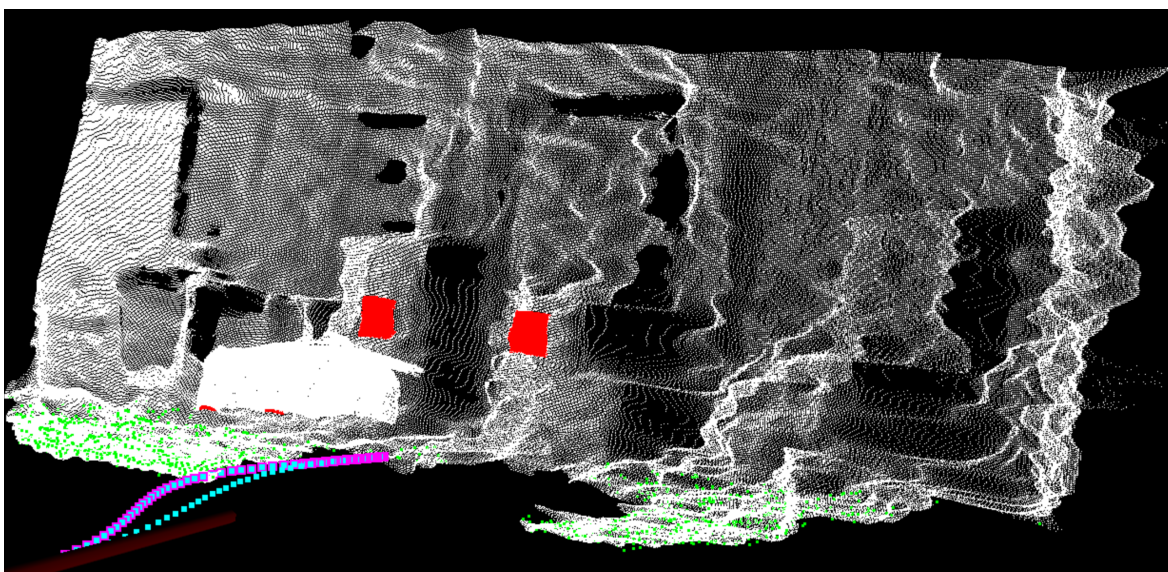
The calibration procedure aims to study initially the behaviour of a commercial power wheelchair (model GR558 of Nuova Blandino) equipped with the traditional control devices (commercial joystick and driver).

During this first part was collected information about the kinematic parameters characterizing the commercial wheelchair such as the value related to the velocity profiles. The test was carried out by connecting the traditional driver to two motors equipped with two magnetic encoders mounted on the hubs of the wheels, as shown in Fig. 5.12. In this way it was possible to measure the effective speed of the wheels during the execution of forward and backward movements as well as pure rotation on the spot. The data acquisitions were performed on all the 5 driving modality, from the slowest speed profile to the fastest one. From the tests was extracted information about the full speed and the acceleration following a step input. From an operative point of view, the test was carried out applying a step on the joystick in the three manoeuvre for each level of speed. After some seconds the joystick was realised, leaving it to return in the normal position. From the recorded data was calculated the full speed value with an uncertainty level of 95% and an estimation of the acceleration value during the rising edge.

As overall results, the Fig. 5.13a shows 5 levels of speed related to the different driving modality on a forward movement. In particular, the maximum full speed recorded range



(a) Point cloud frames collected with Kinect v2



(b) Point cloud frames collected with Intel RealSense D435

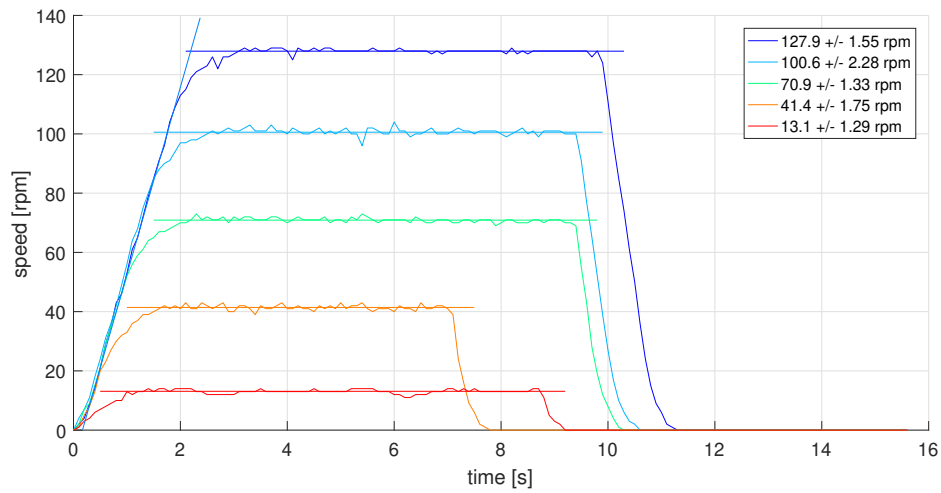
Fig. 5.11 Point cloud frames collected with the two cameras.

Table 5.3 Pros and cons of depth Kinect v2 and Intel RealSense D435.

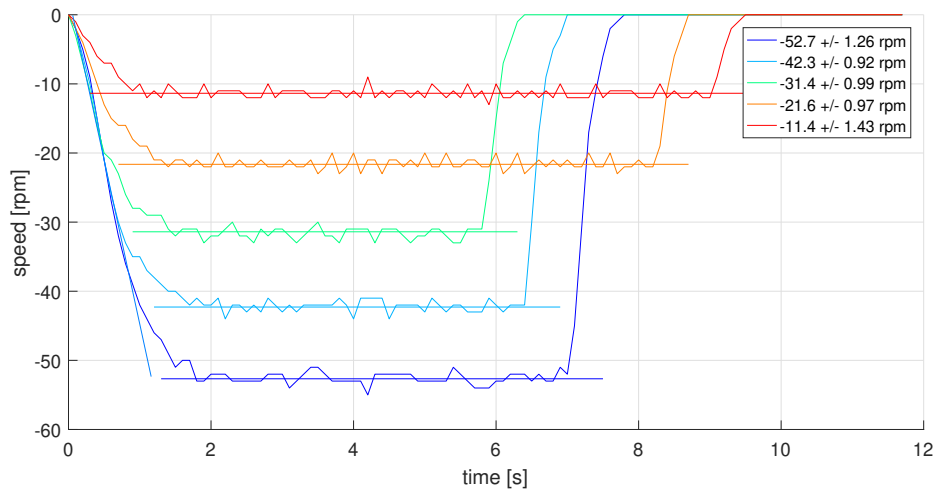
	Pros	Cons
Kinect v2	<ul style="list-style-type: none"> • Higher FOV • Higher resolution of depth and RGB video • Lower noise, better quality and accuracy of point cloud • Higher overall tracking quality can be expected 	<ul style="list-style-type: none"> • Requires external power supply
Intel RealSense D435	<ul style="list-style-type: none"> • Up to 90 FPS • High resolution of depth map • Very compact 	<ul style="list-style-type: none"> • Very low quality of depth map (high noise, many artifacts) • RGB camera has significantly lower FOV



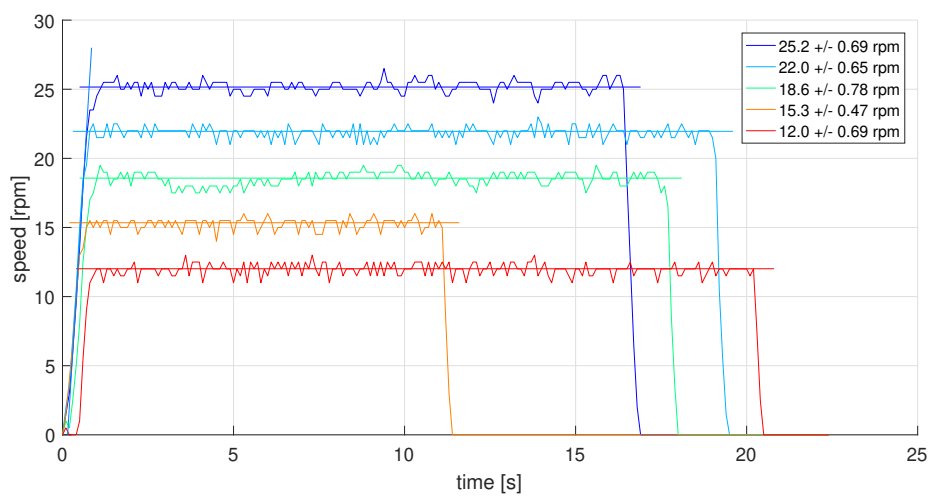
Fig. 5.12 Testbed for the calibration of the wheelchair kinematic parameters.



(a) Forward movement.



(b) Backward movement.



(c) Lateral movement.

Fig. 5.13 Velocity profiles resulting from the amaryllis on the commercial wheelchair.

Table 5.4 Ziegler-Nichols Tuning Formula for Step Response Method.

Controller	K_p	T_i	T_d
P	T/L	-	-
PI	$0.9T/L$	$L/0.3$	-
PID	$1.2T/L$	$2L$	$0.5L$

from 128 rpm in the highest configuration, to 13 rpm the slowest one with a step of about 30 rpm. Moreover, the acceleration estimated is equal to 63 rpm/s. It could be considered the same for the 5 levels of speed.

The same test on the backward movement, Fig. 5.13b, reports a maximum full speed value of -53 rpm. The step between a level and the following is of almost 10 rpm obtaining in this way a minimum speed of -11 rpm. The acceleration is equal to -47.5 rpm/s.

As regards the pure rotation around the middle point of the wheelbase of the driving wheels, it is possible to notice values of lower full speed values with respect to the previous cases, Fig. 5.13c. Indeed, the maximum speed is equal to 25 rpm. The acceleration is equal to 40 rpm/s.

The second part of the procedure involved the calibration of the feedback control system by estimating the parameters related to the proportional and integrative gains.

The speed control of a vehicle represents one of the fundamental parts of the navigation process. The driver installed on the prototype involves a PID regulator, that is the most used one in industrial applications, able to guarantee a rotation speed of the wheels as close as possible to the set value. This regulator executes a control action proportional to the error identified by a feedback system that uses the speed estimation obtained from the encoders mounted on the wheels hubs. On the RoboteQ driver, it is possible to set the gains related to the PID regulator (proportional K_p , integrative K_i and derivative K_d). Only the proportional and integral components are used in the specific case of speed control.

The gains estimation of the controller was performed by using the open loop Ziegler-Nichols method [1]. The procedure involves the application of a step input to the system to be controlled, and acquire the information related to its response, Fig. 5.14. The PID gains can be achieved directly as a function of T/L and L , as shown in Table 5.4

Where $K_i = K_p/T_i$ and $K_d = K_p \cdot T_d$.

The obtained response of the system is fitted with polynomials having the proper degree. In the specific case here presented was used a fourth-degree polynomial, Fig. 5.15. In the inflection point is determined the tangent and thus the incidence points with the x axis and

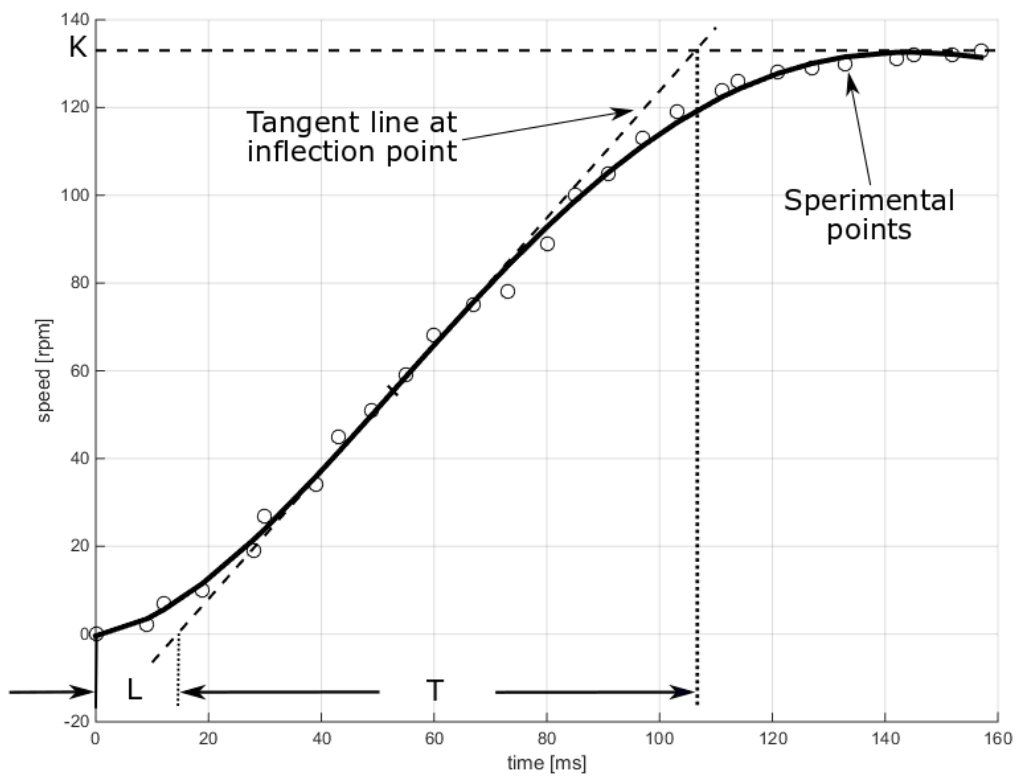


Fig. 5.14 Theoretical open loop system step response.

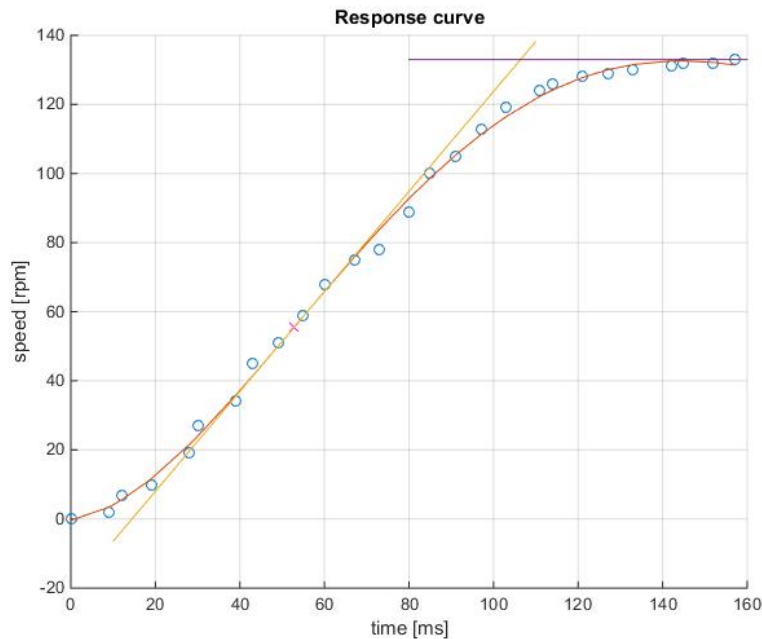


Fig. 5.15 Measured open loop system step response.

the steady-state value. The parameters useful to determine the gains is determined by means of the incidence points.

5.5 Prototype: software

The navigation of the eye-controlled wheelchair is managed by a micro-services architecture software. A micro-services architecture provides that the entire application is structured as a collection of loosely coupled services. This type of structure improves, as main benefit, the modularity of the system. As a direct consequence, the application became easier to understand, to develop, to expand and test, but also more resilient to architecture erosion. Chen [17] reports, among other things, the main benefits achieved the usage of micro-services and describes the new challenges that have arisen from its usage. Indeed, despite all the benefits, the micro-services architecture is not a silver bullet. This type of structure can introduce problematic situation without the proper management, introducing in this way complexity and challenges in the system.

The micro-services architecture used in the prototype of eye-controlled wheelchair is characterized by 8 services that manage:

- Human-machine interface

- Camera acquisition
- Path planning
- Path following
- Autonomous navigation
- Serial communication
- Management of the wheelchair layout (tilt of the sit)
- Status management of the system

The communication between the services was performed through the ZeroMQ, a high-performance asynchronous messaging library and, specifically, publish-subscribe patterns. This is a data distribution pattern useful to connect a set of publishers to a set of subscribers.

5.5.1 Human Machine Interface

The frontal monitor displays the HMI, shown in Fig. 5.16, and presents the navigation options to the user. It is the first service of the micro-services based software architecture. This includes:

- A video stream from the camera on the background
- The buttons to start/stop the navigation on the foreground
- The detected POIs with the identified feasible paths on the top of all

The HMI was developed using Unity 3D, one of the current state of the art game engine, and coded with the C# programming language.

The graphical engine considers the role of the uncertainty coming from eye-tracking and its effect on the human-machine interaction, proportionally adapting the size of the buttons and pins depending on the magnitude of such parameter. This is computed online, exploiting a modified moving average (MMA), also called running moving average (RMA) or smoothed moving average (SMMA), of the gazed point over the monitor in time:

$$\overline{\Delta p}_{k+1} = \frac{(N-1) \cdot \overline{\Delta p}_k + \Delta p_k}{N} \quad (5.4)$$

Where:

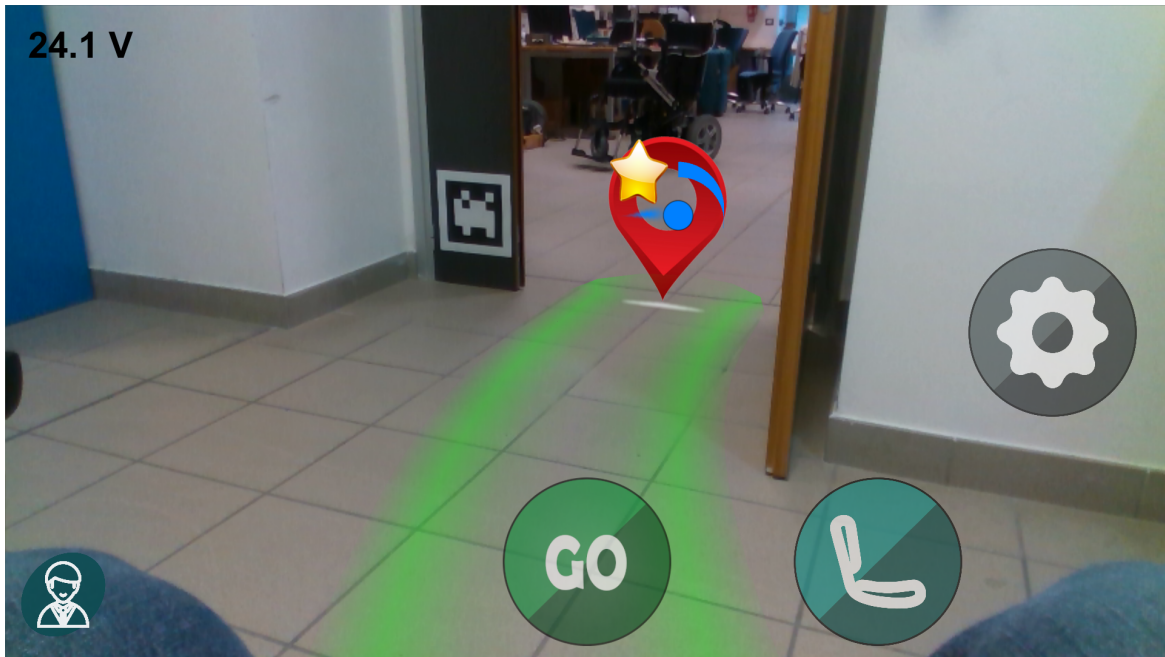


Fig. 5.16 The Human Machine Interface shown on the frontal monitor.

- $\overline{\Delta p_k}$ is the value of the exponential moving average at a step k ;
- ΔP_k is the difference of the gaze position in two subsequent steps;
- N is the number of samples considered in the moving average, set in the proposed application set to 10.

A uniform weighting of $1/N$ was considered for all the samples in the average.

The presented organization achieved the main advantage of fast, reliable and structured access from high-level software interfaces to low-level variables, modules, and functions, enabling the natural integration of kinematic information into the AR. The results were a natural, simple and efficient HMI from which derived a smooth and comfortable control of the motion of the wheelchair.

5.5.2 Camera acquisition

The camera acquisition service performs the capture of the video stream coming from the 3D cameras. In particular, 2 different services were developed for the camera acquisition, the first for the Kinect v2.0 and the second for the Intel RealSense D435. The architecture of the entire application allows to choose the preferred input devices only by changing this service and without modifying other parts of the software.

This service elaborates the data coming from the 3D camera generating two separate data flows the RGB and the point cloud frames. The acquisition rate can be configured basing on the status of the navigation process in order to optimize the performance of the entire system for example in terms of HMI refresh rate or planning speed. The video streams are sent to the HMI and to the path planning service to performs the visualization and the analysis of the surrounding environment. The modularity of the architecture is ensured by a custom data encoding.

5.5.3 Path planning

The path planning procedure analyses the RGB frames in order to detect some *markers* in the field of view of the 3D camera. It is used in the semi-autonomous navigation driving mode. The markers are connected to some Point Of Interest (POI) that are placed in a specific position and attitude with respect to the marker. A **.json* map file reports the list of markers with the related POIs. The path is divided into two parts: a dynamic and a static section. The map file includes also position and attitude of each marker with respect to the absolute reference system as well as a list of *passing points*. The planning algorithm uses these position to determine the second part of the path that is fixed with respect to the POI. This method is considered very useful in some particular situations such as the passage through a door or to approach a table or a bed. The fixed path supports the control of a power wheelchair during difficult manoeuvres. Therefore, the localization algorithm determined the dynamic part that is connected to each passing points as shown in Fig. 5.17. In the figure are placed two markers linked to two POIs that are placed on the left and on the right of each marker. The algorithm searches the marker in the RGB frames, determine the position and the attitude of each POI detected and then plan the best path to reach the target. The entire navigation process is widely described in Section 7.1.1.

5.5.4 Path following

The fourth service is dedicated to the odometric localization and to the path following task, with which a vehicle is able to reach a specific final pose (position and attitude) starting from a certain initial point, by following a reference path and considering a maximum deviation from it. The path following task is different from the trajectory following due to the absence of a temporal law. Indeed, the goal is to approach as much as possible the vehicle to the reference path without considering the time spent to reach it.

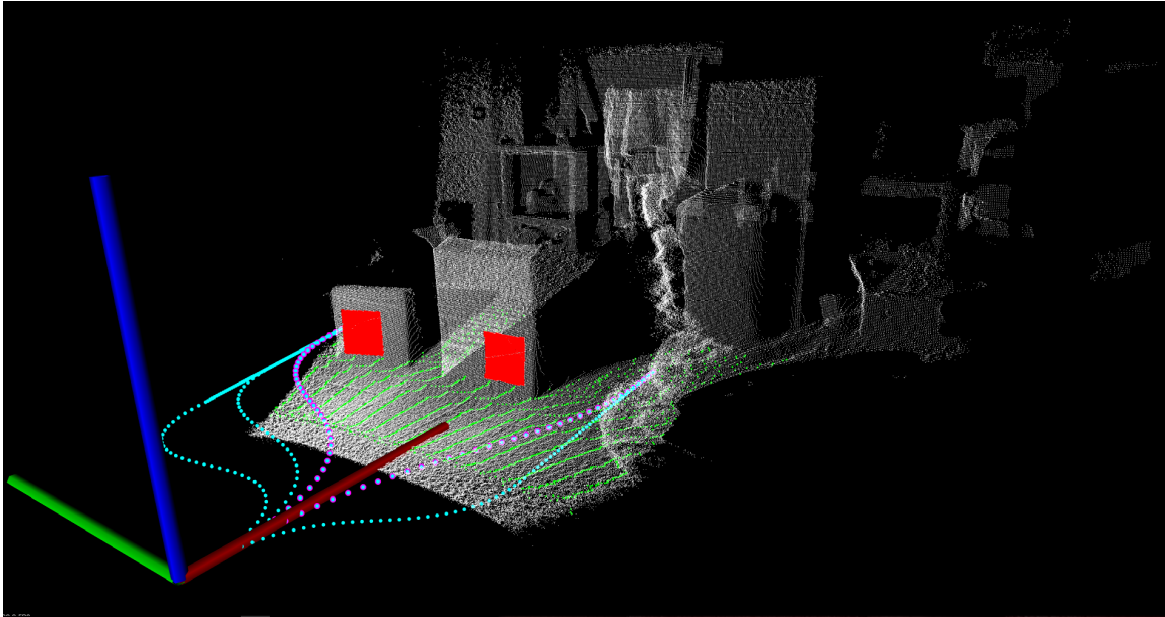
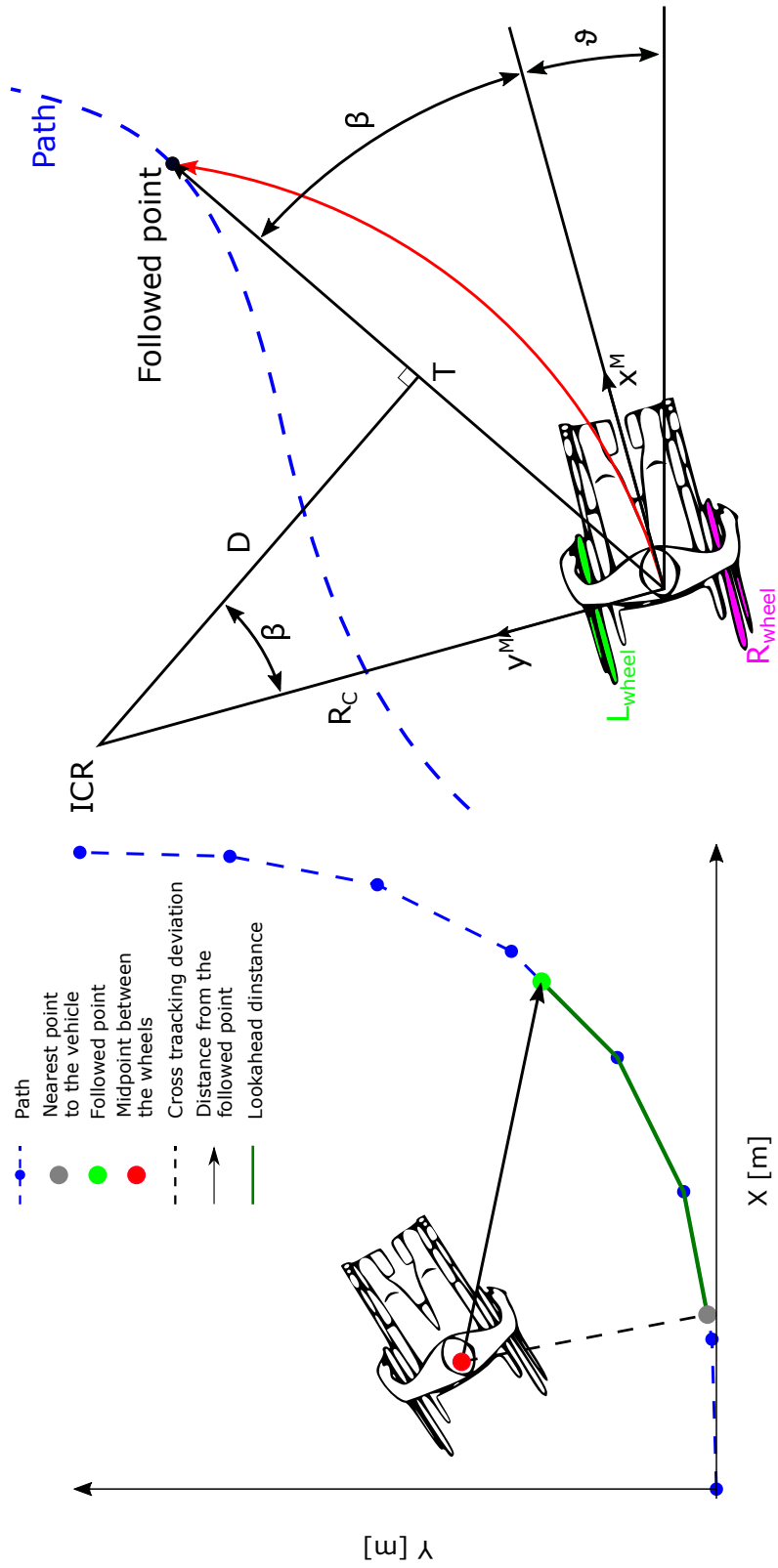


Fig. 5.17 Path planning process.

The odometric localization aims to determine the actual pose of the wheelchair relative to the starting position. In the prototype, this localization algorithm was derived from the odometric recursion from [24], as explained in Section 7.1.1.

The path following algorithm used in the work here reported is based on the Arc Path Following (APF) controller for rhombic like vehicle reported that is presented by Silva et al. [70]. The path following task uses the information coming from the localization processes and determines the nearest point of the reference path. To this position, it is added certain distance as curvilinear coordinate (look ahead distance), obtaining in this way the point that has to be reached as shown in Fig. 5.18a. After that, the algorithm determines the Instantaneous Centre of Rotation (ICR) required to create the circular path that connects the actual position to the tracking point, Fig. 5.18b.



(a) Path followed by the wheelchair

(b) Arc Path Following controller representation

Fig. 5.18 Path following graphical representation.

5.5.5 Serial communication

This service is dedicated to the management of the data exchange between the Windows PC and the RoboteQ SDC2160 DC motor controller through an RS-232 serial interfaces. The data exchanged are related to:

- Speed of the wheels (acquired and setted);
- Encoder ticks;
- Electro-mechanical brake status (acquired and setted);
- Actuators signals (for example tilt of sitting);
- Safety button status;
- Switch of requirement;
- Battery voltage;
- Watchdog counter.

5.5.6 Management of the wheelchair layout

This service is directly connected with the tilt state of the state machine described in the following section. The wheelchair is stopped and the HMI shows the page related to the setting of the layout of some part of the system. In particular, on the prototype developed was possible to change the attitude of the sit by choosing the proper button on the screen. In this way, the system acts on a piston connected to the sit.

5.5.7 Status management of the system

The overall application, running on the Windows PC, was developed using a state machine, a concept used in designing computer programs or digital logic. There are two different types of state machines: finite and infinite. The application developed on the eye-controlled wheelchair includes the first type, the most widely used. This type of state machine is composed of a finite number of states, transition, and actions that are modelled with a specific flow where the logic path is detected when certain conditions occur. A state machine workflow is characterized by an active state that performs basic tasks such as reading a series of inputs. Basing on this basic logic operations, each state specifies which is the following state and when the switch should be performed. The main benefits of using a state machine are hereafter reported:

- A very clean layout or map of the application control;
- Very clear point to add new functionalities of features;
- Cleaner, smaller and very specific code to each state;
- It is easy to extend the application logic by simply adding other states.

The master service (service number 9) manages the status of the state machine. It collects information the requests from all the other services, decides the right time to perform the switch notifying it to all the services. The states used in the application are:

Idle: the wheelchair is stopped, the user can choose to start the navigation or change the main setting (maximum speed or sitting layout);

Manual: direct navigation is activated, the user is driving the wheelchair by looking on the screen;

SemiAuto: semi-automatic navigation is activated, the wheelchair is following the selected path;

Tilt: the HMI shows the page useful to change the tilt angle of the sit, the wheelchair is stopped in this state;

Sleep: the HMI is switched off to optimize the power consumption;

Error: some dangerous situations was detected, the system remains in safe mode until the alerts will be solved.

In addition, the master service manages the acknowledge and *keep alive* signals. All the services notify periodically that they are working properly. If the master service doesn't receive the *keep alive* notification within a certain time it put the system in safe mode (error status).

Chapter 6

Wheelchair Direct Eye Control

6.1 Direct Drive Modality

The direct drive modality, also called "manual navigation", aims to provide versatile maneuverability, with reduced jerks, and an overall comfortable experience [55]. The wheelchair user can act directly on the motor by selecting the desired velocities that are proportional, under different laws, to the gaze position on the screen. During the research work, the development of the direct drive modality involved two different phases in order to design the Human Machine Interaction (HMI) and optimize the related parameters.

In the first phase was developed two different HMIs interfaces using a novel paradigm of HCI by means of a Virtual Reality (VR) environment. Both the HMIs was evaluated inside a simulated environment by using a set of metrics as inclusive as possible to assess the user performances.

During the second phase, an optimized version of the best interaction design resulted from the previous phase, was included on the prototype of eye-controlled wheelchair. It was then compared with a common commercial driving technology involving the joystick inside an environment structured with an advanced motion tracking system able to localize an object with high accuracy and precision.

The test to evaluate the performance of the HMIs was planned starting from the main property of the system such as usability or comfort of the motion but also considering the main feature of the vehicle. Moreover, the evaluation includes information about eye tracker uncertainty to achieve better performances in usability, comfort during navigation and fault tolerance to noise induced by the intrinsically low accuracy of the interface.

6.1.1 Interaction design in VR simulated environment

As mentioned previously, the HMIs developed aims to minimize the stress of the patient resulting from the intensive use of the system, and at the same time maximize his driving performances and motion comfort. For this reason, the HMI has to be as much intuitive as possible for all the users (i.e. for youngsters and elderly). Moreover, the computed commands must take into account the metrological performances of the eye tracker and the physiological characteristics of the users.

For this purpose, the 3D visible environment was projected on the screen and, on the top part (1/3 of the screen), was overlapped the buttons to start and stop the simulation. This area is the one where the eye tracker is typically subject to a lower accuracy and where the ceiling and a narrow part of the walls are projected, so it has been used for general-purpose commands.

The control of the wheelchair is performed in the remaining central and bottom area. The VR environment was used to develop and optimize the two HMI strategies.

According to the first strategy, the whole screen was divided using a 3x3 grid of virtual buttons. As shown in Fig. 6.1 the top row and the first and third element of the bottom row are reserved for the customization of the graphical interface. The other four areas are used to perform the control of the wheelchair and, in particular, each button corresponds to a fixed set point of maximum linear and rotational speed. The information about the uncertainty gives a measure of the precision of the eye tracker. The HMI strategy takes into account the uncertainty to evaluate the compatibility of the estimated point of sight on the screen with the possible commands. The values of compatibility are multiplied by the velocity set point in order to obtain two simultaneous movements, as in Eq. 6.1.

$$\begin{cases} v_f = C_f \cdot V_{MAX} \\ \dot{\theta}_r = C_r \cdot \dot{\theta}_{MAX} \end{cases} \quad (6.1)$$

Where:

- v_f is the linear velocity;
- C_f is the compatibility with the forward button;
- V_{MAX} is the reference for the linear velocity;
- $\dot{\theta}_r$ is the rotational velocity;
- C_r is the compatibility with the turning right button;

- $\dot{\theta}_{MAX}$ is the reference for the angular velocity;

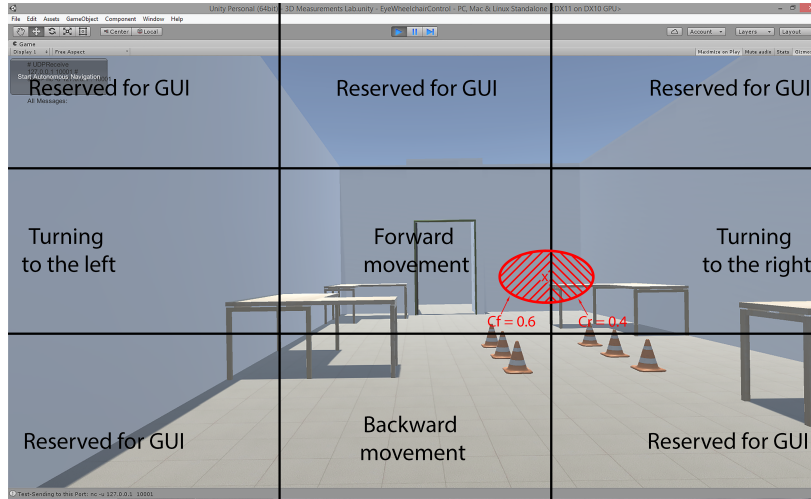


Fig. 6.1 HMI with 3X3 grid buttons. Cf forward and Cr right turning compatibilities.

The second HMI strategy foresees a continuous variation of the two set point velocities with the aim to increase manoeuvrability, reduce jerks, and thus increase comfort, Fig. 6.2. In particular, the traction speed has a trend following a rational control function with two cubic polynomials (Eq. 6.2):

$$F(y) = \frac{-2.29y^3 + 1.18y^2 + 1.13y - 0.017}{y^3 - 4.38y^2 + 1.71y + 2.22} \quad (6.2)$$

The parameters in Eq. 6.2 are obtained by fitting the function model with a set of reference 2D points (screen position vs speed) using a trust region routine. The values of y are in the range from -0.5, corresponding to the bottom side of the screen, to 1 in the top side. The rotation speed follows a linear law from the value -1 rad/s on the left side of the screen to 1 rad/s on the right side, as reported in Eq. 6.3.

$$G(x) = \begin{cases} \frac{3}{W} \cdot x + \frac{1}{2} & (\text{leftside}) \\ \frac{3}{W} \cdot x - \frac{1}{2} & (\text{rightside}) \end{cases} \quad (6.3)$$

where:

- W is the screen width;

For both control functions, a flat zone around the zero, where the wheelchair does not move was inserted. The amplitude of this area is defined to be comparable to the maximum

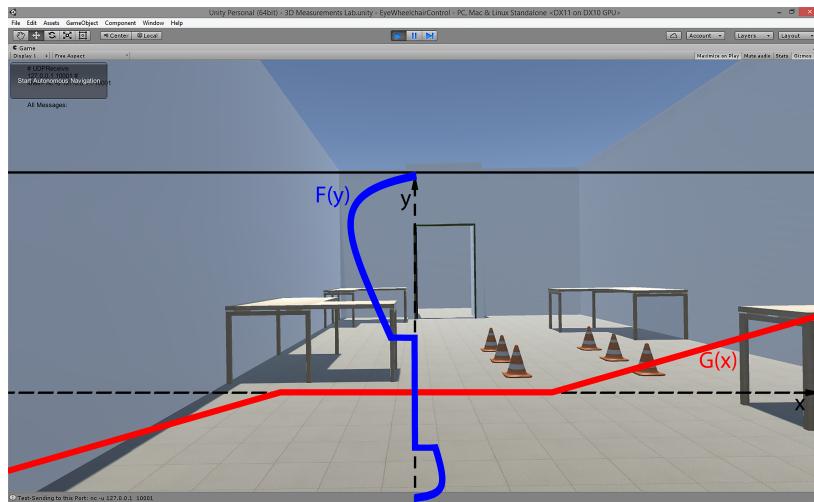


Fig. 6.2 HMI with control functions for translation and rotation.

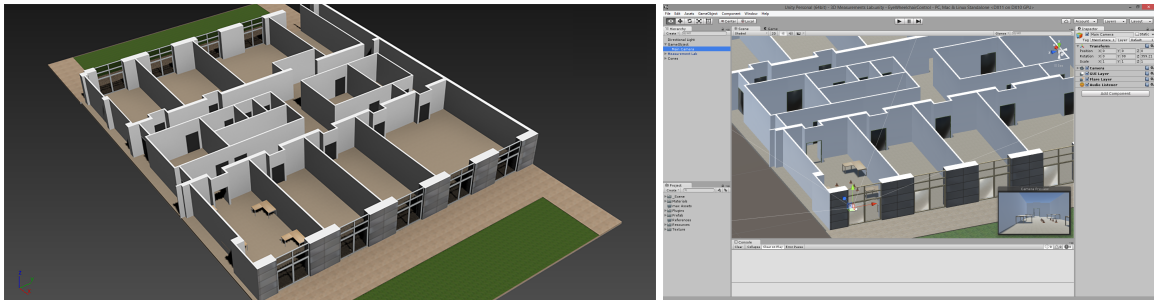


Fig. 6.3 On the left: the 3D environment of the mechatronics laboratory in the modelling application. On the right: the corresponding Unity 3D scenario (Game engine)

eye tracker uncertainty. The reference speed was calculated multiplying the maximum speed by the value of the previous functions.

The eye-controlled Virtual Reality environment

The 3D virtual scenario represents the environment of the mechatronics laboratories of the industrial department. It is developed starting from the 2D map, and completing the missing information using a common 3D modelling application (Fig. 6.3).

The HMI interaction and the wheelchair simulation was developed with UNITY 3D. The game engine permits to obtain a better realistic simulation from a graphical point of view, taking into account the collision with the wall (bouncing on collision) and the dynamics of the wheelchair.

Furthermore, the simulation takes into account the dynamics of the vehicle by means of the field “mass” applied to the rigid body component and viscous friction. Both the kinematics and friction models are very simplified. The kinematics of the wheelchair is a unicycle while the friction simulates the rotational friction along the wheel axis and the wheel lateral slippage. The control of the wheelchair is achieved providing a reference velocity that the object reaches imposing a maximum acceleration law (bang-bang control) to the rigid body. Each dynamical update is computed at a fixed timestamp like in a real-time operating system, see Eq. 6.4. During each “FixedUpdate” cycle, the application estimates the variation of the linear and rotational velocity taking into account the HMI commands that provide the reference linear and angular velocities. In this way, the behaviour of the two velocities follows a common trapezoidal trend characterized by a speed limit equal to the reference provided by the HMI, shown in Fig. 6.11.

$$\begin{cases} v_k = v_{k-1} + a \cdot \Delta t_{frame} \\ \dot{\theta}_k = \dot{\theta}_{k-1} + \alpha \cdot \Delta t_{frame} \end{cases} \quad (6.4)$$

Where:

- v_k is the linear velocity at k-th frame;
- a is the bang-bang maximum forward acceleration;
- $\dot{\theta}_k$ is the rotational velocity at k-th frame;
- α is the bang-bang maximum angular acceleration;
- Δt_{frame} is the time between two consequent frames;

6.1.2 Interaction design on the eye controlled wheelchair

The driving interface is based on a continuous law that controls two set point velocities, frontal and angular in order to provide a versatile manoeuvrability, with reduced jerks, and overall comfortable experience. The idea is similar to the ones proposed in the previous chapter and published on [55] with some modification in the functions to calculate the velocities to reduce jerks and increase the manoeuvrability and thus the comfort. The main difference involves the part of the HMI devoted to the GUI and thus to start/stop of the manual navigation or to select the backward movement. On the real prototype, the eye tracker is mounted on the monitor that is placed in front of the user. The video stream coming from the 3D camera is displayed on the screen. It is augmented with the information related to

the GUI such as the start/stop or backward buttons, the planned path or the points of interest detected. Some test on the first prototype highlighted the importance to tilt the camera in order to see a part of the user body (i.e. feet or knee) inside the interface, increasing in this way the depth perception. Usually, with this camera attitude and the limited vertical field of view of the camera, the top part of the interface shows the surrounding environment at a distance of few meters resulting very important for the control of the wheelchair. Due to these reasons, the area of the HMI devoted to the GUI was moved to the central bottom part of the screen leaving all the other part to the velocity estimation.

Each set point velocity is characterized by two part: a control law with a linear trend normalized with respect to the size of the screen (Eq. 6.5) and a maximum speed selected by the user. The values of velocity are calculated by multiplying the result of the control law (between 0 and 1) by the maximum value of speed. In particular, the control law values increase moving the gaze from the central bottom part of the screen to the external corners, where it takes the maximum value. The proposed control laws foresee the continuous variation of frontal and angular velocities with two, different, shapes: rationale for the forward direction, and a linear for the rotational one. For both control functions, a *rest zone* in the central bottom part of the monitor was defined. When looking at such area, the wheelchair does not move. The amplitude of the area is defined to be comparable to the maximum eye tracker uncertainty, basically 100pixel in our initial setup [34] and the dynamically adjusted with respect to the uncertainty value. The forward control law value starts to increase after 25% of the height of the monitor while the rotation value remains zero in the 30% central part of the screen. By looking in the central bottom part of the screen the two values of control law are set to zero, leaving in this way the space for the start and stop buttons. In the same central bottom part of the screen are located the reverse buttons. The maximum values of speed can be changed by the user selecting the different drive modalities, from the slowest to the quickest one.

Equation 6.5 determines the control value of the forward velocity. The variable y is calculated considering the gaze position according to the reference system of Fig. 6.4 and normalizing it with respect to the screen height.

$$F(y) = \frac{-2.29y^3 + 1.18y^2 + 1.13y - 0.017}{y^3 - 4.38y^2 + 1.71y + 2.22} \quad (6.5)$$

The value of y is determined using the Eq.6.6:

$$y(y_P) = \frac{y_P - y_{NAZ}}{H - y_{NAZ}} \quad (6.6)$$

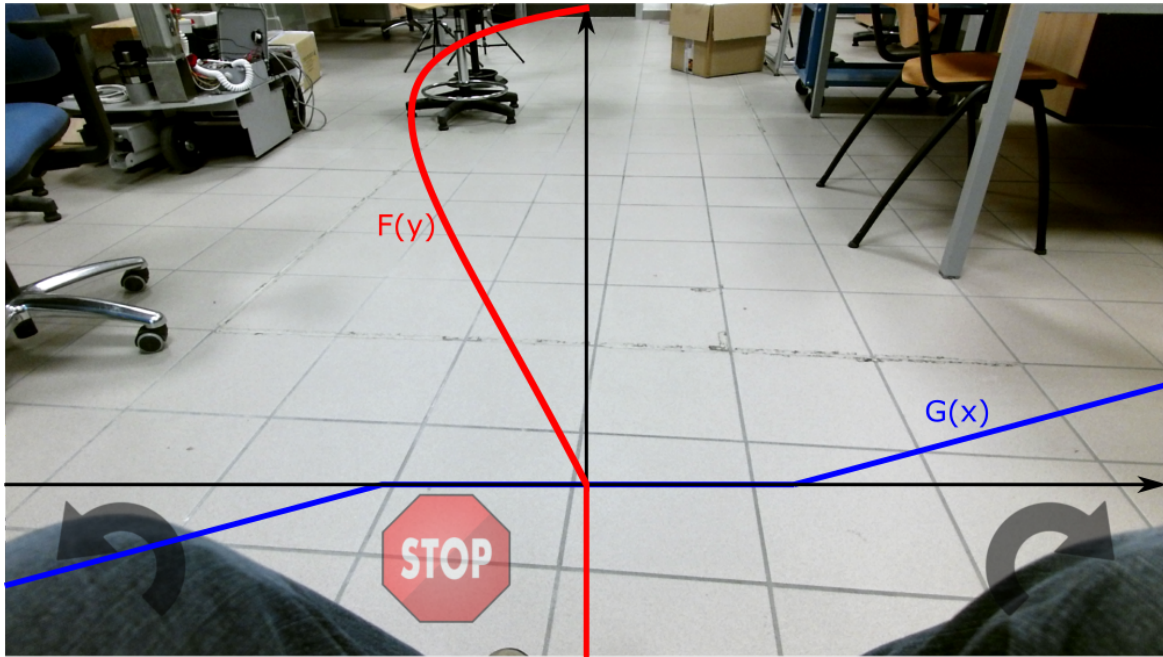


Fig. 6.4 Control laws of the velocity profiles.

Where:

- y_P is the actual position, along y direction, of the gaze on the screen;
- H is the height of the screen;
- y_{NAZ} is the part of the screen where the speed has to be set to zero;

The forward speed (Eq. 6.7) is simply determined by multiplying the positive value of the control calculated above (Eq. 6.5) by the maximum value of forward speed.

$$FrwSpeed = \begin{cases} V_{frwMax} \cdot F(y), & \text{if } F(y) > 0 \\ 0, & \text{if } F(x) \leq 0 \end{cases} \quad (6.7)$$

Where: V_{frwM} is the maximum values of the forward speed.

The lateral speeds are calculated using the same approach of the forward velocity. The control law for the right and left movement are represented by the Eq. 6.8. Also in this case, the variable y_P is calculated considering the gaze position according to the reference system of Fig. 6.4 and normalizing it with respect to the screen width.

$$\begin{aligned} G_{Left}(x_P) &= \frac{2 \cdot (x_P + x_{NAZ})}{W - x_{NAZ}}, \\ G_{Right}(x_P) &= \frac{2 \cdot (x_P - x_{NAZ})}{W - x_{NAZ}} \end{aligned} \quad (6.8)$$

Where:

- x_P is the actual position, along x direction, of the eye on the screen;
- W is the width of the screen;
- x_{NAZ} is the part of the screen where the speed has to be set to zero;

The lateral speed is determined using the Eq. 6.9.

$$\begin{aligned} LatSpeed_{Right} &= \begin{cases} V_{latMax} * G_{Right}(x_P), & \text{if } G_{Right}(x_P) > 0 \\ 0, & \text{if } G_{Right}(x_P) \leq 0 \end{cases} \\ LatSpeed_{Left} &= \begin{cases} V_{latMax} * G_{Left}(x_P), & \text{if } G_{Left}(x_P) < 0 \\ 0, & \text{if } G_{Left}(x_P) \geq 0 \end{cases} \end{aligned} \quad (6.9)$$

Where: V_{latM} is the maximum values of the lateral speed.

For both control functions, the *rest zone* is defined in the central bottom part of the monitor, gazing at that area implies no motion by the wheelchair. The dimensions are around equal to 1/3 of the screen resolution for both directions and are dynamically adjusted by linearly increasing them with respect to the online assessment of eye tracker uncertainty up to a maximum of 1/2.

The eye tracker uncertainty is also considered in the identification of the speed: the most probable value of the velocity function insider the uncertainty area of the gazed point is considered as the target value. The reference speed for the driver is obtained by multiplying the maximum speed by the aforementioned value.

6.1.3 Test plan

The assessment of a driving performance has to evaluate the limitations that characterize the system and its interfaces. From Literature, it is possible to identify some methodologies and guideline, usually derived from known drive tests, like the Miller Road Test [78].

The performance evaluation of the manual navigation driving technique explained above was performed through two different scenarios. The first one included the VR-based simulation of an indoor environment in order to evaluate the two innovative HMIs. Fig. 6.5 shows the virtual test environment developed in Unity 3D game engine. In the second scenario was compared the performances of the prototype of eye-controlled wheelchair developed with respect to a commercial wheelchair controlled through a standard joystick. The evaluation involves the design of a specific environment to collect the position and the attitude of the wheelchair with high accuracy and repeatability (millimeters) in order to analyse the driving behaviour of the subject with respect to the driving interface. The designed environment includes some standardized movements for the wheelchair user capability assessment, Fig. 6.6.

The first step of the experimental verification was the definition of suitable metrics useful to quantify the driving performance, the usability of the HMI and the comfort of the user. Therefore, a complete and meaningful evaluation should consider different metrics related to the vehicle management, the comfort of the user, but also his/her cognitive and the emotive response of to different stimuli [54, 72, 79].

Hereafter, the main categories considered for both the scenarios are:

- **Vehicle Metrics**

- **Manoeuvrability Metrics:** related to vehicle position and orientation, lane positioning, driving speed, vehicle steering angle, brake distances. These metrics assess the skill and driving capability of the user.
- **Comfort Metrics:** related to the motion characterization, longitudinal and lateral acceleration, jerk, vibrations, smoothness [14]. Derived from standard ISO 2631-1 [33], these metrics identify under which conditions the driving results comfortable, uncomfortable, or even potentially harmful for the subject.

- **Human Metrics**

- **Cognitive Metrics:** related to the locus of attention or cognitive workload of the driver, usually obtained through interaction with an examiner under the different testing condition, i.e. detection of signs, time to perform a given computation, the accuracy in committing items to memory. These metrics assess the level of mental load required to use the interface and to drive.
- **Subjective Metrics:** include norms of driving performance that are difficult to assess by automated means or do not include cognitive issues of driving workload,

interactions with the domestic spaces, responses to persons, obstacles, etc. Direct feedback from subjects, useful for usability estimation.

More in detail, the metrics adopted for the kinematic analysis were:

- *Circuit*: the user has to follow a given path marked on the floor. The performed path is recorded and compared with a reference one, which must be followed minimizing the lateral displacement of the wheelchair. In Fig. 6.5 and Fig. 6.6 the path following test is highlighted with "A". The path designed for the evaluation of the interface on the real prototype (Fig. 6.6, A) considers the skills related to the WST protocol.
- *Manoeuvring*: the user has to drive through a series of cones as quickly as possible, without touching any of them. The cones are positioned on a wide flat section of the floor. The time to complete the manoeuvring task is recorded. In the simulated environment, each cone touched or knocked over is recorded and considered as an error score. In this case, the manoeuvring score is calculated as the time to complete the task plus a time penalty for each error. The manoeuvring test is marked in Fig. 6.5 and Fig. 6.6 with the letter "B".
- *Depth perception*: the user has to drive from a starting point till an ending reference marked on the floor, represented by a line on the ground. He/she has to complete the task at the highest possible speed but stopping as close as possible to the reference. The deviation between the final position of the wheelchair and the reference is recorded. In the simulated environment, the time taken to complete the task is recorded. In this case, the depth perception score is calculated as the time required to complete the task, plus a penalty score depending on the final gap between the wheelchair and the target. Fig. 6.5 and Fig. 6.6 highlight the depth perception test with the letter "C".
- *Comfort assessment*: parameter calculated from the longitudinal and the lateral acceleration and jerk analysis. The standard ISO 2631-1 proposes a comfort assessment based on the root mean square (RMS) of the weighted accelerations:

$$a_{RMS}(kT) = \left[\frac{1}{T} \int_0^T a_w^2(t) dt \right]^{\frac{1}{2}} \quad (6.10)$$

where:

- $a_w(t)$ is weighted acceleration. Horizontal (lateral and longitudinal) accelerations are weighted using a human transfer function defined in the standard;

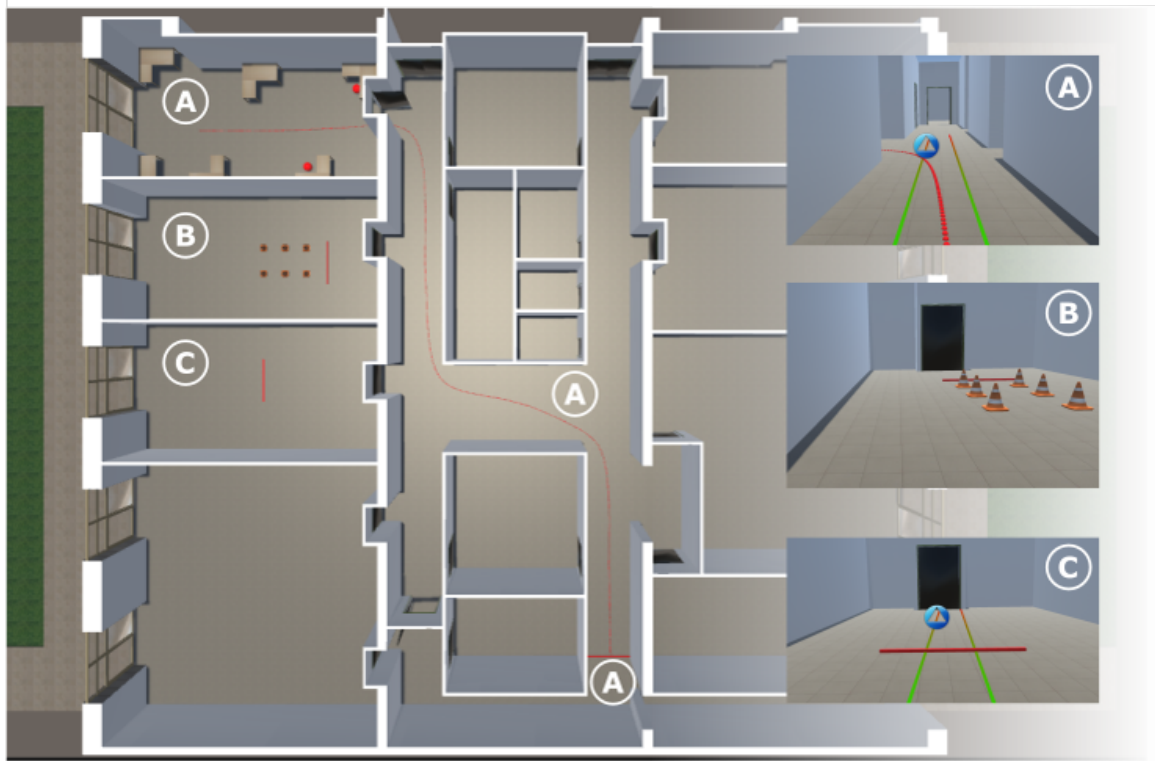


Fig. 6.5 UNITY virtual test environment.

- T is the time interval for the RMS evaluation;
- $a_{RMS}(kT)$ is weighted RMS acceleration, function of the k -th T period;

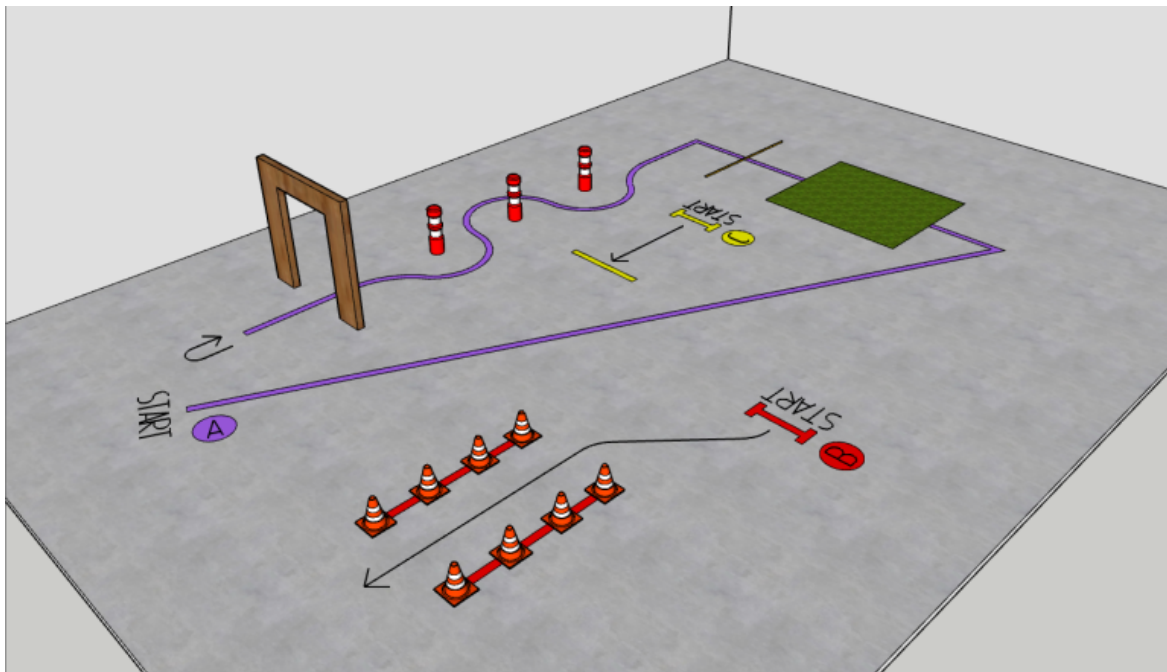


Fig. 6.6 Rendering of the real test environment.

6.2 HMI performance evaluation in VR environment

As previously mentioned, the development of the direct drive modality foresaw two phases in order to design the HMI and optimize the related parameters. The first phase involved, as presented in the previous chapter, the development of two HMIs interfaces and a VR environment where the two strategies were tested. The evaluation of the performance of the two HMI included seven subjects.

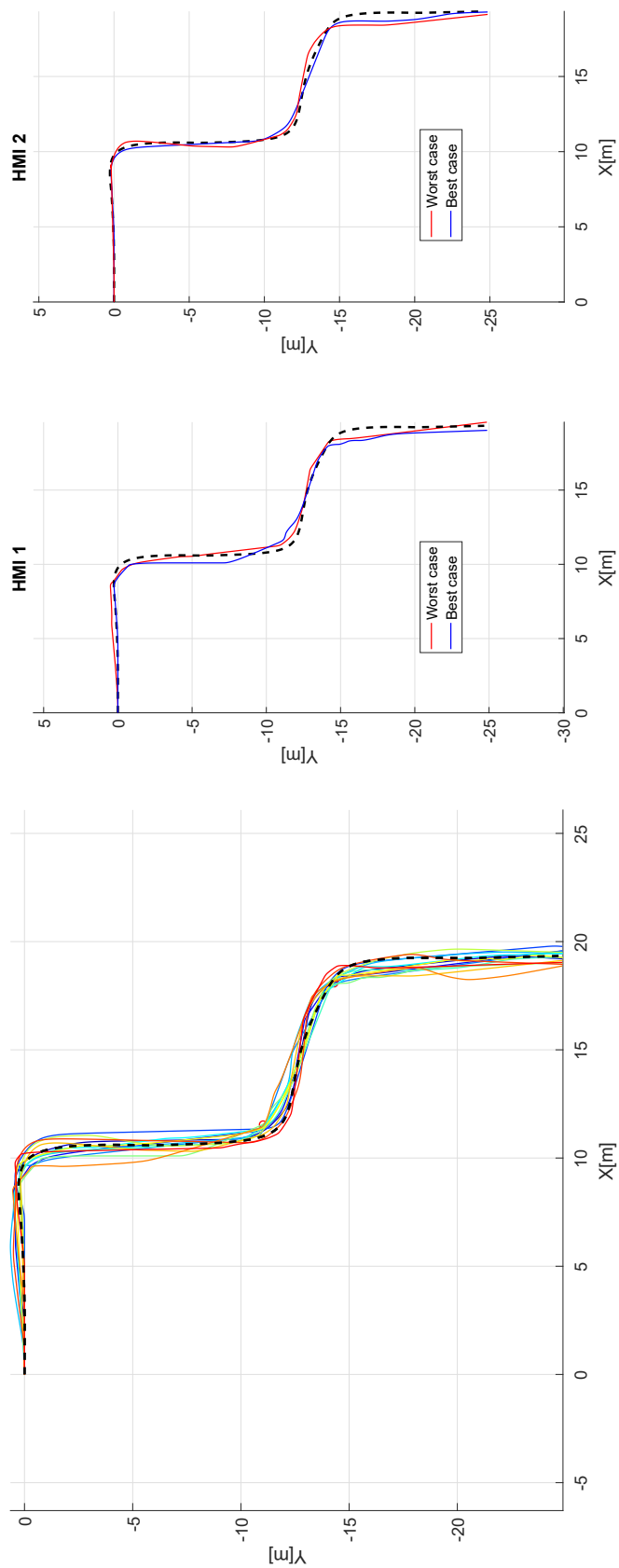
The assessment of the driving performance is performed evaluating some metrics related to the vehicle, to the comfort and to the user feeling. Each user performed the three task showed in Fig. 6.5 that is useful to evaluate metrics such as circuit, manoeuvring, depth perception and comfort. The evaluation is based on a penalty score for each metric considered. In this way, it is possible to merge all the features affecting the performance such as the deviation from the reference path, the time, the number of collisions, the speed or the accelerations. For this purpose was defined some weighting factors that are multiplicative coefficients used to combine the different elements of the test into a homogeneous representation as a unique meaningful penalty score. Higher penalty scores characterize the worse overall driving performance. The weights are defined by the designer of the tests considering the purposes of the simulation, the application field and the potential risk levels of the equivalent real application. The values are defined before the testing phase and kept constant for all subjects. For the sake of completeness, each factor of the penalty function is provided separately.

The test protocol starts with a training phase during which each user familiarizes with both the HMI. In this initial part, the subjects perform a sufficient number of trials to fully understand and properly manage the driving technique (self-assessment given by the users). The subjects can take all the time they need to practice on each task of the test and on the environment by using an ocular control technology.

After the training phase, the subject is instructed on the parameters of test that are under monitoring, the associated metrics, and weighting factors. At this point, the subjects performed each test once. The data is here recorded and analysed using the metrics described in subsection 6.1.3.

6.2.1 Results analysis of the circuit metric

The objective of the test is to follow a given path inside an indoor environment. The main difficulty of the test is to not collide with the walls while following the reference.



(a) Full set of executed paths

(b) Best and the Worst case for both HMIs

Fig. 6.7 Paths performed during the circuit test in VR.

All subjects reached the final position with a very limited number of collisions performing similar trajectories. However, the paths obtained using the second HMI achieved smoother trajectories compared to the ones obtained using the first HMI. Fig. 6.7 shows the best and worst obtained paths (lowest and highest penalty) for both the HMIs. Eq. 6.11 indicates the metric used to assess the driving performances of the subjects and the HMIs. In Table 6.1 the results of the tests are reported.

$$P_{Ci} = \Delta t + wf_{RMS} \cdot \Delta p_{RMS} + wf_{hit} \cdot N_{hits} \quad (6.11)$$

Where:

- P_{Ci} is the penalty score of the circuit test;
- Δt is the time interval from the first motion till the reaching of an imaginary line at the end of the circuit;
- Δp_{RMS} is the RMS distance from the reference path;
- wf_{RMS} is the weighting factor for RMS distance: 1 seconds for each 0.1 meters. The value is meant to penalize those trajectories affected by a displacement bias or ones with a strong variability around the reference trajectory;
- N_{hits} corresponds to the number of collisions with the environment;
- wf_{hit} is the weighting factor for collisions: 2 seconds for each collision. The value is the same used for the manoeuvrability metric;

Fig. 6.8 shows the comparison between the penalty scores achieved with the two HMIs. Lower values of penalty scores correspond to better driving performances. Six out of seven subjects achieved better performances (lower penalty) with second HMI. The parameter that mostly influences such results it is the time required to complete the task: when using the first HMI the users are usually slower. Such operative condition is due to a limitation in performing the turns maintaining a constant frontal speed. With the first HMI, the user can control only one element per time, frontal or angular velocity; the compatibility analysis on the active areas helps the user to provide hybrid driving control in speed but still such driving interface implies a strong loss in the management of the frontal feed. We can then conclude that the second HMI seems to provide a more agile driving experience.

Table 6.1 Results of circuit metric.

Subject	HMI	Time [s]	RMS D [m]	Collisions	Penalty [s]
1	1	160.8	0.270	0	163.5
	2	133.4	0.195	1	137.3
2	1	139.2	0.309	0	142.3
	2	127.2	0.333	0	130.5
3	1	146.2	0.240	0	148.6
	2	133.1	0.282	1	137.9
4	1	121.6	0.397	0	125.6
	2	121.1	0.233	0	123.4
5	1	132.4	0.207	0	134.5
	2	135.7	0.235	0	138.1
6	1	149.7	0.533	0	155.0
	2	149.5	0.328	0	152.8
7	1	158.7	0.248	0	161.2
	2	140.9	0.242	0	143.3

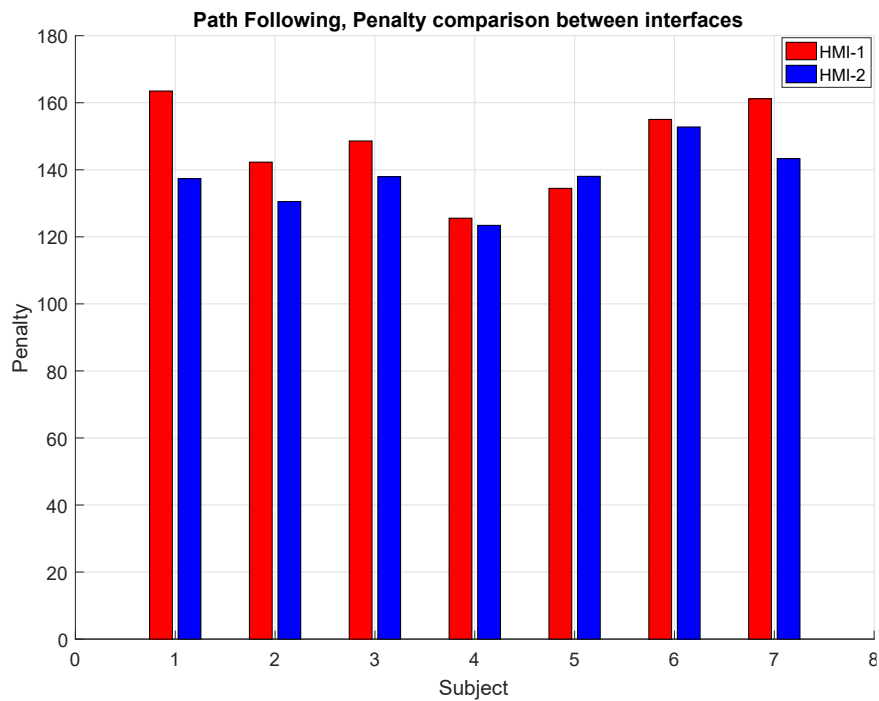


Fig. 6.8 HMIs penalties comparison for the circuit test in VR.

6.2.2 Results analysis of comfort metric

The aim of this metric is to assess the level of comfort experienced by the user on the virtual wheelchair. The metric is developed according to the ISO 2631-1 guidelines and the related literature [14]. Table 6.2 reports result of the tests related to the comfort metrics. The assessment of the performance concerning the comfort of the user is determined though Eq. 6.12 indicates the metric used.

$$P_{Co} = wf_{RMS} \cdot \bar{a}_{RMS} + wf_{RMS} \cdot \max(a_{RMS}) \quad (6.12)$$

Where:

- P_{Co} is the penalty score for comfort analysis;
- \bar{a}_{RMS} is the mean of the RMSs accelerations (longitudinal and lateral) along the path (period for the RMS evaluation set to 2 seconds);
- $\max(a_{RMS})$ is the maximum value of the RMSs longitudinal accelerations (frontal and lateral) along the path;
- wf_{RMS} is the weighting factor for the comfort level: 0 if a_{RMS} is within the range of comfort, 2^n otherwise, where n is an index of the level of comfort (1 is *a little uncomfortable*, 5 *extremely uncomfortable*). The values are set to penalize the occurrence of acceleration spikes and continuous variations of acceleration associated to an RMS value over threshold;

In all tests, the resulting acceleration, main parameter for the comfort assessment, remains under the threshold associated to the *comfortable* level (an RMS less than 0.314 m/s^2). Nevertheless, it must be underlined that the level of RMS accelerations is lower in the case of the first HMI; such result is mainly due to a more stable frontal speed when moving. With the second HMI, the continuous control law, together with the eye tracker uncertainty, causes small but continuous variations of the frontal speed, with associated frontal accelerations, resulting in a potentially less comfortable driving experience.

6.2.3 Results analysis of manoeuvring metric

The objective of this test is passing through a set of cones, starting the manoeuvre aligned with the passing direction but from both a lateral and longitudinal displacement. This test mimics a change of line manoeuvre. In Fig. 6.9 the overall results are shown. The first

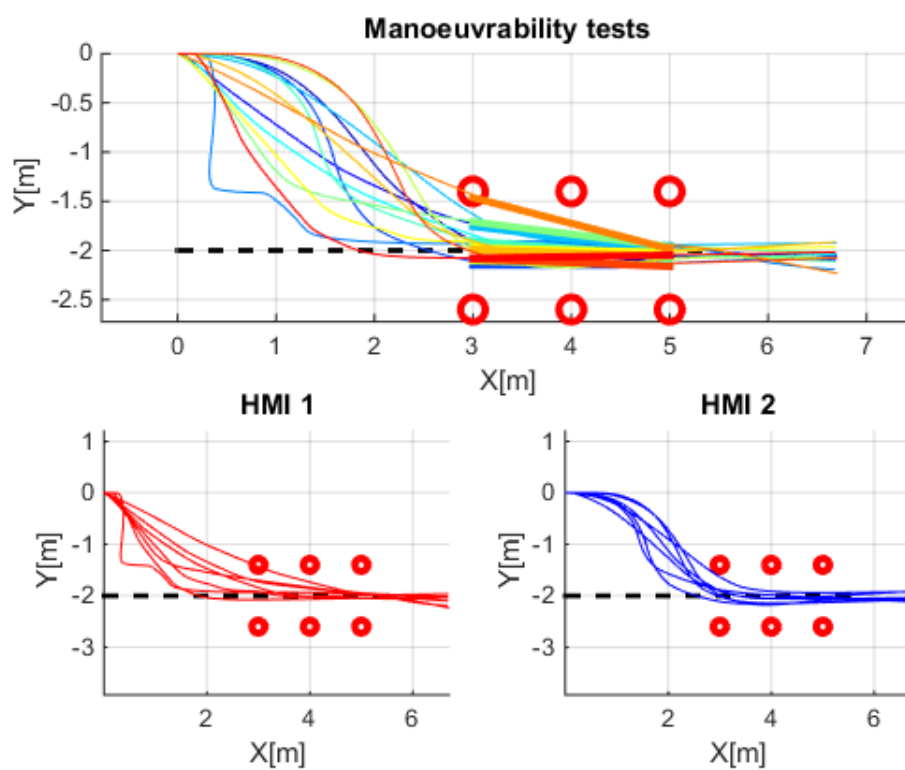


Fig. 6.9 Paths performed during the manoeuvring test in VR. On the top: full set of executed paths. On the bottom: a comparison between the path obtained the single HMI.

Table 6.2 Results of comfort metric.

Subject	HMI	Mean a RMS [m/s^2]	Max a RMS [m/s^2]	Penalty [s]
1	1	0.016	0.043	0
	2	0.039	0.140	0
2	1	0.015	0.073	0
	2	0.022	0.091	0
3	1	0.012	0.052	0
	2	0.029	0.113	0
4	1	0.020	0.056	0
	2	0.021	0.089	0
5	1	0.020	0.057	0
	2	0.029	0.129	0
6	1	0.022	0.061	0
	2	0.049	0.167	0
7	1	0.015	0.044	0
	2	0.030	0.095	0

important noticeable element is that subjects involved in the tests perform smoother motions using the second HMI.

The metric used for the assessment of the manoeuvrability is presented in Eq. 6.13, and Table 6.3 reports the data collected and the results of the metric.

$$P_M = \Delta t + wf_{hit} \cdot N_{hits} + |\vartheta| \cdot wf_{\theta} \quad (6.13)$$

Where:

- P_M is the penalty score of the manoeuvring test;
- Δt is the time interval from the first motion till the reaching of an imaginary line at the end of the cones;
- N_{hits} corresponds to the number of cones hit in the test;
- wf_{hit} is the weighting factor for hitting a cone: 2 seconds for each cone. The weighting factor is chosen to penalize a potentially dangerous manoeuvre due to a collision with objects or environment. The specific value of 2 seconds is set in order to assign a moderate penalty to the score;

Table 6.3 Results of manoeuvring metric.

Subject	HMI	Time [s]	Cone Hits	Entry angle [rad]	Penalty [s]
1	1	40.0	2	-0.113	56.9
	2	28.1	1	-0.060	37.0
2	1	44.9	0	-0.011	46.1
	2	27.3	2	0.001	31.4
3	1	31.1	1	-0.087	43.1
	2	25.8	1	-0.121	41.6
4	1	29.5	2	-0.124	47.7
	2	27.1	0	-0.071	35.2
5	1	34.9	0	-0.022	37.5
	2	25.4	2	-0.023	32.0
6	1	39.1	2	-0.255	72.3
	2	29.7	0	-0.035	33.7
7	1	42.2	0	0.015	43.9
	2	26.1	2	-0.037	34.4

- ϑ is the angle of the trajectory performed through the cones as linear segment
- wf_{θ} is the weighting factor for the alignment mismatch between the reference direction (defined by the cones) and ϑ : 2 seconds for each degree. The factor is chosen to penalize the wrong positioning during the manoeuvre. The value is equal to wf_{hit} in order to give the same importance to both elements in the test

According to the application, each weighting factor value can be increased or reduced. An example could be the HMI control of a space rover, in this case, the main objective is to avoid collisions with obstacles (i.e. rocks) and so wf_{hit} should be increased. In the case of long vehicles, the alignment with the loading station is a mandatory requirement, in those cases, it would be recommendable a higher value of wf_{θ} . In our case the alignment is an important parameter since the capability to reach a position in space with the desired attitude is a fundamental element for usability of the system as far as the user, in this way, minimizes the need for continuous realignments.

In Fig. 6.10 the relation between the penalty scores achieved using the first HMI or the second one are reported. The distributions underline and confirm what already stated in the circuit metric, namely that the second HMI offers a more agile interface. When using the second HMI the users are able to perform the task in a less amount of time. Regarding the

accuracy in manoeuvring, no explicit evidence was found to state that the second HMI is better than the first one. The number of cone hits and angular driving does not highlight the presence of particular trends; in fact, the accuracy seems then related more to the driving skills of the subject rather than to the HMI used.

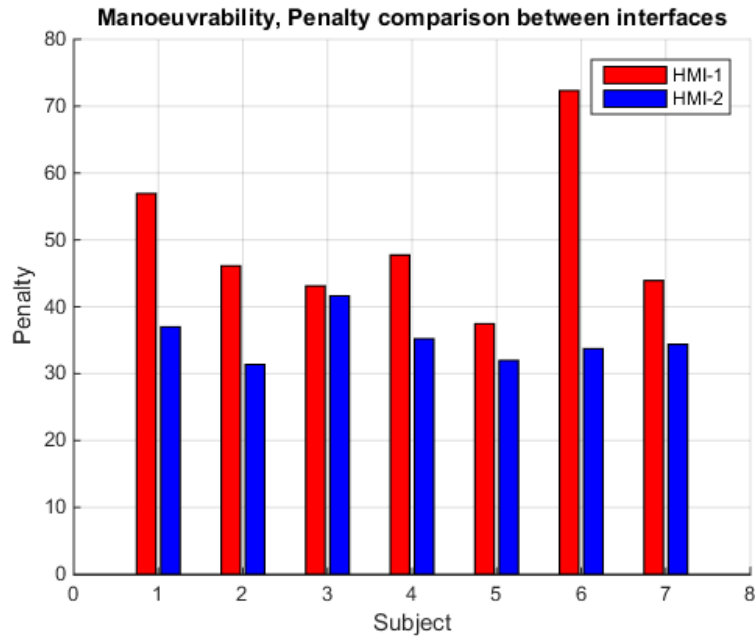


Fig. 6.10 HMIs penalties comparison for the manoeuvring test in VR.

6.2.4 Results analysis of depth perception metric

In this case, the analysis aims at assessing the depth perception of the subjects when using the proposed HMIs. The test requires the movement at the maximum possible speed and stopping the motion as close as possible to a transversal line placed 5 meters 5 meters ahead of the starting position. The difficulty of the test is that the frontal view displayed on the monitor implies the visual loss of the ending line when the wheelchair approaches the line, due to the limited field of view of the virtual (and real) camera. This element forces the subjects to extrapolate the position of the line in order to estimate the relative distance and perform the stop manoeuvre at the proper time.

The metric used to assess the depth perception is the one in Eq. 6.14. Table 6.4 reports the collected data and the corresponding results.

$$P_D = \Delta t + w f_p \cdot |\Delta p| + w f_v \cdot \Delta v \quad (6.14)$$

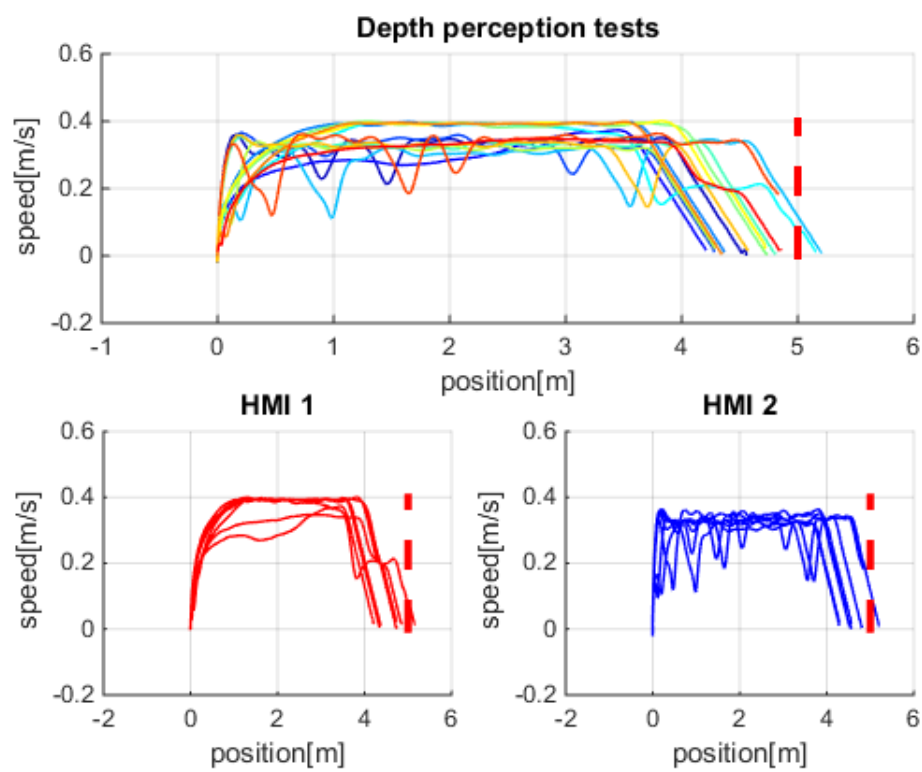


Fig. 6.11 Speed of the virtual wheelchair during the depth perception test in VR referred to the position. On the top: full set of performed speed. On the bottom: a comparison between the speed obtained using the single HMI.

Where:

- P_M is the penalty score of the depth perception test;
- Δt is the time interval from the first motion till the reaching of the target;
- Δp is the distance between the ending line and the vehicle when this one is stopped (end of the test);
- wf_p is the weighting factor for the final distance: 2 seconds for each 0.1 meters before the line, 3 seconds for each 0.1 meters after the line (the crossing of a limit it is commonly considered a worse scenario than an early stop);
- Δv is the difference between the maximum admissible speed and the one reached by the user;
- wf_v is the weighting factor for the maximum speed mismatch: 0.5 seconds for each 1 m/S. The difference between the maximum possible speed and the one reached by the subject is a parameter also related to the time used to finish the test. This weighting factor is set to have a moderate effect on the metric since the time it is already included and the element of main interest is the distance from the reference line;

In Fig. 6.12 the relation between the penalty scores achieved using the first HMI or the second one are shown. The distributions are similar, not underlying particular evidence or differences in performances in depth perception. None of the subjects, independently of the HMI, managed to stop closer than 10 centimeters from the line.

An interesting fact can however be derived from Fig. 6.11. The main discrepancy between the HMIs is the speed management. When using the first HMI, the subjects are able to maintain a more stable speed. Such trends can be addressed to the behaviour of the eyes during the motion. During the approach to the line, the user tends to gaze such a specific point on the display, tracking it, in order to have a spatial reference. When the line exits from the field of view, the subject loses the reference marker and starts using the eyes in a more proper way, controlling the velocity through the HMI. This behaviour has different results in the two HMIs. In the first HMI, it has a limited influence thanks to the intrinsic filtering effect coming from the rather large dimensions of the active areas (variations of gaze inside the active square do not influence the final velocity command). In the second HMI, the variation of gaze causes a variation of the frontal speed, so the subject must continuously correct the speed.

Table 6.4 Results of depth perception metric.

Subject	HMI	Time [s]	Distance [m]	Max Speed [m/s]	Penalty [s]
1	1	20.3	-0.787	0.373	28.2
	2	22.6	-0.439	0.361	27.0
2	1	19.7	-0.631	0.398	26.0
	2	20.0	-0.720	0.366	27.2
3	1	25.1	0.157	0.396	29.8
	2	24.7	0.203	0.346	30.8
4	1	23.3	-0.267	0.400	26.0
	2	22.7	-0.194	0.352	24.7
5	1	17.8	-0.280	0.400	20.6
	2	19.0	-0.719	0.339	26.2
6	1	22.8	-0.655	0.398	29.4
	2	21.1	-0.428	0.359	25.4
7	1	22.8	-0.138	0.347	24.2
	2	16.0	-0.158	0.364	17.6

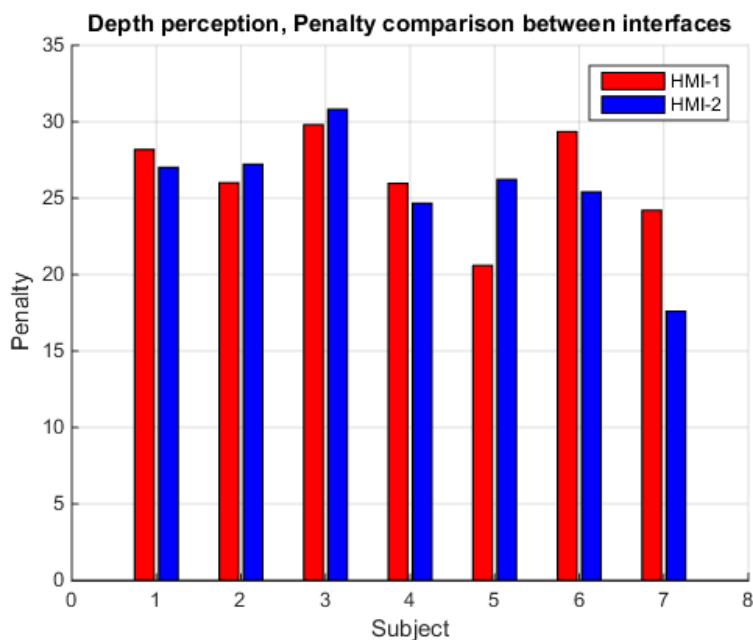


Fig. 6.12 HMIs penalties comparison for the depth perception test in VR.

6.2.5 Discussion of the results

This paper focuses on the development of optimized strategies of HMI based on eye trackers by means of a Virtual Reality (VR) environment where several motion metrics were evaluated. To this aim, we developed two HMI. The first HMI is button based while the second one embeds a continuous control law. Both were tested with seven subjects.

For the circuit metrics, all subjects managed to achieve the goal with a very limited number of collisions. However, the tests performed using the second HMI achieved paths definitively smoother than the ones from the first HMI. It is possible to conclude that the second HMI provides a more agile driving experience.

Regarding comfort, in all the tests the horizontal acceleration remains under the threshold associated to the *comfortable* level. Nevertheless, it must be underlined that the level of RMS accelerations is lower in case of the first HMI; this result is mainly due to a more stable frontal speed when moving. With the second HMI, the continuous control law, together with the eye tracker noise, causes small but continuous variations of the frontal speed leading to a potentially less comfortable driving experience.

Regarding manoeuvrability, the second HMI offers a more agile interface, performing the same task in less time. About accuracy in manoeuvre, no explicit evidence was found to state that the second HMI is better than the first one. The number of cone hits and angular displacements varies between subjects and interfaces without a specific trend; the accuracy seems then related more to the driving skills of the subject rather than to HMI used.

Regarding depth perception, the distributions are similar, not underlying particular differences in performances. None of the subjects, independently of the HMI, managed to stop closer than 10 centimeters from the line.

As an overall conclusion, we can state that the first HMI is more suitable for precise and localized manoeuvre close to a target while the second HMI is much better for driving until the approach.

6.3 HMI performance evaluation in real environment

As anticipated in the previous chapter, one of the main topics of this thesis is the performance evaluation of the direct drive modality. The driving performance was evaluated through a test campaign in which the novel eye tracking control technology was compared with a standard joystick. The experimental test is very similar to the one proposed by Letaief et al. [50]. A pool of subjects tested both technologies following a specific test plan. The group of subjects involved in the test was chosen to be more heterogeneous as possible with the following different features:

- Age;
- Gender;
- Degree of mobility;
- Regular user of power or manual wheelchairs;

The test was structured considering information from the literature such as the standardized method WST (Wheelchair Skills Test) for the evaluation of the wheelchair users and also the regulation for the comfort evaluation of a vehicle.

Furthermore, the evaluation included also some subjective metrics regarding the feeling with the interfaces used, the workload required to drive the eye-controlled wheelchair and some personal interests to explore the correlation between the daily activities and the performance reached.

All the tests involving subjects were evaluated and approved by the *Human Research Ethics Committee* of the University of Trento in compliance with the regulation on privacy. In particular, all the data regarding both the motion metrics but also the subjective metrics was stored without reporting any information that can be used to link the test with a specific subject. The data collected was marked with an ID like *R_M_xxxx*. Clinical details were not recorded except to the rough information about the degree of mobility that was classified in two levels: full mobility or reduced mobility.

This chapter exposes both the procedure carried out during the test and also the obtained results complete with the observations.

6.3.1 Test environment design

The test was carried out inside one of the university laboratories located at the BIC (Business Innovation Centre) facility in Pergine Valsugana (TN - Italy). The laboratory is provided of

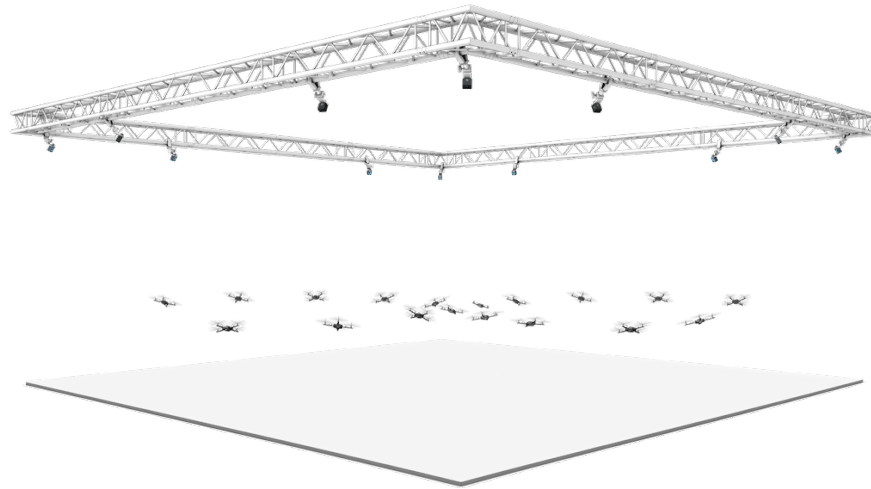


Fig. 6.13 "*OptiTrack*" simulated environment.

an advanced motion capture system of "*OptiTrack*" able to localize and track objects inside a drone arena where it is mounted on Fig. 6.13. The workspace of the motion capture system has an area of about 15 x 10 meters where the paths related to the motion test was designed considering the skills reported on the WST protocol.

"*OptiTrack*" motion capture system

The tracking of the wheelchair movement performed during the test was carried out using the "*OptiTrack*" marker-based motion capture system from NaturalPoint. The main component characterizing this motion capture system are:

Marker "*OptiTrack*" motion capture systems can use both passive and active markers as indicators for 3D position and orientation. An appropriate marker setup is essential for both tracking quality and reliability of captured data. All markers must be properly placed and must remain securely attached to surfaces throughout capture. In addition to marker placements and marker counts, the tracking quality is influenced by:

- **Marker size:** the size of the marker affects its visibility. Larger markers can be tracked at longer distances, but they are less suitable for tracking fine movements or smaller objects. On the other hand, smaller markers enhance precise tracking, such as facial and microvolume tracking, but have difficulty being tracked at long distances and are more likely to be occluded during capture. A proper choice of the marker size optimizes the object tracking.

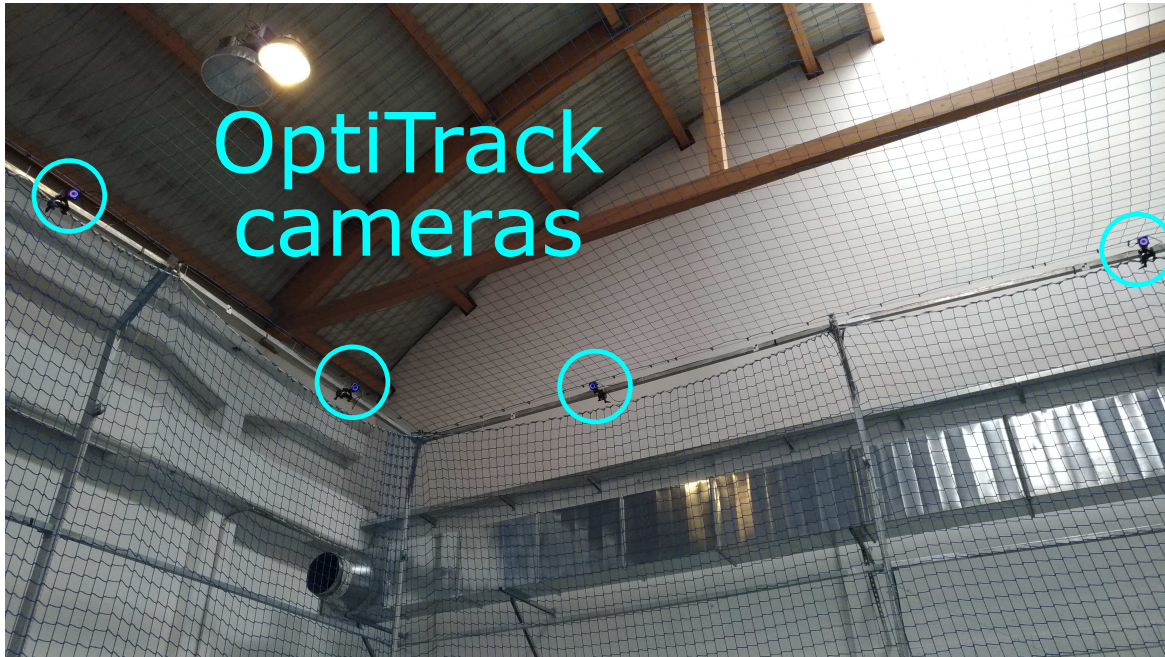


Fig. 6.14 Drone arena equipped with the set of cameras and the safety nets.

- Marker shape: "*OptiTrack*" cameras can track any surface covered with retro-reflective material but markers should be completely spherical with a smooth and clean surface for the best results. Hemispherical or flat markers, such as retro-reflective tape on a flat surface, can be tracked effectively from straight on, but when viewed from an angle, they will produce a less accurate centroid calculation. Therefore, non-spherical markers will have a less trackable range of motion when compared to tracking fully spherical markers.
- Marker surface: All the markers must have a well-maintained retro-reflective surface that satisfies the brightness threshold to be recognized. Worn markers with damaged retro-reflective surfaces will appear to a dimmer image in the camera view, limiting the tracking performance.

The tracked objects are represented by sets of spheres with a diameter ranging from 6.4 mm to 19 mm that are mounted on plastic rigid bodies. Each sphere is covered with reflective material in order to make it as much visible as possible. One or more rigid bodies with the proper set of sphere identify the object to be tracked. Alternatively, active (LED) markers can be used but they must be properly configured and synchronized with the system. Proper marker placement is vital for quality of motion capture data because each marker on a tracked subject is used as indicators for both position and orientation.

Cameras "OptiTrack" motion capture systems used for the test is composed of 14 infra-red and RGB cameras equipped with an Infra-Red (IR) illuminant. These cameras track any surfaces covered with retro-reflective material, which is designed to reflect incoming light back to its source. Infra-Red light emitted from the camera is reflected by passive markers and detected by the camera's sensor. The captured reflection is used to determine the marker 2D position. After that, the 2D marker locations are used to compute 3D positions through reconstruction. Increasing the number of cameras can help improve the tracking performance in terms of precision but also allows to track objects partially occluded. The cameras are attached on a metallic structure of a cage. Some flexible safety nets are placed around the arena to ensure the security of the user and the people around. Fig. 6.14 shows the drone arena equipped with the cameras and safety nets. The cameras are attached on a metallic structure of a cage. Some flexible safety nets are placed around the arena to ensure the security of the user and the people around. Fig. 6.14 shows the drone arena equipped with the cameras and safety nets.

Software platform Motive is a specific proprietary software platform designed to control motion capture systems for various tracking applications. It runs on a server PC, collects and analyse the information coming from the cameras to determine the position of an object in real-time. Motive not only allows the user to calibrate and configure the system, but it also provides interfaces for both capturing and processing of 3D data. The captured data can be both recorded or live-streamed to other pipelines. Motive obtains 3D information via Reconstruction, which is the process of compiling multiple 2D images of markers to obtain 3D coordinates. Using 3D coordinates from tracked markers, Motive can obtain 6 Degree of Freedom (3D position and orientation) data for multiple rigid bodies and skeletons, and enable tracking of complex movements in the 3D space. The video stream of each camera is analysed by Motive applying some filters on the images. It identifies the position of each marker (sphere), that was previously defined as part of an object, with respect to the reference system. The information from all the cameras is combined in order to obtain the 3D position of the marker inside the workspace. The 3D position of the markers can be resolved with millimeter accuracy. The real-time data streaming rate is 100 fps.

the accuracy and the precision of the tracking system depend on many factors such as the cameras arrangement, the efficiency of the calibration process and the illumination conditions. The uncertainty estimation of the system was performed through a repeatability test. A rigid body was placed inside the workspace of the motion capture system following a 5 x 3 grid and collecting the proper amount of sample of each position. The repeatability analysis highlighted a mean dispersion of 0.72 mm with an interval of confidence of 90%. Fig. 6.15

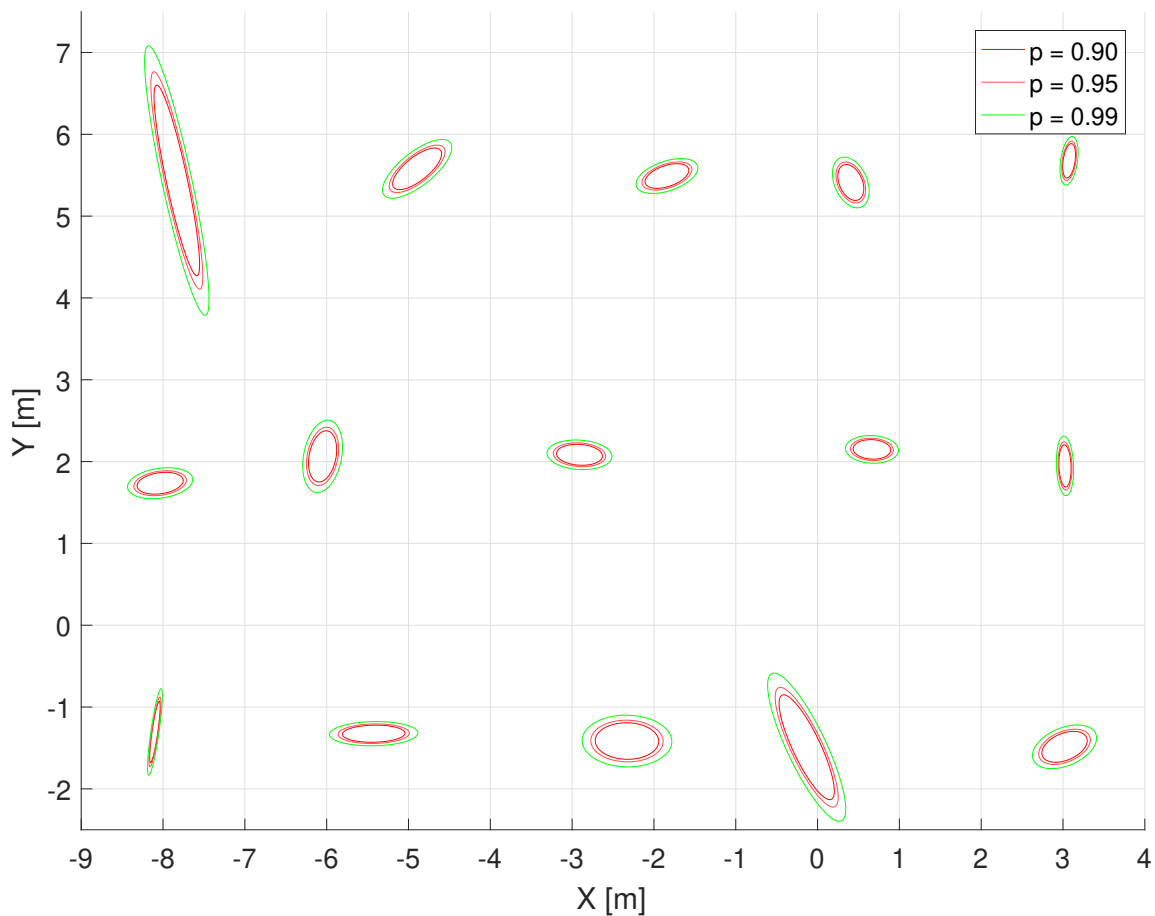


Fig. 6.15 Uncertainty analysis of the Optitrack motion capture system. For greater readability the uncertainty ellipses are represented with a positive scale factor of 1000.

shows the results of the uncertainty analysis with an interval of confidence of 90%, 95%, and 99%. The upper right corner presents the higher value of uncertainty but the precision of the localization remains good for the research purposes.

As previously introduced, the markers (reflective sphere) are used as the reference for the tracking of the wheelchairs inside the drone arena. The "*OptiTrack*" motion capture system is based on multi-markers plastic rigid bodies where the sets of markers are placed. Each rigid body can include a maximum of six reflective markers. The usage of a single marker allows to determine only its 3D position, while the complete reconstruction of positions and attitudes require at least three markers. The markers can be mounted on the single rigid body with different configurations, considering the distances between every sphere, to optimize the identification of the object. If two markers are too close together, it was also noticed that sometimes the system fuses the two spheres compromising the identification of the rigid body especially when the object is at a high distance from the cameras or when viewed from

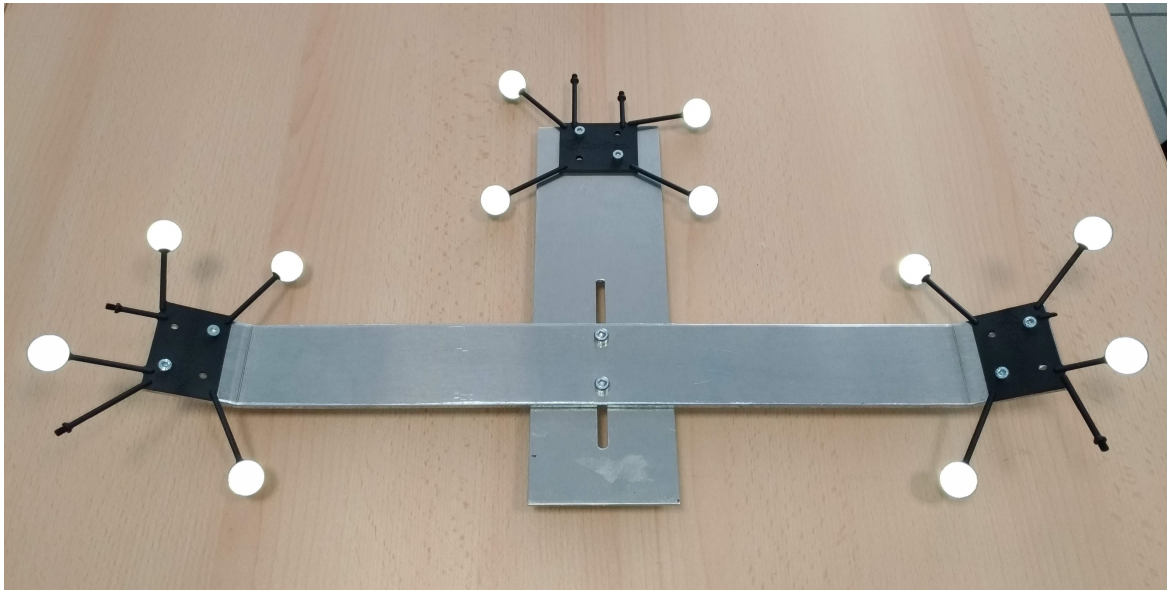


Fig. 6.16 "Optitrack" tracking object with three rigid bodies.

an angle. If any markers related to a rigid body are taken off or merged with others, the rigid body will become unlabelled, and the corresponding data will be either lost or approximated. Due to these reasons, on the wheelchair was mounted three rigid bodies with four marker on each one and the displacement shown in Fig. 6.16 to increase the traceability of the vehicle. The marker was placed on the single rigid body using different configurations and optimizing the distances between the spheres to create three different objects to be tracked.

Wheelchair Skills Test (WST)

The Wheelchair Skills Test (WST) is a standardized evaluation method useful to evaluate and document some ability of wheelchairs in an easy and low-cost way. The WST is included in the Wheelchair Skills Program (WSP) developed by the Wheelchair Research Team at Dalhousie University and Capital Health in Halifax, Nova Scotia in Canada starting using methodology based on the extensive motor-learning. In addition to the WST, the WSP includes the Wheelchair Skills Training Program (WSTP) and the related materials.

During the first step of the rehabilitation process, the WST may be used to determine which skills need to be addressed by the patients. Another usage could be represented by the wheelchair evaluation during the design process of the devices. The evaluation process here explained refers to this last usage. During the tests was used an Italian version 4.2 of the WST translated by a local rehabilitation centre. That version was approved by the authors of the WST and it is under validation.

The Italian version of the WST 4.2 implies the evaluation of 32 skills on a manual or a powered wheelchair that the user has to complete. The official version of the tests involves the assignment of a score, by some physiotherapists, to each skill in order to calculate the whole score of the user. This research work exploits the WST, and the associated testing guidelines, in the evaluation of the controllability of the wheelchair only, in terms of self-motion capabilities achieved by the user accordingly to used HMI. The original testing sequence was revised to organize a meaningful and effective experimental campaign, considering only those tests that present relation with the considered topic and achievable with both HMIs. Due to the nature of the technology under evaluation and to the physical condition of the users involved in the use of the technology developed, some of these skills are not valuable. Therefore, the solution under evaluation is addressed for people that are (or will be) almost completely paralyzed. Table 6.5 reports the full skill list from WST (Version 4.2¹) with the corresponding Italian translation. In bold the points considered for the design of the experiment and testing track.

Table 6.5 Wheelchair Skills Test skills, in bold the points considered for the design of the experiment.

Original version		Italian version	
N	Skills	N	Skills
1.	Moves controller/tiller away and back	1.	Sposti il comando di guida avanti e indietro e infine lo rilasci
2.	Turns controller on and off	2.	Accenda e spenga la carrozzina
3.	Selects drive modes and speeds	3.	Selezioni le diverse modalità (profili) di guida e le varie velocità possibili
4.	Operates body positioning option	4.	Utilizzi i comandi per variare la postura
5.	Disengages and engages motors	5.	Disinserisca e inserisca i motori
		6.	Dia le istruzioni per disinserire e inserire i motori
6.	Operates battery charger	7.	Colleghi la carrozzina al carica-batterie

¹<https://wheelchairskillsprogram.ca/en/skills-manual-forms-version-4-2-wst/>

- | | |
|---|--|
| | 8. Dia le istruzioni per collegare la carrozzina al caricabatterie |
| 7. Rolls forwards (10 m) | 9. Si sposti avanti per 10 m |
| 8. Rolls backwards (2 m) | 10. Si sposti indietro per 2 m |
| 9. Turns while moving forwards (90°) | 11. Esegua una svolta di 90° mentre sta andando avanti |
| 10. Turns while moving backwards (90°) | 12. Esegua una svolta di 90° mentre sta andando indietro |
| 11. Turns in place (180°) | 13. Giri di 180° sul posto |
| 12. Manoeuvres sideways (0.5 m) | 14. Si sposti lateralmente di 50 cm (con manovre combinate) |
| 13. Gets through hinged door | 15. Varchi una porta a battente (in entrambe le direzioni) |
| 14. Reaches high object (1.5 m) | 16. Raggiunga un oggetto a 1.5 m di altezza |
| 15. Picks object up from floor | 17. Raggiunga un oggetto da terra (es. quaderno ad anelli) |
| 16. Relieves weight from buttocks (3 s) | 18. Sollevi il peso dal sedile per 3 secondi (anche un lato per volta) |
| 17. Transfer to and from bench | 19. Si trasferisca su una panca e ritorni sulla carrozzina |
| 18. Rolls 100 m | 20. Si sposti in avanti per 100 m |
| 19. Avoids moving obstacles | 21. Eviti degli ostacoli con movimenti a zig-zag |
| 20. Ascends 5° incline | 22. Salga su una superficie con una pendenza di 5° (circa 8%) |
| 21. Descends 5° incline | 23. Scenda da una superficie con una pendenza di 5° (circa 8%) |
| 22. Ascends 10° incline | 24. Salga su una superficie con una pendenza di 10° |
| 23. Descends 10° incline | 25. Scenda da una superficie con una pendenza di 10° |
| 24. Rolls across side-slope (5°) | 26. Avanzi su una superficie inclinata lateralmente di 5° |
| 25. Rolls on soft surface (2 m) | 27. Avanzi 2 m su una superficie cedevole (es. prato) |



Fig. 6.17 Drone arena with the drawn paths

- | | |
|---------------------------------------|--|
| 26. Gets over gap (15 cm) | 28. Superi un avvallamento di 15 cm |
| 27. Gets over threshold (2 cm) | 29. Superi una soglia di 2 cm |
| 28. Ascends low curb (5 cm) | 30. Salga uno scalino di 5 cm |
| 29. Descends low curb (5 cm) | 31. Scenda da uno scalino di 5 cm |
| 30. Gets from ground into wheelchair | 32. Partendo da terra salga sulla carrozzina |
-

Paths design

The experimental verification related to the comparison between the eye-controlled technique and the standard commercial joystick involved the design of three different paths considering parameters like the WST evaluative skills discussed in the previous chapter and shown in the real scenario of Fig. 6.17 and in the rendering of Fig. 6.6.

Path A - Circuit It is the longest path and consists of the following of a line drawn on the floor that includes the evaluation of the WST skills. On this path are collected information about the position of the wheelchair with respect to the reference line and the acceleration applied to the device;

Path B - Parking During the test, the user starts from a fixed position and drives through a series of cones, positioned on a wide flat section of the path, as quickly as possible without touching any of them. The starting point and the cones are placed to force the user to perform a curve and a reverse curve before entering the corridor. By means of this test, it is possible to evaluate the driving capability performing tight manoeuvres and passing through narrow spaces

Path C - Braking The user has to start from a fixed position, move forward for few meters and then stops with the center of rear wheels as close as possible to a reference line drawn on the floor keeping the gaze in front of him. By means of this test, it is possible to evaluate the depth perception of the surrounding environment and the capability of stopping on the desired position.

6.3.2 Testing protocol

The testing protocol starts with a brief description of the project followed by a complete explanation about the operations that have to be performed, the behaviour of the system and how the wheelchair works. After that, the testing protocol continues as follows:

1. 15 minutes of free practice
2. Execution of the path A in the forward direction and then, after a turning on the spot of 180°, come back in the backward direction to the starting point. This task has to be executed for 5 times so at the end each user performs the path for 10 times;
3. Execution of path B for 10 times;
4. Execution of path C for 10 times;

The four steps were performed initially with the standard wheelchair, controlled by the joystick, and then with the prototype of eye-controlled wheelchair. The test was not randomized to minimize the stress resulting from the transfer among the two systems, especially for disabled subjects. During the tests were recorded information from the accelerometers and the positions of the wheelchair. The mean time to execute the whole set of tests was about 1.5 hours. At the end of the entire test protocol, the subjects were asked to fill questionnaires related to the workload, the interface usage/feelings, and personal interests.

6.3.3 Metrics evaluation features

The performance analysis of the system was carried out by evaluating specific motion metrics to compare the proposed solution with a standard joystick interface. The test campaign involved a pool of 36 subjects divided, basing on the degree of motor impairment of the users, in two groups:

21 full mobility users who haven't any mobility limitation

15 reduced mobility users having difficulties in the movement and use motor aids ranging from manual to power wheelchairs based on the degree of motor impairment.

Fig. 6.28 reports all the data collected from the "*OptiTrack*" motion capture system related to the position of both the wheelchairs during the tests. From the figure, it is quite easy to identify the three different paths characterizing the test.

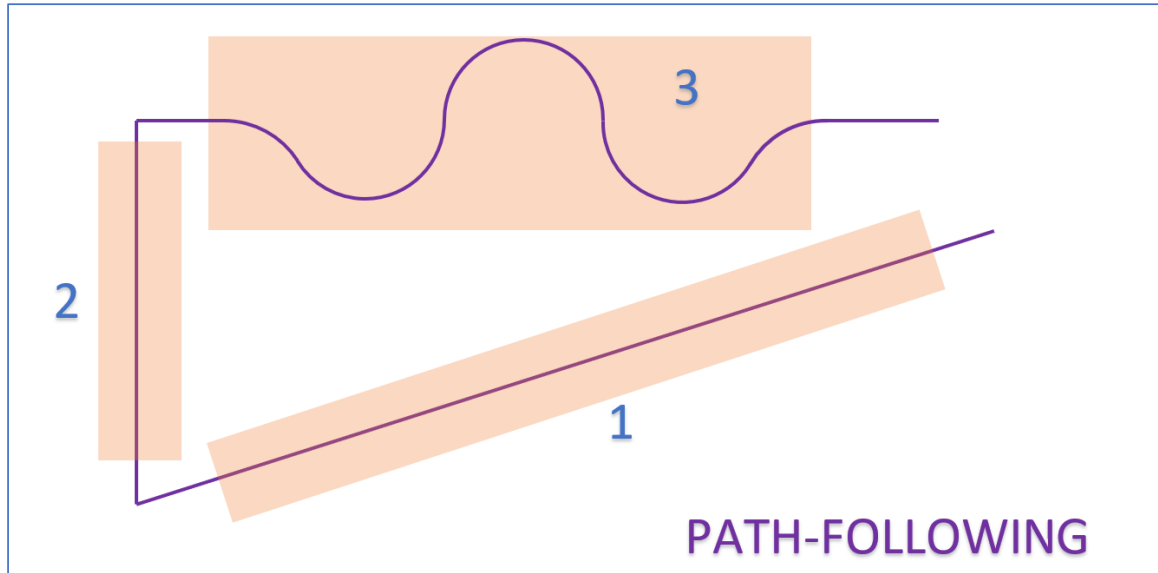
Instead, Fig. 6.19 shows the information coming from the accelerometers along the path following test. The graphs highlight that the *Z* component has a mean value equal to 1 g due to the gravity that is aligned to the *Z* axis as reported in Fig. 6.20. Furthermore, the *X* component is not equal to zero due to the misalignment of the sensor with the floor. To these data is applied a roto-translation matrix calculated during the calibration phase of the accelerometers. On the graphs it is possible to distinguish the various parts of the path following test:

- The first curve between the first and the second section the spike along the *X* axis at almost 22 seconds
- The overcoming of the obstacle (2 cm threshold) with the discontinuity along the *Z* axis at almost 28 seconds
- All the curved part of the path with the discontinuity along the *X* and *Y* axis between 30 and 55 seconds

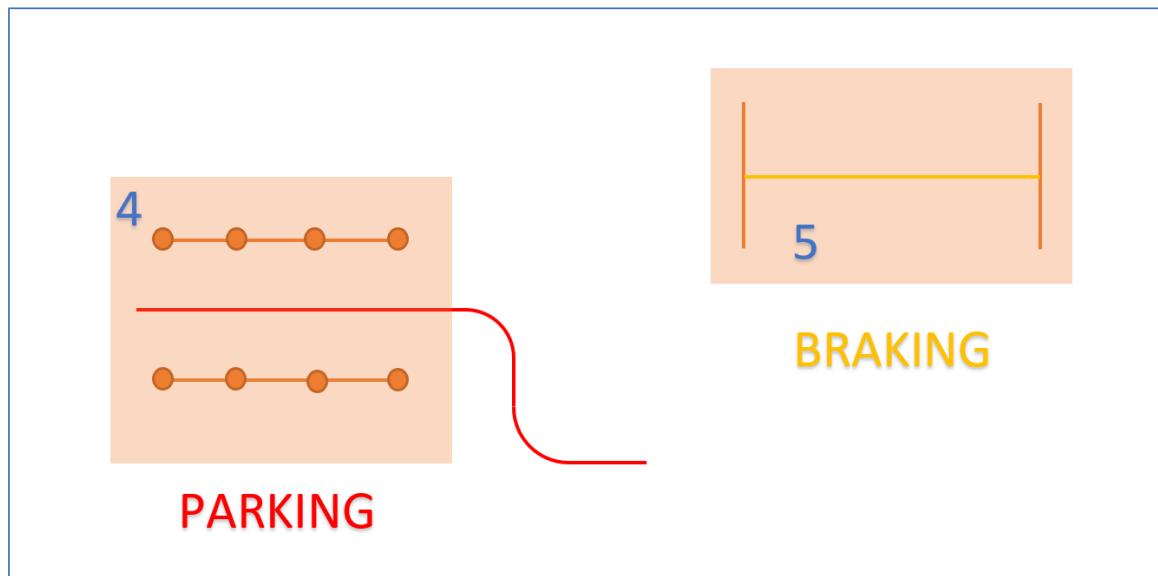
For a better objective evaluation of the performances, the reference of the path following test (Fig. 6.6, A) was subdivided into three sub-parts, to isolate the data for the analysis on specific metrics:

Straight section crossing diagonally the arena (1)

Bumpy section where are placed a grassy carpet and a threshold to overcome (2)



(a)



(b)

Fig. 6.18 Schematic representation of the sections considered in the analysis

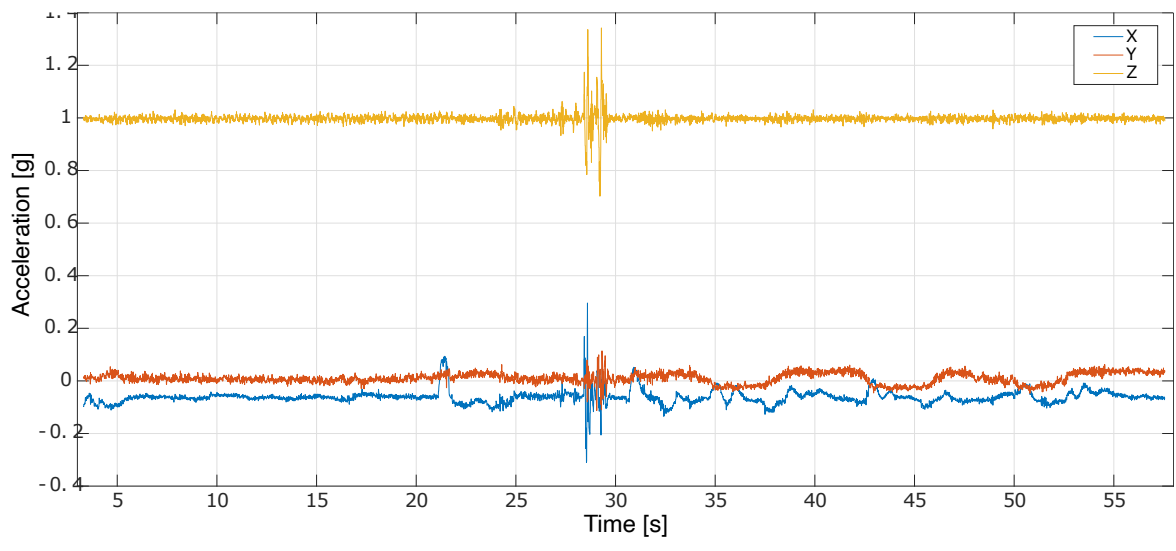


Fig. 6.19 Example of acceleration data from a specific subject related to the path following test.

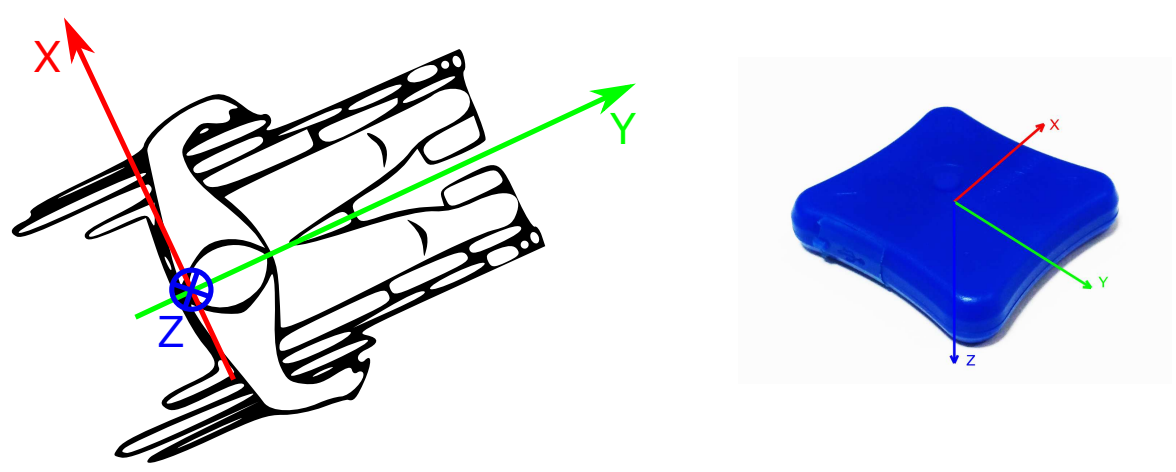


Fig. 6.20 Wheelchair reference system.

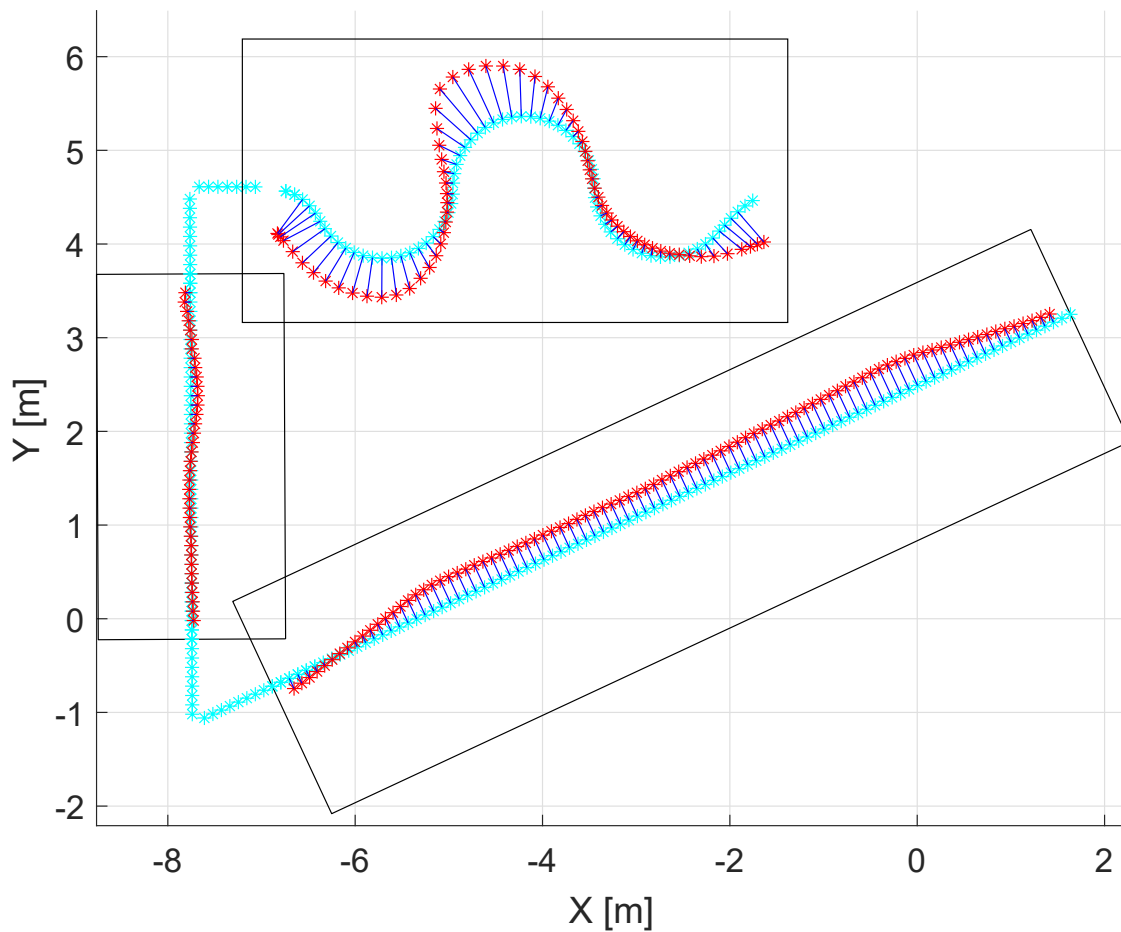


Fig. 6.21 Path segmentation for the path following test with representation of the deviations.

Curved section where are placed the three aligned cones that must be bypassed (3)

Fig. 6.18a shows the three section characterizing the path following test just described.

The manoeuvring and the depth perception performance are evaluated along two specific paths (4 & 5), Fig. 6.18b.

On the reference path was selected a series of equally spaced points having a distance of 20 cm between them. For each point, inside the predefined section (Fig. 6.18a), the distance of the wheelchair from the reference path was recorded by selecting the nearest point of the performed path. Fig. 6.21 shows the segmentation of the reference path with the cyan markers while the red markers represent the path really performed by the user. The distances between each point of the reference and the closest point of the real performed path are highlighted with blue lines. The average value of these deviations was used as a reference measurement feature for all the testing conditions. In the section from 1 to 4, the parameter

evaluated is called mean deviation with its module while, in the braking test (5-th section), was evaluated the module of the braking distance.

Moreover, on the section 4 and 5 were considered additional elements, that is specific for these tests, such as the maximum reached speed, the accelerations (frontal and lateral) to which the wheelchairs are subjected and the angles related to the entrance and the exit from the corridor (the two series of cones).

All the evaluated features are calculated for each subject driving both the -eye-controlled wheelchairs and the common commercial one with the joystick.

The full list of the evaluated features are reported in Table 6.21 and hereafter explained:

Mean deviation - e_m : it is the mean value of the distances to the reference lines. For the path following test (section 1, 2 and 3), it is the distance between each point of the reference and the corresponding closest point of the path performed by the user. The points of the reference path evaluated are those included inside the predefined sections (Fig. 6.18a), neglecting the starting end final part of the path and the curves. The closest point is determined drawing a line orthogonal to the reference on the points. Also in the parking test (section 4), the mean deviation is determined with respect to a reference that is, in this case, the center line of the corridor. As in the path following test, the reference line is segmented and the closest point is extracted using the orthogonal line passing through each point on the reference. On the test environment, the reference was an imaginary line in the center of the two series of cones, it was not drawn on the floor. The initial part of the path useful for the alignment with the corridor is not considered. The braking test (section 5) is evaluated by using a specific feature called mean braking distance described below.

Module of mean deviation - $|e_m|$: it is simply the absolute value of the mean deviation described above.

Efficiency in speed control - v_{eff} : it is the average speed calculated on the path. The two interfaces provide different maximum navigation velocities. In particular, the maximum speed value of the joystick wheelchair is 0.7 m/s while on eye-controlled wheelchair it was set to 0.5 m/s. Due to this reason the velocities were normalized to 1, considering as reference parameter the capability in reaching the maximum value, thus and efficiency in the utilization. This parameter ensures the homogeneity among the interfaces. The mean speed was calculated on the path effectively performed by the user and not on the reference.

Table 6.6 Evaluated features for each considered section of path.

Feature	Sym	1	2	3	4	5
Mean deviation	e_m	✓	✓	✓	✓	
Module of mean deviation	$ e_m $	✓	✓	✓	✓	
Efficiency in speed control	v_{eff}	✓	✓	✓	✓	✓
Frontal weighted average acceleration	a_{wf}	✓	✓	✓		
Lateral weighted average acceleration	a_{wl}	✓	✓	✓		
Entrance angle	θ_s				✓	
Exit angle	θ_e				✓	
Braking distance	e_b					✓
Module of braking distance	$ e_b $					✓

Frontal and lateral weighted average accelerations - a_{wf} & a_{wl} : it is the weighted quadratic acceleration determined according to the regulations UNI ISO 2631, previously defined and hereafter reminded:

$$a_w = \left[\frac{1}{T} \int_0^T a_w^2(t) dt \right]^{\frac{1}{2}} \quad (6.15)$$

where $a_w(t)$ is weighted acceleration. This feature is evaluated for both the frontal and lateral accelerations.

Entrance and exit angles - θ_s & θ_e : it is related to the attitude of the wheelchair at the start of section 4. This feature represents the angle with which the user approaches the corridor. A value of 0 degree indicates that the user entered in the corridor parallel to the walls. Similarly, the exit angle is referred to the attitude of the wheelchair at the end of the corridor.

Mean braking distance - e_b : it is mean deviation evaluated, when the user stopped the wheelchair, as the distance between the mid-point of the rotation axis of the rear wheels and the reference line drawn on the floor. This feature is evaluated only on the braking test (section 5).

Module of braking distance - $|e_b|$: it is simply the absolute value of the mean braking distance described above.

6.3.4 Subjective evaluation features

The performance evaluation included not only the motion metrics but also other features related to the subject, to the interface used and to the feeling perceived using the system (subjective metrics).

For this purpose, was drafted a questionnaire regarding some personal information such as the occupation, the daily usage of devices like PC, smartphone or game console, the feeling with the technology or the free-time activities. The intensive use of these devices should provide on the subject a better feeling with the graphical interfaces and therefore, a better interaction reactivity with the elements commonly used on the HMIs. Indeed, the analysis includes also the evaluation of the possible correlation between personal interests and the results obtained from the practical tests. Fig. 6.22 shows the questionnaire about the personal information of the subject that was collected and subsequently evaluated together with the motion metrics. This questionnaire was submitted to each subject at the end of the tests.

The information related to the personal interest of the subject and to the type of controlled, used during the test, was elaborated in order to get some numerable features considering a two-level classification. For each topic, the multiple-choice was grouped to obtain two answers and simplifying in this way the analysis. The features obtained are hereafter described:

Mobility level value 0 for full mobility subject, 1 for reduced mobility subject.

Type of controller value 0 for the joystick and 1 for the ocular HMI

Age value 0 for under 40 subject, 1 for over.

Technology value 1 if the subject performs at least two activities with the smartphone (such as Call/SMS, Internet, Photo/Video, Games) and/or with the PC (such as Mail, Film, Writing, Internet, Game, Social Network), 0 otherwise.

Free-time activities value 1 if the subject performs at least two activities in the free-time, 0 otherwise.

The feature classification just described may be considered too generic because it doesn't consider the frequency with which the subject performs, for example, a specific activity with a device. However, the analysis aims to connect driving performance with the variety of different activities that may be linked to the level of experience in the usage of informatics technologies.

A good HMI must be as much user-friendly as possible, especially due to the delicate health conditions of the users. Therefore, the evaluation of the system that considers also the

Università degli Studi di Trento - DII

RoboEye

ID _____

Questionario interessi

Età:	<input type="checkbox"/> 0 – 18	<input type="checkbox"/> 19 – 24	<input type="checkbox"/> 25 – 34	<input type="checkbox"/> 35 – 44
	<input type="checkbox"/> 45 – 54	<input type="checkbox"/> 55 – 64	<input type="checkbox"/> Più di 65	
Sesso:	<input type="checkbox"/> Maschio <input type="checkbox"/> Femmina			
Professione:	<input type="checkbox"/> Impiegato	<input type="checkbox"/> Operaio	<input type="checkbox"/> Libero professionista	<input type="checkbox"/> Imprenditore
	<input type="checkbox"/> Pensionato	<input type="checkbox"/> Studente	<input type="checkbox"/> Casalinga	<input type="checkbox"/> Disoccupato
	<input type="checkbox"/> Altro _____			
Hai uno smartphone?	<input type="checkbox"/> Sì <input type="checkbox"/> No			
Se sì, lo usi quotidianamente?	<input type="checkbox"/> Sì <input type="checkbox"/> No			
Per fare cosa?	<input type="checkbox"/> Telefono/SMS	<input type="checkbox"/> Internet	<input type="checkbox"/> Foto/video	<input type="checkbox"/> Giochi
	<input type="checkbox"/> Altro _____			
Hai un PC?	<input type="checkbox"/> Sì <input type="checkbox"/> No			
Se sì, lo usi quotidianamente?	<input type="checkbox"/> Sì <input type="checkbox"/> No			
Per fare cosa?	<input type="checkbox"/> Leggere mail	<input type="checkbox"/> Guardare film	<input type="checkbox"/> Scrivere documenti	
	<input type="checkbox"/> Navigare in internet	<input type="checkbox"/> Giocare	<input type="checkbox"/> Social network	
	<input type="checkbox"/> Altro _____			
Ti piace la tecnologia?	<input type="checkbox"/> Sì <input type="checkbox"/> No			
Quali dispositivi usi maggiormente?	<input type="checkbox"/> Smartphone	<input type="checkbox"/> PC	<input type="checkbox"/> Console di gioco	
	<input type="checkbox"/> Televisore			
	<input type="checkbox"/> Altro _____			
Cosa fai nel tempo libero?	<input type="checkbox"/> Sport	<input type="checkbox"/> Lettura	<input type="checkbox"/> Eventi culturali	
	<input type="checkbox"/> Esco con gli amici	<input type="checkbox"/> Guardo Tv / Uso PC	<input type="checkbox"/> Cinema	
	<input type="checkbox"/> Altro _____			
Note:	<hr/> <hr/> <hr/> <hr/>			

Fig. 6.22 Questionnaire on personal interests.

opinions of the user from a cognitive and emotive point of view represents a fundamental element for the human-machine interface assessment. For this reason, two questionnaires were included in the testing sessions carried out in the real environment, to evaluate the usability of the system (if it requires too much energy to maneuver the wheelchair) but also to understand how much the human-machine interface results intuitive.

Also in this case, the information from the questionnaires was elaborated to extract numerable results. Table 6.7 reports the data considered that are related to interface and in particular to the usability, to the trust, and to the satisfactoriness.

Fig. 6.23 shows the questionnaire related to the workload required to drive the wheelchair while Fig. 6.24 to 6.27 shows the questionnaire related to the Interface.

6.3.5 Experimental results

The analysis of Variance (ANOVA) was used to analyse if statistically significant differences were present in the feature base considered in the experiment.

The analysis of variance included the evaluation of all features listed in Table 6.6. In the following subsections are reported the most interesting results achieved from the analysis. Table 6.8 reports the entire set of p-values for the entire feature set, considering the subject and interface as factors. Fig. 6.6 shows the full set of paths recorded during the tests.

Section 1

The initial step of the analysis considered only the first straight part of the path following test, marked as section 1 in Fig. 6.18a. The other parts of the path, where are placed obstacles and curves, are analysed separately. The goal of this part of the test was to follow a straight line drawn on the floor.

The first feature evaluated is the wheelchair deviations in position from the reference along the straight section of the path following test. The reference path was segmented by selecting a series of equally spaced points having a distance of 20 centimeters. The deviation is determined as the shortest distance between each point of the segmented reference and the path performed by the wheelchairs.

The figures ranging from 6.29 to 6.31 show the probability density functions referring to the deviation from the reference performed by different type of subjects (full mobility users or reduced mobility users) and with different input interfaces (joystick and gaze-based).

Comparing the deviation from the reference path related to the full population, shown in Fig. 6.29, it is possible to notice that the variability of the data related to the gaze-based wheelchair is much higher than the joystick one, Fig. 6.29a. Instead, the same analysis on the

Table 6.7 Subjective features evaluated.

Usability
(a) I think that I would like to use this system frequently
(b) I found the system unnecessarily complex
(c) I thought the system was easy to use
(d) I think that I would need the support of a technical person to be able to use this system
(e) I found the various functions in this system were well integrated
(f) I thought there was too much inconsistency in this system
(g) I would imagine that most people would learn to use this system very quickly
(h) I found the system very cumbersome to use
(i) I felt very confident using the system
(j) I needed to learn a lot of things before I could get going with this system
Trust
(a) I believe the system is a competent performer
(b) I trust the system
(c) I have confidence in the advice given by the system
(d) I can depend on the system
(e) I can rely on the system to behave in consistent ways
(f) I can rely on the system to do its best every time I take its advice
Satisfactoriness
(a) Useful-Useless
(b) Pleasant-Unpleasant
(c) Bad-Good
(d) Nice-Annoying
(e) Effective-Superfluous
(f) Irritating-Likable
(g) Assisting-Worthless
(h) Undesirable-Desirable
(i) Raising alertness-Sleep inducing

RoboEye

ID: _____

**You have now completed your first test drive.
Please, rate your workload during this drive by putting a cross on each scale below.**

Workload

1. The factors defined below describe different components in the driving task you carried out during the test.

Please, read the definitions of the components and make an estimation.

a. Make an estimation on how difficult it was to drive mentally. How much **mental activity** (finding the way, looking for information, to handling traffic situations, thinking, calculating, deciding, etc.) was required during driving? Was the task easy or demanding, simple or complex in this respect? How large demand on thinking, deciding and looking for information was required during driving?

Very low | _____ | Very high
mental activity | _____ | mental activity

b. Make an estimation on how difficult it was to drive physically. How much **physical activity** (pushing the pedals, steering, etc.) was required? Was the task easy or demanding, slow or brisk, restful or laborious? How large demand on physical activity was required during driving?

Very low | _____ | Very high
physical activity | _____ | physical activity

c. Make an estimation on how much **time pressure** you felt during driving due to the traffic conditions (e.g. did you feel other cars making you drive faster?). Was the pace slow or rapid, leisurely or frantic? How large was the time pressure during driving?

Very low | _____ | Very high
time pressure | _____ | time pressure

d. Make an estimation on how successful you think you were in driving. How satisfied are you with your **own driving performance**?

Very low | _____ | Very high
performance | _____ | performance

e. Make an estimation on how hard you had to work (to find the way, to look for information, to handle the traffic conditions, to think, to make decisions, to turn the steering wheel, etc.) to accomplish your level of performance when driving. How large was your **effort** when driving?

Very low | _____ | Very high
effort | _____ | effort

f. Make an estimation on how **frustrated** you felt due to the driving task and to traffic conditions. Did you feel insecure, discouraged, irritated, stressed and annoyed versus secure, gratified, content, relaxed and complacent? How high was your level of frustration during driving?

Very low | _____ | Very high
frustration | _____ | frustration

If You have further comments or remarks, You are welcome to make them here:

Fig. 6.23 Workload questionnaire.

University of Trento - DII

RoboEye

ID. _____

Please, read the questions carefully and don't hesitate to ask for help if needed.

Your evaluation of the system is important to us!

INTERFACE: _____

Understanding the system

1. Are you aware of any limitations of the system? If yes, please explain.

2. During the learning phase of the usage of the system, were there especially difficult things to learn? If yes, please explain.

Fig. 6.24 Interface questionnaire (page 1).

University of Trento - DII

RoboEye

ID _____

Usability (SUS)

3. Please, indicate below to what extent you agree with the following statements

	Strongly disagree				Strongly agree
a. I think that I would like to use this system frequently	<input type="checkbox"/>				
b. I found the system unnecessarily complex	<input type="checkbox"/>				
c. I thought the system was easy to use	<input type="checkbox"/>				
d. I think that I would need the support of a technical person to be able to use this system	<input type="checkbox"/>				
e. I found the various functions in this system were well integrated	<input type="checkbox"/>				
f. I thought there was too much inconsistency in this system	<input type="checkbox"/>				
g. I would imagine that most people would learn to use this system very quickly	<input type="checkbox"/>				
h. I found the system very cumbersome to use	<input type="checkbox"/>				
i. I felt very confident using the system	<input type="checkbox"/>				
j. I needed to learn a lot of things before I could get going with this system	<input type="checkbox"/>				

Trust

4. Please, indicate below to what extent you agree with the following statements

	Strongly disagree				Strongly agree
a. I believe the system is a competent performer	<input type="checkbox"/>				
b. I trust the system	<input type="checkbox"/>				
c. I have confidence in the advice given by the system	<input type="checkbox"/>				
d. I can depend on the system	<input type="checkbox"/>				
e. I can rely on the system to behave in consistent ways	<input type="checkbox"/>				
f. I can rely on the system to do its best every time I take its advice	<input type="checkbox"/>				

Fig. 6.25 Interface questionnaire (page 2).

University of Trento - DII

RoboEye

ID _____

Other possible issues

6. Did you encounter any other benefits when using the system compared to driving without the system?

7. Did you encounter any other problems when using the system compared to driving without the system?

9. Your gender Male Female

10. Your age 18-24 25-44 45-64 65-70

11. If you have further comments or remarks, You are welcome to write them here:

Fig. 6.27 Interface questionnaire (page 4).

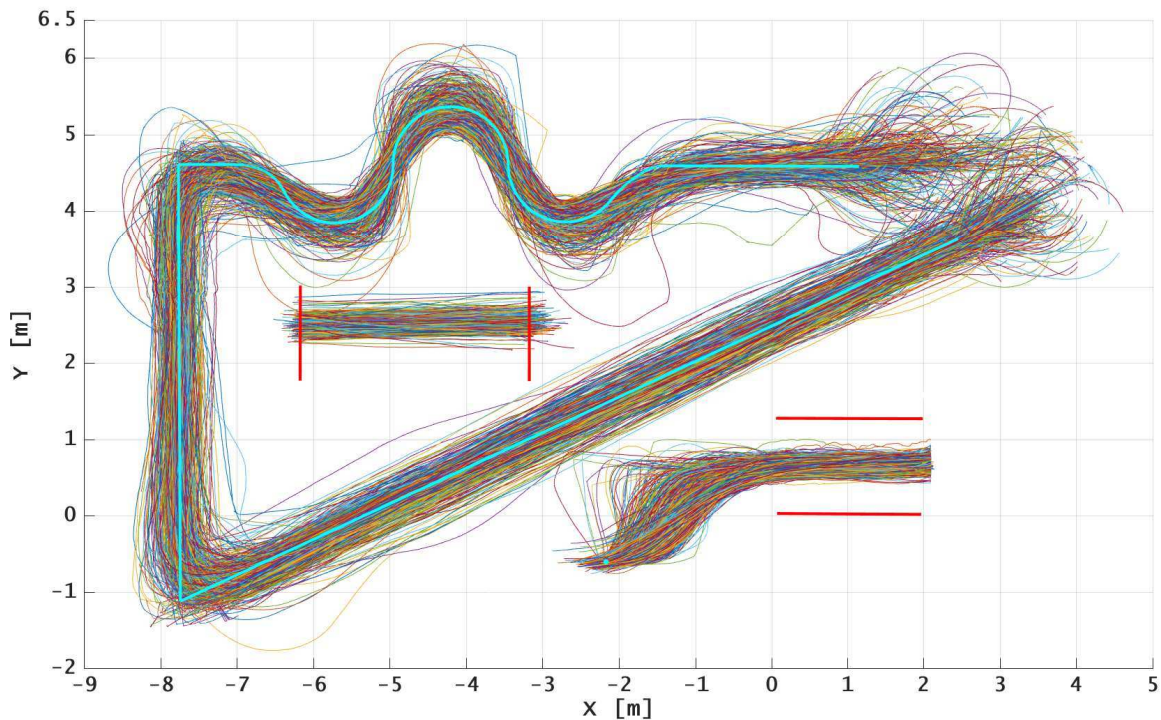


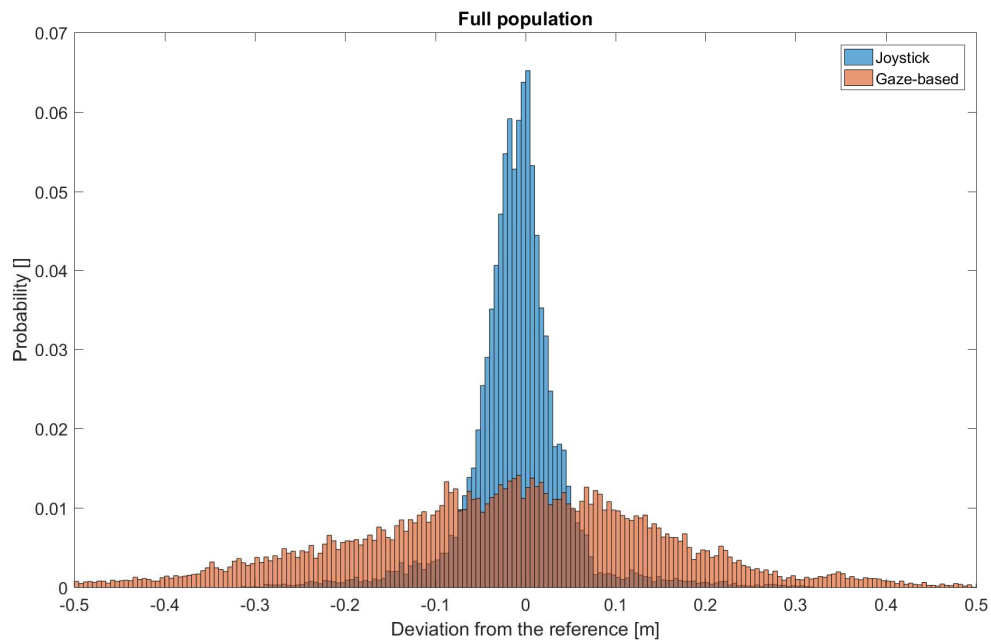
Fig. 6.28 Full set of paths recorded during the tests.

entire population referred to the type of user shows a comparable variability on the deviation of the full mobility users and the reduced mobility users, Fig. 6.29b.

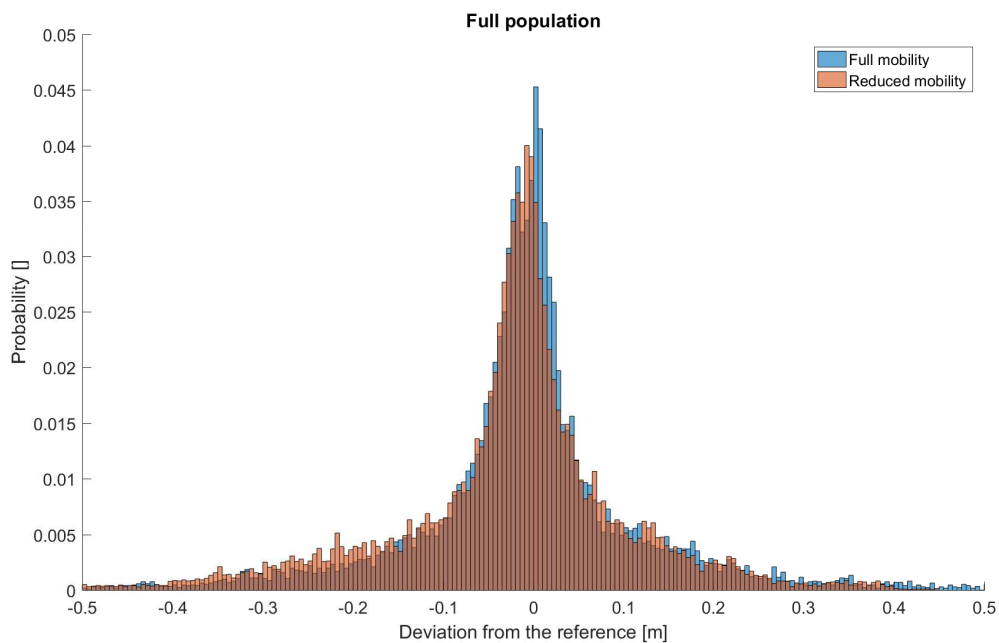
In the same way, it is interesting to focus the analysis of the probability density function, initially on the subject type and then on the interfaces. In particular, the comparison of the deviation between the joystick and gaze-based interface shows the same behaviour for both the cases of full and reduced mobility users, Fig. 6.30a and 6.30b.

The comparison on user types highlights a good overlap in the data both in the case of full and reduced mobility subjects that used the joystick, Fig. 6.31a, and the eye-controlled wheelchair, Fig. 6.31b. The histograms show a wider distribution for the gaze-based interface. Moreover, analysing the effect of the subject type it is possible to notice a slightly higher variability in the case of reduced mobility users with respect to the full mobility users.

The performance evaluation continues with the analysis of variance (ANOVA 2 way). ANOVA produced a p-value for the subject of 33%, 16% for the interface, and a 3% for the interaction of the parameters (Fig. 6.32b). This suggests that no marked differences can be found in the following of a straight path with both interfaces, despite a correlation in the performances is suggested with the subject. Fig. 6.32a shows the box plot for the section and feature type. In both the box plots the two median values are approximately the same while the reduced mobility users and the gaze-based interface presents respectively the high

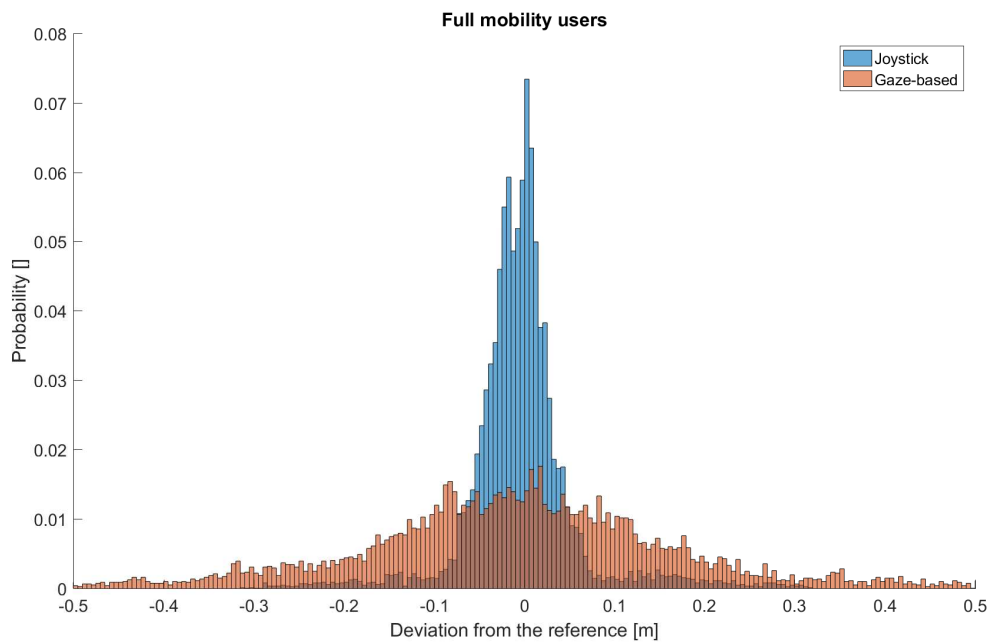


(a)

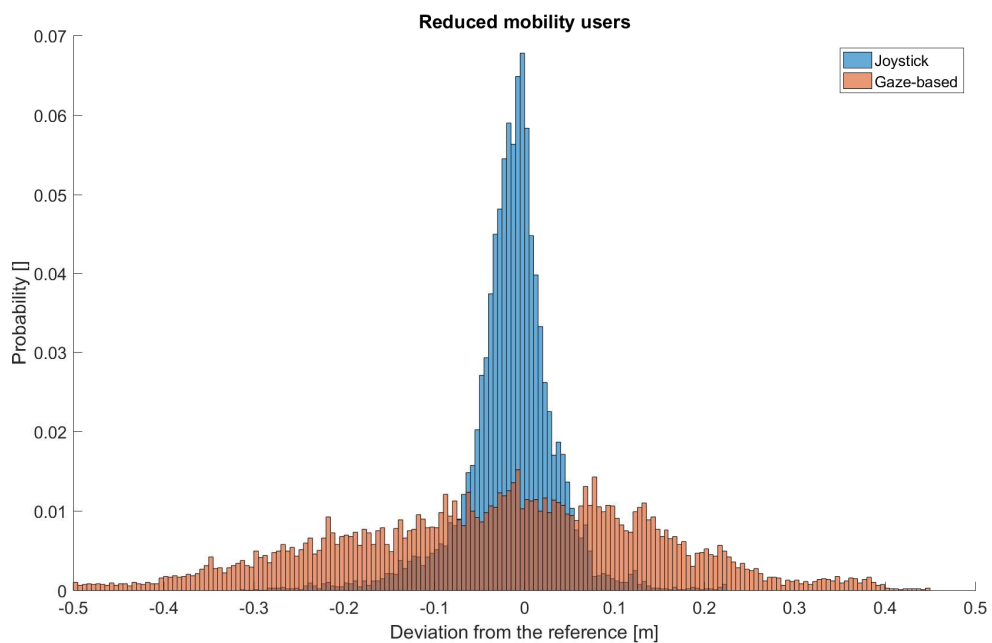


(b)

Fig. 6.29 Comparison of the deviation from the reference path related to the full population along the straight part of the path following test (section 1). Subfigure *a* shows the comparison between the control interface for both the subject type while the subplot *b* highlights the difference between the subjects using both the interfaces

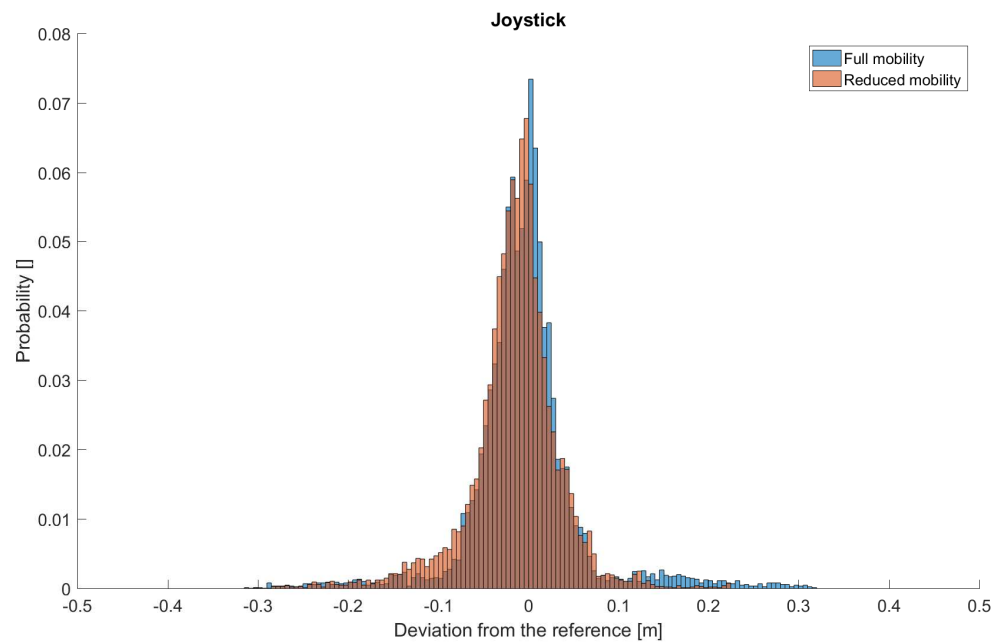


(a)

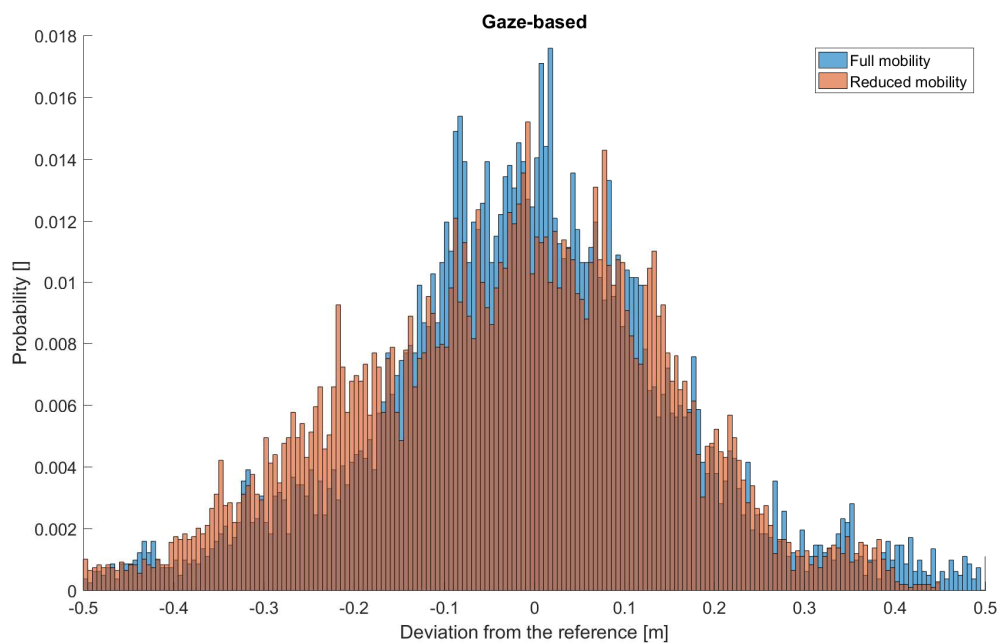


(b)

Fig. 6.30 Comparison of the deviation from the reference path between interfaces performed by full mobility users (a) and reduced mobility users (b) along the straight part of the path following test (section 1).

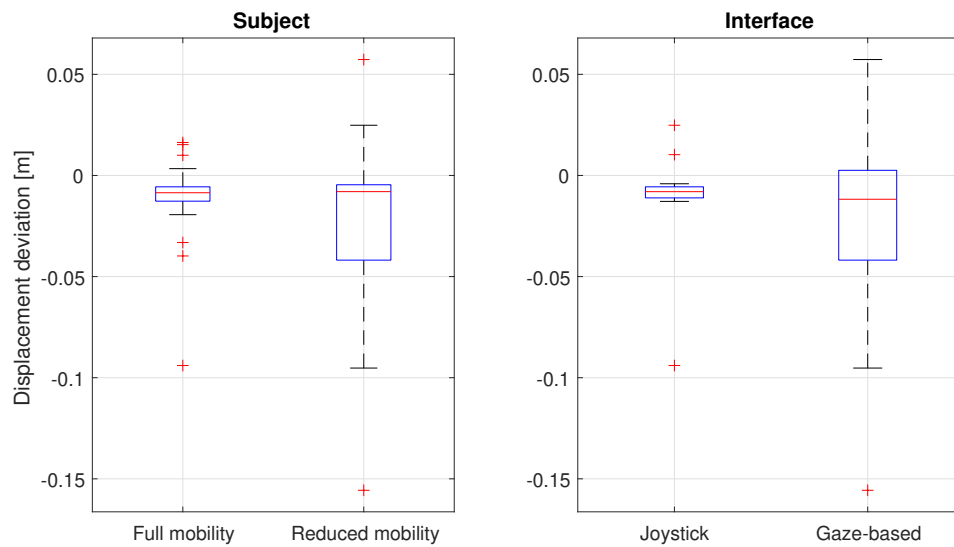


(a)



(b)

Fig. 6.31 Comparison of the deviation from the reference path between subjects driving a classic joystick wheelchair (a) and the gaze-based prototype (b) along the straight part of the path following test (section 1).



(a)

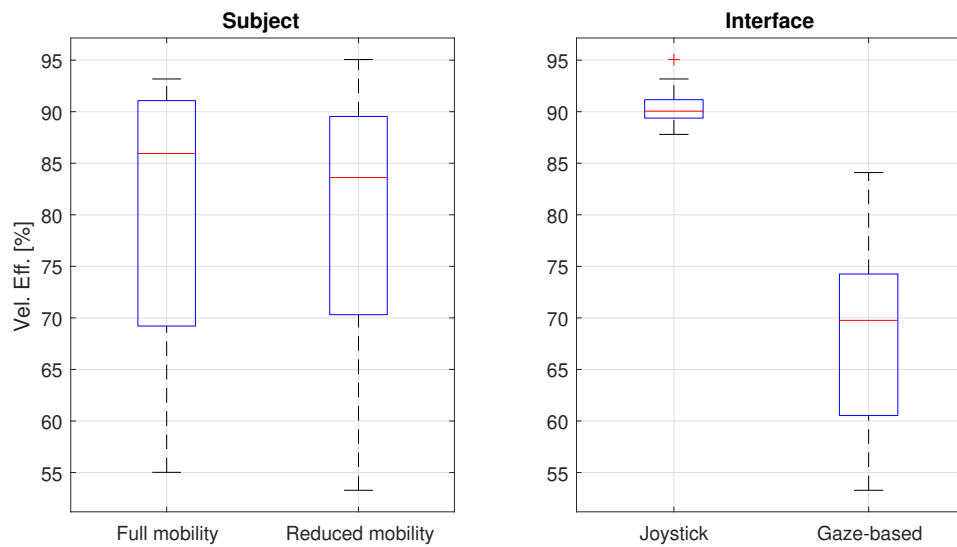
ANOVA Table					
Source	SS	df	MS	F	Prob>F
Subject	0.00109	1	0.00109	0.99	0.325
Interface	0.00225	1	0.00225	2.04	0.1606
Interaction	0.0057	1	0.0057	5.19	0.0282
Error	0.04396	40	0.0011		
Total	0.053	43			

(b)

Fig. 6.32 ANOVA analysis for the mean deviation (e_m) for the path following test, along the section 1 with the box plots of the mean deviation related to subject (left) and interface (right).

variability with respect to the full mobility users and the joystick. This behaviour confirms the trend observed in the evaluation of the probability density function.

As for the velocity efficiency, the ocular interface presented a lower efficiency than the joystick, Fig. 6.33a. Indeed, the median velocity efficiency value of the gaze-based interface is 70%, while it is 90% in the case of the joystick. ANOVA returned a p-value related to the interface of 0% indicating that the interface has a strong influence on the velocity efficiency, Fig. 6.33b. Furthermore, the gaze-based values have a much higher variability with respect to the joystick. Considering the ANOVA analysis associated with the subject the box plot shows a similar behaviour of both the median and the variability values. This is confirmed by the p-value of 41% related to the subject indicating that the subject doesn't have any influence



(a)

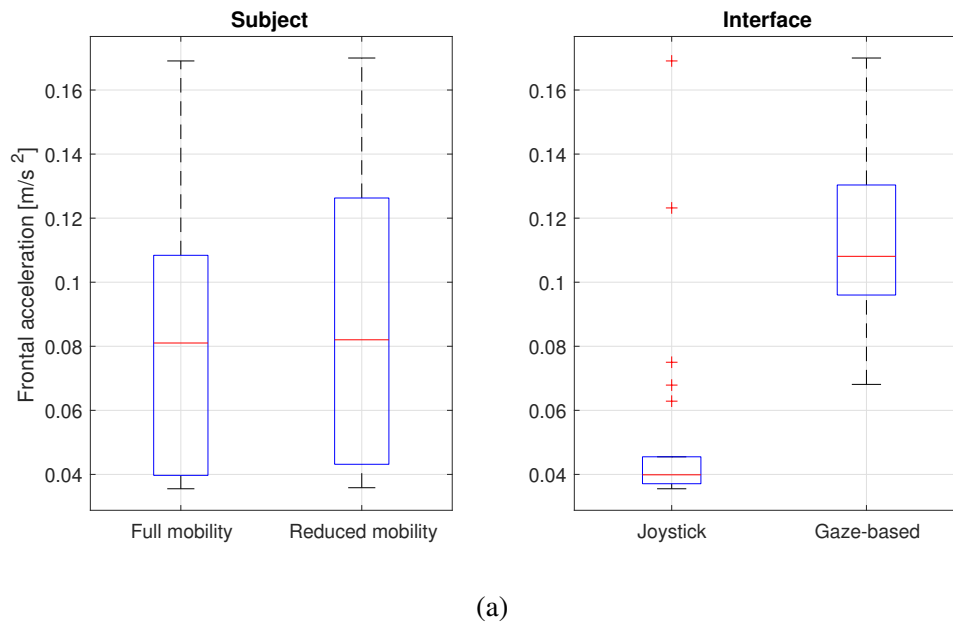
ANOVA Table					
Source	SS	df	MS	F	Prob>F
Subject	24.92	1	24.92	0.69	0.4104
Interface	5428.18	1	5428.18	150.76	0
Interaction	6.76	1	6.76	0.19	0.667
Error	1440.21	40	36.01		
Total	6900.08	43			

(b)

Fig. 6.33 ANOVA analysis for the efficiency in speed control (v_{eff}) for the path following test, along the section 1 with the box plots of the efficiency related to subject (left) and interface (right).

on the performance. The interaction p-value of 67% means that the two parameters subject and interface don't present a statistically significant correlation.

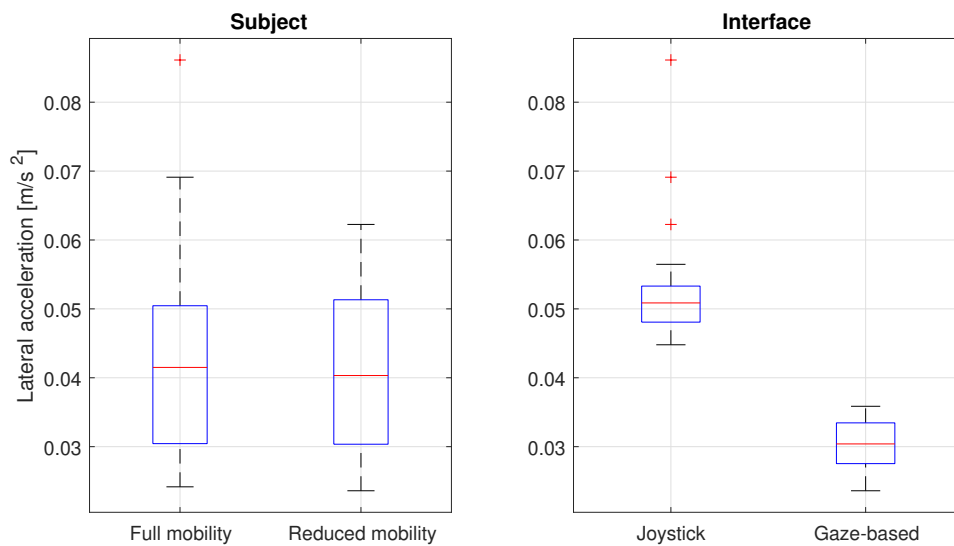
The results about the accelerations show that the subject doesn't influence the performance in both the frontal and the lateral accelerations. The ANOVA tables (Fig. 6.34b and 6.35b) reports a p-value related to the subject of 42% for the frontal acceleration and of 29% for the lateral one. A p-value of 0% on both ANOVA tables suggests that the interface has a strong influence on the acceleration. In the case of the interaction, the p-values of 40% and 48% for the frontal and the lateral accelerations indicate that the subject and the interface features don't present a statistically significant correlation. It is important to notice that the maximum value of both frontal and lateral accelerations remained inside the *not uncomfortable* region



ANOVA Table					
Source	SS	df	MS	F	Prob>F
Subject	0.00061	1	0.00061	0.67	0.4179
Interface	0.03979	1	0.03979	44.03	0
Interaction	0.00067	1	0.00067	0.74	0.3952
Error	0.03615	40	0.0009		
Total	0.07722	43			

(b)

Fig. 6.34 ANOVA analysis for the frontal weighted average acceleration (a_{wf}) for the path following test, along the section 1 with the box plots of the acceleration related to subject (left) and interface (right).



(a)

ANOVA Table					
Source	SS	df	MS	F	Prob>F
Subject	0.00006	1	0.00006	1.14	0.2925
Interface	0.00578	1	0.00578	114.07	0
Interaction	0.00003	1	0.00003	0.5	0.4842
Error	0.00203	40	0.00005		
Total	0.00789	43			

(b)

Fig. 6.35 ANOVA analysis for the lateral weighted average acceleration (a_{wl}) for the path following test, along the section 1 with the box plots of the acceleration related to subject (left) and interface (right).

of the regulation UNI ISO 2631, having an upper limit of 0.315 m/s^2 . Anyhow, using the gaze-based interface the users suffered smaller lateral acceleration compared to the joystick. The frontal accelerations present the opposite behaviour, with lower acceleration values for the joystick interface.

Section 2

The second part evaluated is related to the bumpy section where are placed a grassy carpet and a 2 centimeters threshold to overcome. It is the second part of the path following test, marked as section 2 in Fig. 6.18a. As in section 1, the subject had to follow a straight line drawn on the floor minimizing the disturbance effects introduced by both the soft surface and the threshold.

The first feature analysed is the deviation of the wheelchair from the reference path, that is calculated as the shortest distance between the points obtained with the segmentation and the wheelchair position.

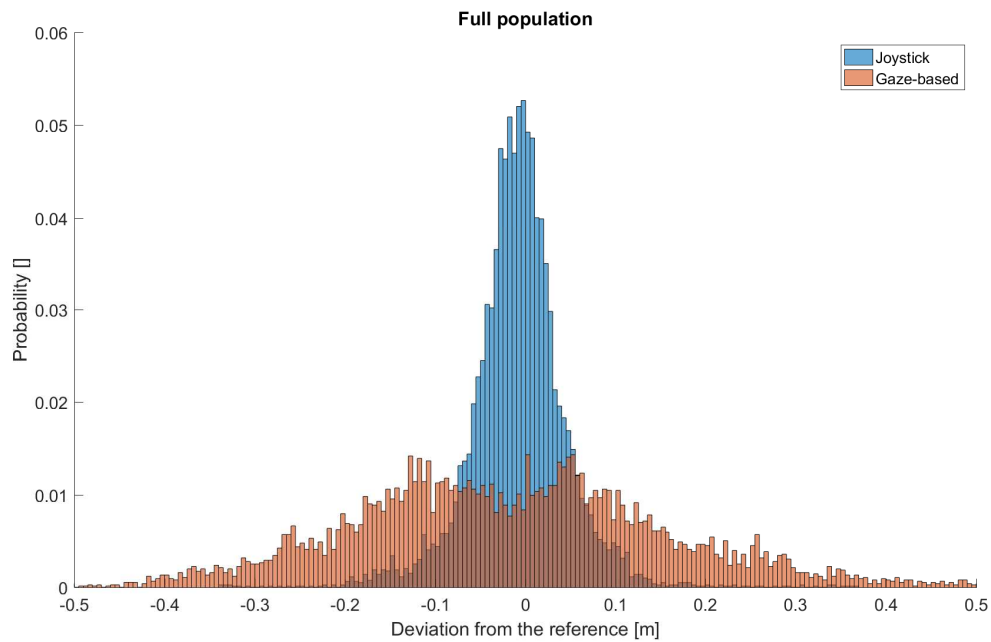
The probability density functions related to the deviation from the reference are shown in the figures ranging from 6.36 to 6.38. The data were recorded from a different type of subjects (full mobility users or reduced mobility user) driving wheelchairs with different input interfaces (joystick and gaze-based).

Comparing the deviation from the reference path related to the full population, shown in Fig. 6.36, it is possible to notice that the results are similar to the histograms obtained from the section 1. The variability of the data related to the gaze-based wheelchair is much higher than the joystick one, Fig. 6.36a. The same analysis on the entire population referred to the type of user shows a comparable variability on the deviation of the full mobility users and the reduced mobility users, Fig. 6.36b.

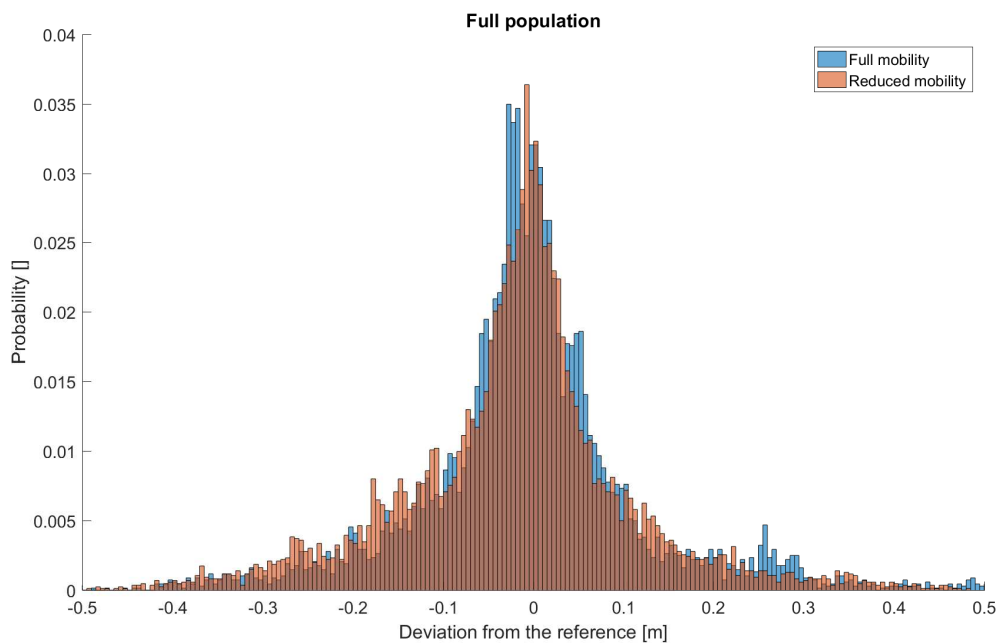
As in section 1, the analysis of the probability density function regarding individually the two specific subject type shows the same behaviour, Fig. 6.37a and 6.37b. The deviation obtained with the gaze controlled wheelchair presents a higher variability for both the full and reduced mobility users.

The comparison on user types highlights a good data overlapping in the case of both the full and the reduced mobility subjects that used the joystick, Fig. 6.38a, and the eye-controlled wheelchair, Fig. 6.38b. The histograms show a wider distribution for the gaze-based interface.

The analysis of variance ANOVA 2 way on the mean deviation (e_m) highlights that the subject is a significative parameter, even if with low influence. Fig. 6.39 shows the results of the analysis, on the top are presented the two boxplots regarding the subject and the interface while, on the bottom, the ANOVA table is reported. The resulting p-value is of 4.9% for the subject, that is very close to the traditional limit of 5% lesser than witch the test can be

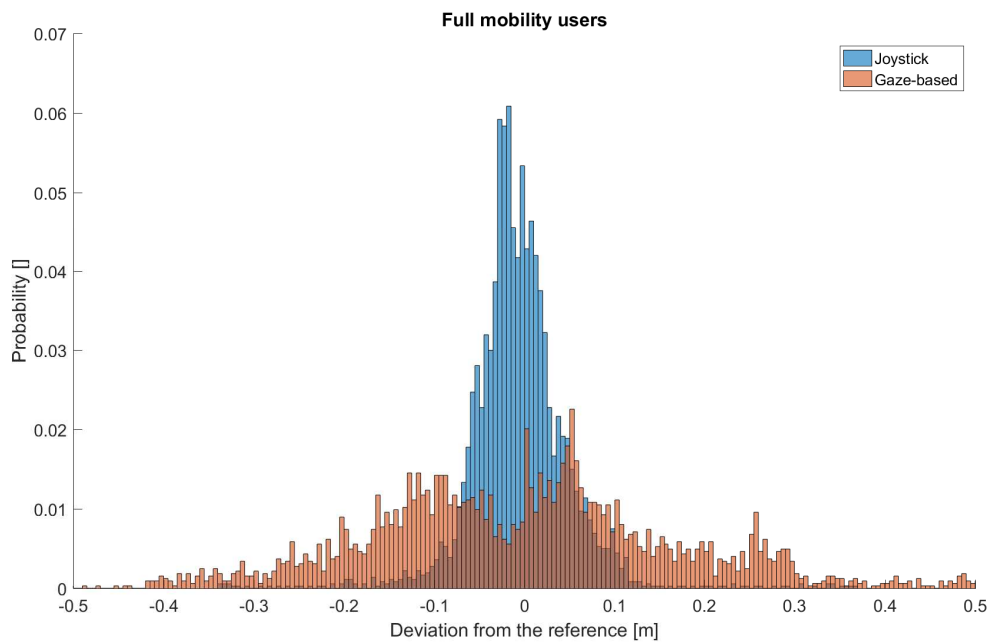


(a)

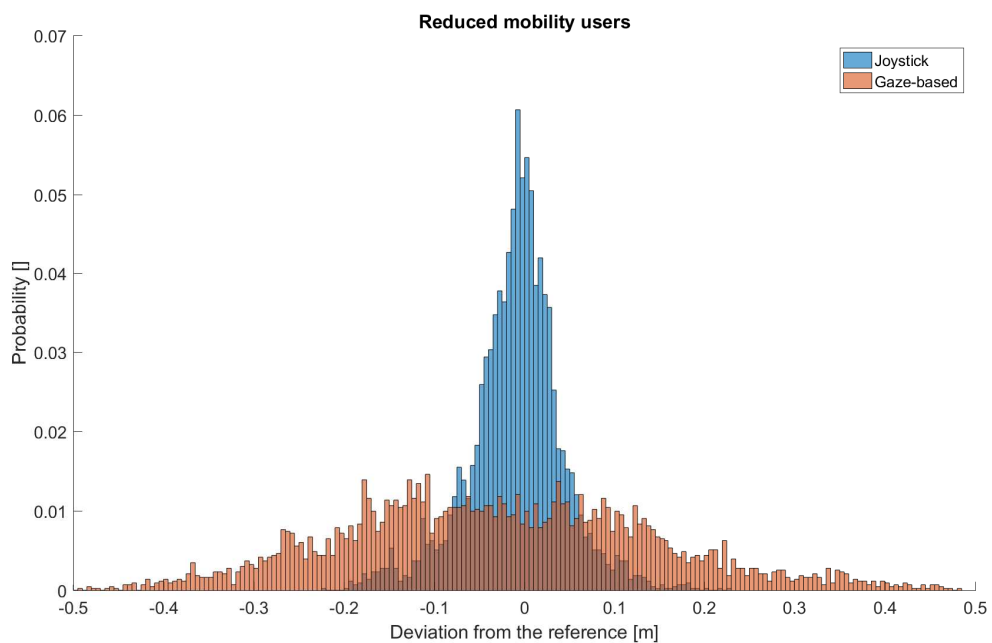


(b)

Fig. 6.36 Comparison of the deviation from the reference path related to the full population along the bumpy part of the path following test (section 2). Subfigure *a* shows the comparison between the control interface for both the subject type while the subplot *b* highlights the difference between the subjects using both the interfaces

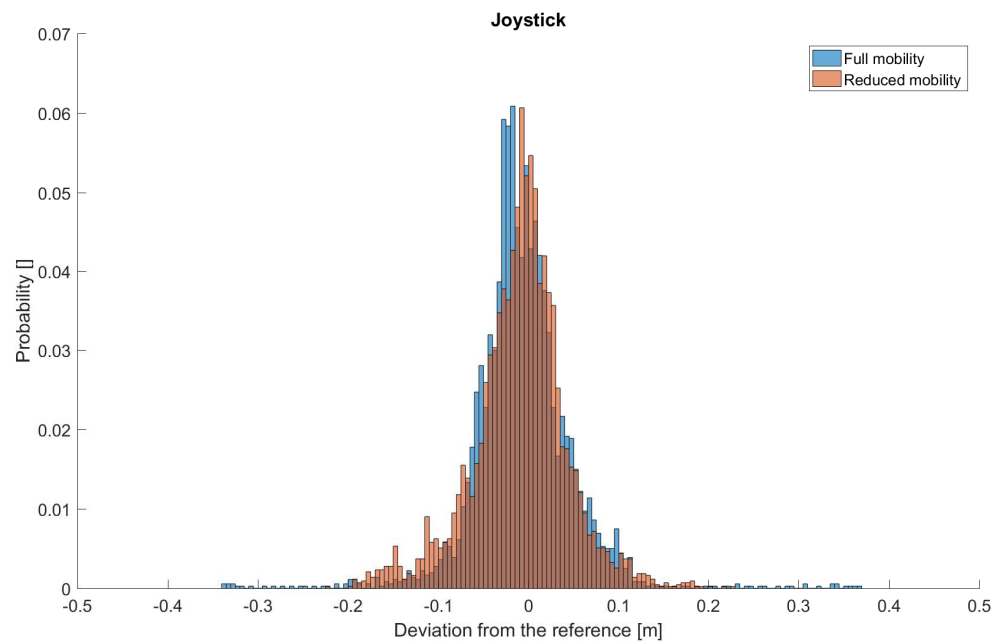


(a)

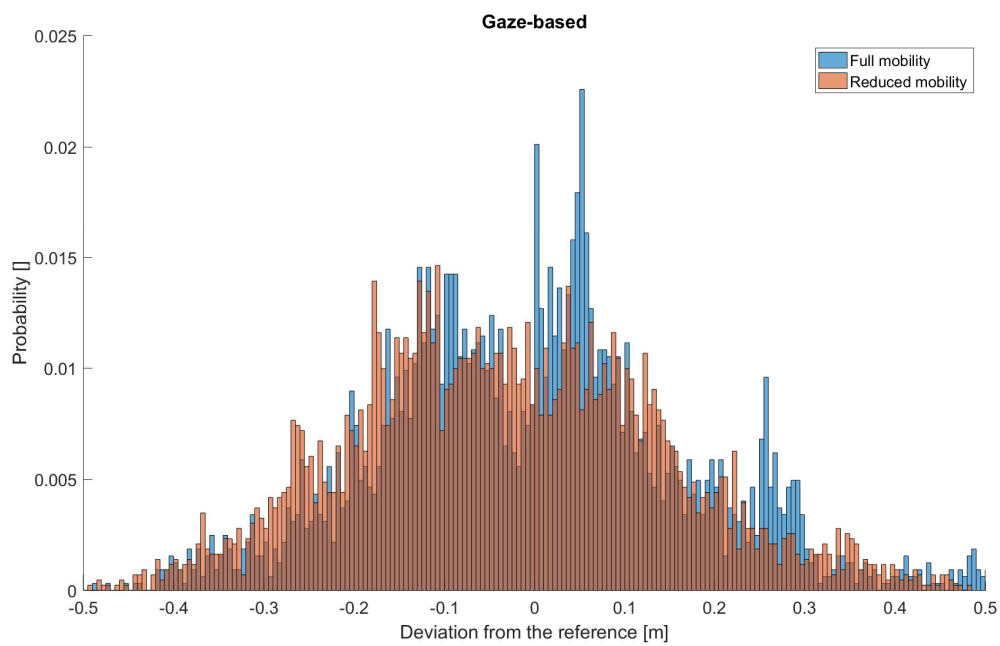


(b)

Fig. 6.37 Comparison of the deviation from the reference path between interfaces performed by full mobility users (a) and reduced mobility users (b) along the bumpy part of the path following test (section 2).

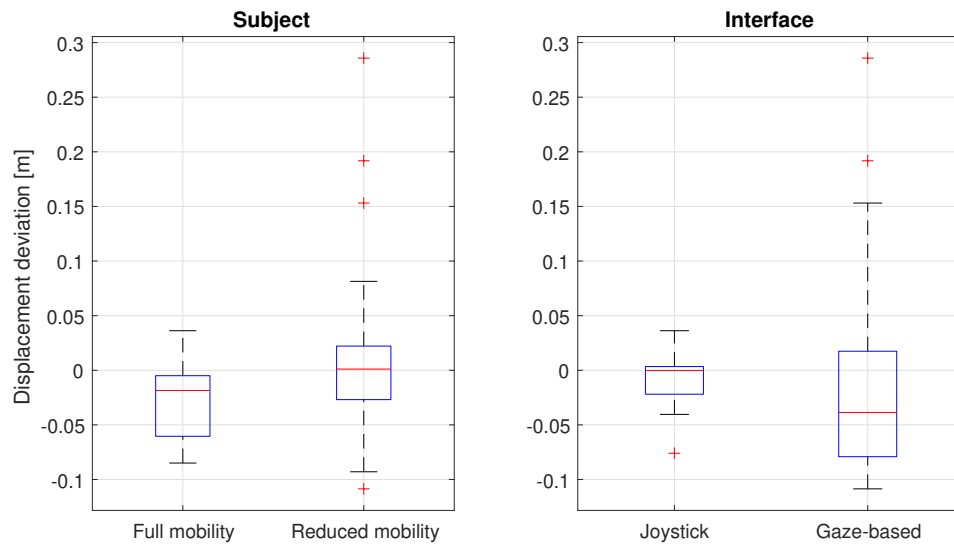


(a)



(b)

Fig. 6.38 Comparison of the deviation from the reference path between subjects driving a classic joystick wheelchair (a) and the gaze-based prototype (b) along the bumpy part of the path following test (section 2).

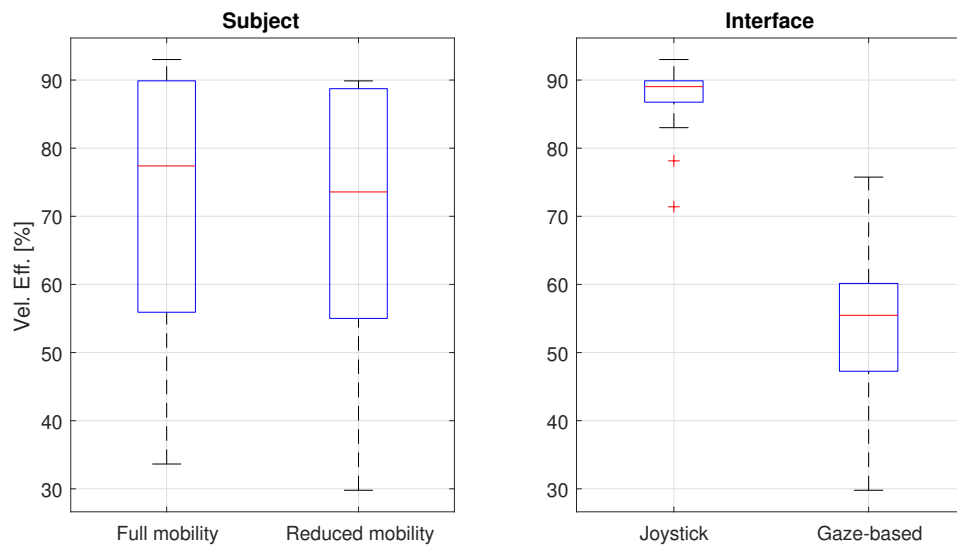


(a)

ANOVA Table					
Source	SS	df	MS	F	Prob>F
Subject	0.02	1	0.02	4.12	0.049
Interface	0.00002	1	0.00002	0	0.9477
Interaction	0.01151	1	0.01151	2.37	0.1313
Error	0.19393	40	0.00485		
Total	0.22546	43			

(b)

Fig. 6.39 ANOVA analysis for the mean deviation (e_m) for the path following test, along the section 2 with the box plots of the mean deviation related to subject (left) and interface (right).



(a)

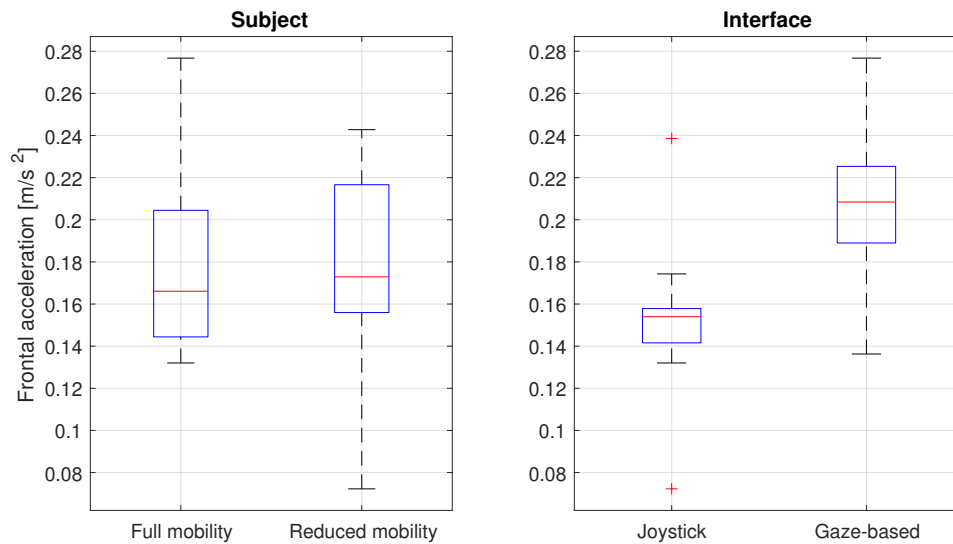
ANOVA Table					
Source	SS	df	MS	F	Prob>F
Subject	56.4	1	56.4	0.67	0.418
Interface	12031.3	1	12031.3	142.81	0
Interaction	15.5	1	15.5	0.18	0.6703
Error	3369.8	40	84.2		
Total	15473.1	43			

(b)

Fig. 6.40 ANOVA analysis for the efficiency in speed control (v_{eff}) for the path following test, along the section 2 with the box plots of the efficiency related to subject (left) and interface (right).

said to be significant. A p-value of 95% for the interface and 13% for the interaction suggest that the interface doesn't affect the performance, as well as the interaction between the two features don't present a statistically significant correlation. The differences between the performed path and the reference are similar to the values obtained in the first section. In contrast, the dispersion analysis ensures that the standard deviation of the distances obtained by full mobility users is wider than the previous case. In this case, the boxplot related to the subject analysis shows comparable standard deviations of the two subject types.

The next step of the analysis focuses on the average velocity, in terms of efficiency in the usage of the interface (v_{eff}). A p-value close to 0% for the interface highlights a significant difference among the two input technology. In contrast, a value of 42% for the subject

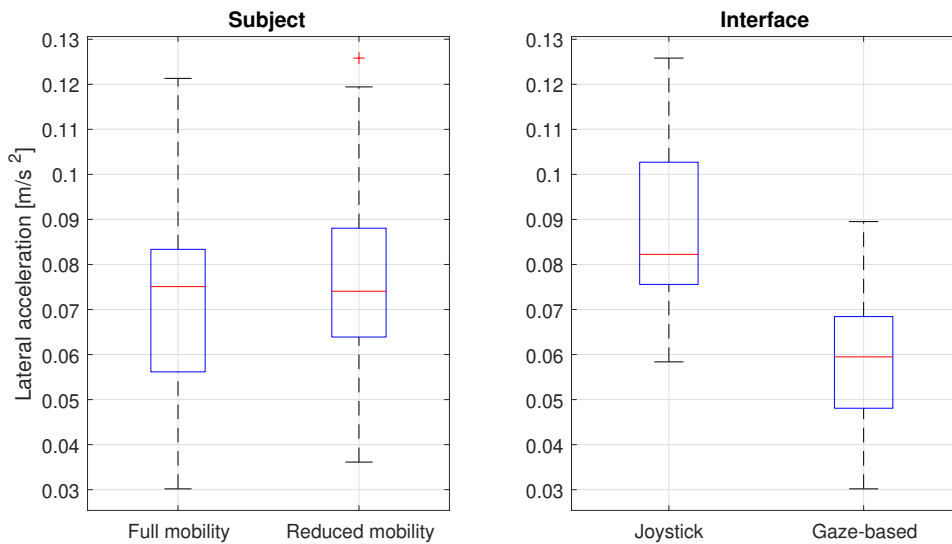


(a)

ANOVA Table					
Source	SS	df	MS	F	Prob>F
Subject	0.0003	1	0.0003	0.33	0.5695
Interface	0.03325	1	0.03325	36.65	0
Interaction	0.00016	1	0.00016	0.17	0.6803
Error	0.03628	40	0.00091		
Total	0.06999	43			

(b)

Fig. 6.41 ANOVA analysis for the frontal weighted average acceleration (a_{wf}) for the path following test, along the section 2 with the box plots of the acceleration related to subject (left) and interface (right).



(a)

ANOVA Table					
Source	SS	df	MS	F	Prob>F
Subject	0.00035	1	0.00035	1.13	0.2934
Interface	0.00894	1	0.00894	28.82	0
Interaction	0.00017	1	0.00017	0.56	0.4588
Error	0.01241	40	0.00031		
Total	0.02188	43			

(b)

Fig. 6.42 ANOVA analysis for the lateral weighted average acceleration (a_{wl}) for the path following test, along the section 2 with the box plots of the acceleration related to subject (left) and interface (right).

suggests no discrepancies among the two testing groups, Fig. 6.40. It follows that the joystick interface performed in a more efficient way than the ocular one, but at the same time both interfaces performed in a way that is independent from the subject type. A p-value of 67% for the interaction of the subject versus the interface indicates that there isn't any significant correlation from a statistical point of view. It is interesting to notice that the efficiency in speed control reached by full and reduced mobility subjects are similar in terms of both the mean value and the standard deviation. A bigger disparity is highlighted, as previously mentioned, in the ANOVA analysis on the interface in which the speed obtained with the joystick interface wheelchair provided the highest efficiency and the lower variability.

As for the acceleration, the analysis variance shows a behaviour very close to the one observed in section 1. The main differences are related to the median values of acceleration that is more or less doubled as well as the variability with respect to the previous case, Fig. 6.41a and 6.42a. The results of ANOVA suggests that the subject doesn't influence the performance in both the frontal and the lateral accelerations. Indeed, the p-value of the subject is 57% for the frontal acceleration and 29% for the lateral one, Fig. 6.41b and 6.42b.

Moreover, the ANOVA tables report a p-value of 0% for the interface in the case of both the frontal and lateral acceleration. This suggests that the interface has a strong effect on the accelerations. Considering the interaction, subject and interface features don't present a statistically significant correlation; the p-values are 68% and 45% respectively for the frontal and lateral acceleration.

Also in this case, the maximum values of frontal and lateral acceleration remained inside the *not uncomfortable* region of the regulation UNI ISO 2631, having an upper limit of 0.315 m/s^2 . Anyhow, using the gaze-based interface the users suffered smaller lateral acceleration compared to the joystick. The frontal accelerations present the opposite behaviour, with lower acceleration values for the joystick interface.

Section 3

The third part of the analysis concerns the curved part of the path following test, marked as section 3 in Fig. 6.18a. It is the last part of the path following test. In this section, are placed three aligned cones that must be bypassed. As in the previous two sections, the user has to follow a reference path drawn on the floor in order to pass through the cones. The curved path resulted to be the most tricky due to the reduced distance between the cones requiring the precise manoeuvres. Therefore, the user must maintain the attention not only on the line to be followed but also on the environment surrounding the vehicle. This task requires the usage of the peripheral view.

The first feature evaluated is the wheelchair deviations in position from the reference along the curved part of the path following test, determined as the shortest distance between each point of the segmented reference and the path performed by the wheelchairs.

The figures ranging from 6.43 to 6.45 show the probability density functions referring to the deviation from the reference performed by different type of subjects (full mobility users or reduced mobility users) and with different input interfaces (joystick and gaze-based).

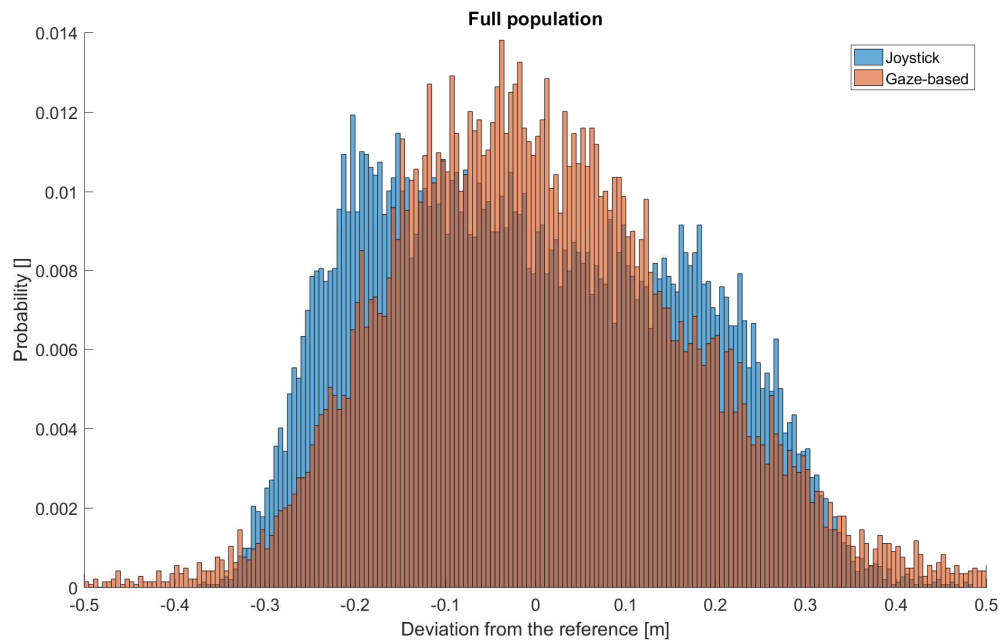
The deviation from the reference path, related to the full population and reported in Fig. 6.43, shows that the behaviour of the probability density function is different compared to the previous cases. The variability of the wheelchair positions related to the gaze-based interface is higher with respect to the joystick one. Moreover, it is interesting to notice that the probability density function of the gaze-based interface presents a shape very similar to a Gaussian distribution. Instead, the histogram concerning the joystick interface is characterized by two symmetric peaks around the zero. The reason of this behaviour can be observed in Fig 6.46 where the blue lines indicate the full set of paths performed by using the joystick. It is evident that during the test with the commercial wheelchair the users systematically passed in the internal part of the curves, introducing in this way the two mean deviations, on the left and on the right of the reference.

The same analysis on the entire population referred to the type of user shows a comparable variability on the deviation of the full mobility users and the reduced mobility users, Fig. 6.43b.

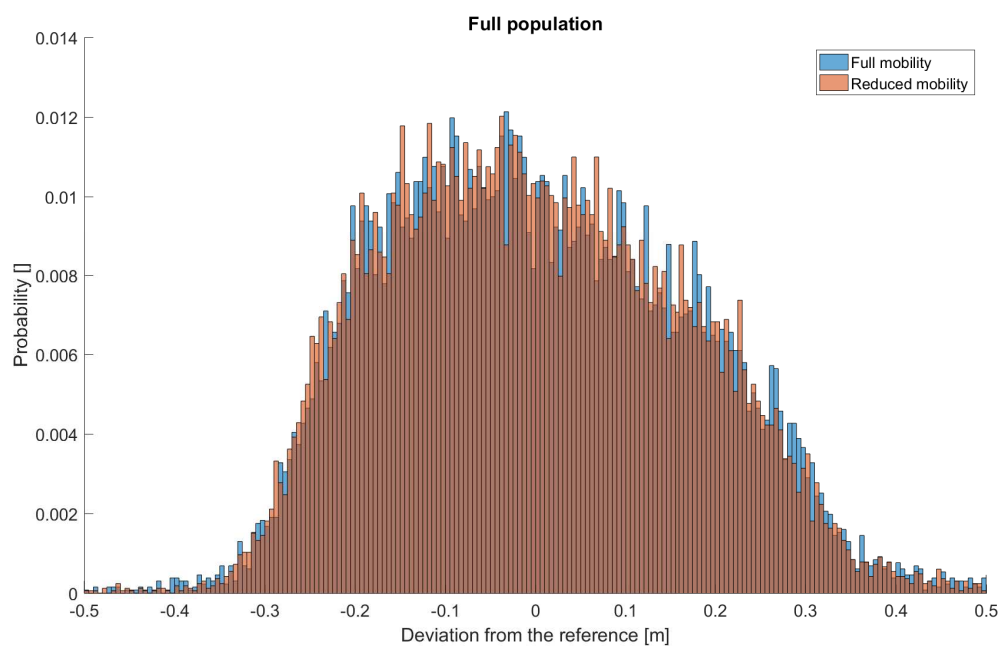
In the same way, it is interesting to focus the analysis of the probability density function, initially on the subject type and then on the interfaces. In particular, the comparison of the deviation between the joystick and gaze-based interface shows the same behaviour for both the cases of full and reduced mobility users, Fig. 6.44a and 6.44b. The histograms show a wider distribution for the joystick interface.

The comparison on user types highlights a good overlap in the data both in the case of full and reduced mobility subjects that used the joystick, Fig. 6.45a, and the eye-controlled wheelchair, Fig. 6.45b.

The analysis of variance on the displacement variation highlights the relevant role of the interface, Fig. 6.47. With a p-value on this factor of 1.5%, the outcome of the test is that the ocular interface performs generally in a worse way than the joystick. That comes from the higher variability of in the performed paths previously explained. However, the module of the median deviation obtained with the gaze-based interface is smaller with respect to the joystick one. As for the subject, no marked differences can be stated (p-value of 18%) and the median values of e_m are very similar. The only difference is the higher data variability

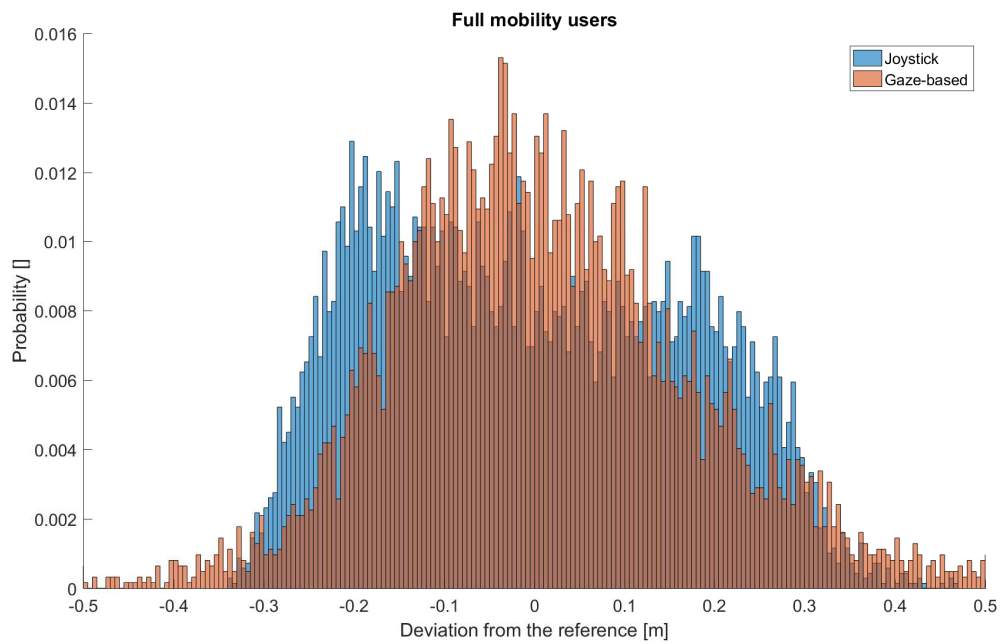


(a)

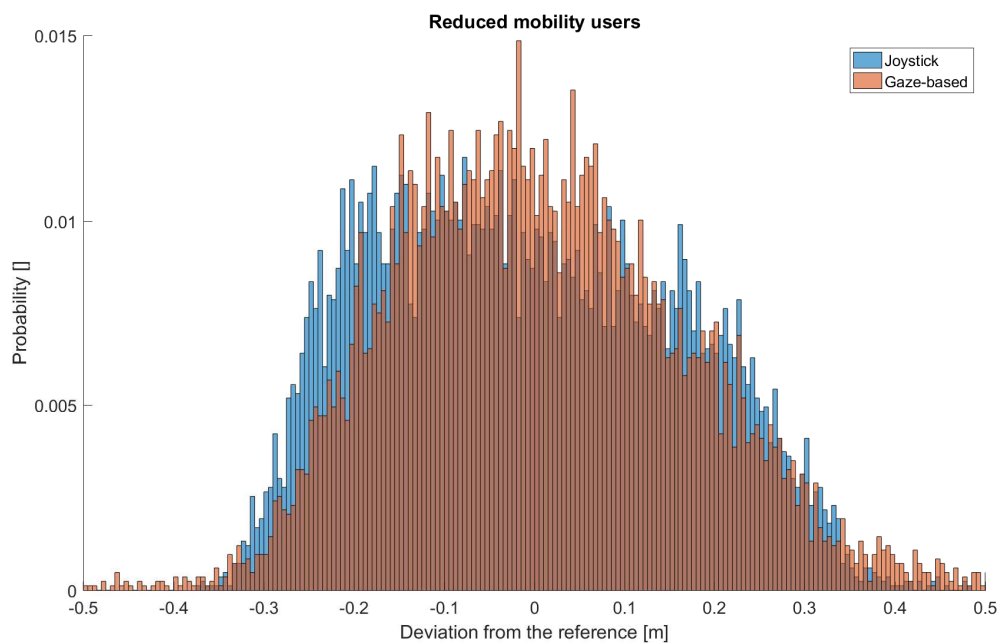


(b)

Fig. 6.43 Comparison of the deviation from the reference path related to the full population along the curved part of the path following test (section 3). Subfigure *a* shows the comparison between the control interface for both the subject type while the subplot *b* highlights the difference between the subjects using both the interfaces

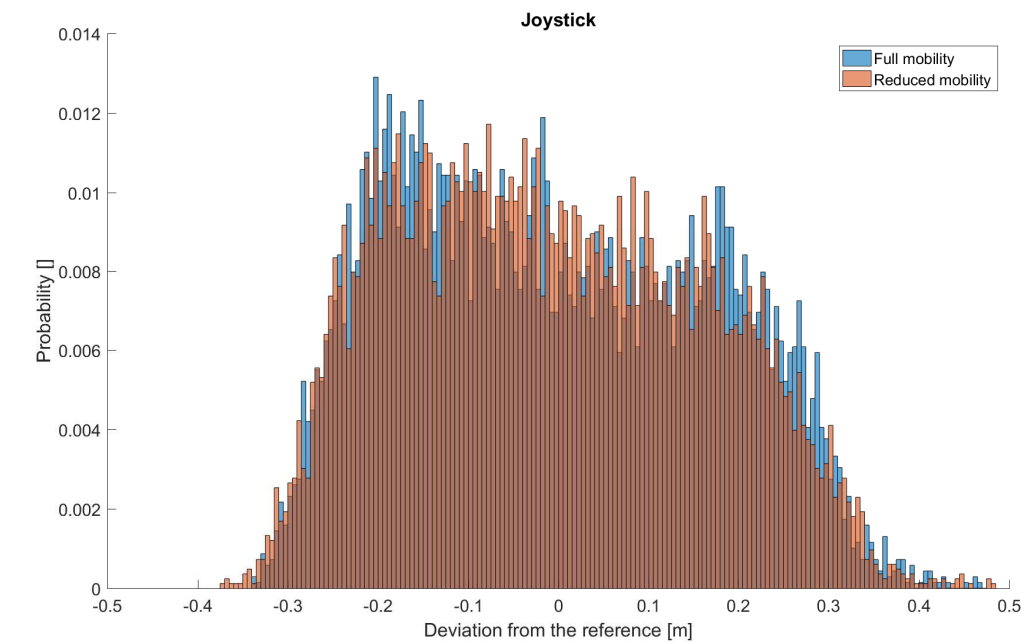


(a)

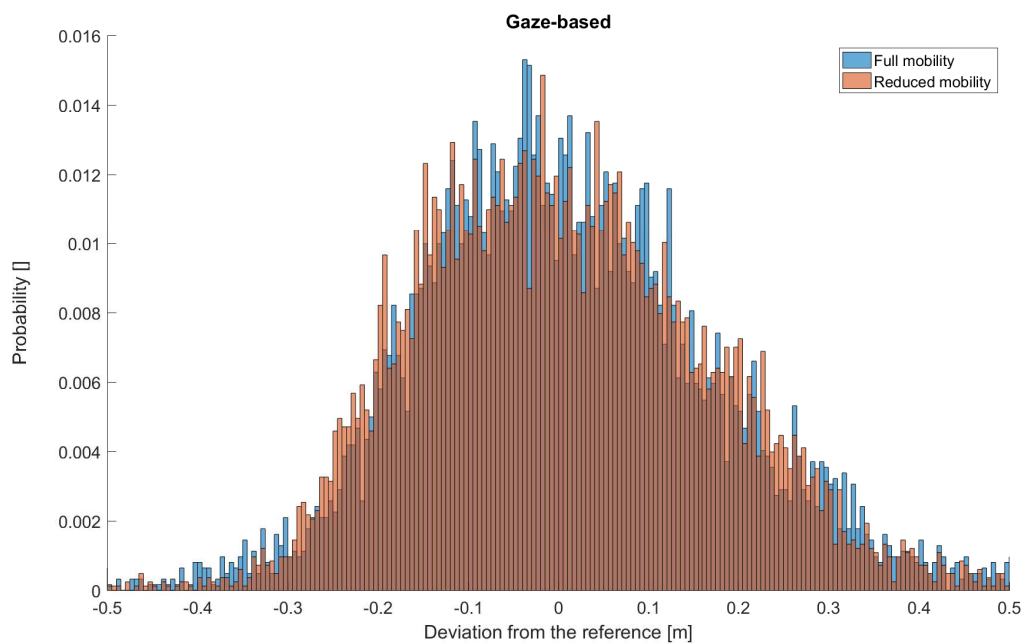


(b)

Fig. 6.44 Comparison of the deviation from the reference path between interfaces performed by full mobility users (a) and reduced mobility users (b) along the curved part of the path following test (section 3).



(a)



(b)

Fig. 6.45 Comparison of the deviation from the reference path between subjects driving a classic joystick wheelchair (a) and the gaze-based prototype (b) along the curved part of the path following test (section 3).

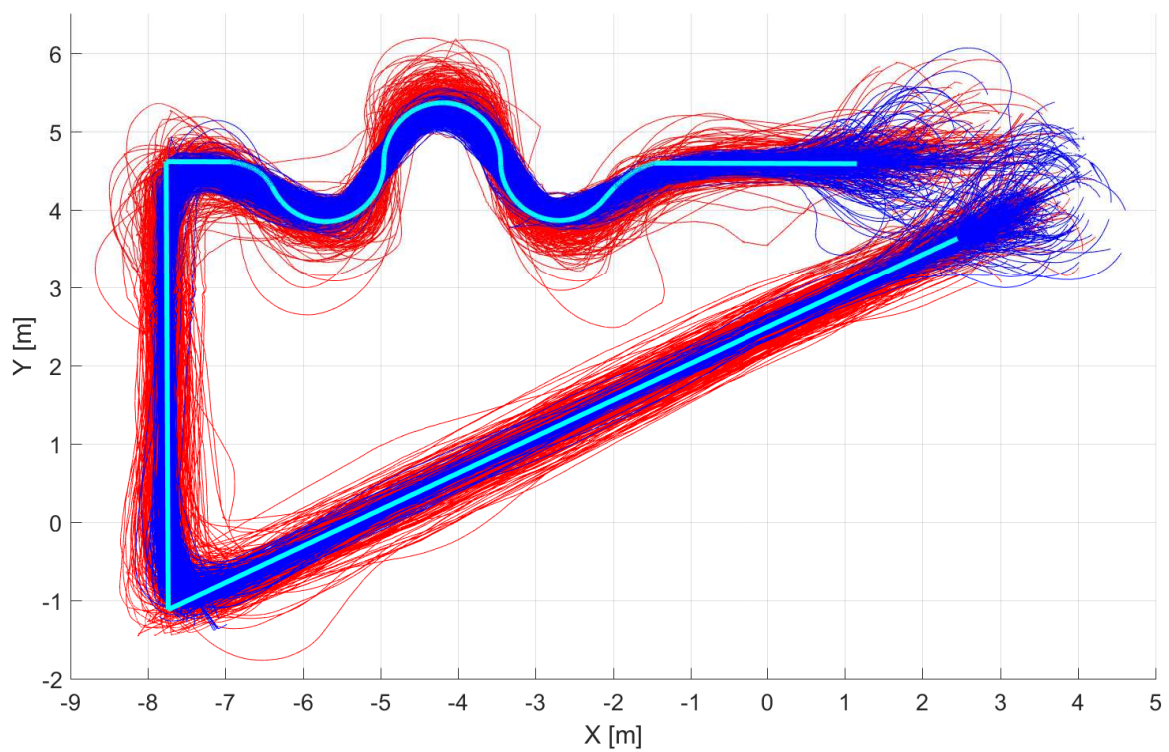
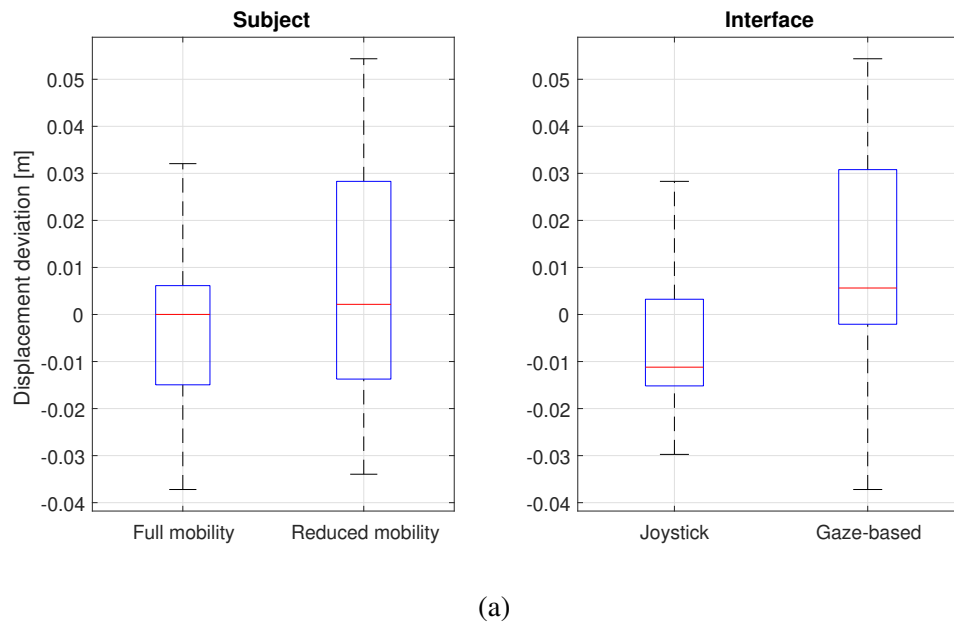


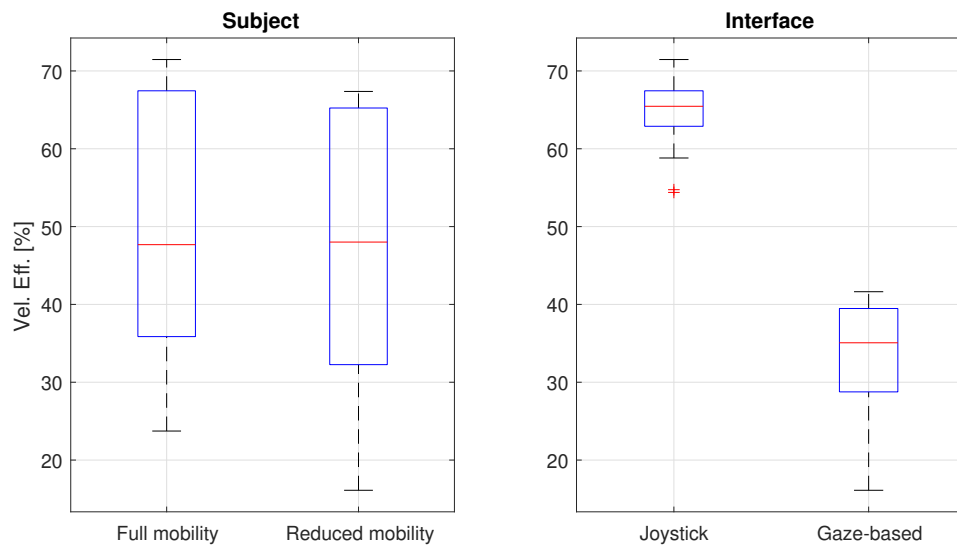
Fig. 6.46 Full set of paths related to the path following test. The blue and the red paths were performed by using respectively the joystick and the gaze-based wheelchairs.



ANOVA Table					
Source	SS	df	MS	F	Prob>F
Subject	0.0008	1	0.0008	1.89	0.1765
Interface	0.00268	1	0.00268	6.34	0.0159
Interaction	0	1	0	0	0.9861
Error	0.01692	40	0.00042		
Total	0.0204	43			

(b)

Fig. 6.47 ANOVA analysis for the mean deviation (e_m) for the path following test, along the section 3 with the box plots of the mean deviation related to subject (left) and interface (right).



(a)

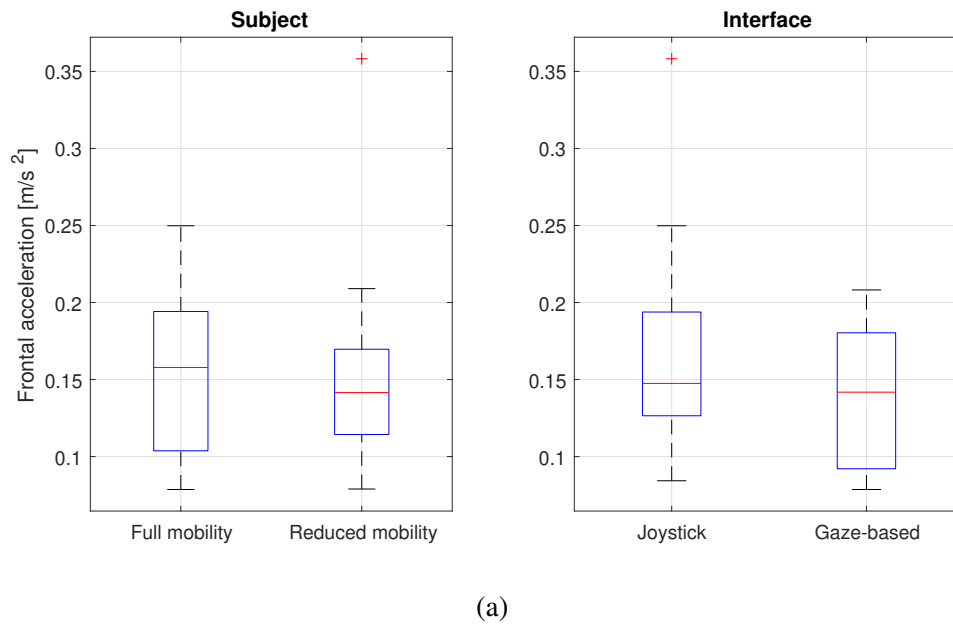
ANOVA Table					
Source	SS	df	MS	F	Prob>F
Subject	100.6	1	100.6	2.67	0.1103
Interface	11040.2	1	11040.2	292.67	0
Interaction	1.2	1	1.2	0.03	0.857
Error	1508.9	40	37.7		
Total	12651	43			

(b)

Fig. 6.48 ANOVA analysis for the efficiency in speed control (v_{eff}) for the path following test, along the section 3 with the box plots of the efficiency related to subject (left) and interface (right).

obtained by users with reduced mobility. A p-value of 99% for the interaction suggests that the two features don't present a statistically significant correlation.

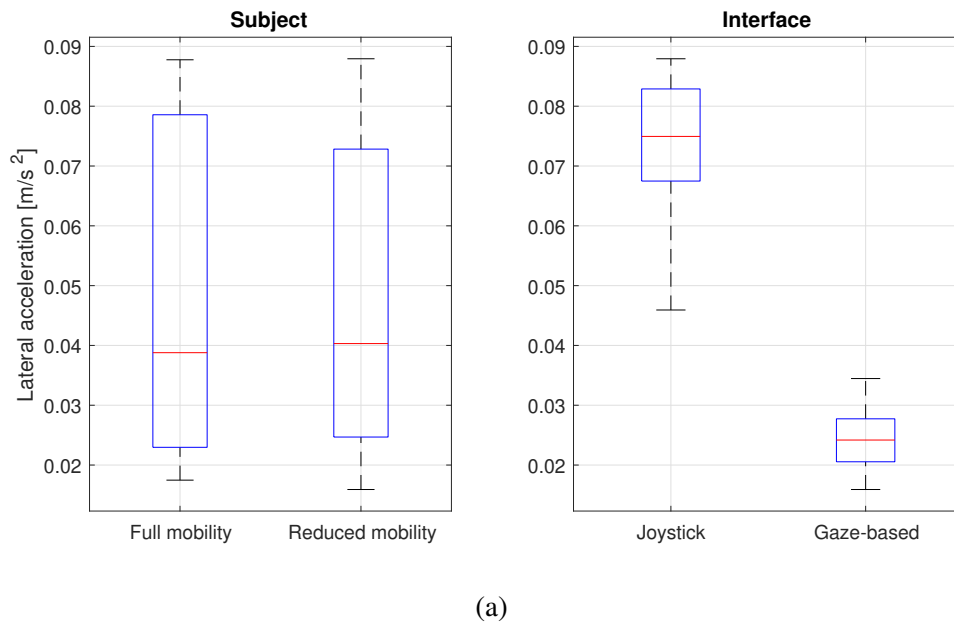
As for the average velocity in terms of efficiency in the usage of the interface (v_{eff}), a p-value of 0% for the interface highlights a significant difference among the two input technology, Fig. 6.48b. In particular, the speed values coming from the joystick interface presents higher efficiency. The median value is more than double with respect to the gaze-based interface. Also the variability is smaller. In contrast, a p-value of 11% for the subject indicates that there aren't any differences among the two testing groups, Fig. 6.48. This feature doesn't have any influence on velocity efficiency. In this case, the data collected from



ANOVA Table					
Source	SS	df	MS	F	Prob>F
Subject	0.00002	1	0.00002	0.01	0.9387
Interface	0.00741	1	0.00741	2.51	0.1207
Interaction	0.00002	1	0.00002	0.01	0.9315
Error	0.11783	40	0.00295		
Total	0.12528	43			

(b)

Fig. 6.49 ANOVA analysis for the frontal weighted average acceleration (a_{wf}) for the path following test, along the section 3 with the box plots of the acceleration related to subject (left) and interface (right).



(a)

ANOVA Table					
Source	SS	df	MS	F	Prob>F
Subject	0	1	0	0.04	0.8479
Interface	0.02566	1	0.02566	246.49	0
Interaction	0.00001	1	0.00001	0.07	0.791
Error	0.00416	40	0.0001		
Total	0.02984	43			

(b)

Fig. 6.50 ANOVA analysis for the lateral weighted average acceleration (a_{wl}) for the path following test, along the section 3 with the box plots of the acceleration related to subject (left) and interface (right).

full and reduced mobility users are very similar in terms of median value and variability. A p-value of 86% for the interaction of the subject versus the interface indicates that there isn't any significant correlation from a statistical point of view.

The analysis about the frontal acceleration highlights a p-value of 93% and 12% respectively for the subject and the interface, Fig. 6.49b. This means that the two feature doesn't have any influence on the performance regarding, in this case, the comfort of the user. Moreover, the data collected from both the user types and by both the interfaces are very similar in terms of median value and variability as shown in Fig. 6.49a.

A p-value of 93% for the interaction indicates that there isn't any significant correlation between the subject and interface.

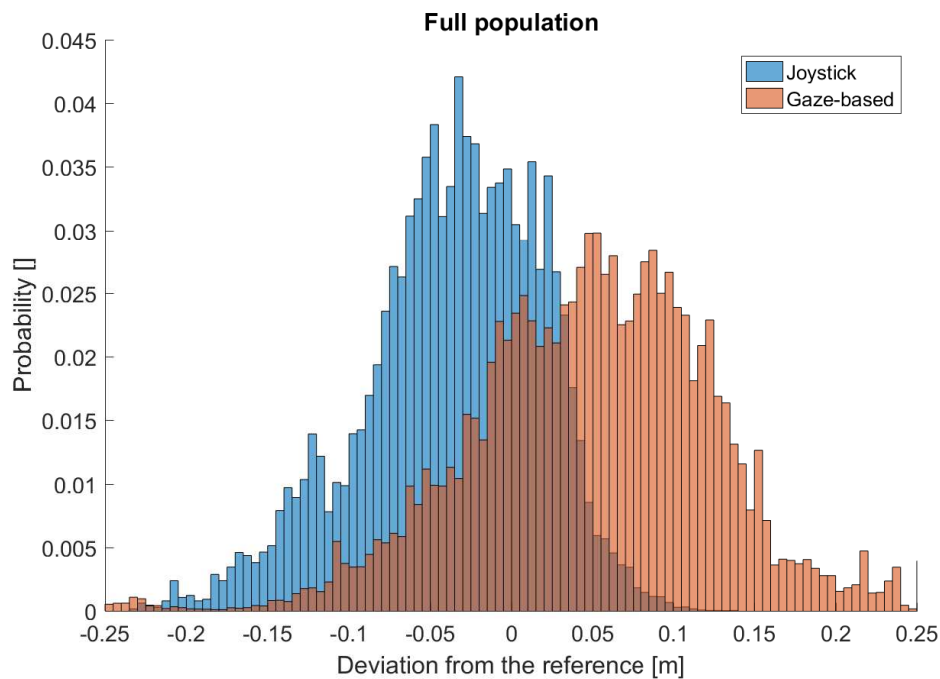
The results of the ANOVA on the lateral acceleration suggests a strong influence of the interface on the performances. Indeed, the ANOVA table of Fig. 6.50b reports a p-value regarding the interface feature of 0%. In particular, the median values obtained with the joystick are three times the ones recorded with the gaze-based interface, Fig. 6.50a. This means that in this case, the joystick interface performs in a worse way than the gaze-based. In contrast, the subject doesn't influence the lateral acceleration with a p-value of 85%. In this case, both the median and the variability is very similar.

As for the interaction between feature and interface the analysis of variance returns a p-value of 79% indicating that there isn't any significant statistical correlation between the features.

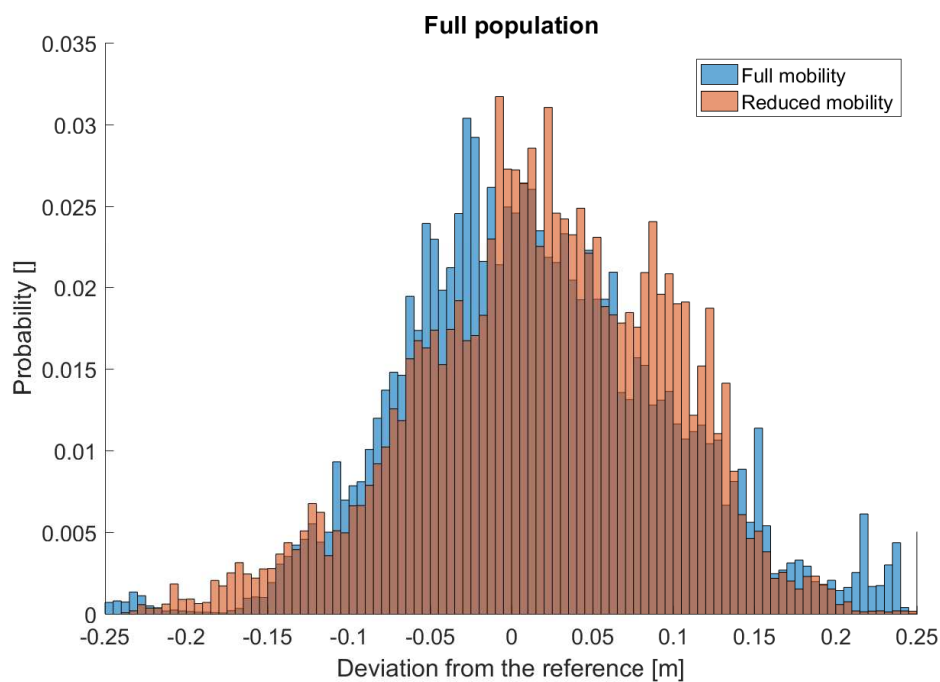
Anyhow, the maximum value of both frontal and lateral accelerations remains inside the *not uncomfortable* region of the regulation UNI ISO 2631, having an upper limit of 0.315 m/s^2 .

Section 4

The fourth part evaluated is related to the parking test, marked as section 4 in Fig. 6.18b. This test is finalized to analyse the performance of manoeuvring task as well as the passage through a corridor without any lines drawn on the floor to be followed. Regarding this topic, the users highlighted a completely different driving feeling, especially concerning the eye-controlled wheelchair. Their attention was not focused on a line drawn on the floor, placed in the central part of the screen, but widely to search some reference points laterally in the surrounding environment. Therefore, also in this case, the peripheral view assumes a key role in the control of the wheelchair.

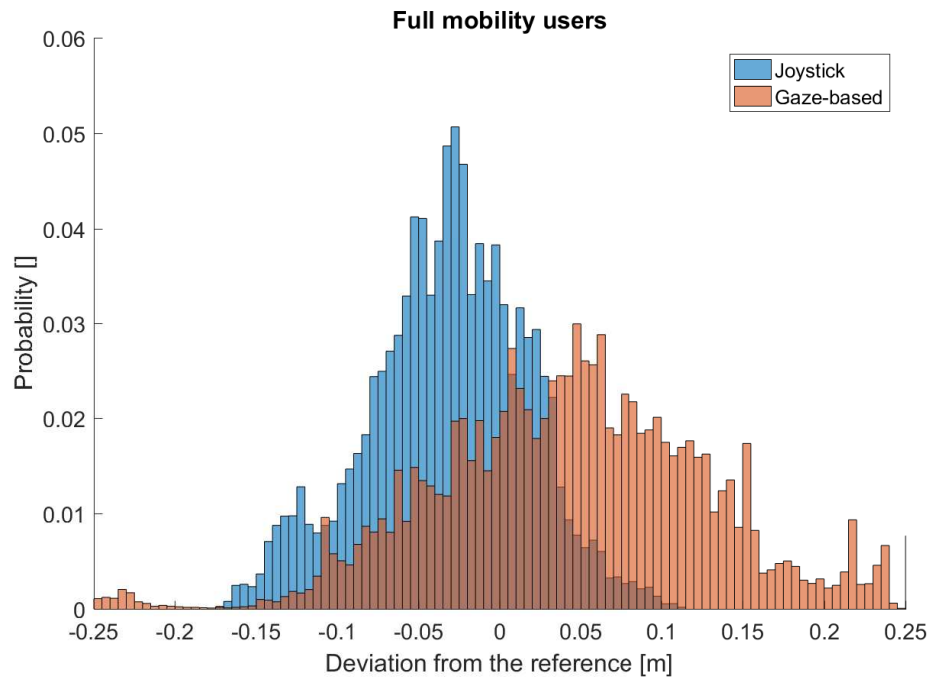


(a)

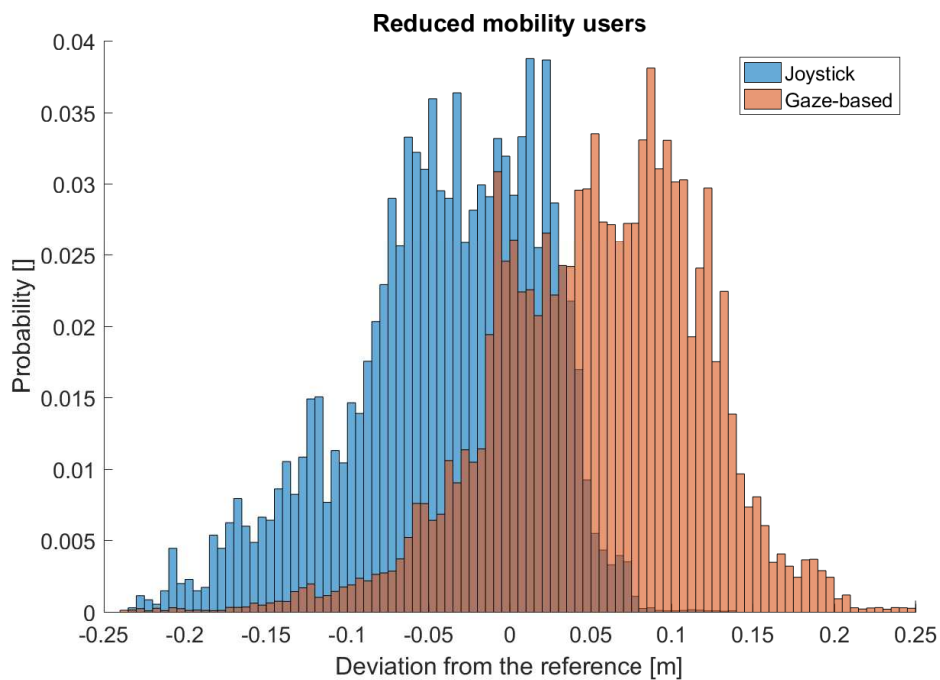


(b)

Fig. 6.51 Comparison of the deviation from the reference path related to the full population along the parking test (section 4). Subfigure *a* shows the comparison between the control interface for both the subject type while the subplot *b* highlights the difference between the subjects using both the interfaces



(a)



(b)

Fig. 6.52 Comparison of the deviation from the reference path between interfaces performed by full mobility users (a) and reduced mobility users (b) on the parking test (section 4).

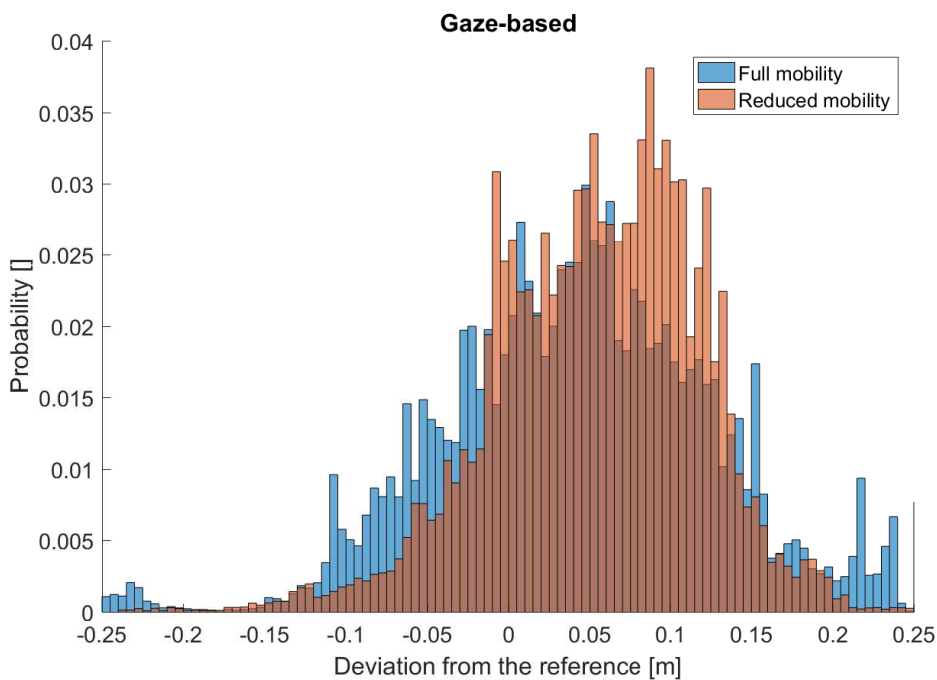
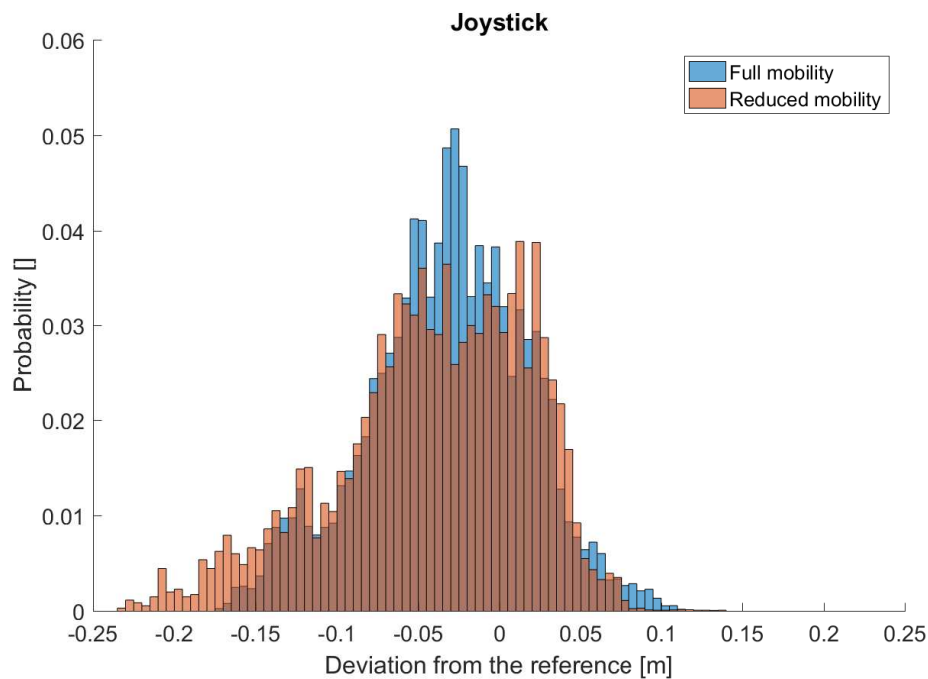


Fig. 6.53 Comparison of the deviation from the reference path between subjects driving a classic joystick wheelchair (a) and the gaze-based prototype (b) along the parking test (section 4).

The parking test aims to evaluate the driving capability performing tight manoeuvres and passing through narrow spaces. During the test the user started from a fixed point and drove as quickest as possible through a series of cones that are positioned on a wide and flat of the floor, as shown in Fig. 6.18b, without touching any of them. The starting point and the series of cones were placed in such a way to force the user to perform the curve and the reverse curve before entering the corridor.

The first feature evaluated is the wheelchair deviations in position from an ideal reference line placed in the middle of the corridor. It was determined as the point to line distance between the reference line and the path performed by the wheelchairs. The figures ranging from Fig. 6.51 to 6.53 show the probability density functions referring to the deviation from the reference performed by different type of subjects (full mobility users or reduced mobility users) and with different input interfaces (joystick and gaze-based). The first results of the test are related to the behaviour of the probability density function of the deviation from the reference. The deviation values have a positive sign on the left part of the reference while the sign is negative on the right side. The variability of the wheelchair position performed with the gaze-based interface is slightly higher than the joystick one, as shown in Fig. 6.51a. Moreover, it is possible to notice a difference regarding the expected values of the Gaussian distribution. The deviations obtained with the joystick present an expected value lower than zero while, the data collected with the gaze-based interface have an expected value greater than zero. This difference can be noticed also in Fig. 6.54c on which the paths obtained with the joystick are mainly placed on the right with respect to the reference (cyan line). Contrary, the path performed with the eye-controlled wheelchair is located to the left of the reference.

The same analysis on the entire population referred to the type of user shows a comparable variability on the deviation of the full mobility users and the reduced mobility users, Fig. 6.51b.

It is also interesting to analyse the probability density function separately, before on the subject type and then on the interfaces. The comparison of the deviation between the joystick and gaze-based interface shows the behaviour previously explained with the positive and the negative expected values, Fig. 6.52a and 6.52b. In the case of the full mobility users, the gaze-based data shows a wider distribution.

The comparison on user types highlights a good overlap in the data both in the case of full and reduced mobility subjects that used the joystick, Fig. 6.53a, and the eye-controlled wheelchair, Fig. 6.53b.

As explained before, the manoeuvring test shows a discrepancy in the final reached position, Fig. 6.55a, with a median of -2.8 cm for the joystick and of 3.4 cm for the ocular

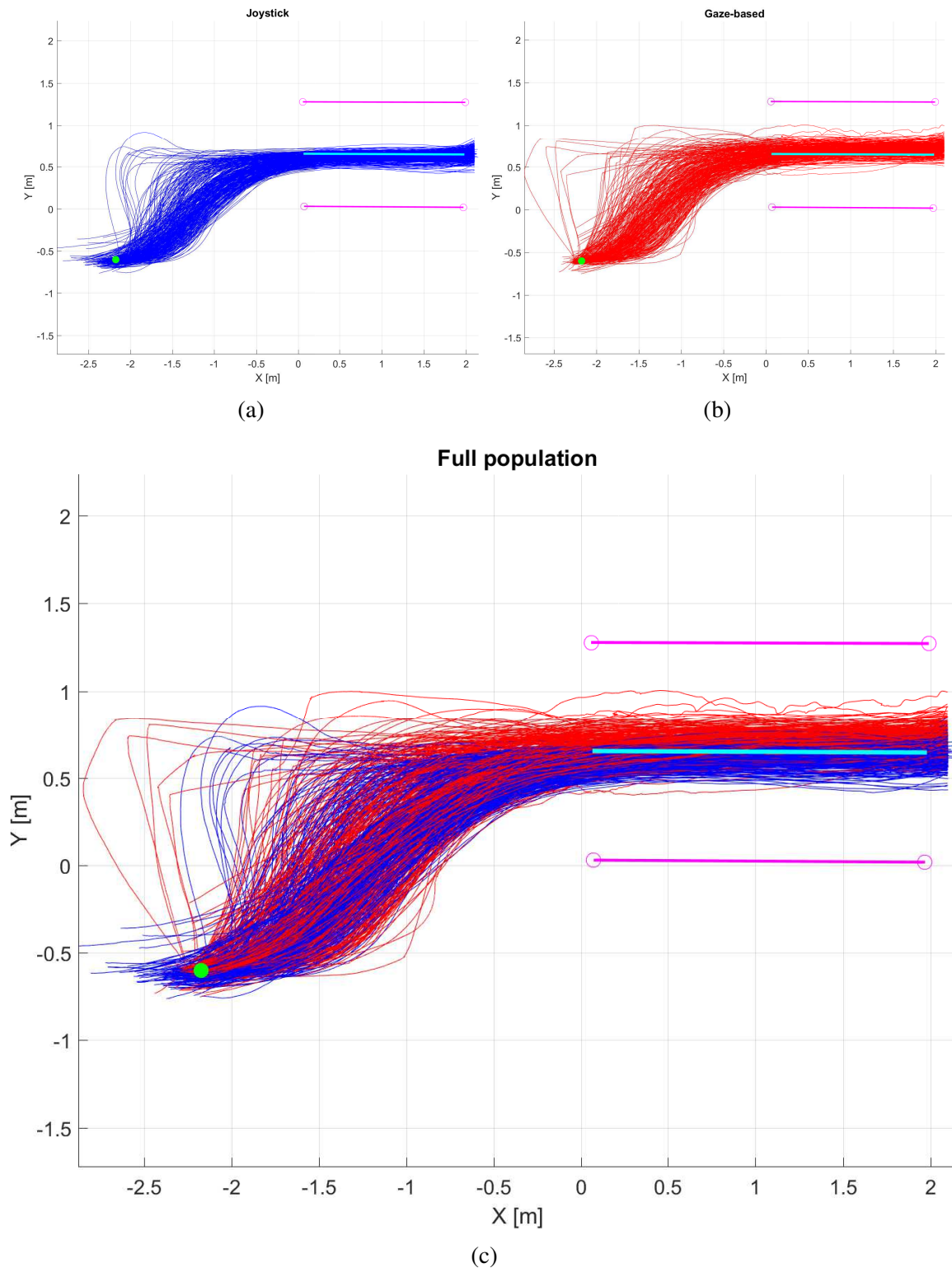
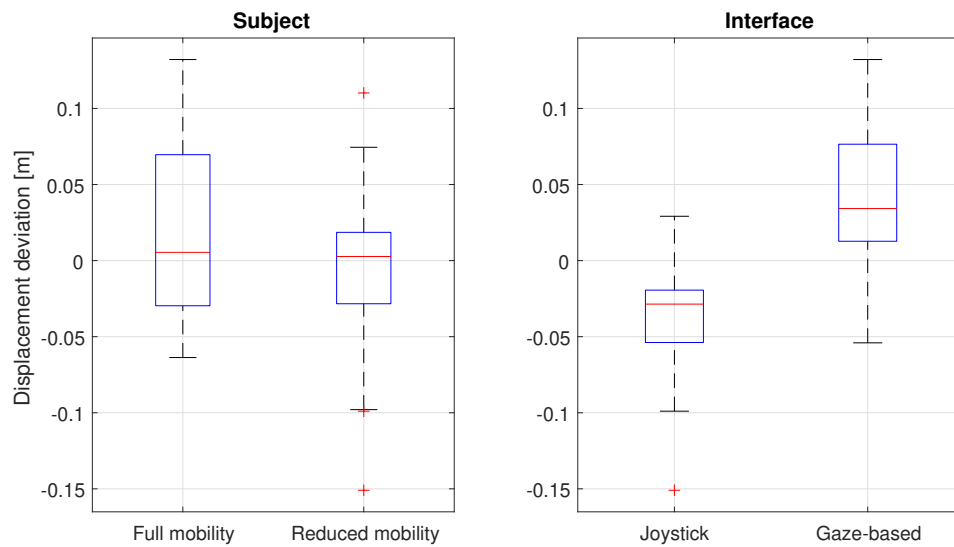


Fig. 6.54 Full set of paths related to the parking test. The blue and the red paths were performed by using respectively the joystick and the gaze-based wheelchairs. Subfigures *a* and *b* show the only the data related to the joystick and to the gaze-based control, while subfigure *c* contains the full set of data.



(a)

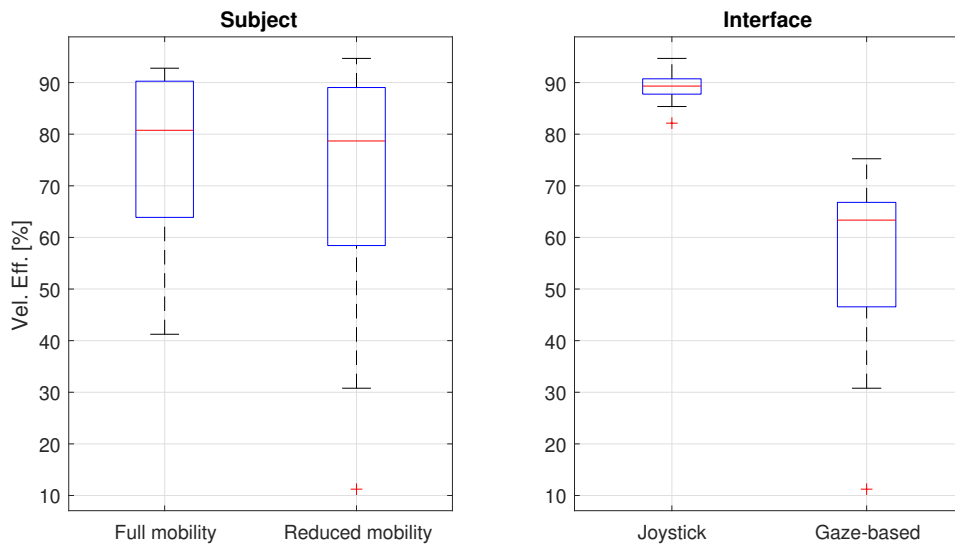
ANOVA Table					
Source	SS	df	MS	F	Prob>F
Subject	0.00838	1	0.00838	4.56	0.0388
Interface	0.07151	1	0.07151	38.95	0
Interaction	0.00012	1	0.00012	0.07	0.797
Error	0.07343	40	0.00184		
Total	0.15344	43			

(b)

Fig. 6.55 ANOVA analysis for the mean deviation (e_m) for the parking test, with the box plots of the mean deviation related to subject (left) and interface (right).

HMI. Despite the absolute value of the error is similar, the outcome suggests that the two interfaces cause different behaviours during the execution of a manoeuvre. The analysis of variance regarding the subject returns a p-value of 4% that confirms a difference in the performance depending on the user. As regards the interface, a p-value of 0% suggests that this feature has a strong effect on the mean deviation. Considering the interaction, subject and interface features don't present a statistically significant correlation with a p-value of 80%.

Anyhow, from an operative point of view, the similarity of the error suggests that the interfaces can be considered in first approximation similar (p-value of 8% for the $\log_{10}|e_m|$), Table 6.8.

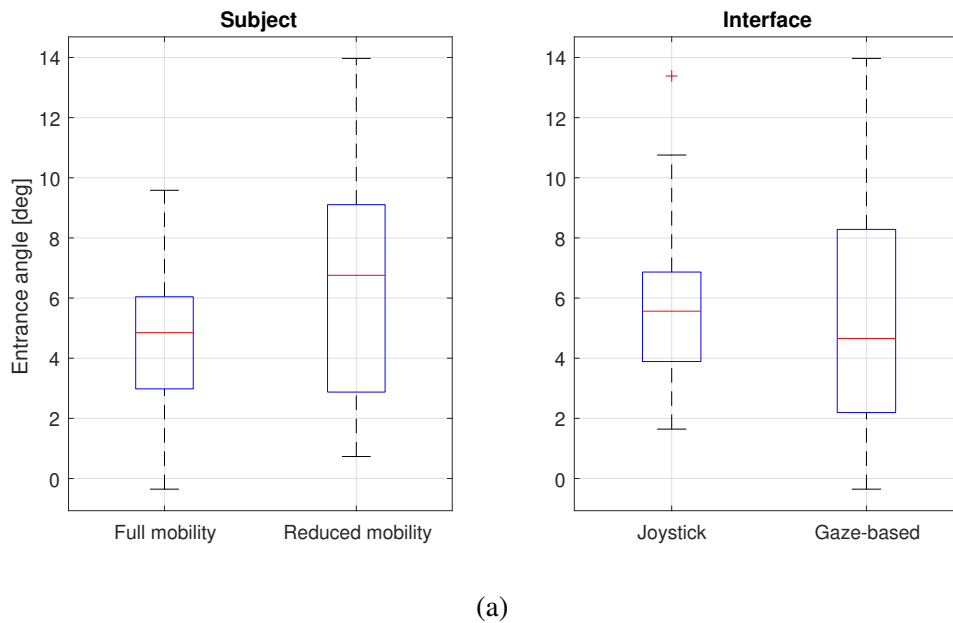


(a)

ANOVA Table					
Source	SS	df	MS	F	Prob>F
Subject	517.2	1	517.2	3.79	0.0586
Interface	11934.5	1	11934.5	87.49	0
Interaction	294.1	1	294.1	2.16	0.1499
Error	5456.6	40	136.4		
Total	18202.5	43			

(b)

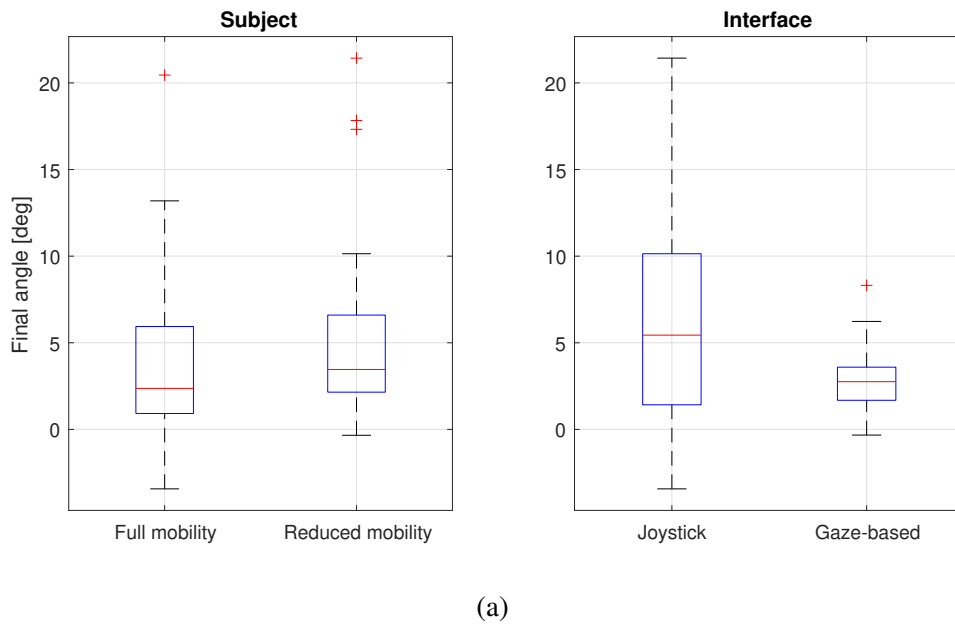
Fig. 6.56 ANOVA analysis for the efficiency in speed control (v_{eff}) for the parking test, with the box plots of the efficiency related to subject (left) and interface (right).



ANOVA Table					
Source	SS	df	MS	F	Prob>F
Subject	46.601	1	46.6007	4.21	0.0467
Interface	3.813	1	3.8128	0.34	0.5604
Interaction	5.366	1	5.3663	0.49	0.4901
Error	442.434	40	11.0609		
Total	498.214	43			

(b)

Fig. 6.57 ANOVA analysis for the entrance angle (θ_s) for the parking test, with the box plots of the angle related to subject (left) and interface (right).



(a)

ANOVA Table					
Source	SS	df	MS	F	Prob>F
Subject	19.82	1	19.824	0.72	0.4003
Interface	141.36	1	141.361	5.15	0.0286
Interaction	57.02	1	57.018	2.08	0.1571
Error	1096.97	40	27.424		
Total	1315.17	43			

(b)

Fig. 6.58 ANOVA analysis for the exit angle (θ_e) for the parking test, with the box plots of the angle related to subject (left) and interface (right).

The analysis on the average velocity, in terms of efficiency in the usage of the interface (v_{eff}) returns a p-value of 0% indicating a significant difference among the two input technology, Fig. 6.56b. The speed values coming from the joystick interface ($\sim 90\%$) presents higher median efficiency than the gaze-based one ($\sim 63\%$) as shown in Fig. 6.56a. Furthermore, the gaze-based interface provides a higher variability. Contrarily, a p-value of 6% for the subject indicates that there aren't any differences among the two testing groups. The data collected are very similar from both median and variability point of view. This means that the subject doesn't influence velocity efficiency. A p-value of 15% for the interaction of the subject versus the interface indicates that there isn't any significant correlation from a statistical point of view.

The next step of the analysis focuses on the initial attitude of the wheelchair at the entrance of the corridor. The ANOVA table, shown in Fig. 6.57b, reports a p-value of 4.7% that is near to the limit of the significance level of 0.05 indicating that a difference exists on the evaluated feature. From the boxplot related to the subject it is possible to deduce that the reduced mobility users turn into the corridor with a higher median angle and obtaining a greater deviation, Fig. 6.57a.

A p-value of 56% for the subject suggests no discrepancies among the two testing groups. In this case, joystick and ocular interfaces provide similar values of median while the variability related to the gaze-based technique is higher. This behaviour is confirmed in Fig. 6.54 in which is quite evident that the paths obtained with the gaze-based wheelchair have higher dispersion in terms of attitude.

A p-value of 49% for the interaction of the subject versus the interface indicates that there isn't any significant correlation from a statistical point of view.

As for the final attitude of the wheelchair, which should be ideally alighted with the cones that mark the area, a p-value of 3% confirms a difference in the interfaces, Fig. 6.58b. In this case, the ocular interface is the best performing one, with both a minor bias and variance in the results Fig. 6.58a. Indeed, the final attitude obtained with the gaze-based wheelchair has a median value of about 3° while the data coming from the joystick wheelchair have a deviation value of more than 5° . Furthermore, the joystick interface presents much greater variability.

The analysis of variance regarding the subject returns a p-value of 40% that there are no differences in the performance depending on the user. This thesis is supported by the boxplot where both the data related to the full and reduced mobility users obtained about the same median and variability values.

Considering the interaction, subject and interface features don't present a statistically significant correlation with a p-value of 16%.

Section 5

The last section evaluated in these tests was designed to analyse specifically the perception capability of the surrounding environment as well as the ability to stop the wheelchair on the desired position by using the two different interfaces. The user has to start from a fixed position, move forward for few meters and then stops with the center of rear wheels as close as possible to a reference line drawn on the floor keeping the gaze in front of him.

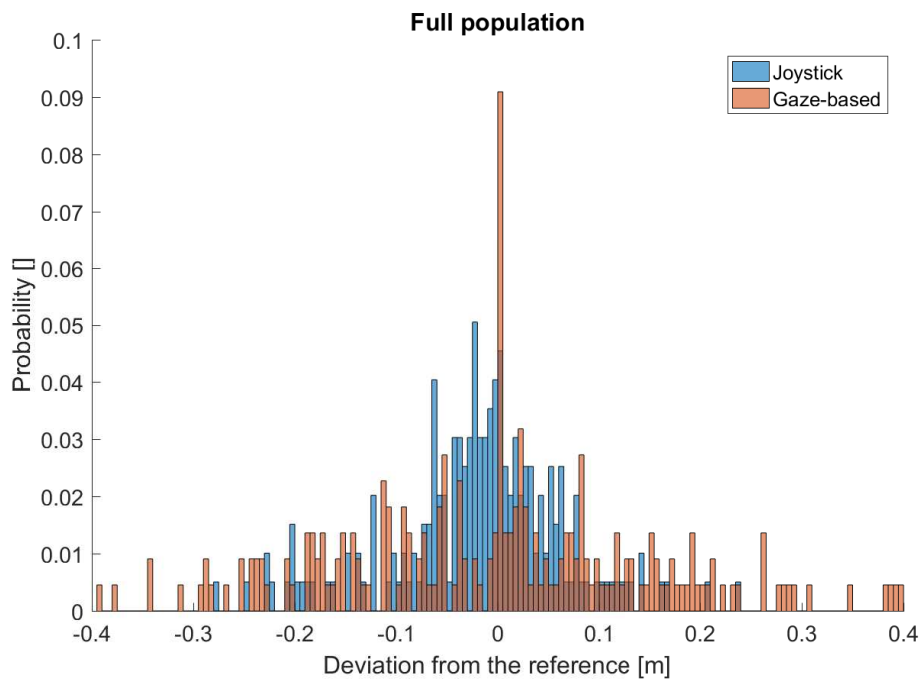
As in the previous cases, the first feature evaluated is the deviation in position from a reference line placed on the floor. It was calculated the distance between the point to line distance between the reference line and the middle point of the rear wheel axes. The figures ranging from Fig. 6.59 to 6.61 show the probability density functions referring to the deviation from the reference performed by different type of subjects (full mobility users or reduced mobility users) and with different input interfaces (joystick and gaze-based). The variability of the wheelchair position resulted from the gaze-based interface is slightly higher than the joystick one, as shown in Fig. 6.59a.

The same analysis on the entire population referred to the type of user shows a comparable variability on the deviation of the full mobility users and the reduced mobility users, Fig. 6.59b.

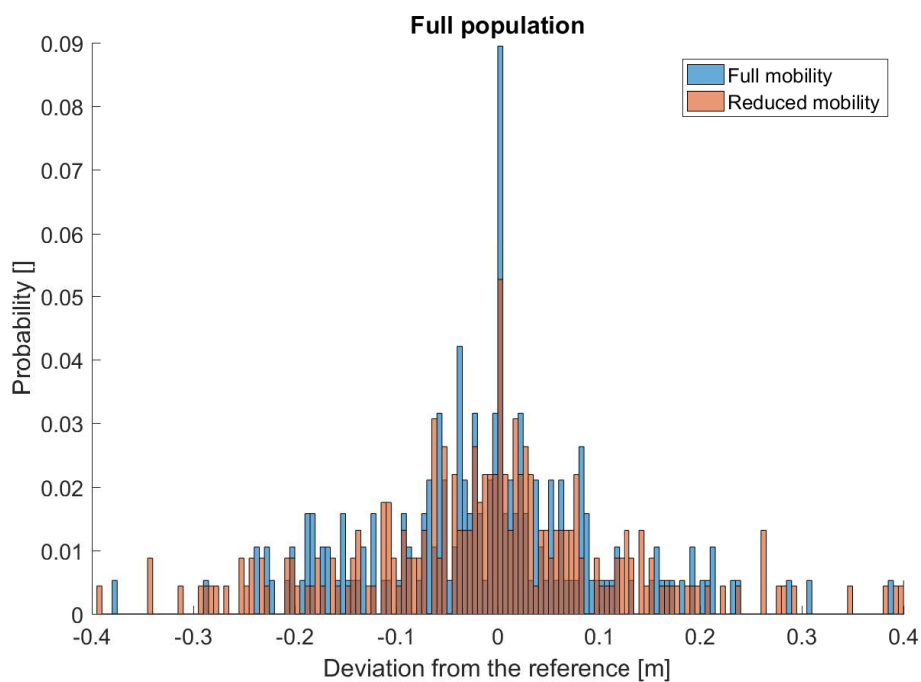
It is also interesting to analyse the probability density function separately, before on the subject type and then on the interfaces. In this case, the limited number of samples collected makes it difficult to extract some considerations from the distribution analysis. From the comparison of the deviation between the joystick and gaze-based interface, it is possible to notice the behaviour previously explained with the gaze-based data having wider distribution compared to the joystick ones for both the full and reduced mobility users, Fig. 6.60a and 6.60b

The corresponding comparison on user types highlights a good overlap in the data both in the case of full and reduced mobility subjects that used the joystick, Fig. 6.61a, and the eye-controlled wheelchair, Fig. 6.61b.

The analysis of variance regarding the braking distance shows similar behaviour for both the subject and the interface features. In particular, Fig. 6.62a related to the subject and the interface reports approximately the same median values. The only difference can be noticed in the case of the interface where the variability of the data collected with the gaze-based technology is higher than the joystick. Indeed, the p-values for subject and interface were



(a)



(b)

Fig. 6.59 Comparison of the deviation from the reference path related to the full population along the braking test (section 5). Subfigure *a* shows the comparison between the control interface for both the subject type while the subplot *b* highlights the difference between the subjects using both the interfaces

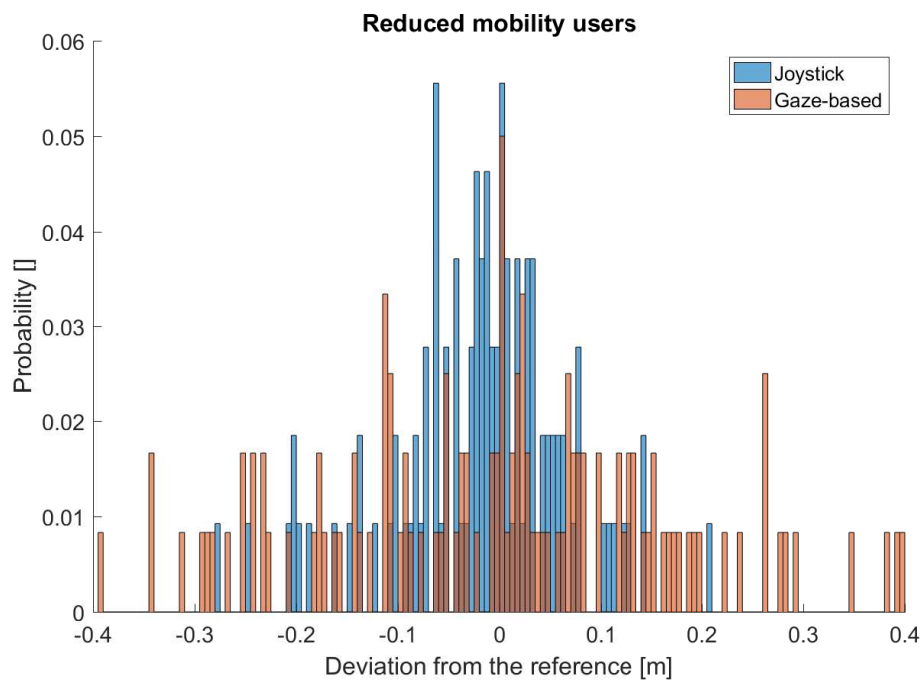
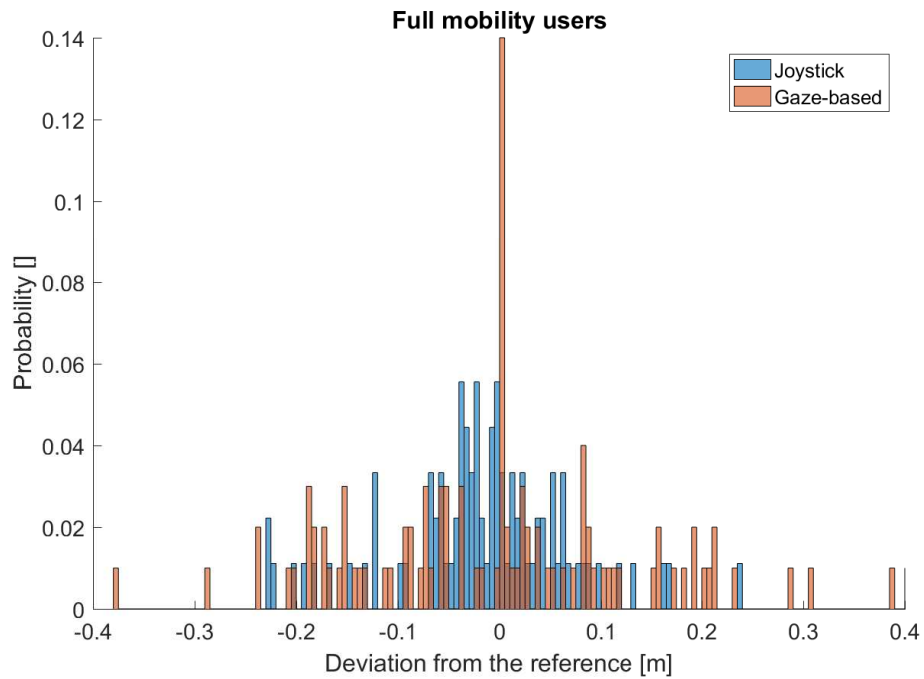
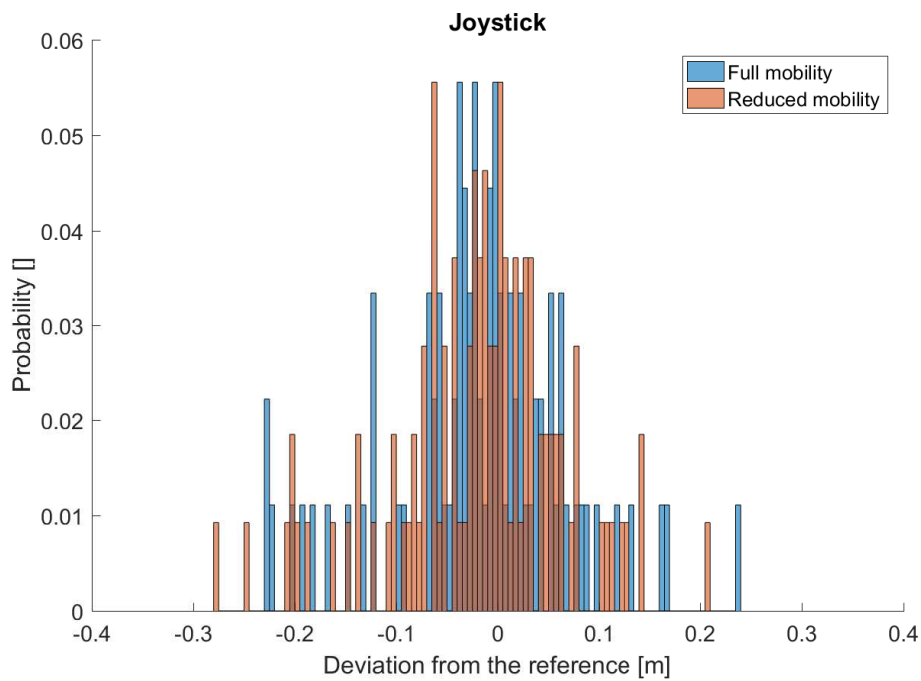
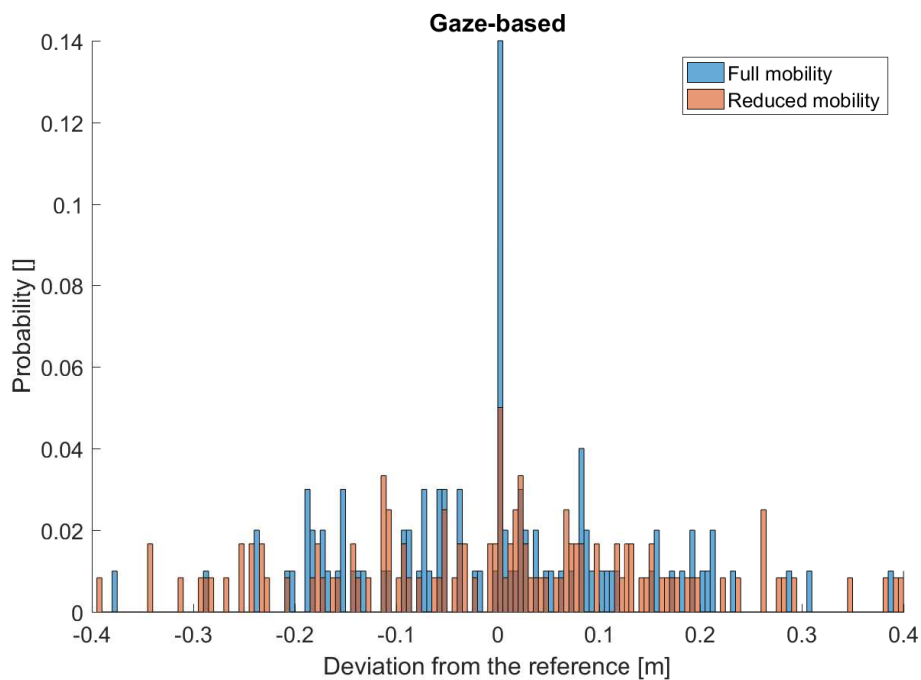


Fig. 6.60 Comparison of the deviation from the reference path between interfaces performed by full mobility users (a) and reduced mobility users (b) along the curved part of the braking test (section 5).



(a)



(b)

Fig. 6.61 Comparison of the deviation from the reference path between subjects driving a classic joystick wheelchair (a) and the gaze-based prototype (b) along the braking test (section 5).

95% and 37% respectively, Fig. 6.62a. Despite a higher variability in the final reached position in the case of the ocular HMI, no statistical significant difference can be found from samples data. That could be related to a worse perception of the environment, especially for the depth, from the usage of the monitor as a visual reference rather than the eye directly.

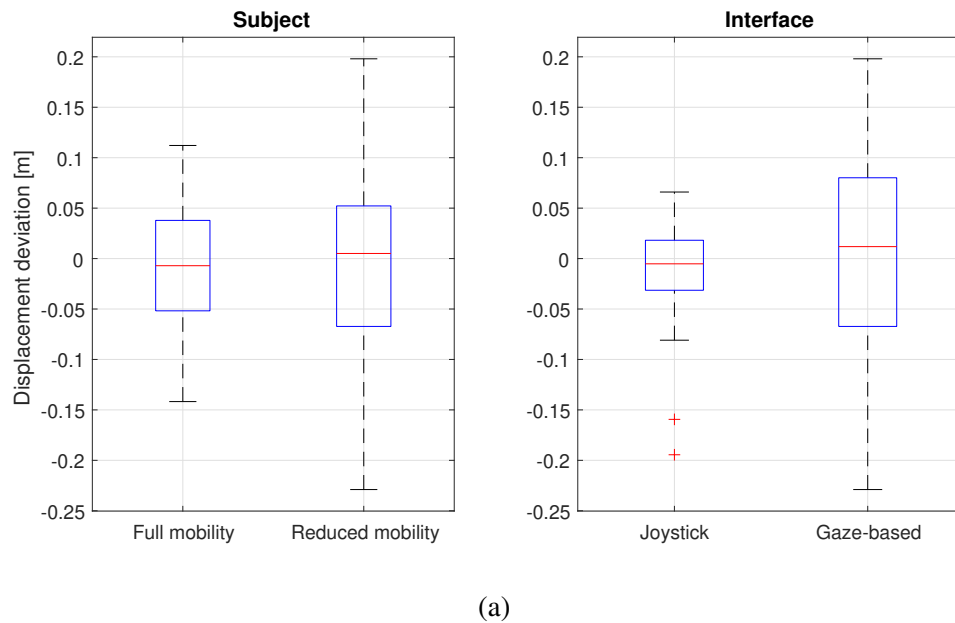
Considering the interaction, subject and interface features don't present a statistically significant correlation with a p-value of 20%.

As for the interface evaluation of the maximum reached velocity, the joystick shows a higher efficiency, while the ocular HMI presents a much lower median value together with a relevant variability in the results, Fig. 6.63a. Indeed, the p-value is 0%, suggesting that this parameter has a strong effect on the speed efficiency, as reported in Fig. 6.63b.

On the other hand, the analysis of variance regarding the subject returns a p-value of 10% highlighting no statistical significant difference can be found from samples data.

Also the interaction between subject and interface don't present a statistically significant correlation with a p-value of 19%.

The results highlight then that the interfaces result both effective, despite a difference in efficiency, for the approach of the wheelchair to a specific area or object, such as furniture (i.e. a desk).

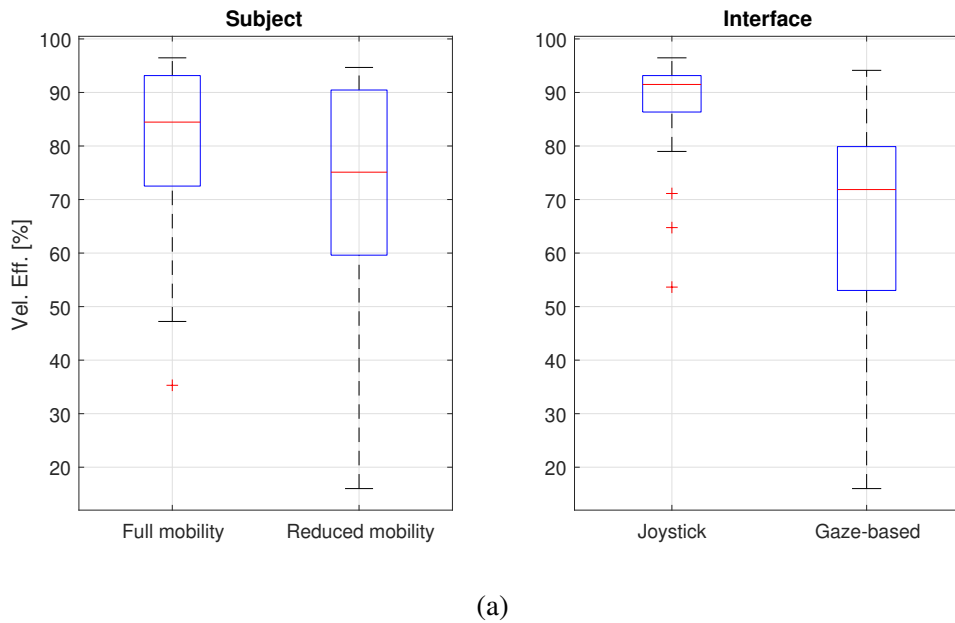


(a)

ANOVA Table					
Source	SS	df	MS	F	Prob>F
Subject	0.00003	1	0.00003	0	0.9478
Interface	0.00601	1	0.00601	0.83	0.3683
Interaction	0.01234	1	0.01234	1.7	0.1996
Error	0.29025	40	0.00726		
Total	0.30863	43			

(b)

Fig. 6.62 ANOVA analysis for the braking distance (e_b) for the braking test, with the box plots of the deviation related to subject (left) and interface (right).



ANOVA Table					
Source	SS	df	MS	F	Prob>F
Subject	680.72	1	680.72	2.83	0.1001
Interface	4892.74	1	4892.74	20.36	0.0001
Interaction	428.02	1	428.02	1.78	0.1895
Error	9610.54	40	240.26		
Total	15612.02	43			

(b)

Fig. 6.63 ANOVA analysis for the efficiency in speed control (v_{eff}) for the braking test, with the box plots of the efficiency related to subject (left) and interface (right).

Table 6.8 P-values from ANOVA analysis among the considered feature for the vehicle metrics. The considered factors are: subject, non-disabled vs. disabled, and interface, joystick vs. ocular. S-H represents the interaction between subject and interface.

Feature	S 1		S 2		S 3		S 4		S 5	
	Sbj.	HMI S-H								
e_m	33%	16%	3%	3%	18%	2%	99%	4%	0%	80%
$ e_m $	17%	0%	26%	24%	41%	76%	5%	56%	8%	2%
v_{eff}	41%	0%	67%	67%	11%	0%	86%	6%	0%	15%
a_{wf}	42%	0%	40%	68%	94%	12%	93%			
a_{wl}	29%	0%	48%	46%	85%	0%	79%			
θ_s								5%	56%	49%
θ_e								40%	3%	16%
e_b								95%	37%	20%
$ e_b $								37%	0%	94%

Table 6.9 Classification of the influence factor

Feature	False (0)	True (1)
Age	1 ÷ 4	5 ÷ 7
PC usage	0 ÷ 2	3 ÷ 7
Smartphone usage	0 ÷ 2	3 ÷ 5
Activities during free time	0 ÷ 2	3 ÷ 7

6.3.6 Influence factors in the usage of ocular HMI

Until now, the analysis of the result involved only the two parameters that were considered more influential: motor disability of the subjects and type of interface. This chapter evaluates the performance considering, in addition, other influence factors, as described in section 6.3.4, such as *age*, *PC usage*, *Smartphone usage* and *number of activity carried out during the free-time*. The data was obtained through a questionnaire about the personal interest of the subjects. The numeric values collected with the questionnaire was elaborated with a binary classification under the rules reported in Table 6.9. In order to reduce the number of features that have to be iterate during the analysis, the parameters *PC usage* and *Smartphone usage* was merged through a boolean multiplication, obtaining the *feeling with the technology*.

The first part of this analysis focused then on the ocular interface only, with the objective of highlighting possible relations among its performances and the user. The feature considered are: *mobility level*, *age* and *feeling with the technology*.

Fig. 6.64 reports the interaction plot for the error e_m along the straight part of the path following test (section 1). The results suggest that a young full mobility user tends to perform better than an older one (over 40), as well as, the feeling with the technology seems to represent a key factor in driving with this HMI. Contrary to what was expected, a user that is accustomed to a monitor and the interaction with a software interface manages to worse follow the reference on the ground. A high number of activities carried out during the free time has a slightly positive effect on the performance of full mobility user while, on the subject with reduced mobility, has a negative effect.

Along the bumpy part of the path following test, Fig. 6.65, the ANOVA analysis returned the same trends obtained in section 1. The only difference can be noticed in the effect of the technology, especially for the reduced mobility users. In this case, the higher usage of technology corresponds to a lower mean deviation from the reference path.

From the results along the curved part of the path following test (section 3) it is interesting to notice that older subjects obtained better performances than the younger ones, Fig. 6.66.

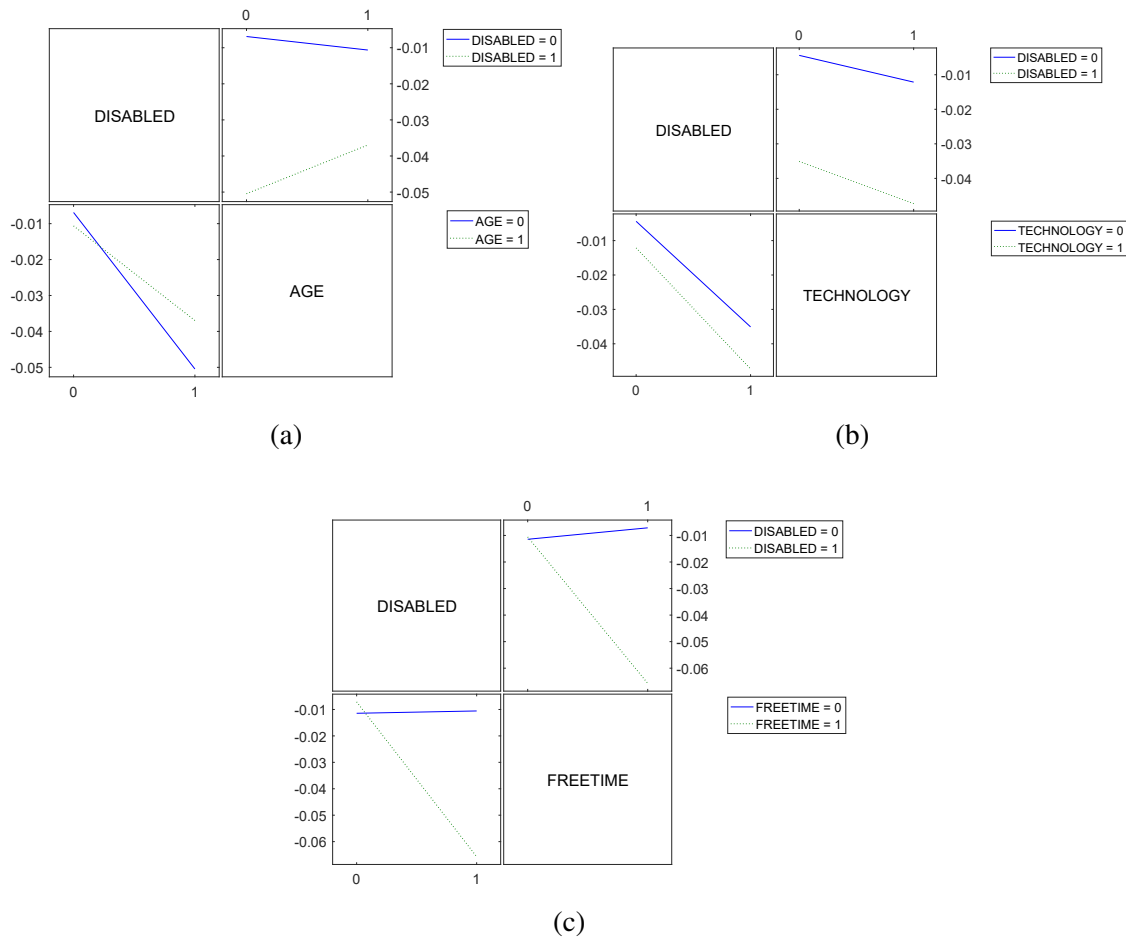


Fig. 6.64 Influence factors evaluation on the mean deviation (e_m) of the wheelchair along the straight part of the path following test.

A different trend can be found in the parking test (section 4), Fig. 6.67 in which the increasing age has a positive effect on the reduced mobility users while the older full mobility users obtained a higher deviation compared to the younger subjects. Furthermore, a higher number of activities carried out in the free-time is connected to the worst performances for both the subject with full and reduced mobility.

As for the analysis along the braking test (section 5), shown in Fig. 6.68, age and the number of activities carried out in the free-time have a negative effect respectively on the full and reduced mobility users. Focusing on the reduced mobility subject, the increasing age brings a positive contribution while the higher feeling with the technology has a negative effect on the performances. The explanation could be related to the difficulty in moving the gaze away from the monitor, with a consequent loss in the depth perception for the reference on the ground, and thus a higher deviation in the braking distance.

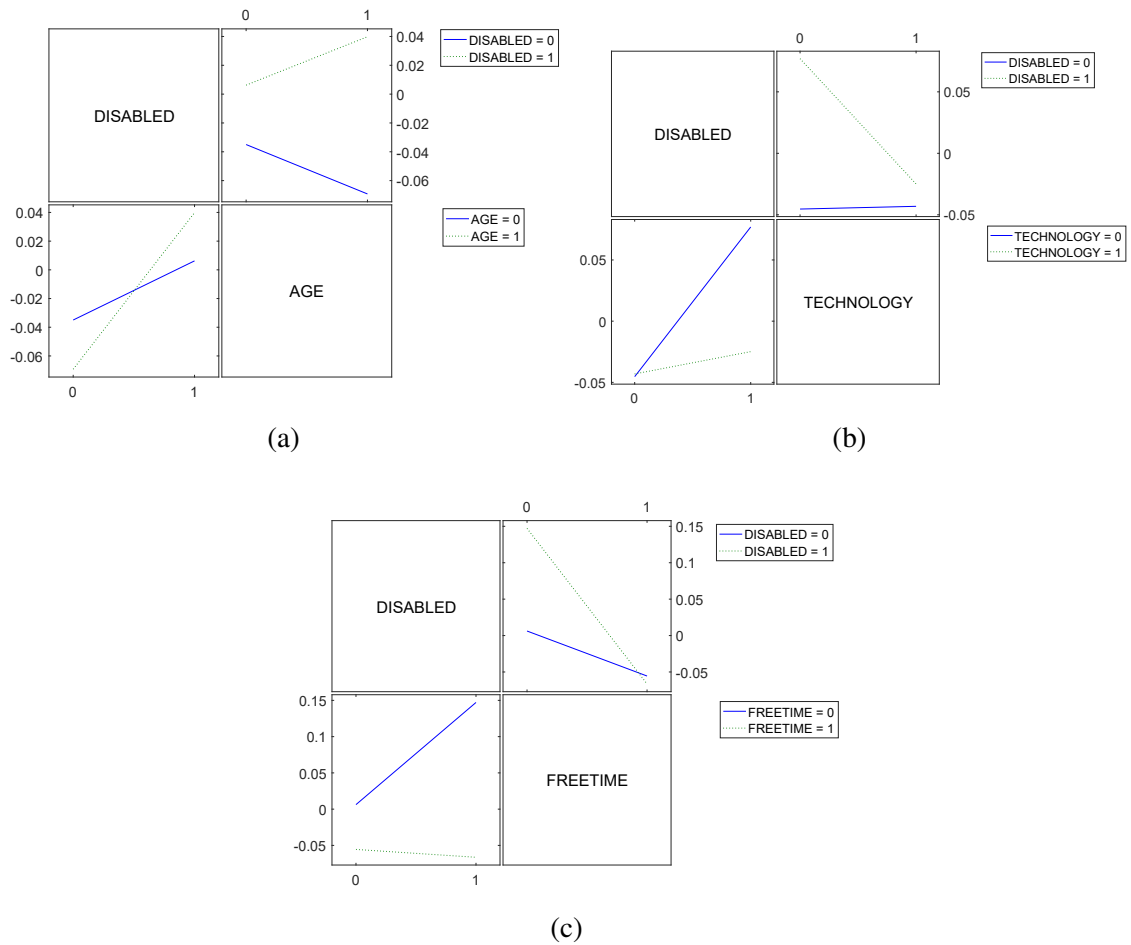


Fig. 6.65 Influence factors evaluation on the mean deviation (e_m) of the wheelchair along the bumpy part of the path following test.

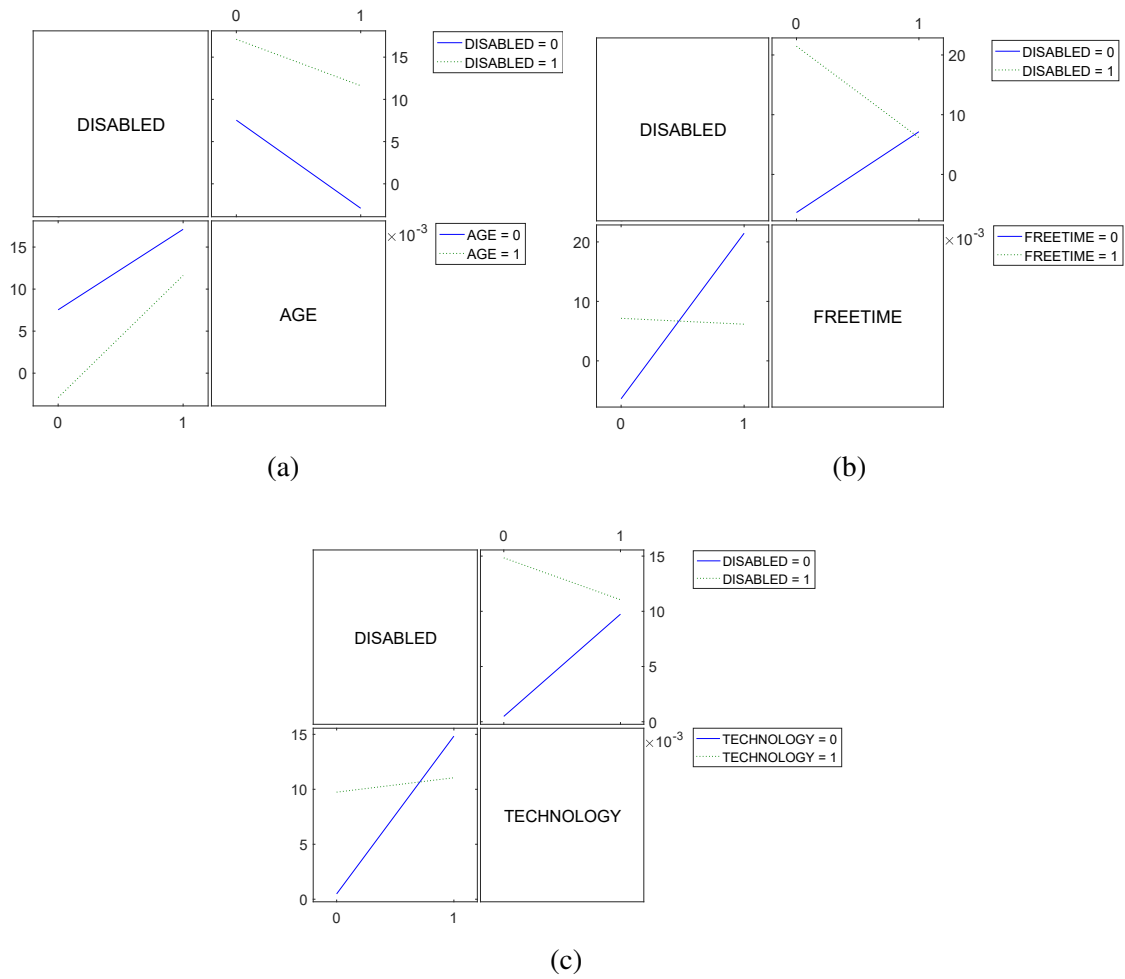


Fig. 6.66 Influence factors evaluation on the mean deviation (e_m) of the wheelchair along the curved part of the path following test.

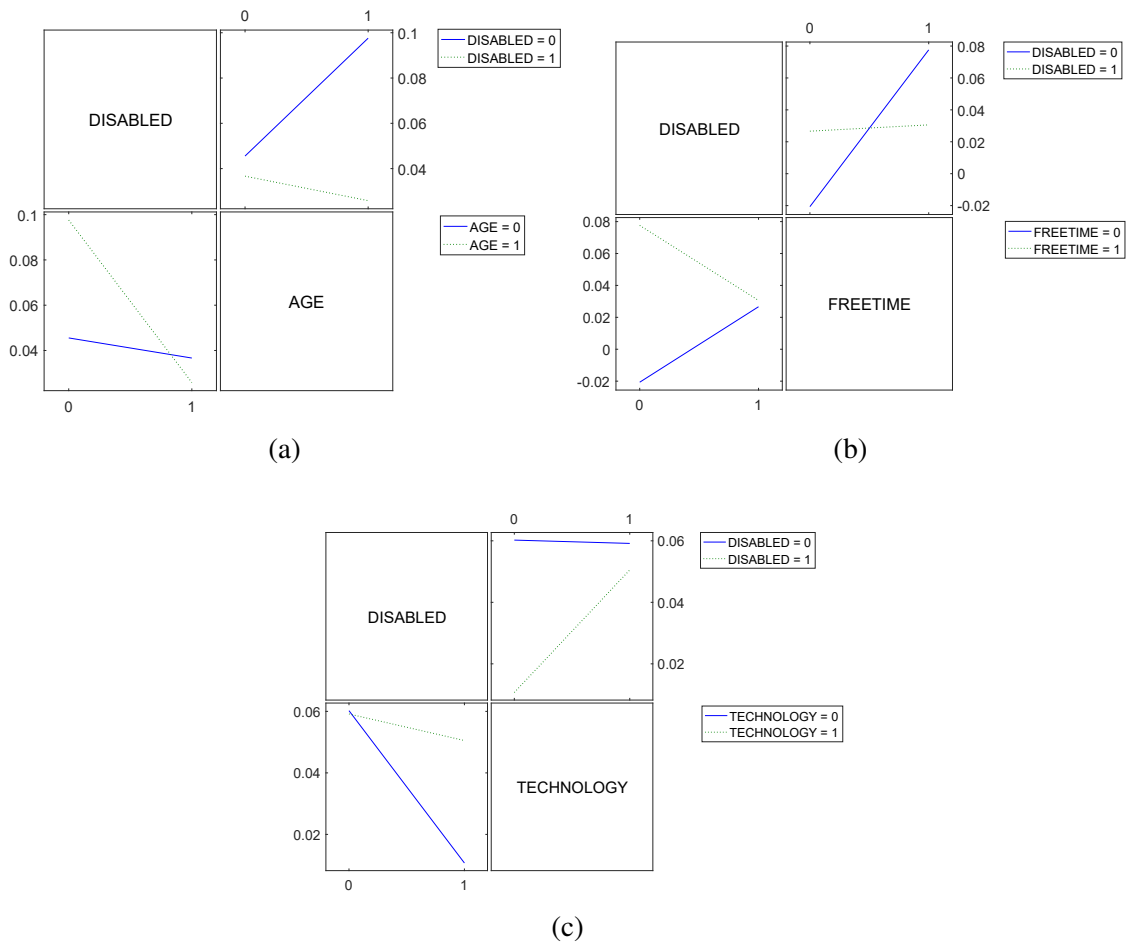


Fig. 6.67 Influence factors evaluation on the mean deviation (e_m) of the wheelchair along the parking test.

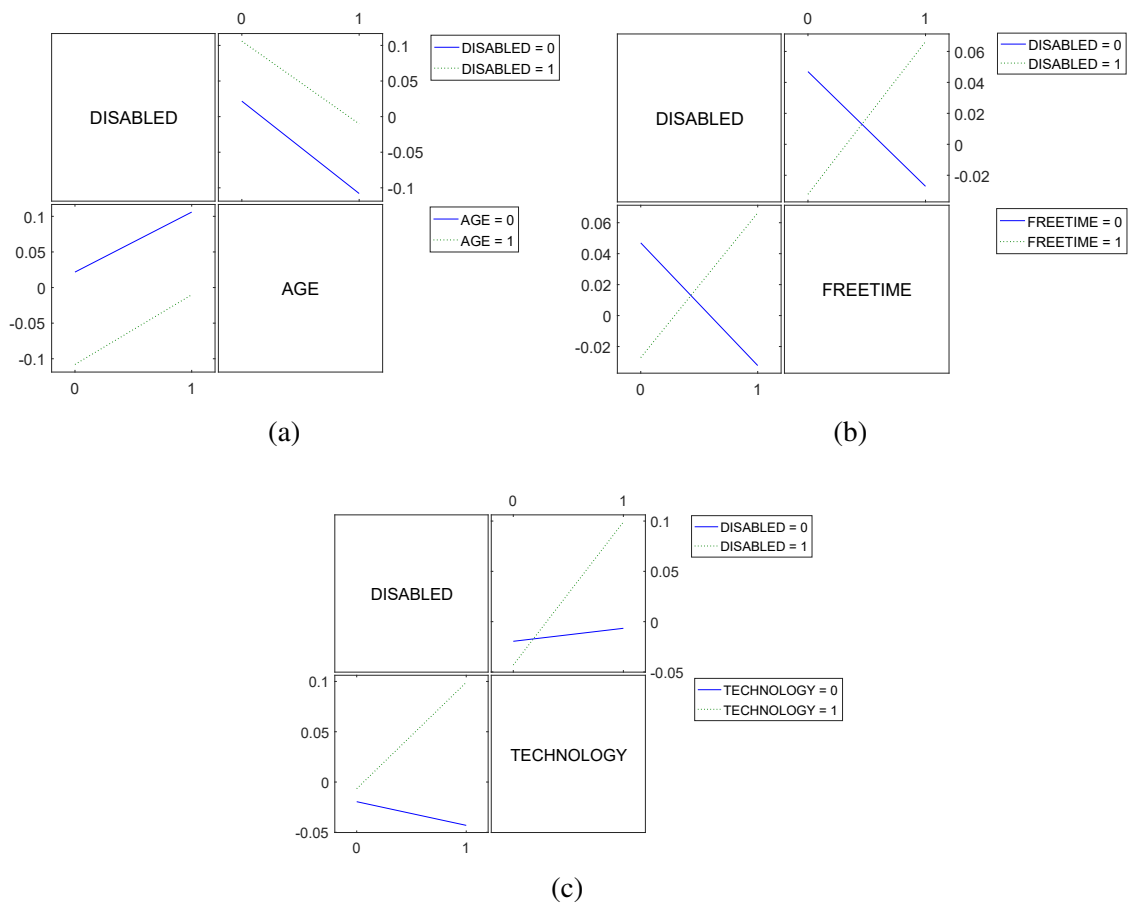


Fig. 6.68 Influence factors evaluation on the mean deviation (e_m) of the wheelchair along the braking test.

The figures ranging from Fig. 6.69 to 6.73 shows the analysis on different combinations of influence factors related to each part of the test for both the joystick and the ocular interface. The feature considered is the module of the mean deviation ($|e_m|$);

6.3.7 Human metrics

A questionnaire, shown in the figures ranging from Fig. 6.24 to 6.27, was provided to the subjects for both interfaces asking for feedback on the usability and the feeling associated to the usage. In Table 6.10 are listed the points of the questionnaire and the average values. The results were scaled in a range from 1, related to the lowest value, to 5 for the highest value. The second column, marked with *J*, refers to the joystick interface while the third column is related to the ocular HMI and marked as *O*. The elements evaluated were usability, trust, and satisfactoriness.

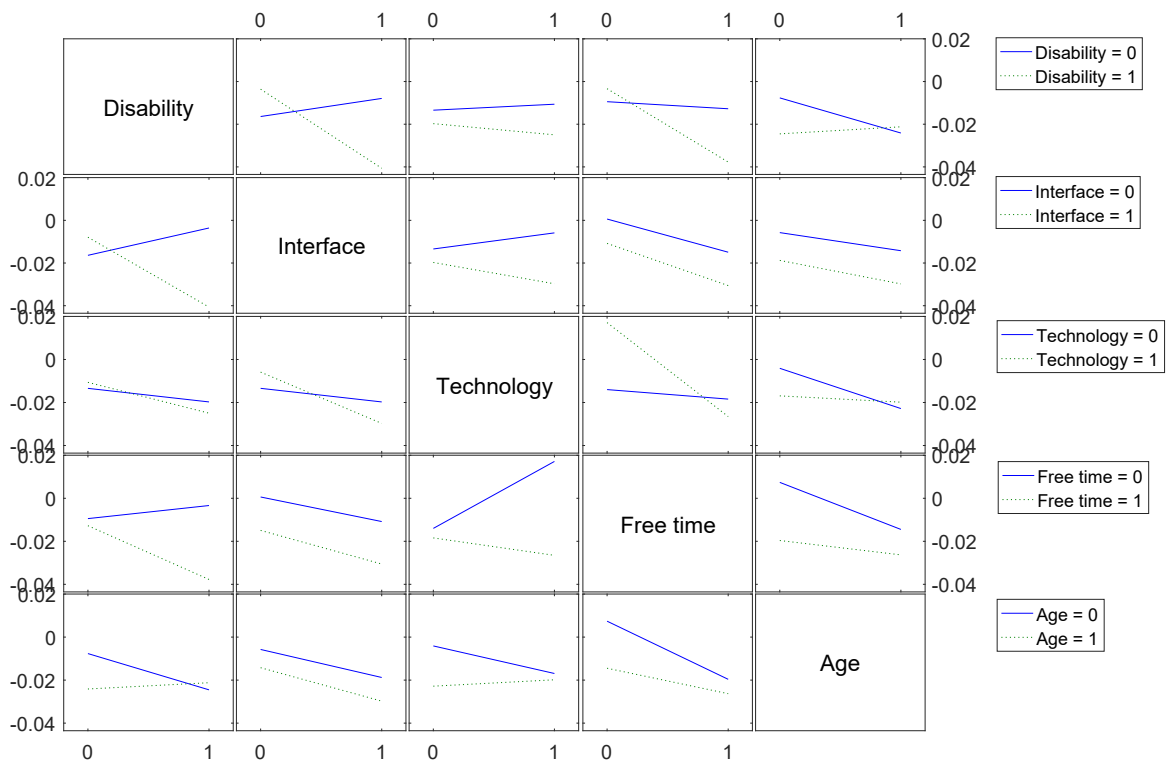
The values resulted similar for most of the points in the questionnaire. The main difference can be found in the perception of the usability of the system. The ocular interface seems at first glance less intuitive and more difficult to use than the joystick as reported in points *c* and *d* of the usability feature. That represents a predictable outcome given the novelty of the ocular interface with respect to a more standard one like the joystick.

6.3.8 Workload

This part evolves the information collected about the perceived feeling and workload in driving for the ocular HMI only. That data was recorded through the questionnaire shown in Fig. 6.23. Five points were considered:

1. Mental workload in the usage of the interface;
2. Physical workload;
3. Temporal pressure as the feeling of a delayed control in driving;
4. Satisfaction of the driving performances
5. Effort during the driving;
6. Frustration.

The average scores, on a scale from 1 to 5 were 1 is a low workload and 5 intensive, are reported in Table 6.11.



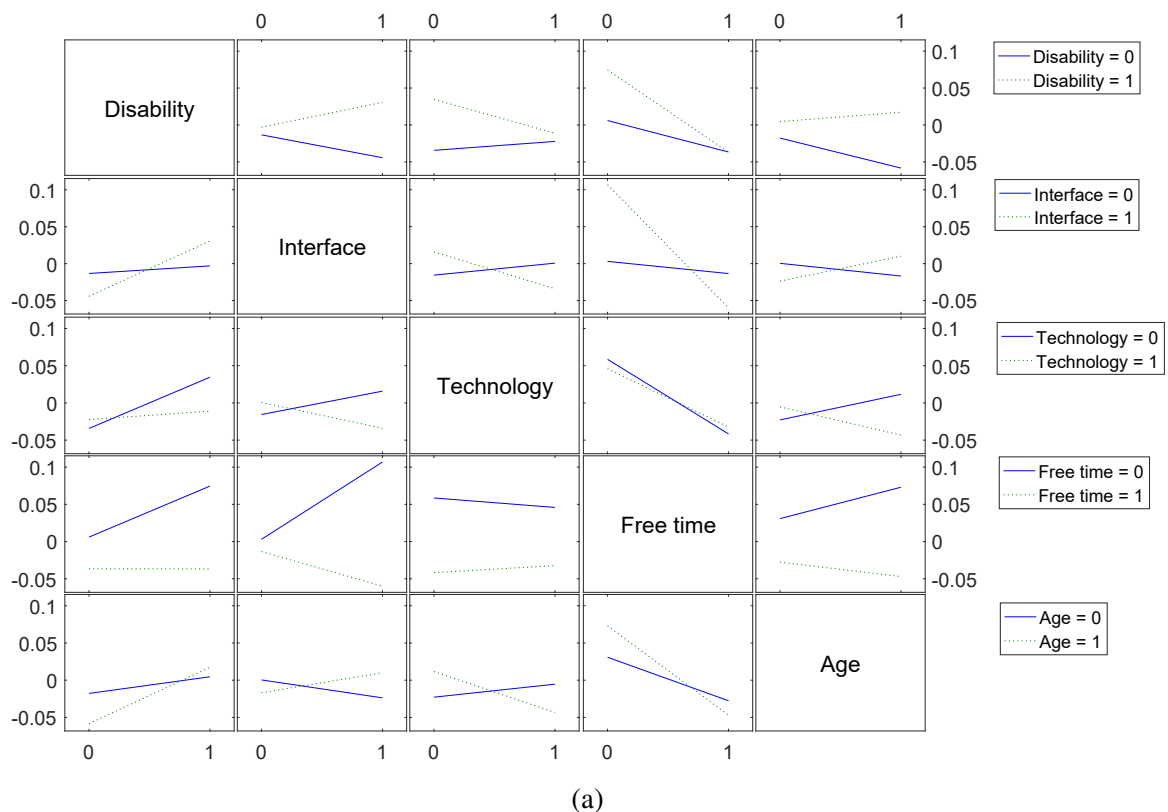
(a)

Analysis of Variance					
Source	Sum Sq.	d.f.	Mean Sq.	F	Prob>F
Disability	0.00165	1	0.00165	1.8	0.1911
Interface	0.00109	1	0.00109	1.18	0.2859
Technology	0.00006	1	0.00006	0.07	0.7921
Free time	0.00045	1	0.00045	0.49	0.4896
Age	0.00166	1	0.00166	1.82	0.1887
Disability*Interface	0.0068	1	0.0068	7.42	0.011
Disability*Technology	0.00029	1	0.00029	0.32	0.5758
Disability*Free time	0.00604	1	0.00604	6.59	0.0159
Disability*Age	0.00064	1	0.00064	0.7	0.4115
Interface*Technology	0.00006	1	0.00006	0.07	0.7956
Interface*Free time	0.00077	1	0.00077	0.84	0.3664
Interface*Age	0.0008	1	0.0008	0.87	0.3595
Technology*Free time	0.0002	1	0.0002	0.22	0.6407
Technology*Age	0.00113	1	0.00113	1.23	0.2761
Free time*Age	0.00178	1	0.00178	1.94	0.1747
Error	0.02568	28	0.00092		
Total	0.053	43			

Constrained (Type III) sums of squares.

(b)

Fig. 6.69 Interaction plot of the module of the mean deviation (e_m) of the wheelchair along the straight part of the path following test

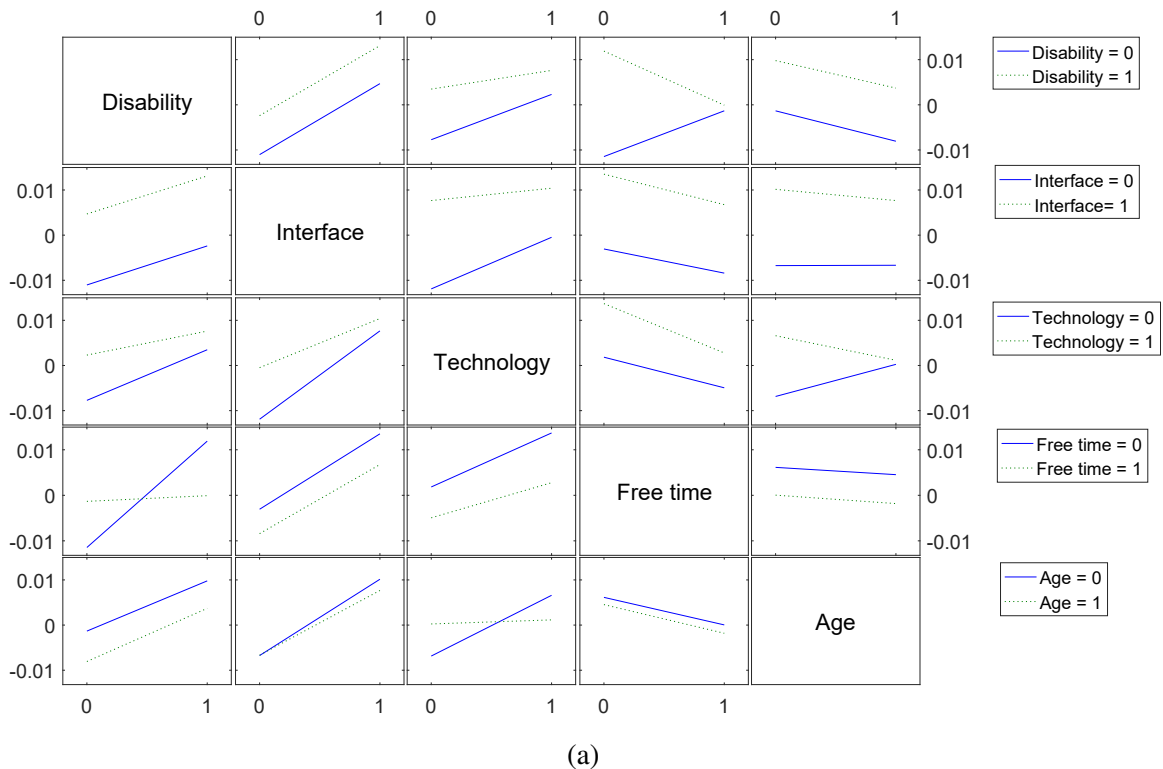


Analysis of Variance					
Source	Sum Sq.	d.f.	Mean Sq.	F	Prob>F
Disability	0.00473	1	0.00473	1.97	0.171
Interface	0.00545	1	0.00545	2.27	0.1429
Technology	0.00022	1	0.00022	0.09	0.7638
Free time	0.02085	1	0.02085	8.7	0.0064
Age	0.00026	1	0.00026	0.11	0.7423
Disability*Interface	0.00068	1	0.00068	0.29	0.5975
Disability*Technology	0.00009	1	0.00009	0.04	0.8444
Disability*Free time	0.00475	1	0.00475	1.98	0.1704
Disability*Age	0.00127	1	0.00127	0.53	0.4732
Interface*Technology	0.00184	1	0.00184	0.77	0.3878
Interface*Free time	0.03641	1	0.03641	15.19	0.0006
Interface*Age	0.00065	1	0.00065	0.27	0.6062
Technology*Free time	0	1	0	0	0.9936
Technology*Age	0.00016	1	0.00016	0.07	0.8001
Free time*Age	0	1	0	0	0.9798
Error	0.06711	28	0.0024		
Total	0.22546	43			

Constrained (Type III) sums of squares.

(b)

Fig. 6.70 Interaction plot of the module of the mean deviation (e_m) of the wheelchair along the bumpy part of the path following test

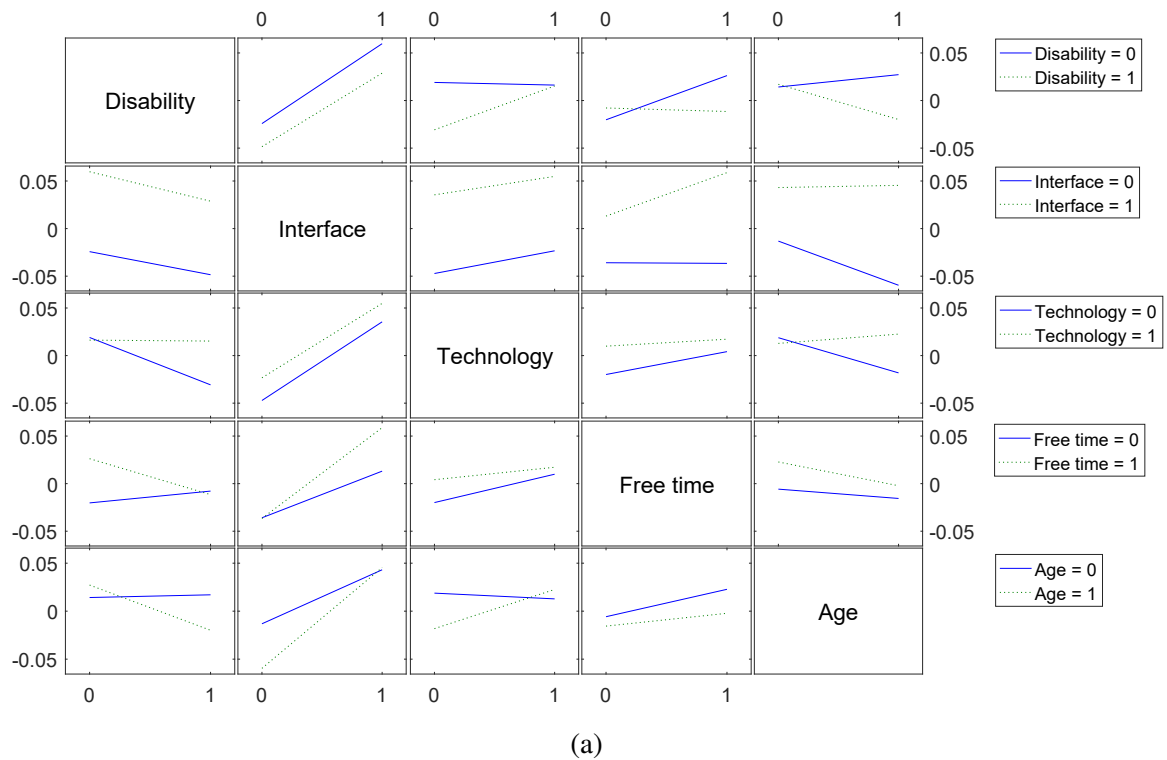


Analysis of Variance					
Source	Sum Sq.	d.f.	Mean Sq.	F	Prob>F
Disability	0.00291	1	0.00291	6.92	0.0137
Interface	0.00194	1	0.00194	4.61	0.0406
Technology	0	1	0	0.01	0.9379
Free time	0.00042	1	0.00042	1.01	0.3242
Age	0.00135	1	0.00135	3.19	0.0848
Disability*Interface	0.00004	1	0.00004	0.09	0.7724
Disability*Technology	0	1	0	0	0.9585
Disability*Free time	0.00361	1	0.00361	8.56	0.0067
Disability*Age	0.00057	1	0.00057	1.36	0.2533
Interface*Technology	0.00032	1	0.00032	0.76	0.3901
Interface*Free time	0.00001	1	0.00001	0.02	0.8847
Interface*Age	0.00014	1	0.00014	0.33	0.5695
Technology*Free time	0.00034	1	0.00034	0.81	0.3755
Technology*Age	0.00014	1	0.00014	0.33	0.5722
Free time*Age	0.00175	1	0.00175	4.14	0.0514
Error	0.0118	28	0.00042		
Total	0.0204	43			

Constrained (Type III) sums of squares.

(b)

Fig. 6.71 Interaction plot of the module of the mean deviation (e_m) of the wheelchair along the curved part of the path following test

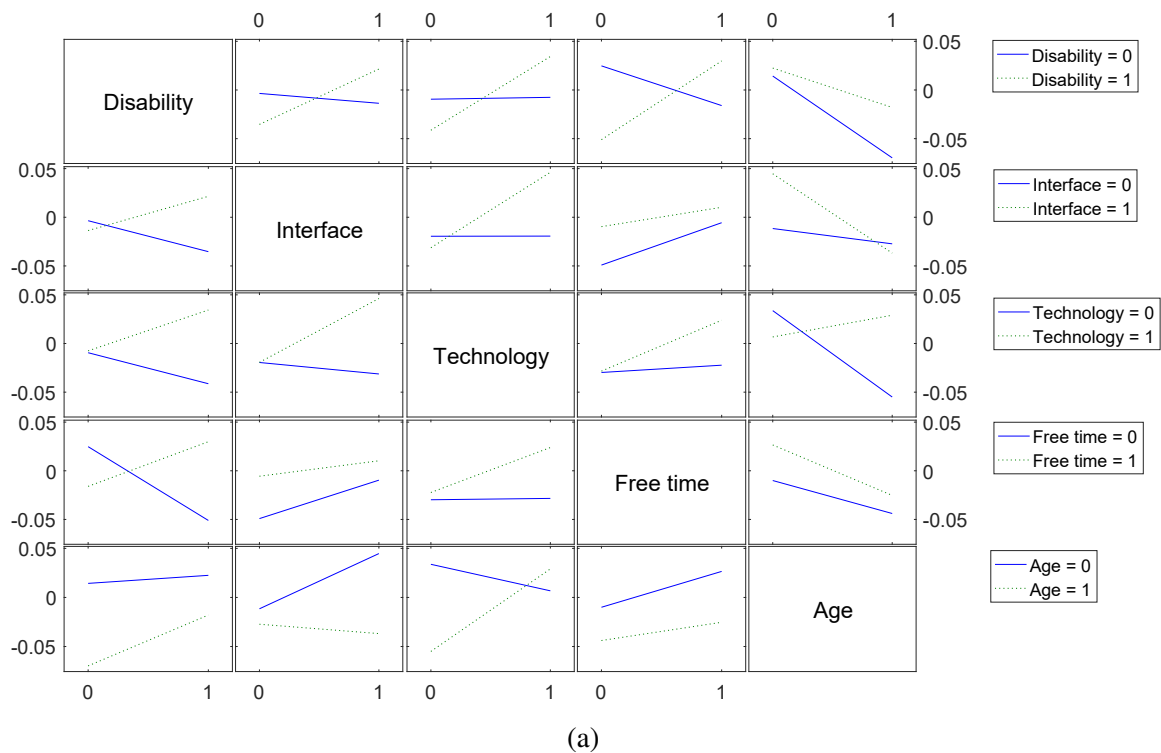


Analysis of Variance					
Source	Sum Sq.	d.f.	Mean Sq.	F	Prob>F
Disability	0.00195	1	0.00195	1.74	0.1983
Interface	0.04871	1	0.04871	43.31	0
Technology	0.0077	1	0.0077	6.85	0.0141
Free time	0.00077	1	0.00077	0.68	0.4164
Age	0.00217	1	0.00217	1.93	0.1756
Disability*Interface	0.00129	1	0.00129	1.15	0.2931
Disability*Technology	0.00205	1	0.00205	1.82	0.1881
Disability*Free time	0.0005	1	0.0005	0.44	0.5124
Disability*Age	0.00077	1	0.00077	0.69	0.4136
Interface*Technology	0.00028	1	0.00028	0.25	0.6231
Interface*Free time	0.0036	1	0.0036	3.2	0.0843
Interface*Age	0.00836	1	0.00836	7.43	0.0109
Technology*Free time	0.00246	1	0.00246	2.19	0.1504
Technology*Age	0.002	1	0.002	1.78	0.1928
Free time*Age	0.00357	1	0.00357	3.17	0.0857
Error	0.03149	28	0.00112		
Total	0.15344	43			

Constrained (Type III) sums of squares.

(b)

Fig. 6.72 Interaction plot of the module of the mean deviation (e_m) of the wheelchair along parking test



Analysis of Variance					
Source	Sum Sq.	d.f.	Mean Sq.	F	Prob>F
Disability	0.00122	1	0.00122	0.24	0.6281
Interface	0.00665	1	0.00665	1.31	0.2623
Technology	0.00477	1	0.00477	0.94	0.3407
Free time	0.00084	1	0.00084	0.17	0.6872
Age	0.00059	1	0.00059	0.12	0.7353
Disability*Interface	0.02262	1	0.02262	4.45	0.0439
Disability*Technology	0.00008	1	0.00008	0.02	0.9028
Disability*Free time	0.02561	1	0.02561	5.04	0.0328
Disability*Age	0.00029	1	0.00029	0.06	0.8122
Interface*Technology	0.00374	1	0.00374	0.74	0.3982
Interface*Free time	0.0002	1	0.0002	0.04	0.8427
Interface*Age	0.01822	1	0.01822	3.59	0.0686
Technology*Free time	0.00163	1	0.00163	0.32	0.5751
Technology*Age	0.0154	1	0.0154	3.03	0.0926
Free time*Age	0.01503	1	0.01503	2.96	0.0964
Error	0.14218	28	0.00508		
Total	0.30863	43			

Constrained (Type III) sums of squares.

(b)

Fig. 6.73 Interaction plot of the module of the mean deviation (e_m) of the wheelchair along braking test

Table 6.10 Subjective features results.

Usability		J	O
(a)	I think that I would like to use this system frequently	4.2	3.7
(b)	I found the system unnecessarily complex	1.2	1.4
(c)	I thought the system was easy to use	4.8	3.6
(d)	I think that I would need the support of a technical person to be able to use this system	1.4	2.4
(e)	I found the various functions in this system were well integrated	4.6	4.3
(f)	I thought there was too much inconsistency in this system	1.2	1.5
(g)	I would imagine that most people would learn to use this system very quickly	4.3	3.7
(h)	I found the system very cumbersome to use	1.1	1.8
(i)	I felt very confident using the system	4.6	3.6
(j)	I needed to learn a lot of things before I could get going with this system	1.4	2.2
Trust			
(a)	I believe the system is a competent performer	4.8	4.2
(b)	I trust the system	4.7	4.2
(c)	I have confidence in the advice given by the system	4.7	3.7
(d)	I can depend on the system	4.1	3.6
(e)	I can rely on the system to behave in consistent ways	4.7	4.0
(f)	I can rely on the system to do its best every time I take its advice	4.7	4.0
Satisfactoriness			
(a)	Useful-Useless	1.2	1.4
(b)	Pleasant-Unpleasant	1.6	1.9
(c)	Bad-Good	4.8	4.7
(d)	Nice-Annoying	1.8	1.9
(e)	Effective-Superfluous	1.3	1.5
(f)	Irritating-Likable	4.3	4.1
(g)	Assisting-Worthless	1.3	1.3
(h)	Undesirable-Desirable	4.6	4.6
(i)	Raising alertness-Sleep inducing	1.8	2.1

Table 6.11 Workload results.

Workload	Score
Mental workload in the usage of the interface	3.4
Physical workload	2.4
Temporal pressure as the feeling of a delayed control in driving	3.2
Satisfaction of the driving performances	3.2
Effort during the driving	3.4
Frustration	2.1

The results suggest a non-negligible workload, both mental and physical, in the usage of the interface, and that the user must focus on what he is doing to achieve a satisfactory driving performance. However, a low value in the frustration point suggests that the HMI successfully manages to provide a good driving experience, with minimum errors that are generally considered not relevant by the user.

6.3.9 Discussion of the results

From the highlighted elements, the outcome of the experiment is that the ocular interface does not manage to achieve the same driving performance and experience of a standard joystick. The differences found in the results are mainly due to the interface, since to statistical significant elements can be found on the user, characterized by for both full and reduced mobility. That was confirmed both from vehicle and subject metrics. The joystick resulted in more intuitive and able to provide a better driving experience, usually characterized by better accuracy and control.

The analysis foresaw the design of testing procedure from the Wheelchair Skill Test, with the objective of assessing similarities or differences among the two interfaces. That results fundamental for the usage of the gaze-based interface as, necessary, substitute in the transition from the joystick in case of heavily invalidating pathologies. Several cinematic quantities were considered, so as more subjective elements from feedback provided by the same testers through questionnaires.

The experimental results show that, in general, the ocular controller is less accurate than the joystick, especially in case of reduced mobility users. Most of the difficulties are related to depth and environmental perception. Additionally, it is necessary to remember that the human eye is mainly conceived for exploration and less for control. Due to this reason, looking at a fixed point for a lot of time results in a non-trivial operation that requires a

certain amount of both mental and physical workload from the user. However, with a training phase, the users can easily learn how to manoeuvre in a proper way the wheelchair.

One critical element is represented by the different efficiency in the usage of the interface in terms of navigation velocity. The joystick manages to provide a driving experience in most of the time close to the maximum velocity, and thus a high efficiency. The ocular ones achieve, instead, a lower performance. That could be related to the usage of the interface. By gazing at the top part of the monitor, the user tends to lose control on what is close to the wheelchair that is located in the bottom part of the screen. For such a reason, it seems that the user tends to navigate at a lower velocity, gazing mostly in the middle region of the screen and losing in this way the efficiency but feeling safer.

The outcome of this experimental part suggests that the joystick remains the best interface for the drive of a wheelchair. Anyhow, the gaze-based HMI manages to achieve performances very close to the joystick. Therefore, it results in a suitable alternative for those users that are affected by an impairing pathology and the initial option is no more valid.

Chapter 7

Robotic feature modality using mixed reality

Although direct control represents a very natural and effective way of controlling the motion, it may result fatiguing if used for long periods due to the necessity of keeping the attention on the monitor. An innovative drive modality, called semi-autonomous navigation and presented on Maule et al. [56], was developed to solve the problem of fatigue by enabling the wheelchair to reach autonomously the selected target position. This foresees the use of visual marker and Augmented Reality (AR) to localize specific points of interest (POI) in the domestic environment and then drive the wheelchair there.

The concept of the innovative semi-autonomous driving technique comes from the industrial field where robotic applications are commonly used ad support for the worker.

Robotics is the discipline concerning the development and the realization of automatic devices able to partially or fully substitute the human work in tasks that are considered difficult, dangerous, boring or where particular repeatability is required. Applications of this kind range from industrial to medicine.

It is well known that, during the history of humanity, the people tried to use their intelligence in order to develop tools, machines or in general devices able to support the human. This phenomenon has deep historical roots. It started a few thousands of years ago to supply to the weakness of the humans in the military field, such as eyesight limitation.

Over the years, people introduced and developed the automation process especially for civil and industrial applications due to economic, scientific or safety reasons, but also social and philosophical in second place. Despite the ancient origins, the actual concept of automation was introduced by the Czech playwright Karel Capek who wrote the play Rossum's Universal Robots (R.U.R.), in 1920. On this occasion, he coined the term *robot* that derived from *robota*, a Slav word that means executive labours.

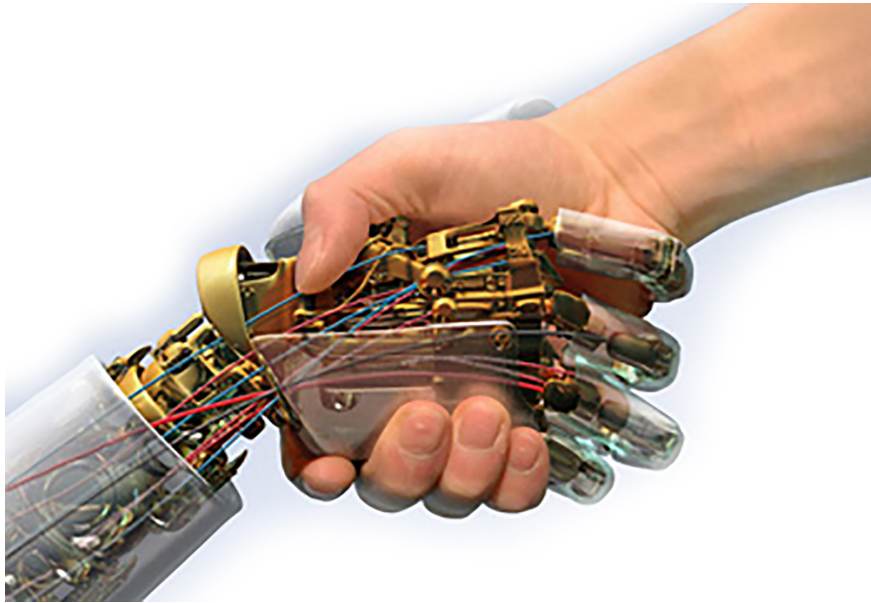


Fig. 7.1 Robotics: a collaboration concept.

More recently, in the 1940s, the well-known Russian science fiction writer Isaac Asimov introduced the concept of robot as a human appearance automaton devoid of feelings. It was programmed by the human to satisfy certain rules of ethical conduct. With Asimov introduced the terms robotics as the science studying robots based on three fundamental laws:

1. A robot may not injure a human being or, through inaction, allow a human being to come to harm.
2. A robot must obey the orders given by human beings, except when such orders would conflict with the first law.
3. A robot must protect its own existence, as long as such protection does not conflict with the first or second law.

These laws provided behaviour rule that the design of a robot has to consider and follow. Since then the robot has achieved the connotation of industrial device or product designed by special technicians, the engineers.

Asimov, with her science fiction plays, influenced the common vision of the people which imagined the robot as a humanoid having visual, communication and motor capabilities. According to scientific interpretation, a robot is independent of its external appearance. The capability of a machine to act on the surrounding environment, with actions governed by specific rules is the fundamental concept to define it as a robot. These rules characterize the

behaviour of the device which interacts with the external environment acquiring data on its status and acting the proper drivers. With regard to this concept, robotics is commonly defined as the science studying the *intelligent connection between perception and action*, [69].

According to the previous definition, a robotics system is a complex system functionally composed by multiple subsystems. The fundamental part of a robot is the mechanical system that allows the device to interface with the surrounding environment, by acting its parts such as wheels or mechanical legs. The development and the realization of a mechanical system are strongly related to the context where the robot has to operate.

The motor capabilities, both locomotion, and manipulation, performed by the mechanical part of a robot are executed by an actuation system, and in particular by servomotors, drivers and transmissions.

The perception is assigned to a sensory system which acquires information about the surrounding environment and about the internal status of the mechanical system using for example position transducers such as encoders, cameras or laser scanners. After that, the measurements acquired are converted in electrical signals and sent to the control system.

The smart connection between perception and action is realized by the control system. It manages the execution of movements starting from some specific requests (such as from a planning task) taking into account the actual status of the robot coming from sensory systems.

In conclusion, robotics can be considered as an interdisciplinary topic concerning the cultural areas of mechanics, electronics, programming, and controls.

The development of the robotic feature on the prototype of eye-controlled wheelchair took into account the idea of robotic as a collaborative concept between human and machine in order to design a semi-autonomous driving technique able to support the users during the most difficult harvesting manoeuvres. In this sense, the HMI plays a fundamental role to obtain a so-called *natural gaze-based wheelchair driving*. Due to this reason, the prototype design focuses also on the development of an Augmented Reality application based on a gaze interaction technology able to control several wheelchair functionalities.

Mixed Reality The concept of Mixed Reality (MR) was defined by Milgram and Kishino [58] as the environment in which the real world and virtual world are merged somewhere along the *reality-virtuality continuum (RV)*. Recently, several applications based on MR interfaces was developed for manufacturing [21], computer-aided instruction [31]. Furthermore, medical visualization is another important field of application for the MR interface, as described by De Cecco et al. [26], where AR is used to enhance the clinician's observation during the assessment of daily living activities. All these applications demonstrate that MR interfaces create an innovative way to interact with the real world.

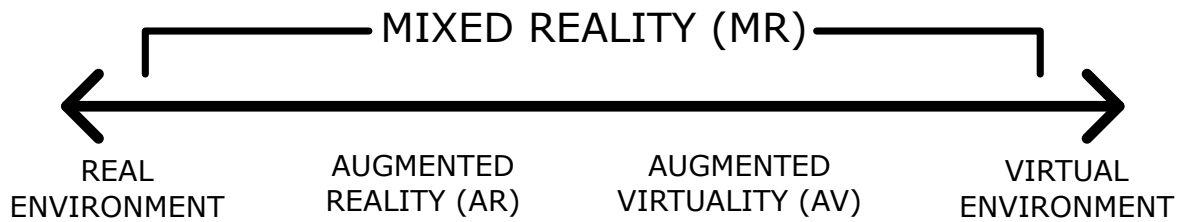


Fig. 7.2 Reality-Virtuality (RV) Continuum.

The reality-virtuality continuum is a continuous scale having as endpoints the real and the virtual environments, Fig. 7.2. The reality-virtuality continuum defined by Milgram and Kishino [58] is related to the mixture of classes objects presented in any particular display situation. In the area between the two extremes is located the mixed reality, where the reality and the virtual are mixed. Within the concept of reality-virtuality continuum is defined the Augmented Reality as the interactive experience of a real-world environment where the objects that reside in the real-world are "augmented" by computer-generated perceptual information [59].

This chapter proposes an integration of our previous gaze-based HMI with a robotic framework able to plan and control a part of the route according to a normal HMI based on Augmented Reality. This novel technology aims to guarantee the freedom of movement and at the same time the comfort of the assisted guide. The proposed AR-based application is able to recognize points of interest (POIs) visible by the camera, to plan a path and gives to the patient the possibility to eventually perform the preferred path after proper checking. From an applicative point of view, when a POI enters in the field of view of the camera the user can select it, starting in this way the navigation. This driving technique is called semi-autonomous navigation.

7.1 Semi-autonomous driving technique

With semi-autonomous navigation, the wheelchair is able to reach a selected target without any other input from the user. To achieve such task, it is necessary to assess the actual position of the wheelchair with respect to the surrounding environment. Given that, the start and the end points, the vehicle calculates the best path to reach the goal. Then another specific algorithm, that calculates the control parameters for the motor, realizes the tracking of the path (path-following task).

The localization algorithm [56] returns the position and the attitude of all POIs detected in the frontal FoV and the AR engine shows pins in correspondence of these plus a manoeuvre calculated by a path planning algorithm [25]. Fig. 7.3 shows an example. The user can

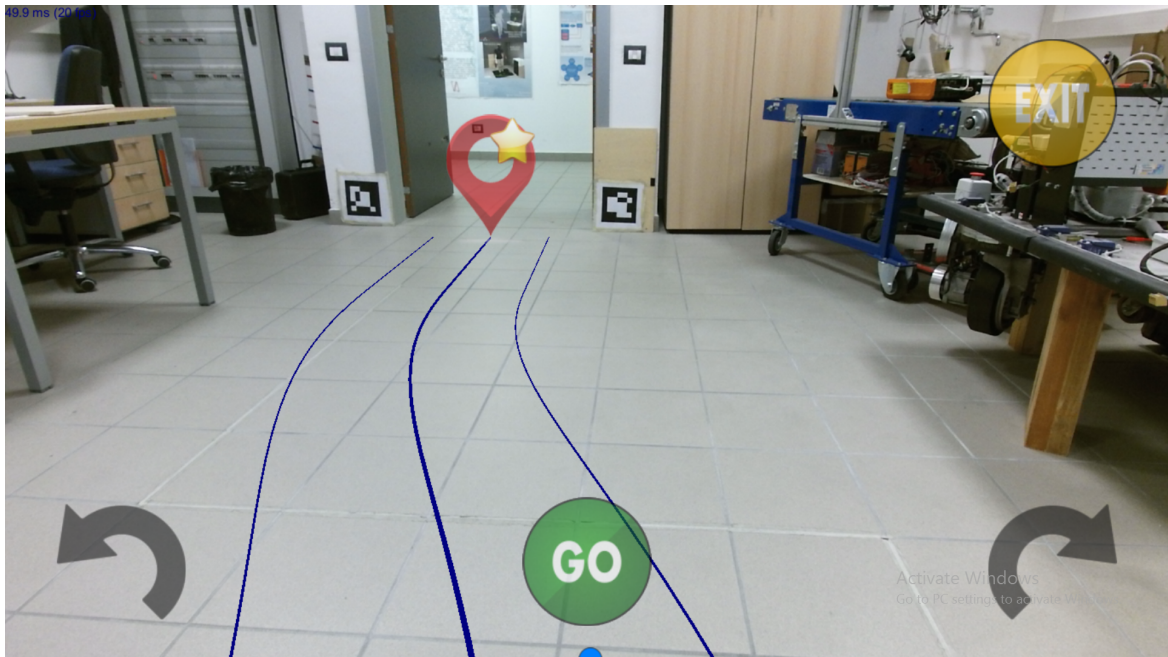


Fig. 7.3 The Human Machine Interface shown on the frontal monitor.

select a POI by gazing at its pin for 2 seconds while a loading circle marks the selection in time. After that, the wheelchair performs the manoeuvre exploiting the path-following task from [25]. At the end of the path, the wheelchair stops automatically allowing the user to select new POI or to switch back to the direct ocular driving.

However, in the context of domestic navigation, a fully dynamic path generation and action could result dangerous from the presence of narrow passages or obstacles. For this reason, the planning tool foresaw the division of the manoeuvre into two sub-parts:

Dynamic path The first part that brings the wheelchair near the POI. This first section is dynamically determined by exploiting a clothoid [25, 9], a curve characterized by continuous third order curvature that ensures the continuity in the jerk and so an optimal comfort level in the navigation. On the top of that, the curve can be expressed analytically [36, 10], providing as advantages a simple data management for the control, HMI and AR, but also it facilitates the identification of obstacles and thus their avoidance. In this way, it is possible to evaluate the feasibility of the planned path.

Static path The fixed conclusive manoeuvre, specifically defined for each POI, ensuring in this way a safe approach or passage toward the target position. The conclusive manoeuvre was associated to a graph based map of the environment containing all POIs' information. Depending on the type of POI, passage (i.e. through doors) or approach point (i.e. for

reaching a desk), a linear or curvilinear segment was defined considering the geometry of the environment, positions of the markers and POI.

Given a selected POI and the complete path, the HMI checks and notifies the presence of obstacles along it. If so, the HMI highlights the path in red, preventing the execution of the manoeuvre. In this case, it is demanded to the user itself to perform a corrective motion and to bring the wheelchair into a suitable condition for a safe manoeuvre. This strategy came from the desire of emphasizing the user's decision rather than the development of a completely autonomous system.

7.1.1 Navigation

Advanced robotics functionalities, based on video and 3D data processing, represent the core element of the semi-autonomous navigation modality. These were derived from specific libraries, that could not be directly coded at HMI level, and were therefore coded in some dedicated C++ services. This was organized into four parallel tasks that perform:

- Images acquisition
- Absolute localization using ToF data stream
- Incremental localization using the encoders and path following task
- Communication with the HMI and the driver

Localization

The localization of the wheelchair is performed by fusing two contributions: odometry from encoder and custom designed absolute localization method based on the data from the TOF.

As for the first, this was derived from the odometric recursion from [24].

$$\begin{cases} x_{k+1} = x_k + \pi \cdot \frac{n_{Rk} \cdot R_R + n_{Lk} \cdot R_L}{n_0} \cdot \cos(\delta_k) \\ y_{k+1} = y_k + \pi \cdot \frac{n_{Rk} \cdot R_R + n_{Lk} \cdot R_L}{n_0} \cdot \sin(\delta_k) \\ \delta_{k+1} = \delta_k + 2\pi \cdot \frac{n_{Rk} \cdot R_R - n_{Lk} \cdot R_L}{n_0 \cdot b} \end{cases} \quad (7.1)$$

Where:

- (x, y, δ) is estimated position and attitude with respect to the fixed reference (initial pose);

- R_R, R_L are the right and left driver wheels' radius;
- n_{Rk}, n_{Lk} are the number of counts from the driving right and left encoder
- n_0 is the number of counts of the driving encoder in one turn;
- b is the wheel base of the differential drive robot

As for the latter, this was designed differently from the canonical ones, which are usually based on the matching of range data with a previously created map [51].

A vision based solution foresees the use of Augmented Reality (AR) functionalities [47, 38] to localize the wheelchair with respect to the POIs without the use of a map. The main advantages are:

- the simplification of the data structure;
- a lower computational cost;
- the possible usage of cheap sensors, that is the only cost of the introduction of visual tags, as spacial anchors, in the domestic environment;

The eye-controlled wheelchair prototype was designed to work mainly in a domestic environment. In such a context, the furnitures represent reliable landmarks since it is very unlikely that these are moved frequently in time. The most interesting furnitures from an operative point of view, like doors, tables and so on, were then referenced using AR tags [67]. For each, a POI was defined as a target pose $[x, y, \theta]$. An operative example is a television: the POI is defined with respect to the marker, placed nearby the device so that the user can reach by mean of the semi-autonomous navigation modality a predefined position and watch it in the most comfortable way.

The steps involved in the localization process are presented in the Algorithm 1 and detailed here:

- 1. Data acquisition** the information concerning the RGB image and the depth stream data are collected from the ToF camera and passed to the processing block;
- 2. Assessment of the 3D camera position** the system determines the transformation, in terms of height and attitude, between the sensor and the ground using a RANdom SAmple Consensus plane fitting (RANSAC) [32]. This task is fundamental to compensate the mobility of the camera on the chassis, especially in the attitude;

Algorithm 1 Localization algorithm

```

while KeepRunning do
  if CameraConnected then
    Acquire RGB and depth frames
    Calculate plane equation relative to the floor
    Determine camera pose w.r.t. the wheelchair
    Transform cloud points into the wheelchair reference system
    Search ArUco marker in the RGB image
    for EachMarkerDetected do
      Determine pose of the POI related to each marker
    end for
    Send POIs detected information to the HMI
  end if
end while

```

3. Roto-translation of the 3D points the depth frames (3D cloud points) are transformed from the ToF reference system to the wheelchair one. This also enables the organization of a more versatile and efficient AR framework;

4. Target detection an ArUco function analyses the RGB frames searching for the markers. If present, the algorithm evaluates their 3D positions by isolating the correspondent 3D points in correspondence of the markers. This strategy, with respect to the standard vision based one, works without the knowledge of the intrinsic parameters of the camera. The main benefit is the avoidance of a calibration phase, otherwise necessary. The localized markers and the corresponding POIs are then passed to the interface as possible target position and anchor for the autonomous navigation.

The two (concurrent) localization modalities are fused to minimize both the influence of the slowness from the TOF camera localization, both the drift error from odometric localization. A Bayesian-based approach was considered from De Cecco et al. [23] for that, resulting in much accurate navigation (if compared to the single localization options) and thus a safer system.

Uncertainty estimation of localization tasks

Any localization process exploited in an autonomous (and also in the semi-autonomous) navigation should include, for the sake of safety, an assessment of the uncertainty of the identified positions.

Uncertainty of odometric localization The uncertainty estimation of the odometric localization is calculated through the algorithm proposed by De Cecco et al. [22] as a function

of the manoeuvre performed by a vehicle in certain given time. It is expressed in terms of covariance matrix of the pose vector (x_k, y_k, δ_k) . The result is a recursive estimation of the covariance that takes into account both the correlation between kinematic parameters and also the uncorrelated effects.

The covariance estimation is determined starting from Equation 7.1 that is used to calculate the position increments at each iteration step. The increment estimation is a non-linear function of the parameters $[n_{Rk}, n_{Lk}, n_0, R_R, R_L, b, \delta_k]$. Considering these parameters, the vector of variable affecting the accuracy of the estimation are is composed by:

$$w_k = [R_R, R_L, b, \delta_k] \quad (7.2)$$

The parameters $[n_{Rk}, n_{Lk}, n_0]$ are neglected as a source of uncertainty because it is constant or its error is commonly compensated for between a step and the following ones.

$$C_{Xk+1} = C_{Xk} + \mathfrak{S}_{\Phi_k} \cdot C_{wk} \cdot \mathfrak{S}_{\Phi_k}^T + \mathfrak{S}_{\Phi_k} \cdot S_{wk} \cdot I_k^T + I_k \cdot S_{wk} \cdot \mathfrak{S}_{\Phi_k}^T + |\Phi_k|^2 \cdot C_{\xi_k} \quad (7.3)$$

Where:

- \mathfrak{S}_{Φ_k} is Jacobian matrix of the non linear function related to the increment estimation;
- C_{wk} is diagonal matrix with covariances of parameters of w_k vector;
- S_{wk} is matrix whose elements are square root of C_{wk} elements
- Φ_k is the non linear function related to the increment estimation;
- C_{ξ_k} is the covariance matrix of a stochastic variable related to the uncertainty of the kinematic model.

the integral term I_k can be calculated using the following recursion:

$$I_k = I_{k-1} + \mathfrak{S}_{\Phi_{k-1}} \cdot S_{wk-1} \quad (7.4)$$

The right part of Equation 7.3 includes five terms. The first one is the covariance matrix related to the previous step while the second one is the uncertainty propagation of the parameters expressed in Equation 7.2. This term considers the parameters of the vector w_k as uncorrelated between the others as well as to itself in the time. The third and fourth elements consider the full correlation of the samples during the integration period. The fifth element is the term related to the uncertainty of the kinematic model. In the uncertainty estimation of the wheelchair prototype, the fifth element was neglected for simplicity. Indeed, in order to

include this term, it is necessary to perform a repeatability analysis to obtain information about the unpredictable source of uncertainty related to the kinematic model. For further details please refer to De Cecco et al. [22].

Uncertainty of marker based localization With regard to the uncertainty estimation of the marker based localization, in the eye-controlled wheelchair prototype, such requirement was achieved through a repeatability analysis that foresaw the measurement of static positions of multiple markers positioned in the FOV of the ToF. The tests considered two conditions, distance and orientation related. In the first, the marker and the wheelchair were aligned, moving the second at different distances, Fig. 7.4 reports the measurements as the point-type markers. In the latter, represented by cross-type markers, the attitude of the wheelchair was changed with respect to the marker, keeping the position fixed.

The experimental evidences highlighted a correlation between the number of 3D points laying inside the marker area and the covariance of the measure. Such observation was then exploited to determine the standard deviation of the (x,y) position of the marker as a function of the number of points detected:

$$\sigma(n_p) = \frac{p_1 \cdot n_p + p_2}{n_p + q_1} \quad (7.5)$$

Where:

- n_p is the number of 3D points detected inside the marker
- p_1, p_2, q_1 are numeric coefficients resulting from the fitting of Equation 7.5 with the experimental data;

Equation 7.5 was applied on the principal decomposition of the 3D point cloud in correspondence of the marker, determining in this way two contributes, frontal and transversal, and successively combining them in a covariance matrix.

7.2 Experimental verification

The passage through a door, or narrow passage in general, is one of the most important tasks for the performance of autonomous domestic mobility. In the case of a semi-autonomous motion, the manoeuvre depends on the localization of the wheelchair with respect to the environment, which is a task mostly demanded to a single device, conveniently organized. In the prototype, the ToF covers such role in combination with the POIs.

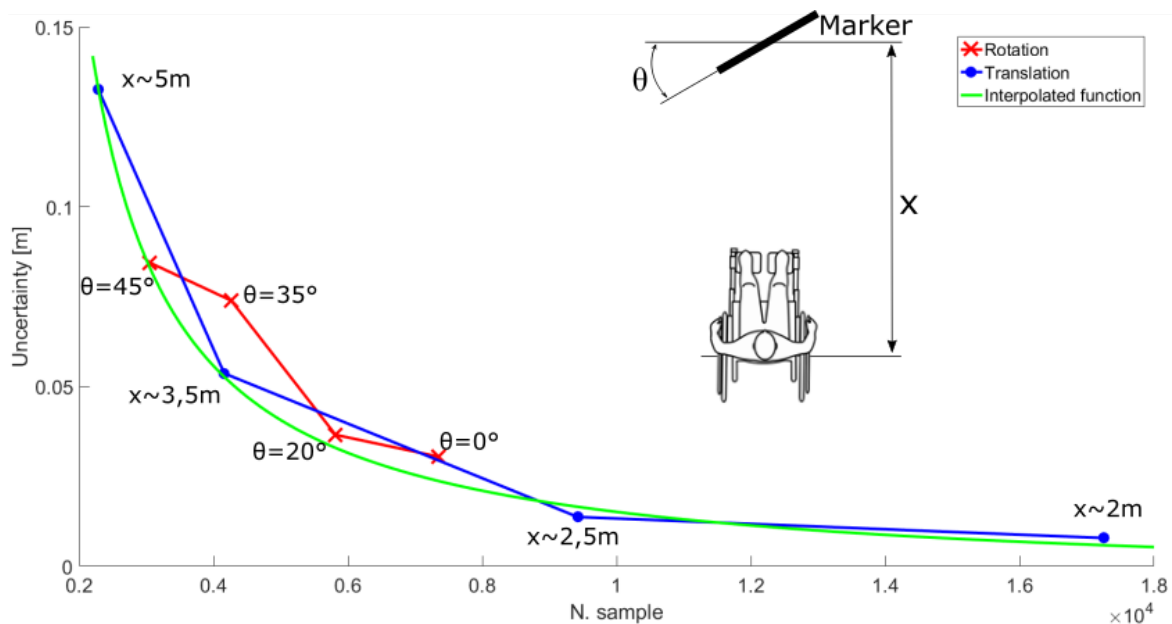


Fig. 7.4 The relation between the standard deviation in the marker localization versus the number of points associated to a marker.

However, the onboard position of such device can be assessed with a limited accuracy since it has to be fixed in a critical spot. From the specifications identified by the testers, to result effective in driving, the ToF has to:

1. be frontal with respect to the system;
2. point toward the floor in order to identify possible obstacles
3. allows an easy repositioning to enable the user to sit on and off the wheelchair (also by mean of assistance equipments)

Such setup implies possible *small* variations in the position of the device from the calibrated reference, either caused by vibrations, the backlash of the mounting system, or mechanic tolerances. That can be modelled as uncertainty in such parameters, resulting in an error that propagates from the initial path planning, when the wheelchair is stationary, along the entire manoeuvre, in which the path is automatically updated every time the target POI falls inside the FoV of the ToF. The result is a non-negligible displacement of the wheelchair from the intended target position, which represents a hazardous condition for the user. For this reason, an error budget analysis was structured to highlight the influence of the uncertainty in the position of the ToF with respect to the performances of the semi-autonomous navigation toward a target POI.

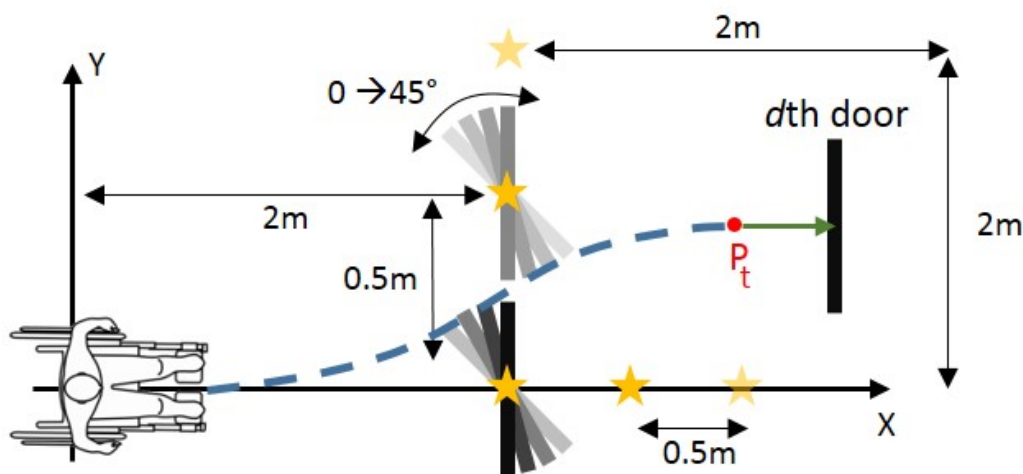


Fig. 7.5 The scheme of the tests used in the Monte Carlo simulation.

7.2.1 Manoeuvre modelling

A Monte Carlo simulation [45] was structured to model the influence of the uncertainty in the position of the ToF along the manoeuvre. Fig. 7.5 shows the considered spatial configuration, which represents an ideal operative scenario: an area starting 2 m away from the wheelchair, 2 m long and 4 m wide. Inside such region, a uniform grid of doors d_{xy} was defined with fixed steps of 0.5 m in the x and y directions. For each d_{xy} , 5 attitudes ranging from 0 to 45° were defined. The simulation considered the wheelchair starting from the origin and the door defined in a position $[x, y, \theta]$. The target pose P_t was defined as a point placed 0.5 m in front of the door.

Only the upper part of the area (positive y s) was considered for symmetry. As further simplification, only positive angles were considered for the attitude of d_{xy} s: negative angles simulate an approach from a high incidence direction, an unlikely operative condition given the vision-based structure of the navigation.

The simulation included the kinematic model of the wheelchair and the uncertainty in the kinematic parameters. The result is a set of covariance matrices along the executed path, which represents the possible *true* position reached by the wheelchair at a defined confidence level [24]. This was set to 99.7% (3σ) to maximize the reliability of the results, and thus the safety of the system.

Given the n th of the N simulation runs and the d th door, the nominal onboard position of the ToF is modified by adding a systematic error randomly selected from a pool of possible uncertainty levels in displacement, named σ_{xy} , and attitude, σ_θ . Such bias remains fixed for the entire duration of the n th run, and cause an error in the generation of the virtual

measurements that link the wheelchair to P_t . To reduce the number of factors in the proposed analysis, the values defined by σ_{xy} represent radial displacements and not independent x and y components. These were instead computed starting from the definition of the distance and randomly selecting a displacement angle (different from θ).

The simulation starts with the initial planning and motion of the wheelchair from the origin toward P_t . After a defined latency, the simulation performs an update of the data as a new measurement of P_t seen from the actual position of the wheelchair. A new path planning and path following operations are then run, structuring a loop that ends when the wheelchair is less than 0.3 m away from P_t . After that, a conclusive planning step is run and the final pose P_{fp} and covariance matrix C_{fp} recorded. As conclusive step, further 100 random seeds are taken from C_{fp} and used to project the position of the wheelchair toward the door's line (a segment of 0.5 m length). Fig.7.6 reports an example of simulation.

The kinematic parameters considered for the wheelchair model were a wheel base of $0.650 \pm 0.005m$ and a wheel radius of $0.155 \pm 0.010m(3\sigma)$. As for the data acquisition process, an update in the planning at 10 Hz was considered, equivalent to a routine every 3 samples from the ToF (native operative frequency of 30 Hz). The speed of the wheelchair was set to 0.5 m/s, the fastest suitable speed for safe domestic usage. Any lower speed reduces the influence of the uncertainty in the final position since it implies a slower motion thus a higher number of updates and so the application of more corrective actions while approaching to the target position.

The considered uncertainty levels in sensor position were chosen accordingly to the hardware configurations, mounting, and fastening options available with standard (certified) mechanical mounts:

- $\sigma_{xy} = [0.001, 0.005, 0.01, 0.02, 0.05]m$
- $\sigma_{\theta} = [0.1, 1, 2, 5, 10]\pi/180[rad]$

For each σ_{xy} - σ_{θ} configuration, 100 trials were run.

Minimum door clearance

The transversal displacement of the wheelchair along the door line was considered as performance factor P_f for each seed. From the distribution P_f , the minimum door clearance $d_{c_{min}}$ was assessed using:

$$d_{c_{min}} = 2 \cdot \left(\Sigma P_f + \frac{3 \cdot \sigma_{P_f} + W_w}{2} \right) \cdot 1.2 \quad (7.6)$$

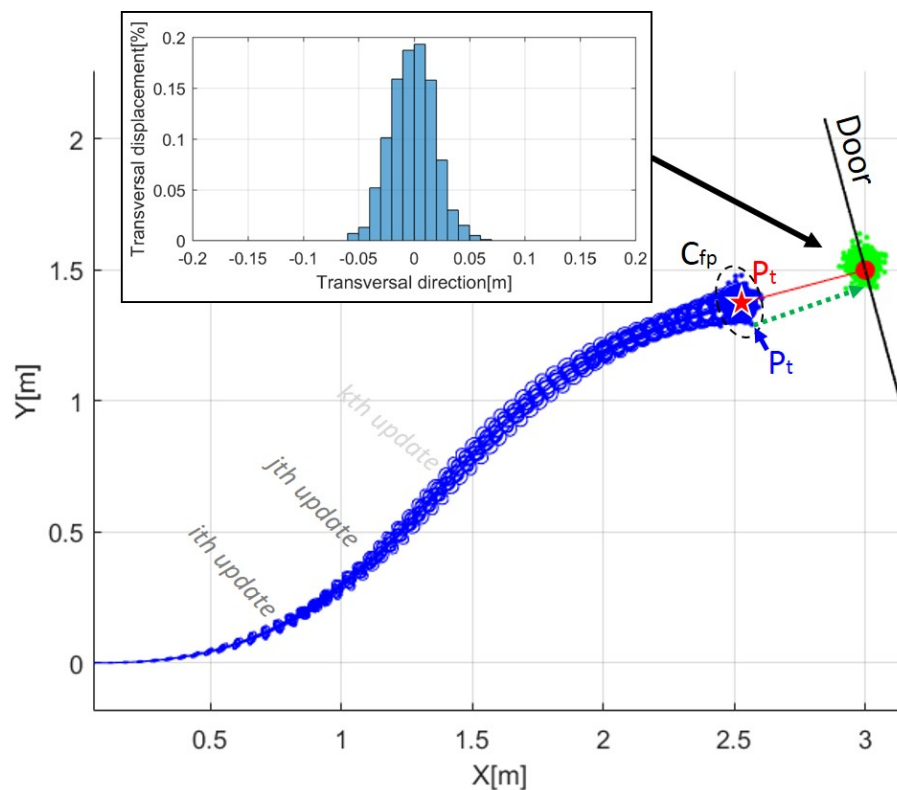


Fig. 7.6 Example of simulation: in black the reference geometry for the door, in red the linear approach to the door, in blue both the ellipses representing the uncertainty propagation along the path for all the simulated paths and the dots the seeds from the final curvilinear positions and covariances, and in green the final positions after the linear conclusive path. The figure reports also the histograms of the performance factor P_f as the final transversal displacement of the wheelchair along the door line.

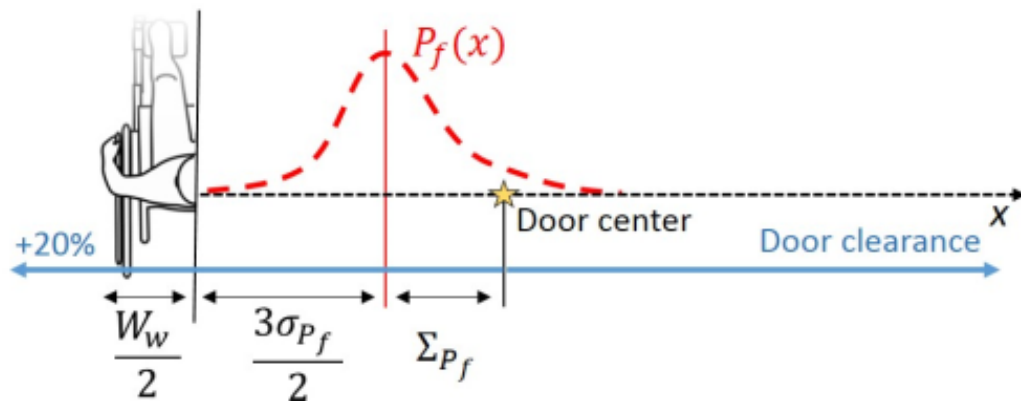


Fig. 7.7 Scheme for the assessment of the minimum door clearance.

W_w is wheelchair width, while Σ_{P_f} and σ_{P_f} represent the systematic and random errors in reaching the door: the first is computed as the mean of the distribution of P_f s, the second as the standard deviation. The value of 1.2 stands as an additional safety factor (20%). Fig. 7.7 reports a geometrical representation of the formula.

Given the multidimensional structure of the data, the 2 σ s and the 3 spatial coordinates of the door, the maximum value among the 5 available was used as a representation of the identified clearance. This condition is the most precautionary since from it derives the widest door clearance.

Fig. 7.8 reports the resulting door clearance organized along the tested xy doors' position at the different levels of σ_{xy} and σ_θ . Fig. 7.9a reports instead the maximum clearance value among the entire tested area.

Minimum door clearance [m]		Safe navigation through a 1.0m door [%]								
0.1	0.99	0.99	0.99	1.00	1.03	100.00	100.00	100.00	100.00	100.00
1	1.01	1.02	1.02	1.02	1.03	99.91	99.90	99.91	99.90	99.90
2	1.06	1.06	1.06	1.06	1.07	99.44	99.42	99.39	99.36	99.27
5	1.22	1.22	1.23	1.23	1.23	83.60	83.52	83.56	83.47	83.48
10	1.56	1.56	1.56	1.56	1.57	54.37	54.44	54.43	54.52	54.65
	0.001	0.005	0.01	0.02	0.05	0.001	0.005	0.01	0.02	0.05
	σ_{xy} [m]					σ_{xy} [m]				

(a) Minimal door clearance with respect to the uncertainty level in sensor position in order to achieve a safe navigation at 99.7% confidence interval

(b) Success rate in case of a door of 1 m width.

Safe navigation through a 1.2m door [%]		Success rate in case of a door of 1.2 m width								
0.1	100.00	100.00	100.00	100.00	100.00	100.00	100.00	100.00	100.00	100.00
1	100.00	100.00	100.00	100.00	100.00	100.00	100.00	100.00	100.00	100.00
2	100.00	100.00	100.00	100.00	100.00	100.00	100.00	100.00	100.00	100.00
5	98.87	98.89	98.88	98.88	98.79	98.87	98.89	98.88	98.84	98.79
10	78.37	78.32	78.32	78.32	78.31	78.37	78.32	78.32	78.32	78.31
	0.001	0.005	0.01	0.02	0.05	0.001	0.005	0.01	0.02	0.05
	σ_{xy} [m]					σ_{xy} [m]				

(c) Success rate in case of a door of 1.2 m width

Fig. 7.9 Success rate in door passage, clearance versus σ_s .

Success rate

The success rate in the navigation through a door for a given clearance d_c was assessed by computing the percentage of seeds that resulted in a passage without an impact, modelled as $P_f(i) \leq 0.5 \cdot (d_c - W_w)$. In Fig.7.9 are shown the percentage for a door of 1 m(a) and 1.2 m(b), standard sizes for domestic environments in which a disabled subject lives [6].

Such results can be used in multiple ways: (i) to determine the minimum door clearance given an uncertainty level in the position of the sensor, (ii) to identify the maximum admissible σ_s given the doors inside a home, or (iii) to identify the best trade-off condition for the design of the wheelchair and the environment in which it will be used.

In this work the focus was on this last point, identifying in the 1.0 m clearance the suitable condition given an assessment of the position of the ToF with σ_{xy} and σ_θ lower than 0.05 m and 2 deg respectively. Among the two, the angular condition resulted in the more restrictive one, and the design of RoboEYE was modified accordingly considering a vertical turnable mount rather than a horizontal one.

The highlighted results are specific for the considered geometry and implementation of the presented system. However, the presented definitions and methodology are general and aimed at including in the design and modeling of the system all the relevant quantity of interest for a better comprehension of the autonomous system, its implications also in relation to the operative environment. The method can be applied directly to different geometries and configuration of a wheelchair, or other similar applications, with just minor modifications in the parameter definition.

7.2.2 Experimental testing

The performances of the semi-autonomous navigation were assessed through a repeatability analysis on the final positions reached by the wheelchair given a set of initial, controlled, states. An experimental test campaign was performed.

Two markers were set at a clearance of 1.2 m, Fig. 7.10 shows the considered scheme and the semi-autonomous navigation activated by pointing as the associated POI. Fig. 7.11 shows the action sequence followed in the tests. The initial position $[x', y', \theta]$ of the wheelchair was referred with respect to the reference frame $[x, y]$, set in the center and aligned along of the door. The following test conditions were achieved:

- fixed initial position and attitude;
- shifts from the initial reference position along the y direction, from $-0.90 \pm 0.01m$ to $+0.90 \pm 0.01m$ with steps of $0.30 \pm 0.01m$;

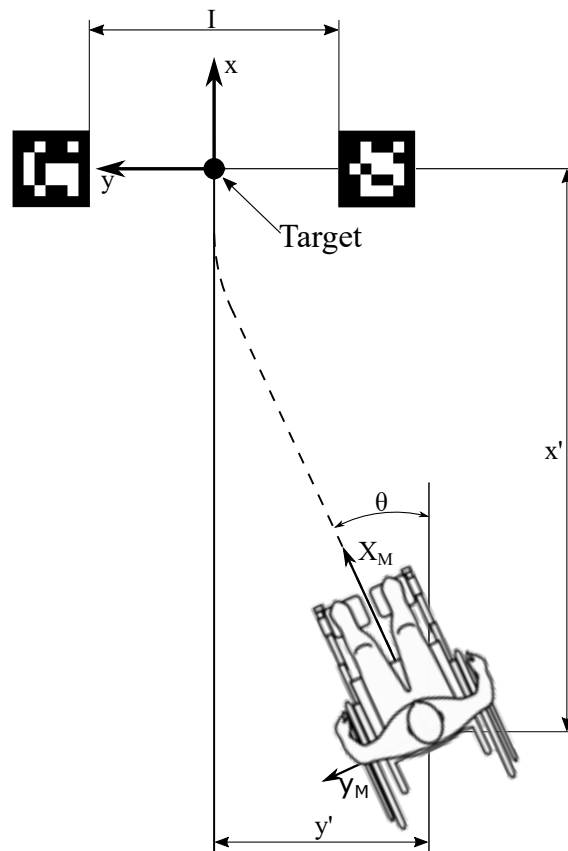


Fig. 7.10 Test scenario related to the semi-autonomous navigation with the wheelchair arrangement with respect to the target pose.

- all the tree initial conditions randomly changed.

Table 7.1 reports the initial condition of the tests.

The outcomes of the test, reported in Fig. 7.12, were:

1. a correlation between the initial shift along the y' direction and the final position reached by the wheelchair, visible in Fig. 7.12b with samples grouped accordingly to their initial starting position;
2. in the case of a variable starting positions, maximum displacements from the target position of 0.18 m along the transversal direction, and 0.08 m longitudinally, Fig. 7.12c;
3. a systematic displacement between the mean position of the sample set and the target, probably deriving from the limited knowledge of extrinsic parameters of the ToF with respect to the wheelchair.

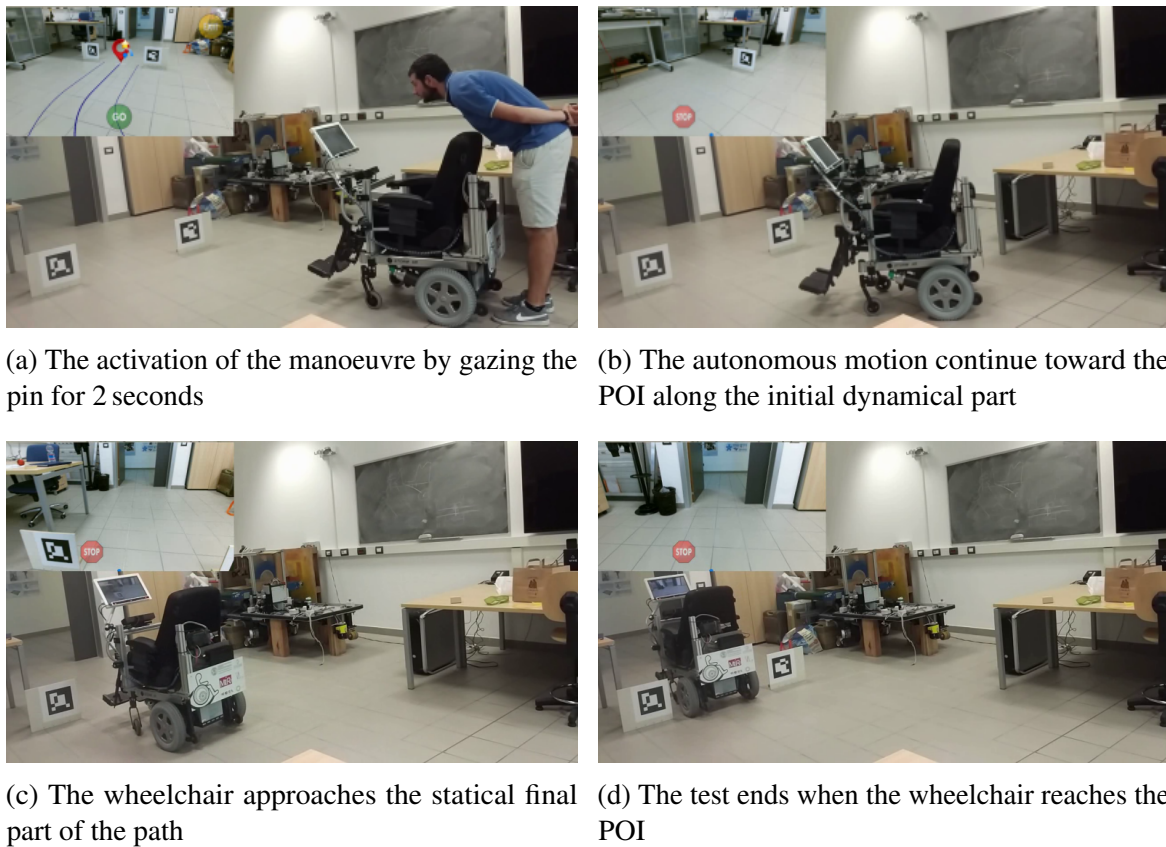


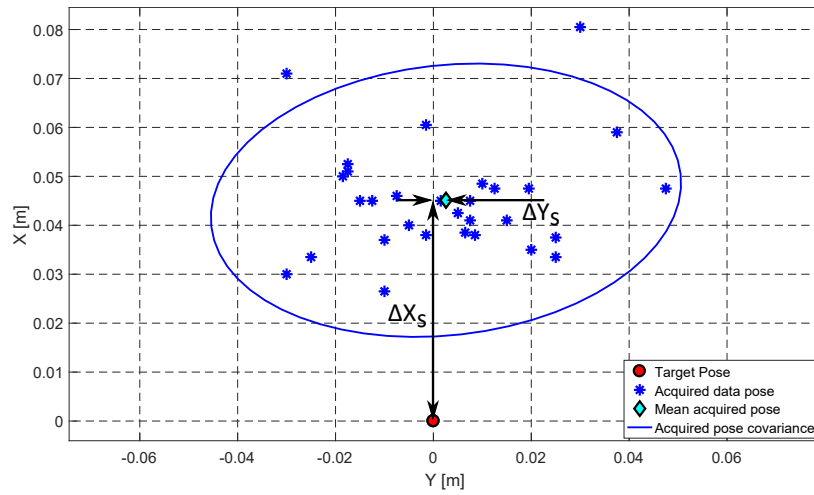
Fig. 7.11 Semi-autonomous navigation action sequence adopted for the repeatability analysis.

Table 7.1 Initial conditions of the repeatability analysis.

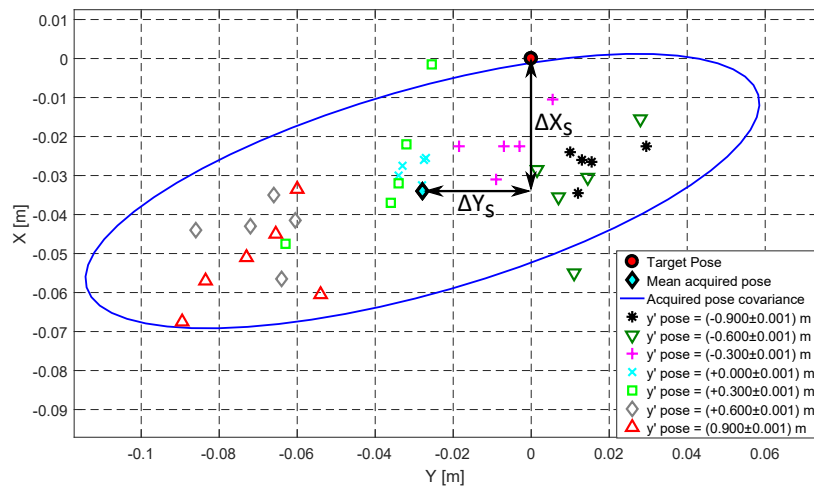
N. test	x' [m]	y' [m]	θ [rad]	N. of samples
1	4.26 ± 0.01	0.61 ± 0.01	0.0 ± 0.1	30
2	4.26 ± 0.01	Variable	0.0 ± 0.1	30
3	Variable	Variable	Variable	30

Table 7.2 Results of repeatability analysis.

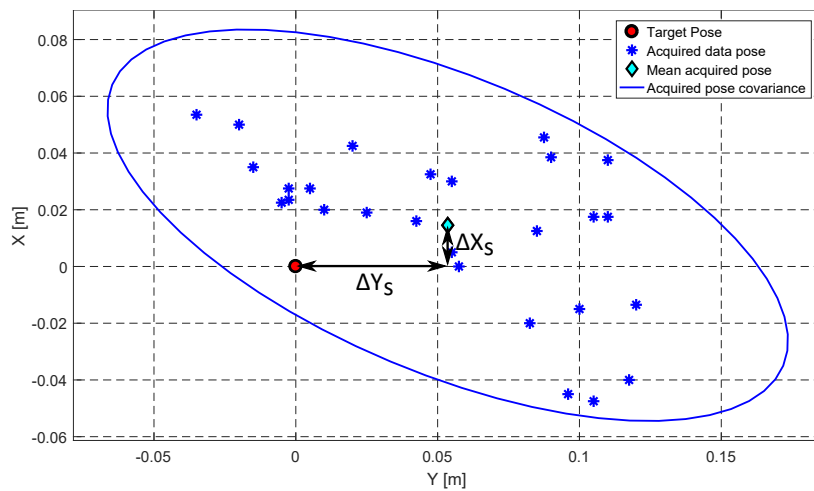
N. test	ΔX [m]	ΔY [m]	σ_{Max} [m]	σ_{min} [m]
1	-0.045	-0.003	0.024	0.014
2	0.034	0.028	0.049	0.013
3	-0.014	-0.054	0.064	0.026



(a) Fixed start point



(b) Variable start point along y'



(c) Random start pose

Fig. 7.12 Repeatability analysis results on semi-autonomous navigation.

Table 7.2 reports the average offset between the target pose and the mean final wheel-chair position, which represents the systematic error and can be compensated with calibration, and the standard deviation which is the index of data dispersion.

7.3 Discussion of the results

This part of the project focuses on the development of an Augmented Reality application based on a gaze interaction technology able to control semi-autonomously a wheelchair in a domestic environment. The performance of the system was evaluated by performing a repeatability analysis on the final positions reached, starting from different positions with respect to the target. In this way, it was possible to assess the influence of the starting position. The repeatability analysis shows a maximum value (test with a complete variable start point, Fig. 7.12) of deviation from the target position, transversal to the final desired direction, of 0.18 m and 0.08 m longitudinally. From this information, we can conclude that, considering the width of the wheelchair of 0.62 m, the minimum space actually required to reach autonomously a target is 0.98 m. Moreover, it is possible to notice a systematic deviation represented by the distances between the mean position of the sample and the target. This deviation can be related to the extrinsic parameters of the camera with respect to the vehicle that are not precisely known. As reported before, the camera is mounted on the chassis through a revolute joint characterized by backlashes in particular in the angle. This causes the systematic deviation highlighted in the final position reached by the wheelchair. Future development is an on-line calibration of the camera extrinsic parameters by considering the changes in terms of position and attitude recorded by the odometric localization and by the camera absolute localization during the execution of the path. In this way, it is possible to compensate the systematic deviation and prevent errors due to the possible variations of the position and attitude of the camera in the long periods. As an overall conclusion, we can say that the semi-autonomous navigation tool developed is suitable for indoor use in common houses having passages wider than 98 centimeters. An improvement of the performance of the overall project can be reached by the implementation of the on-line calibration tool together with an error budget analysis. Architectural house design criteria can take benefits from the error budget results in order to enhance the user mobility experience.

Chapter 8

Conclusions

The thesis presented the guidelines and the design choices taken in the realization of a domestic robotic wheelchair driven by the gaze of the user. The wheelchair, named RoboEye, was developed considering commercial non-contact technology to interface the user with its control.

With respect to other states of the art solutions, RoboEye offers:

1. The minimum invasiveness to the user;
2. It ingrates functionalities derived from the mobile robotics field;
3. It considers the role of the uncertainty in the human-machine interaction;
4. It is based on low-cost hardware solutions.

The result is an efficient and cost-effective system, suitable for the technology transfer to its potential users.

The prototype was equipped with a logic unit that integrated a custom filtering of the eye tracker, the data acquisition and exchange from the equipped sensors, and it manages both the HMI and the driving modalities included in the system. Two options are offered to the user:

Direct ocular control: in which the motion of the wheelchair is directly connected to the gazed point on the monitor;

Semi-autonomous control in which the user has to select only a visual target in order to enable the autonomous manoeuvre toward such point

The direct ocular control was evaluated through a comparison with a classical joystick interface. The analysis was carried out by designing a specific test procedure that includes some point from the Wheelchair Skill Test. During the analysis was considered several kinematic features such as motion and comfort metrics but also subjective feedback provided the testers through questionnaires. The results of the analysis highlight better performances of the joystick with respect to the ocular controller in particular for the full mobility users. This behavior was related to limited depth and environmental perception. An interesting element is the performances of reduced mobility users. Even if the reduced mobility users obtained the worst results compared to the full mobility, their performances obtained with the two different interfaces are comparable. In general, it is necessary to remember that the human eye is an organ mainly devoted to the exploration and not for the control. Therefore, looking at a fixed point for a lot of time requires a certain amount of mental and physical workload for the user, resulting in this way a non-trivial operation. However, with a proper training phase, it is possible to learn how to easily manoeuvre the wheelchair.

As for the second driving modalities, potentially the most hazardous of the two, the performances of the system were evaluated in detail by performing both numeric simulations and experimental verification. The analysis showed a maximum transversal displacement from the target position of $0.18m$, deriving from uncertainties that inevitably affect the knowledge of parameters of kinematics and sensor position. For the considered wheelchair, of $0.62m$ width, the operative outcome is a minimum clearance of $0.98m$ for an autonomous, reliable, and safe navigation through a narrow passage. Such requirement meets the standards for domestic usage of the system, like a house with doors wider than $1m$, which is a common dimension for an environment structured for a wheelchair user.

As a future development, the semi-autonomous navigation can be extended to full-autonomous navigation in order to provide to the wheelchair the capability of moving from one position inside a room to another one inside another room. This feature requires the usage of a global map of the environment as well as an obstacle avoidance task.

The main advantage of the gaze-based control technique is not only related to driving. The technology here presented can also be used for the interaction of a patient with the surrounding environment as well as to the external world. Indeed, as another future development, the usage of a common PC provides to the wheelchair the capability to connect to the home automation system or with to the internet network. Therefore, it is possible to think about a tele-assistance system that enables a caregiver to provide support to the patient. In this way, the wheelchair becomes a sort of "ecosystem" with which the user can drive, manage the home and communicate.

References

- [1] Abdulameer, A., Sulaiman, M., Aras, M., and Saleem, D. (2016). Gui based control system analysis using pid controller for education. *Indonesian Journal of Electrical Engineering and Computer Science*, 3(1):91–101.
- [2] Al-Rahayfeh, A. and Faezipour, M. (2013). Eye tracking and head movement detection: A state-of-art survey. *IEEE journal of translational engineering in health and medicine*, 1.
- [3] Alkhalid, F. F. and Oleiwi, B. K. (2019). Smart autonomous wheelchair controlled by voice commands-aided by tracking system. *IRAQI JOURNAL OF COMPUTERS, COMMUNICATION AND CONTROL & SYSTEMS ENGINEERING*, 19(1):82–87.
- [4] Armanini, A. and Conci, N. (2010). Eye tracking as an accessible assistive tool. In *11th International Workshop on Image Analysis for Multimedia Interactive Services WIAMIS 10*, pages 1–4. IEEE.
- [5] Arthur, K. C., Calvo, A., Price, T. R., Geiger, J. T., Chio, A., and Traynor, B. J. (2016). Projected increase in amyotrophic lateral sclerosis from 2015 to 2040. *Nature communications*, 7:12408.
- [6] Association, I. W. (2014). Best Practice Access Guidelines, Designing Accessible Environments. <https://www.iwa.ie/downloads/about/iwa-access-guidelines.pdf>.
- [7] Baglivo, L. (2005). Navigazione di Veicoli Autonomi: Pianificazione e Controllo di Traiettorie. Appunti per il corso di “Robotica Spaziale” per Ingegneria Aerospaziale. Appunti per il corso di “Robotica Spaziale” per Ingegneria Aerospaziale.
- [8] Bergstrom, J. R. and Schall, A. (2014). *Eye tracking in user experience design*. Elsevier.
- [9] Bertolazzi, E. and Frego, M. (2012). Fast and accurate clothoid fitting. *arXiv preprint arXiv:1209.0910*.
- [10] Bertolazzi, E. and Frego, M. (2018). Interpolating clothoid splines with curvature continuity. *Mathematical Methods in the Applied Sciences*, 41(4):1723–1737.
- [11] Bi, L., Fan, X.-A., and Liu, Y. (2013). Eeg-based brain-controlled mobile robots: a survey. *IEEE transactions on human-machine systems*, 43(2):161–176.
- [12] Brolly, X. L. and Mulligan, J. B. (2004). Implicit calibration of a remote gaze tracker. In *Computer Vision and Pattern Recognition Workshop, 2004. CVPRW'04. Conference on*, pages 134–134. IEEE.

- [13] Buxbaum, L. J., Palermo, M. A., Mastrogiovanni, D., Read, M. S., Rosenberg-Pitonyak, E., Rizzo, A. A., and Coslett, H. B. (2008). Assessment of spatial attention and neglect with a virtual wheelchair navigation task. *Journal of Clinical and Experimental Neuropsychology*, 30(6):650–660.
- [14] Castellanos, J. C., Susin, A. A., and Fruett, F. (2011). Embedded sensor system and techniques to evaluate the comfort in public transportation. In *Intelligent Transportation Systems (ITSC), 2011 14th International IEEE Conference on*, pages 1858–1863. IEEE.
- [15] Cerrolaza, J. J., Villanueva, A., Villanueva, M., and Cabeza, R. (2012). Error characterization and compensation in eye tracking systems. In *Proceedings of the symposium on eye tracking research and applications*, pages 205–208. ACM.
- [16] Champaty, B., Jose, J., Pal, K., and Thirugnanam, A. (2014). Development of eog based human machine interface control system for motorized wheelchair. In *2014 Annual International Conference on Emerging Research Areas: Magnetics, Machines and Drives (AICERA/iCMMD)*, pages 1–7. IEEE.
- [17] Chen, L. (2018). Microservices: architecting for continuous delivery and devops. In *2018 IEEE International Conference on Software Architecture (ICSA)*, pages 39–397. IEEE.
- [18] Clemotte, A., Velasco, M., Torricelli, D., Raya, R., and Ceres, R. (2014). Accuracy and precision of the tobii x2-30 eye-tracking under non ideal conditions. In *InProceedings of the 2nd International Congress on Neurotechnology, Electronics and Informatics*, pages 111–116.
- [19] Clinic, M. (2018). Amyotrophic Lateral Sclerosis (ALS). <https://www.mayoclinic.org/diseases-conditions/amyotrophic-lateral-sclerosis/symptoms-causes/syc-20354022>.
- [20] Cooper, R. A., Ding, D., Simpson, R., Fitzgerald, S. G., Spaeth, D. M., Guo, S., Koontz, A. M., Cooper, R., Kim, J., and Boninger, M. L. (2005). Virtual reality and computer-enhanced training applied to wheeled mobility: an overview of work in pittsburgh. *Assistive Technology*, 17(2):159–170.
- [21] Cruz-Neira, C., Sandin, D. J., DeFanti, T. A., Kenyon, R. V., and Hart, J. C. (1992). The cave: audio visual experience automatic virtual environment. *Communications of the ACM*, 35(6):64–73.
- [22] De Cecco, M., Baglivo, L., and Angrilli, F. (2007a). Real-time uncertainty estimation of autonomous guided vehicle trajectory taking into account correlated and uncorrelated effects. *IEEE Transactions on Instrumentation and Measurement*, 56(3):696–703.
- [23] De Cecco, M., Baglivo, L., Ervas, E., and Marcuzzi, E. (2006a). Asynchronous and time-delayed sensor fusion of a laser scanner navigation system and odometry. In *XVIII IMEKO World Congress, Metrology for a Sustainable Dept*, pages 17–22.
- [24] De Cecco, M., Baglivo, L., and Pertile, M. (2006b). Real-time uncertainty estimation of odometric trajectory as a function of the actual manoeuvres of autonomous guided vehicles. In *Proceedings of the 2006 IEEE International Workshop on Advanced Methods for Uncertainty Estimation in Measurement (AMUEM 2006)*, pages 80–85. IEEE.

- [25] De Cecco, M., Bertolazzi, E., Miori, G., Oboe, R., and Baglivo, L. (2007b). Pc-sliding for vehicles path planning and control: Design and evaluation of robustness to parameters change and measurement uncertainty. In *4th International Conference on Informatics in Control, Automation and Robotics, ICINCO 2007*, pages 11–18.
- [26] De Cecco, M., Fornaser, A., Tomasin, P., Zanetti, M., Guandalini, G., Ianes, P., Pilla, F., Nollo, G., Valente, M., and Pisoni, T. (2017). Augmented reality to enhance the clinician's observation during assessment of daily living activities. In *International Conference on Augmented Reality, Virtual Reality and Computer Graphics*, pages 3–21. Springer.
- [27] De Cecco, M., Zanetti, M., Fornaser, A., Leuci, M., and Conci, N. (2016). Inter-eye: interactive error compensation for eye-tracking devices. In *AIP Conference Proceedings*, volume 1740, page 050007. AIP Publishing.
- [28] Dev, A., Rahman, M. A., and Mamun, N. (2018). Design of an eeg-based brain controlled wheelchair for quadriplegic patients. In *2018 3rd International Conference for Convergence in Technology (I2CT)*, pages 1–5. IEEE.
- [29] Duchowski, A. T. (2002). A breadth-first survey of eye-tracking applications. *Behavior Research Methods, Instruments, & Computers*, 34(4):455–470.
- [30] Duchowski, A. T. (2007). Eye tracking methodology. *Theory and practice*, 328:614.
- [31] Feiner, S., Macintyre, B., and Seligmann, D. (1993). Knowledge-based augmented reality. *Communications of the ACM*, 36(7):53–62.
- [32] Fischler, M. A. and Bolles, R. C. (1981). Random sample consensus: a paradigm for model fitting with applications to image analysis and automated cartography. *Communications of the ACM*, 24(6):381–395.
- [33] for Standardization, I. O. (1997). *Mechanical vibration and shock-Evaluation of human exposure to whole-body vibration-Part 1: General requirements*. The Organization.
- [34] Fornaser, A., De Cecco, M., Leuci, M., Conci, N., Daldoss, M., Armanini, A., Maule, L., De Natale, F., and Da Lio, M. (2017). Eye tracker uncertainty analysis and modelling in real time. In *Journal of Physics: Conference Series*, volume 778, page 012002. IOP Publishing.
- [35] Fornaser, A., De Cecco, M., Leuci, M., Conci, N., Daldoss, M., Maule, L., De Natale, F., and Da Lio, M. (2015). Eye trackers uncertainty analysis and modelling. *XXIII Convegno Nazionale AI VE. LA., Perugia*, pages 12–13.
- [36] Frego, M., Bertolazzi, E., Biral, F., Fontanelli, D., and Palopoli, L. (2017). Semi-analytical minimum time solutions with velocity constraints for trajectory following of vehicles. *Automatica*, 86:18–28.
- [37] Gajwani, P. S. and Chhabria, S. A. (2010). Eye motion tracking for wheelchair control. *International Journal of Information Technology*, 2(2):185–187.
- [38] Garrido-Jurado, S., Muñoz-Salinas, R., Madrid-Cuevas, F. J., and Marín-Jiménez, M. J. (2014). Automatic generation and detection of highly reliable fiducial markers under occlusion. *Pattern Recognition*, 47(6):2280–2292.

- [39] Glenstrup, A. J. and Engell-Nielsen, T. (1995). Eye controlled media: Present and future state. *University of Copenhagen, DK-2100*.
- [40] Guestrin, E. D. and Eizenman, M. (2006). General theory of remote gaze estimation using the pupil center and corneal reflections. *IEEE Transactions on biomedical engineering*, 53(6):1124–1133.
- [41] Hansen, D. W. and Ji, Q. (2009). In the eye of the beholder: A survey of models for eyes and gaze. *IEEE transactions on pattern analysis and machine intelligence*, 32(3):478–500.
- [42] Hansen, D. W. and Pece, A. E. (2005). Eye tracking in the wild. *Computer Vision and Image Understanding*, 98(1):155–181.
- [43] Holmqvist, K., Nyström, M., and Mulvey, F. (2012). Eye tracker data quality: what it is and how to measure it. In *Proceedings of the symposium on eye tracking research and applications*, pages 45–52. ACM.
- [44] Jain, M., Puri, S., and Unishree, S. (2015). Eyeball motion controlled wheelchair using ir sensors. *World Acad. Sci. Eng. Technol. Int. J. Comput. Electr. Autom. Control Inf. Eng.*, 9(4):906–909.
- [45] JCGM (2008). Evaluation of measurement data — Supplement 1 to the “Guide to the expression of uncertainty in measurement” - Propagation of distributions using a Monte Carlo method.
- [46] Johnsson, J. and Matos, R. (2011). Accuracy and precision test method for remote eye trackers. *Tobii Technology*.
- [47] Kato, H. and Billinghurst, M. (1999). Marker tracking and hmd calibration for a video-based augmented reality conferencing system. In *Proceedings 2nd IEEE and ACM International Workshop on Augmented Reality (IWAR'99)*, pages 85–94. IEEE.
- [48] Ktena, S. I., Abbott, W., and Faisal, A. A. (2015). A virtual reality platform for safe evaluation and training of natural gaze-based wheelchair driving. In *2015 7th International IEEE/EMBS Conference on Neural Engineering (NER)*, pages 236–239. IEEE.
- [49] Lahane, P., Adavadkar, S. P., Tendulkar, S. V., Shah, B. V., and Singhal, S. (2018). Innovative approach to control wheelchair for disabled people using bci. In *2018 3rd International Conference for Convergence in Technology (I2CT)*, pages 1–5. IEEE.
- [50] Letaief, M., Rezzoug, N., and Gorce, P. (2019). Comparison between joystick-and gaze-controlled electric wheelchair during narrow doorway crossing: Feasibility study and movement analysis. *Assistive Technology*, pages 1–12.
- [51] Li, Z., Xiong, Y., and Zhou, L. (2017). Ros-based indoor autonomous exploration and navigation wheelchair. In *2017 10th International Symposium on Computational Intelligence and Design (ISCID)*, volume 2, pages 132–135. IEEE.
- [52] Lin, C.-S., Ho, C.-W., Chen, W.-C., Chiu, C.-C., and Yeh, M.-S. (2006). Powered wheelchair controlled by eye-tracking system. *Optica Applicata*, 36.

- [53] Lydall, R. (2014). London scientists unveil wheelchair ‘driven’ by eye-control. <https://rosslydall.wordpress.com/2014/05/12/london-scientists-unveil-wheelchair-driven-by-eye-control/>.
- [54] Mahajan, H. P., Dicianno, B. E., Cooper, R. A., and Ding, D. (2013). Assessment of wheelchair driving performance in a virtual reality-based simulator. *The journal of spinal cord medicine*, 36(4):322–332.
- [55] Maule, L., Fornaser, A., Leuci, M., Conci, N., Da Lio, M., and De Cecco, M. (2016). Development of innovative hmi strategies for eye controlled wheelchairs in virtual reality. In *International Conference on Augmented Reality, Virtual Reality and Computer Graphics*, pages 358–377. Springer.
- [56] Maule, L., Fornaser, A., Tomasin, P., Tavernini, M., Minotto, G., Da Lio, M., and De Cecco, M. (2017). Augmented robotics for electronic wheelchair to enhance mobility in domestic environment. In *International Conference on Augmented Reality, Virtual Reality and Computer Graphics*, pages 22–32. Springer.
- [57] Meimban, R. J. R., Monsura, A. S., Ranada, J. V., and Fernando, A. R. R. (2018). Eye-controlled wheelchair using infrared detection. *International Journal of Simulation–Systems, Science & Technology*, 19(3).
- [58] Milgram, P. and Kishino, F. (1994). A taxonomy of mixed reality visual displays. *IEICE TRANSACTIONS on Information and Systems*, 77(12):1321–1329.
- [59] Milgram, P., Takemura, H., Utsumi, A., and Kishino, F. (1995). Augmented reality: A class of displays on the reality-virtuality continuum. In *Telem manipulator and telepresence technologies*, volume 2351, pages 282–293. International Society for Optics and Photonics.
- [60] Morimoto, C. H. and Mimica, M. R. (2005). Eye gaze tracking techniques for interactive applications. *Computer vision and image understanding*, 98(1):4–24.
- [61] Nyström, M., Andersson, R., Holmqvist, K., and Van De Weijer, J. (2013). The influence of calibration method and eye physiology on eyetracking data quality. *Behavior research methods*, 45(1):272–288.
- [62] Patrick Joyce, Steve Evans, D. H. and Barnes, C. (2015). Open source system to drive powerchairs by eye movement alone - allowing independent mobility when use of a person’s hands isn’t an option. <https://hackaday.io/project/5426-eye-controlled-wheelchair>.
- [63] Pingali, T. R., Dubey, S., Shivaprasad, A., Varshney, A., Ravishankar, S., Pingali, G. R., Polisetty, N. K., Manjunath, N., and Padmaja, K. (2014). Eye-gesture controlled intelligent wheelchair using electro-oculography. In *2014 IEEE International Symposium on Circuits and Systems (ISCAS)*, pages 2065–2068. IEEE.
- [64] Puanhvuan, D., Khemmachotikun, S., Wechakam, P., Wijam, B., and Wongsawat, Y. (2014). Automated navigation system for eye-based wheelchair controls. In *Biomedical Engineering International Conference (BMEiCON), 2014 7th*, pages 1–4. IEEE.
- [65] Purwanto, D., Mardiyanto, R., and Arai, K. (2009). Electric wheelchair control with gaze direction and eye blinking. *Artificial Life and Robotics*, 14(3):397.

- [66] Rayner, K. (1998). Eye movements in reading and information processing: 20 years of research. *Psychological bulletin*, 124(3):372.
- [67] Romero-Ramirez, F. J., Muñoz-Salinas, R., and Medina-Carnicer, R. (2018). Speeded up detection of squared fiducial markers. *Image and Vision Computing*, 76:38–47.
- [68] Shih, S.-W., Wu, Y.-T., and Liu, J. (2000). A calibration-free gaze tracking technique. In *Pattern Recognition, 2000. Proceedings. 15th International Conference on*, volume 4, pages 201–204. IEEE.
- [69] Siciliano, B., Sciavicco, L., Villani, L., and Oriolo, G. (2010). *Robotics: modelling, planning and control*. Springer Science & Business Media.
- [70] Silva, N., Baglivo, L., Vale, A., and De Cecco, M. (2013). Four path following controllers for rhombic like vehicles. In *2013 IEEE International Conference on Robotics and Automation*, pages 3204–3211. IEEE.
- [71] Smith, R. C. and Cheeseman, P. (1986). On the representation and estimation of spatial uncertainty. *The international journal of Robotics Research*, 5(4):56–68.
- [72] Sodhi, M., Reimer, B., Tant, M., Peli, E., Bowers, A., Woods, R., Higgins, K., and Turco, P. (2005). Driver performance evaluation: Considerations underlying selection and design of routes. *Vision in Vehicles X*. Amsterdam: Elsevier Sciences Publishers.
- [73] Tall, M., Alapetite, A., San Agustin, J., Skovsgaard, H. H., Hansen, J. P., Hansen, D. W., and Møllenbach, E. (2009). Gaze-controlled driving. In *CHI'09 Extended Abstracts on Human Factors in Computing Systems*, pages 4387–4392. ACM.
- [74] Valenti, R. and Gevers, T. (2008). Accurate eye center location and tracking using isophote curvature. In *2008 IEEE Conference on Computer Vision and Pattern Recognition*, pages 1–8. IEEE.
- [75] Voronka, N. and Jacobus, C. J. (2001). Low-cost non-imaging eye tracker system for computer control. US Patent 6,299,308.
- [76] Wastlund, E., Sponseller, K., Pettersson, O., and Bared, A. (2015). Evaluating gaze-driven power wheelchair with navigation support for persons with disabilities. *Journal of Rehabilitation Research & Development*, 52(7):815–827.
- [77] White, K. P., Hutchinson, T. E., and Carley, J. M. (1993). Spatially dynamic calibration of an eye-tracking system. *IEEE Transactions on Systems, Man, and Cybernetics*, 23(4):1162–1168.
- [78] Wood, J. M., Mallon, K., et al. (2001). Comparison of driving performance of young and old drivers (with and without visual impairment) measured during in-traffic conditions. *Optometry and Vision Science*, 78(5):343–349.
- [79] Wood, J. M. and Troutbeck, R. (1992). Effect of restriction of the binocular visual field on driving performance. *Ophthalmic and Physiological Optics*, 12(3):291–298.
- [80] Zanetti, M., De Cecco, M., Fornaser, A., Leuci, M., and Conci, N. (2016). The use of inter-eye for 3d eye-tracking systematic error compensation. In *2016 International Symposium ELMAR*, pages 173–176. IEEE.